

ISSN 0970 - 3268

**Journal of
The Indian Association
of Sedimentologists**

VOLUME 33

NUMBERS 1 & 2

JAN- DEC. 2014-16

INDIAN ASSOCIATION OF SEDIMENTOLOGISTS

**JOURNAL OF THE INDIAN
ASSOCIATION OF SEDIMENTOLOGISTS**

**GOVERNING COUNCIL
INDIAN ASSOCIATION OF SEDIMENTOLOGISTS**

President

Prof. G. N. Nayak, Goa

Past Presidents

Prof. S. M. Casshyap, Delhi

Prof. S. K. Tandon, Delhi

Vice-Presidents

Prof. G. M. Bhat, Jammu

Prof. R. Nagendra, Chennai

General Secretary

Prof. Mahshar Raza, Aligarh (Head Quarters)

Joint Secretaries

Prof. R. A. S. Kushwaha, Manipur

Prof. A. V. Joshi, Vadodra

Treasurer

Dr. A.H.M. Ahmad, Aligarh

Chief Editor

Prof. D. Rajasekhar Reddy, Visakhapatnam

Joint Editors

Prof. S. Banerjee, IIT Bombay

Prof. R. Nagendra, Anna University

Prof. K. Mahendra, Goa University

Joint Guest Editors

Dr. S.R. Singarasubramanian, Annamalai University

Foreign Secretary

Prof. Bindra Thusu, (University college) London

Members

Prof. B. P. Singh, Varanasi

Prof. R. N. Hota, Bhubaneswar

Prof. A. L. Ramanathan, JNU, New Delhi

Prof. A. K. Srivastava, Amravati

Dr. S.R. Singarasubramanian, Annamalainagar

Dr. Sarwar Rais, Aligarh

Dr. Abdullah Khan, Aligarh

Dr. V. Sudarshan, Hyderabad

Dr. Senethal Nathan, Pondicherry

Dr. Subir Sarkar, Jadavpur

ISSN 0970 - 3268

Journal of The Indian Association of Sedimentologists



VOLUME 33

NUMBERS 1 & 2

JAN - DEC. 2014-16

INDIAN ASSOCIATION OF SEDIMENTOLOGISTS

Journal of the Indian Association of Sedimentologists

VOLUME 33

NUMBERS 1 & 2

JAN- DEC. 2014-16

The Indian Association of Sedimentologists

© The Indian Association of Sedimentologists

All subscription/orders of the Journal should be sent to
Prof. D. Rajasekhara Reddy, Editor - Journal of IAS,
49-53-8/1, Sneha Apartments, Balaji Hills, Visakhapatnam - 530 013.
E-mail: drsreddy8@gmail.com

Annual Subscription:

Rs. 1,000.00 (In India)

\$ 120.00 (Abroad)

Published by the Indian Association of Sedimentologists.

Head Quarters: Department of Geology, Aligarh Muslim University, ALIGARH – 202 002.

Printed at Ramakrishna Printers, D. No. 49-24-5, Sankaramattam Road, Madhuranagar, Visakhapatnam – 530 016.

JOURNAL OF THE INDIAN ASSOCIATION OF SEDIMENTOLOGISTS

VOLUME 33

NUMBERS 1 & 2

JAN. - DEC. 2014-16

CONTENTS

Lithological Setting and Granulometry of the Lameta Sediments from New Locality Exposed at Pandhari Village, District Betul, Madhya Pradesh	<i>Ashok K. Srivastava and Neelam K. Kandwal</i>	1
A Study on Reservoir Characteristics of the Tipam Sandstones of Miocene Age from Upper Assam Basin, India	<i>Ananya Chutia and Jogendra Nath Sarma</i>	13
Half-Graben Basin Filling Model and New Constraints on Continental Extensional Basin Development – A Case Study from the Kolhan Basin, Eastern India	<i>Subhasish Das Rohini Das and Smruti Rekha Sahoo</i>	25
Stratigraphic Implications of Seismites on Carbonaceous Shales within Siliciclastic Jhuran Formation in Western India	<i>Ashwin Arora</i>	39
Shale Gas Potential of North Cambay Basin, Gujarat, India	<i>Vaishali Sharma and Anirbid Sircar</i>	51
Integrating Field Observations with Sub-Surface Geological Data for better understanding of Depositional Environment	<i>Sankhadip Bhattacharya Rupa Das and W.W Momin</i>	59
Sandstone Petrology of the Kolhan Basin, Eastern India: Implications for the Tectonic Evolution of a Half-Graben	<i>Rohini Das</i>	69
Organic Petrology and Depositional Environments of Lignites of Nagaur, Rajasthan, India	<i>Alok K. Singh and Alok Kumar</i>	79
Paleoclimatic Indicators in the Soil Blanket of Southern Western Ghats (Sahyadri), SW India	<i>Divya V. Padmalal D. Vimal K.C. and Mohanan C.N</i>	91
Periphyton Diatom Assemblages and their relationship to Environmental Characteristics in Cauvery River of Tamil Nadu (Bhavani) by Canonical Correspondence Analysis	<i>Karthikeyan, P. and Venkatachalapathy, R.</i>	99
Uncertainty in Ecological Status Assessments of the Cauvery River, Tamil Nadu, India using of Biological Diatom Indices (IBD)	<i>Karthikeyan, P. and Venkatachalapathy, R.</i>	105

Lithological Setting and Granulometry of the Lameta Sediments from New Locality Exposed at Pandhari Village, District Betul, Madhya Pradesh

ASHOK K. SRIVASTAVA AND NEELAM K. KANDWAL

P.G. Department of Geology, SGB Amravati University, Amravati - 444602

E-mail: ashokamt2000@hotmail.com

Abstract: The Lameta sediments at Pandhari area (lat. 21°22'00.71"N; long. 77°33'00.13"E) is represented by 37m thick column of argillaceous, arenaceous and calcareous sediments. The lowermost argillaceous column is represented by various coloured clays having discontinued thin beds of micritic limestone and irregular calcareous concretions. The arenaceous unit, constituting about 18m middle column, consists of thinly to thickly bedded, grayish to brownish coloured, medium to coarse grained, friable to indurated sandstones having pebbles, chert lenses and irregular concretions, whereas, the calcareous succession in upper part is represented mostly by brecciated, nodular and chertified limestones.

The arenaceous sediments have been subjected for granulometric analysis on the basis of 14 representative samples. Various grain size parameters indicate that sandstones, in general, are medium to fine grained, moderately to poorly sorted, fine to very fine skewed and mesokurtic to leptokurtic in nature. The inter-relationship plots of various parameters are indicative of fluvial environment, in which, the sediments are deposited mostly through rolled and suspension modes.

Keywords: Lithological setting, Granulometry, Lameta, Pandhari.

INTRODUCTION

The Lameta Formation is a significant stratigraphic unit of central and western India covering an area of over 10,000km². It occurs mostly as discontinuous outcrops in different localities of Gujarat, Madhya Pradesh, Maharashtra and rests unconformably on either Precambrian basement or Gondwana sediments and overlain the Deccan basalt. These sediments are considered to be deposited into the five inland fluvio-lacustrine inland basins viz., i) Nand-Dongargaon, ii) Jabalpur, iii) Sagar, iv) Ambikapur-Amarkantak and v) Balasionor-Jhabua (Mohabey, 1996).

These sediments are traditionally considered to be fluvial-lacustrine (Brookfield and Sahni, 1987; Tandon et al., 1995; Mohabey, 1996) however, certain views support coastal-complex settings (Chanda, 1967; Kumar and Tandon, 1979; Singh, 1981; Saha and Shukla, 2010). The formation is well known for dinosaurian remains including bones and eggshells which signifies for various palaeobiological studies (Huene and Matley, 1933; Mohabey, 1983; Khosla and Sahani, 1995; Mohabey, 2001). On the basis of microvertebrates along with other microfossils, palynostratigraphy, magnetostratigraphy and its field relationship with the Deccan Traps and associated Intertrappean beds, the Maastrichtian age is assigned to the formation

(Mohabey et al., 1993; Sahni et al., 1994; Dogra et al., 1994; Hansen et al., 1996; Mohabey, 1996).

The Lameta sediments of the study area is exposed in and around the Pandhari village (lat. 21°22'00.71"N; long. 77°33'00.13"E), lying at extreme south of district Betul Madhya Pradesh, bordering Amravati district of Maharashtra (Fig. 1). The succession, attaining the height of about 37m, is represented by various coloured clays in lower, grayish to brownish coloured arenaceous unit in the middle and the brecciated, nodular and chertified limestones in upper parts. The arenaceous lithounit presently under study, is about 19m thick, mostly represented by thin to thick bedded, medium to coarse grained, friable to hard sandstones having pebbles, chert lenses and irregular concretions. Statistical parameters like mean, standard deviation, skewness and kurtosis have been calculated for interpretation of the nature of sediments, whereas various bivariate plots have been studied to interpret the environment of deposition and pattern of sedimentation.

GEOLOGY AND STRATIGRAPHY OF THE AREA

The Lameta exposure of the study area is one among the few isolated, scattered outcrops laying at the border of districts Amravati, Maharashtra and Betul, Madhya Pradesh. This entire area has been proposed as a new

inland basin of Lameta sedimentation viz., Salbardi-Belkher inland basin (Srivastava and Mankar, 2013). Regionally, the Quartz-feldspathic gneiss of Archaean age forms the basement, over which, the Gondwana rocks rest unconformably. The Lameta Formation rests disconformably over the upper Gondwana sediments and overlain hard and compact, basalt of the Deccan Trap. The Gondwana rock having abundant preservation of gymnosperm and pteridophytic megaflores remains suggests Upper Jurassic to Lower Cretaceous age, correlatable with the Jabalpur Formation (Srivastava et al., 1996, 1999). Alluvium and soil of Quaternary age form top most horizon.

FIELD CHARACTERISTICS OF THE SUCCESSION

The succession attaining the thickness of 37m is well represented by argillaceous, arenaceous and calcareous units in lithostratigraphic order (Fig. 2). The lower argillaceous succession rests over the thinly bedded, light brown coloured sandstone of the Gondwana which is exposed in the close vicinity; however, a clear boundary showing distinct contact in vertical column is not traceable. It is represented by 9m thick, grayish-greenish-yellowish-brownish coloured clays having vast lateral extent (Fig. 3a). The lowermost 3m unit is represented by grayish-black, friable unit having pocketed occurrences of medium gray clay and irregular calc-marl concretions in the range of 2-5cm diameters. The overlying 3m succession is greenish-gray in colour having pockets of brownish-gray clay. It is overlain by 2m thick, grayish-greenish clay having 20-40cm thick, discontinued beds of light to medium gray coloured, micritic limestone which occasionally show chertification. The overlying one-meter succession is yellowish-brown clay having chert lenses. The

boundaries between various coloured clay horizons are often not very distinct due to surficial weathering, vegetation and agricultural activity on the same.

Overlying 19m thick succession is dominantly arenaceous and represented by sandstones of various colours and grain sizes. The lowermost one-meter is brownish gray, medium grained, ferruginous sandstone. Because of poor cementation, it is friable in nature; however, current generated structures are visible at few places. It has a sharp lower contact with yellowish-brown clay and distinctly overlain 1.5m thick light gray, thinly bedded, coarse grained sandstone having rounded to sub-rounded pebbles of quartz and feldspar of 2-5cm diameters. It is followed upward by 2m thick unit of light brownish-gray, medium to coarse grained sandstone which is dominantly massive in nature. It is sharply overlain by equally thick horizon of brownish-gray, coarse grained, friable sandstone. Rounded to sub-rounded clasts of quartz in the range of 2-5cm diameters are abundant. This lithounit is sharply overlain by 5m thick, light to medium brownish, medium to fine grained sandstone (Fig. 3b). The laminated nature of the rock and absence of pebbles clearly distinguishes it from the underlying lithounit. It is succeeded by 2.5m thick, light brownish-gray, compact to friable sandstone, of which, the lower 0.5m is coarse grained and upper 2m is medium grained sandstones. The overlying 5m column is grayish-greenish, medium grained sandstone having abundant sandy concretions. These botryoidal concretions, ranging from 10 to 40cm in lengths are similar in colours as of the host rock however, shows more cementations and argillaceous content therefore harder.

The upper 9m column is calcareous in nature showing distinct boundary with the underlying arenaceous succession. The lower 4m part of the column is pale greenish, typical brecciated limestone which is

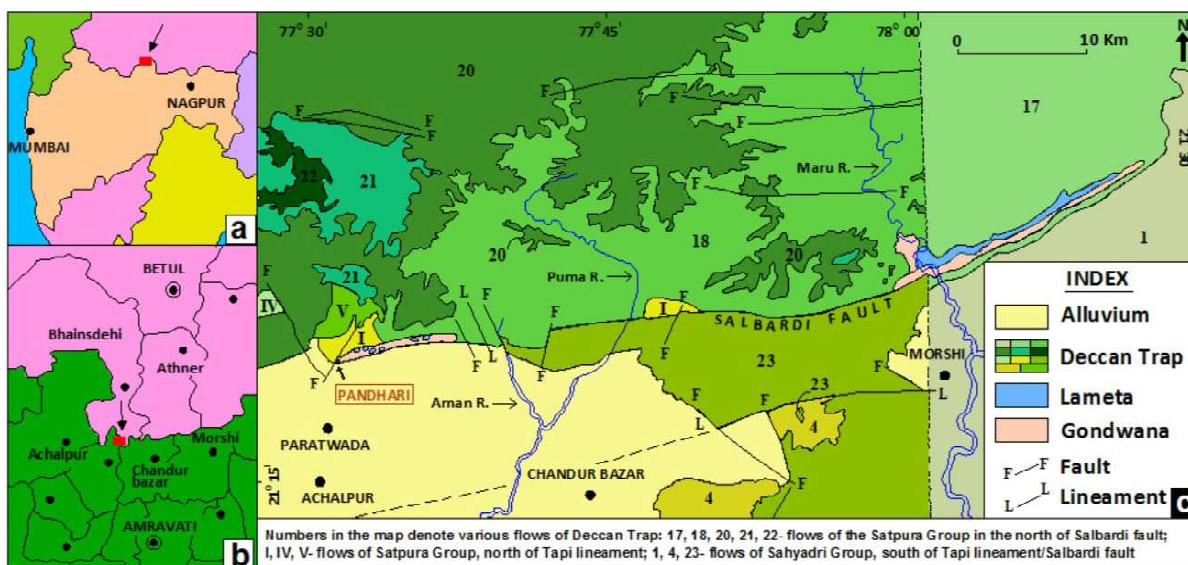


Fig. 1. (a) & (b) Location of the study area in regional set-up and c) geological map of the area.

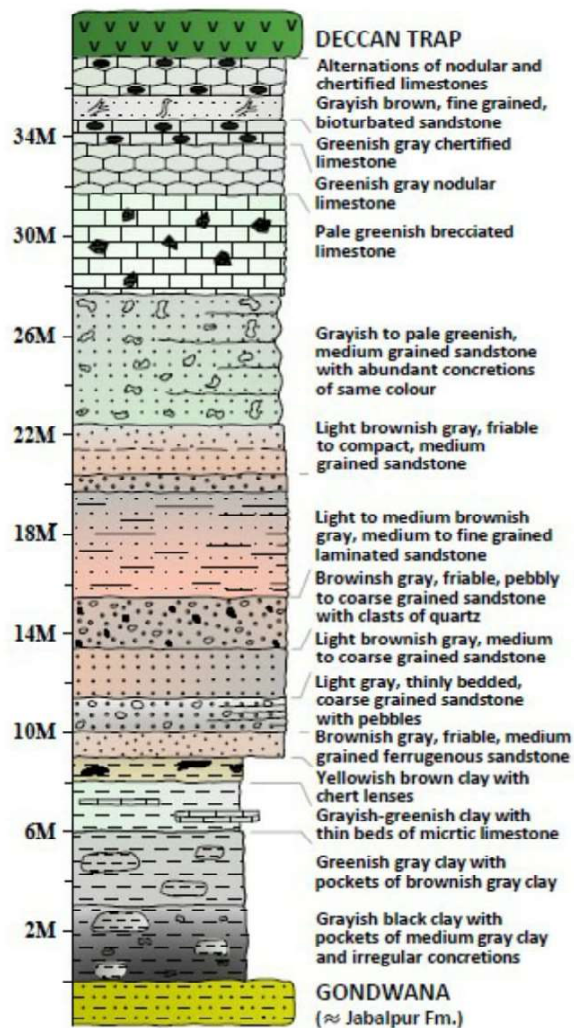


Fig. 2. Sedimentary-log of the Lameta succession.

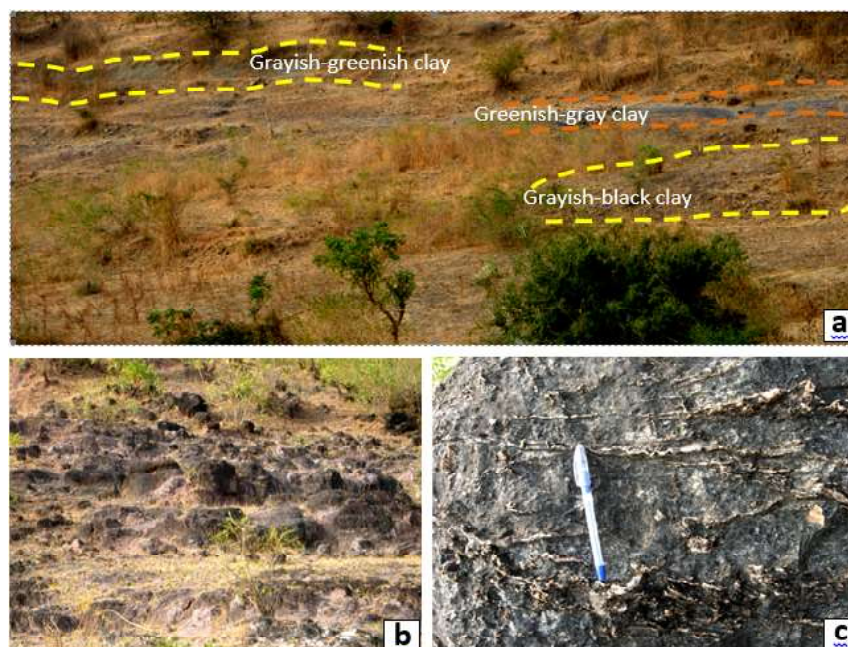


Fig. 3. Field photographs showing (a) grayish-greenish, greenish-gray and grayish-black clayey units; (b) arenaceous lithounit and (c) alternation of nodular and chertified limestone.

sharply overlain by 2m thick greenish-gray limestone having nodular tendency (Fig. 3c). The later shows silicification making it hard and compact in nature. Overlying this is 50cm greenish-gray, hard and compact chertified limestone as a typical marker horizon of the Lameta Formation. It shows faint tendency of flat bedding however, the structures are mostly diffused. Overlying this is one-meter thick grayish-brown, fine grained, bioturbated sandstone marked by cylindrical to inclined burrows of 2-3cm diameters. The topmost 1.5m succession is represented by alternations of nodular and chertified limestones.

SAMPLING AND METHODOLOGY

Total 14 representative samples have been collected from the entire column, mostly at the regular intervals of one-meter or more in the column depending upon lithological variations, contacts or any other significant change. Weathered portion of the rock and loose fragments have been avoided. Broadly, the samples are hard and compact; however, a few samples are friable because of less cementation.

Sieving technique is used for the separation of various size sediments following Ingram (1971). During the initial phase, the samples were disintegrated with the help of wooden mortar so as, to avoid the crushing of the grains. The disintegrated samples then treated with 10% dil. HCl solution to remove the carbonate material and then 6% of Hydrogen peroxide to remove the organic matter followed by washing them by distilled water and air dry. The dried samples then subjected for sieving to separate different size class of the grains. 100gms of sample was subjected for sieving through the sieves arranged at the interval of 8 mesh (-1.25 ϕ), 12 mesh (-0.75 ϕ), 16 mesh (-0.25 ϕ), 22 mesh (0.35 ϕ), 30 mesh (0.75 ϕ), 44 mesh (1.50 ϕ), 66 mesh (2.00 ϕ), 85 mesh (2.60 ϕ), 120 mesh (3.00 ϕ), 170 mesh (3.50 ϕ), 240 mesh (4.10 ϕ) and

followed by pan to collected >240 mesh (4.25 ϕ) fraction. This arrangement was placed to motored sieve-shaker for 30 minutes in order to get the complete separation of various fractions. Further process involved is the weighing of different fractions through digital single pan balance. The weight of different fractions are the basic data used for further calculations and interpretations of various statistical and graphical parameters (Table 1) as proposed by Folk and Ward (1957) and Folk (1980).

RESULTS AND DISCUSSION

Histogram and Frequency Curve

The comparative study of histograms of all the samples showing quantities of various size fractions i.e., granule, very coarse sand, coarse sand, medium sand, fine sand, very fine sand have been made (Fig. 4). The percentage of granule is almost negligible whereas, very coarse sand is also less and present only in a few samples, particularly in lower part of succession. The coarse sand, in general, is high in lower half arenaceous column whereas comparatively less in upper part making up to 14 to 25% of the sediments however, an exceptional value of 73.7% has been noticed in sample no. P19 which is friable, coarse grained sandstone having less cementation. The medium sand constitutes about 25 to 50% fraction of the rocks showing almost equal representation entire columns. The fine sand however, does not show any distinct trend but generally contribute >15% of the rock except in a few samples, though the highest value of 52% is recorded in sample no. P17 which is fine grained sandstone. In general, the fine fractions containing silt and clay normally quantifies for >5%. The cumulative curves also depict the same i.e., a narrow range for granule, very coarse sand and fine fractions, whereas, wider range for coarse medium and fine sands (Fig. 5).

Table 1. Phi values and statistical parameters of the arenaceous sediments.

Sample No. / Grain size	ϕ_{95}	ϕ_{84}	ϕ_{75}	ϕ_{50}	ϕ_{25}	ϕ_{16}	ϕ_5	ϕ_1	Mz	σ_1	SK ₁	K _G	SOS	SKS	C in Micron	M in Micron
P11	3.07	1.92	1.62	0.73	0.5	0.38	-0.43	-0.89	1.01	0.91	0.45	1.28	1.75	1.18	1853	602
P12	3.99	2.76	2.07	1.04	0.56	0.44	-0.27	-0.55	1.41	1.23	0.43	1.15	2.27	1.36	1468	486
P13	4.14	3.11	2.85	2.07	1.34	0.75	0.55	0.34	1.97	1.14	0.02	0.97	1.8	0.55	790	238
P14	3.12	2.14	1.8	1.12	0.62	0.51	0.03	-0.75	1.26	0.88	0.28	1.07	1.55	0.91	1681	460
P15	3.81	2.67	1.86	0.88	0.53	0.4	-0.47	-0.96	1.32	1.22	0.47	1.31	2.14	1.58	1945	543
P16	2.93	1.93	1.73	1.01	0.53	0.37	-0.76	-1.17	3.31	0.95	0.11	1.25	1.85	0.15	2250	496
P17	4.13	2.97	2.81	2.37	1.9	1.77	1.51	0.87	2.37	0.7	0.17	1.18	1.31	0.9	547	197
P18	4.11	2.82	2.5	1.91	1.72	1.63	1.43	1.1	2.12	0.97	0.59	1.42	1.34	1.72	466	266
P19	2.73	1.28	0.74	0.61	0.47	0.41	-0.16	-0.53	0.77	0.66	0.51	4.46	1.45	1.35	1443	655
P20	3.42	2.66	2.12	1.71	1.17	0.75	0.49	0.04	1.71	0.92	-0.06	1.27	1.47	0.49	972	305
P21	3.51	2.7	2.32	1.79	1.38	0.73	0.47	-0.18	1.74	1.38	-0.29	1.32	1.52	0.4	1132	289
P22	4.14	3.13	2.85	2.2	1.74	1.6	0.75	-0.03	2.31	0.9	0.18	1.25	1.7	0.49	1021	217
P23	3.64	2.78	2.4	1.65	0.78	0.66	0.45	-0.11	1.7	1.01	0.16	0.8	1.6	0.79	1079	318
P24	4.17	3.32	2.89	1.96	1.58	1.1	0.57	0.23	2.12	1.1	0.23	1.13	1.8	0.82	1172	257

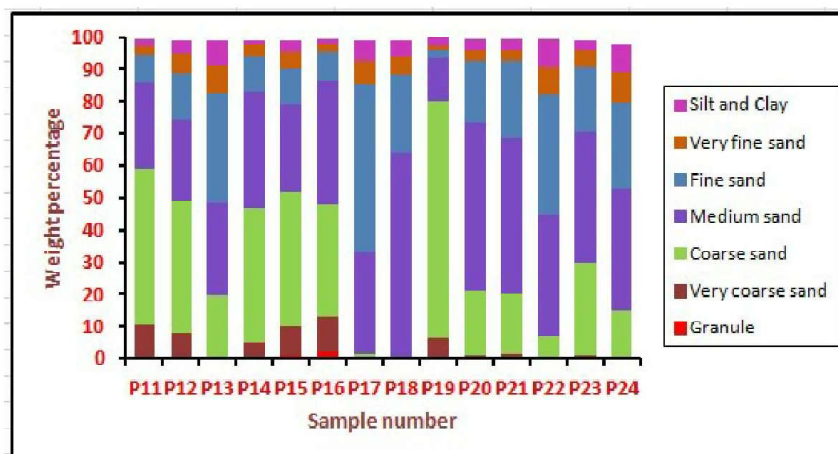


Fig. 4. Histogram showing different grain size classes of all samples.

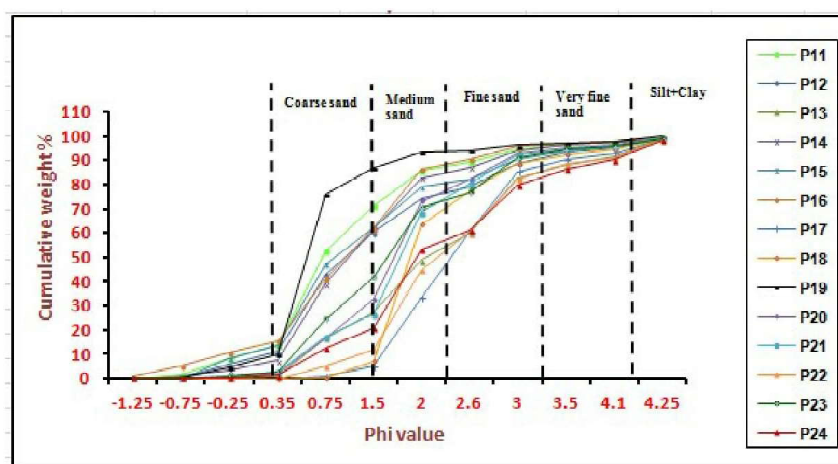


Fig. 5. Cumulative weight percentage curves showing trend of all samples.

Textural Parameters

Various textural parameters i.e., graphic median, graphic mean, graphic standard deviation, graphic skewness and graphic kurtosis have been calculated and interpreted as proposed by Folk and Ward (1957).

Graphic Median (ϕ_{50}): Graphic median (ϕ_{50}) denotes the size for which half of the particles are coarser and half finer by weight. The minimum value obtained is 0.73ϕ where as maximum is 2.37ϕ . In general, the lower part of column lacks any definite trend for different samples whereas, in upper part, these values are mostly high.

Graphic Mean (M_z): Graphic mean measures the central tendency of the sediments which has been calculated by the formula i.e., $M_z = (\phi_{16} + \phi_{50} + \phi_{84})/3$. The mean grain size values range from 0.77ϕ to 3.31ϕ with an average of 1.79ϕ . Majority of the samples are dominated by medium grained sand-size sediments (8 samples) followed by fine grained (4 samples). Coarse and very fine grained categories are represented by one sample each (Fig. 6a).

Graphic Standard Deviation (σ_I): The degree of sorting or uniformity of the particle-size distribution is measured by graphic standard deviation i.e., calculated by the formula $\sigma_I = [(\phi_{84} - \phi_{16})/4] + [(\phi_{95} - \phi_5)/6.6]$. The obtained values range from 0.66ϕ to 1.38ϕ with an average of 0.1ϕ . There is dominance of moderately sorted and poorly sorted sediments represented equally by six samples each. Two samples fall in the moderately well sorted categories which are represented by coarse and fine grained sandstones each (Fig. 6b).

Graphic Skewness (SK_I): The graphic skewness is a measure of symmetry of distribution differentiating i.e., dominance of coarse or fine sediments in the samples and calculated by the formula i.e., $SK_I = [\phi_{16} + \phi_{84} - 2(\phi_{50})/2(\phi_{84} - \phi_{16})] + [\phi_5 + \phi_{95} - 2(\phi_{50})/2(\phi_{95} - \phi_5)]$. Its negative value denotes coarser material in tail or coarse-skewed whereas, fine-skewed represents positive values depicting more fine material in the tail. The present values range from -0.29ϕ (coarse skewed) to $+0.59\phi$ (very fine-skewed), however, there is domination of fine-skewed samples (6 samples) followed by very fine-skewed (5 samples), only one sample fall under the

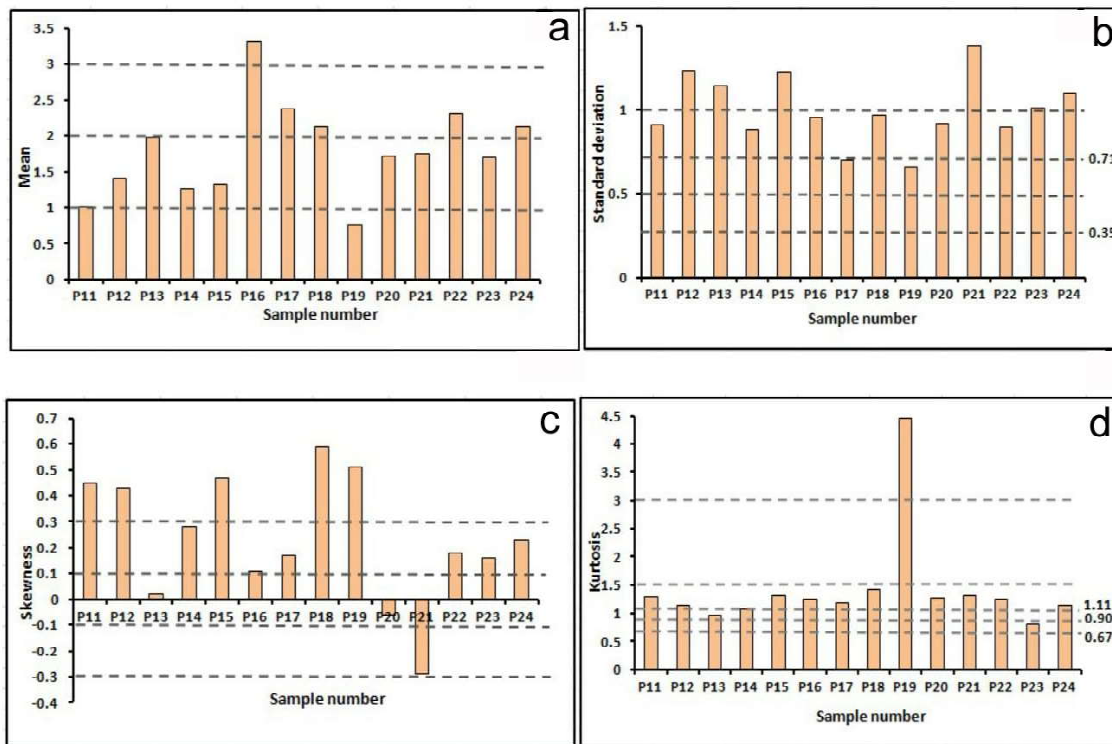


Fig. 6. Comparative histograms of all samples showing (a) mean; (b) standard deviation; (c) skewness and (d) kurtosis. Horizontal dotted lines on each histogram represent the boundary between two successive sub fields of verbal scale for various graphic size parameters respectively.

category of coarse-skewed whereas, near symmetrical is represented by two samples. The average value of 0.23ϕ indicates the dominance of fine-skewed sediments in the admixture showing more sediment in fine tail (Fig.6c).

Graphic Kurtosis (K_G): The graphic kurtosis measures the ratio between the sorting in the tail and the central portion of the distribution and calculated by the formula i.e., $K_G = \phi_{95} - \phi_5 / 2.44(\phi_{75} - \phi_{25})$. Leptokurtic denotes better sorted tails than central portion whereas, platykurtic is reverse condition; if sorting is uniform in both tails and central portion then termed as mesokurtic. The kurtosis values range from 0.80ϕ (platykurtic) to 4.46ϕ (extremely leptokurtic) with an average value of 1.42ϕ indicating leptokurtic nature of the sediments (Fig. 6d).

Bivariate Plots

Bivariate plots between various parameters of the grain size are significant to interpret nature and dynamics of sediments, depositional set-up and energy condition of the depositing medium (Folk and Ward, 1957; Passega, 1957, 1964; Friedman, 1961, 1967; Moiola and Weiser, 1968). These inter-relationship plots show good precision for fluvial, coastal and eolian environments of deposition but least effective for glacial deposits. In the present study, these plots are interpreted for i) nature of

sediments, ii) depositional environment and iii) energy condition of the transporting medium.

Nature of Sediments: Folk and Ward (1957) proposed various inter-relationship plots of mean, standard deviation, skewness and kurtosis depicting nature of sediments in the admixture. The scatter plot between mean vs. standard deviation which give 'M', 'V' or 'inverted V-shaped' trends depends heavily on size range of the sediments. In the present plot, majority of the points closer to a segment of V-shape trend shows smaller size range of the sediments (Folk and Ward, 1957), however, a few distal points show variations in both their size and range (Fig. 7a). The same is also evident by mean values of the sediments showing dominance of medium grain-size sediments. The mean vs. skewness plot of Folk and Ward (1957) depict an established sinusoidal curve which is originally based on the proportions of two size classes i.e., gravel and sand in the sediment admixture. The proportionate change of gravel and sand in the admixture produce either positive or negative skewness depending upon the proportion of size classes present in the admixture; symmetrical in case of equal fractions. In present case, the grain size class is restricted mostly to medium sand size range therefore, the points are not synchronous with the established sinusoidal curve (Fig. 7b). This dominating medium sand size class, forming the principle mode, occasionally loose the symmetrical

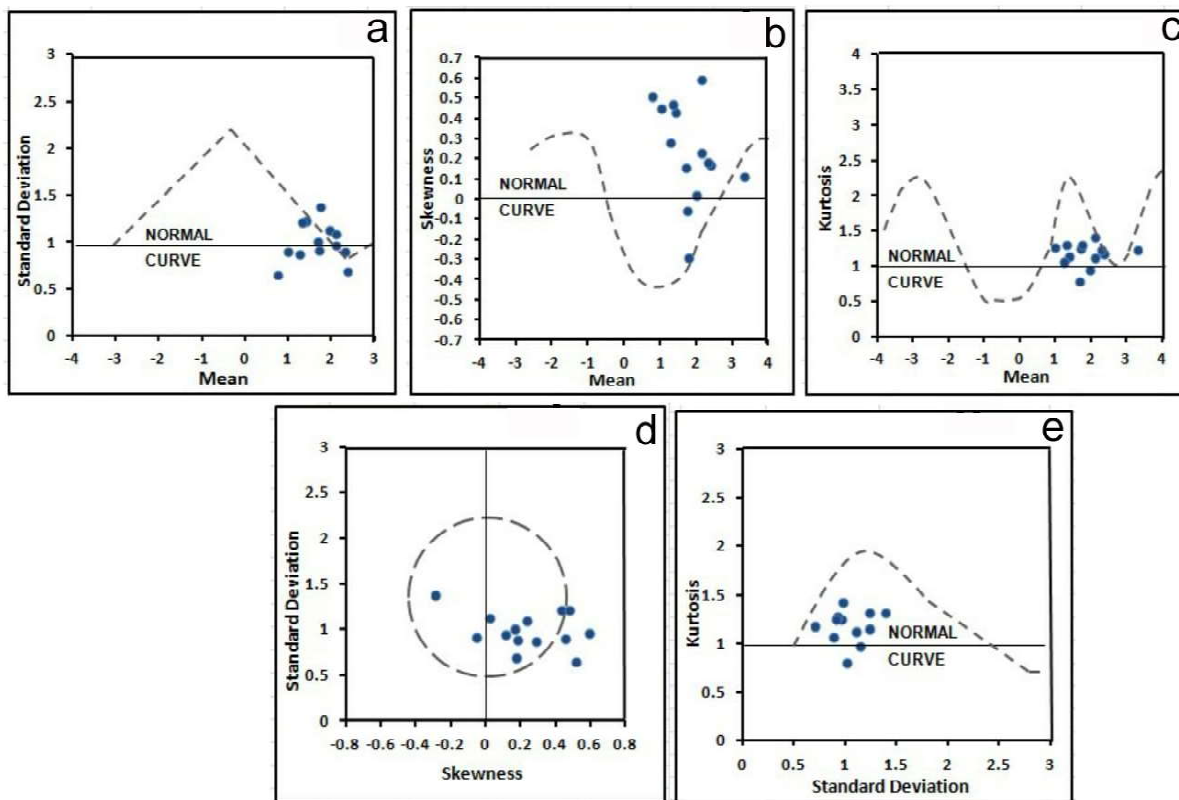


Fig. 7. Bivariate scatter plots of all the samples drawn on the model as proposed by Folk and Ward (1957) (a) mean size vs. standard deviation; (b) mean size vs. Skewness; (c) mean size vs. Kurtosis; (d) skewness vs. standard deviation and (e) standard deviation vs. kurtosis.

distribution because of the influx of coarse or fine sediments in the admixture.

The mean size vs. kurtosis plot is an index of kurtosis which depicts various size classes in the admixture and determines the sorting in peak and tails. This plot is important to differentiate the mode of size classes in sediment admixture (Folk and Ward, 1957). The trend of the points show a 'V' or 'inverted V' shape that depends on the proportion of two modes of the sediments in the admixture. The medium sand size dominated samples are mostly leptokurtic in nature with an average value of 1.42ϕ (Fig. 7c). The plot between skewness vs. standard deviation and standard deviation vs. kurtosis are also helpful in depicting the presence of various size modes in the sediment admixture (Folk and Ward, 1957). In case of previous, both skewness and standard deviation is the function of mean size hence, bears a mathematical relationship. The standard plot between these two parameters for an admixture having unimodal sample with good sorting or equal mixture of two modes, provide nearly equally circular ring. The plot of the studied samples show that most of the points fall in poorly to moderately sorted categories and fine to very fine-skewed range of skewness, however, the graph also shows that though the samples are unimodal, but the second mode is also quite distinct (Fig. 7d). The

same is also evident by standard deviation vs. kurtosis plot (Fig. 7e).

Depositional Environment: It is well defined that certain parameters are very much sensitive to the energy condition of the depositing medium. Their inter-relationship plots are interpreted to differentiate certain specific environments. Friedman (1961, 1967), Muiola and Weiser (1968) have proposed standard plots between mean vs. standard deviation and standard deviation (horizontal axis) vs. skewness (vertical axis) to differentiate between beach and river environments. The plot of standard deviation vs. mean for the present samples are indicative of river environment as proposed by Friedman (1967), Muiola and Weiser (1968) (Fig. 8a). The same is also supported by the plot between standard deviation vs. skewness as proposed by Friedman (1967), Muiola and Weiser (1968) (Fig. 8b). Friedman (1967) added one more plot i.e., Simple Sorting Measure (SOS) and Simple Skewness Measure (SKS) for differentiating between beach and river environments. The plot of present sample shows that all the points fall in the river sector of the standard plot as proposed by Friedman (1967) (Fig. 8c).

Above mentioned all the three plots conform the fluvial environment of deposition for the arenaceous column of the succession. This interpretation is in

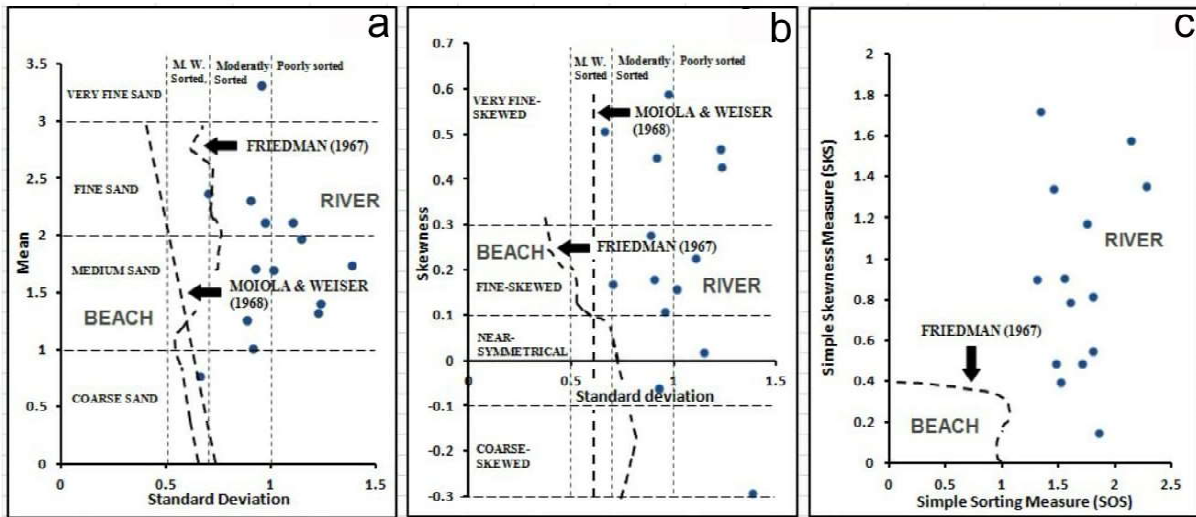


Fig. 8. Bivariate plots showing depositional environment (a) standard deviation vs. mean; (b) standard deviation vs. skewness and (c) simple sorting measure (SOS) vs. simple skewness measure (SKS).

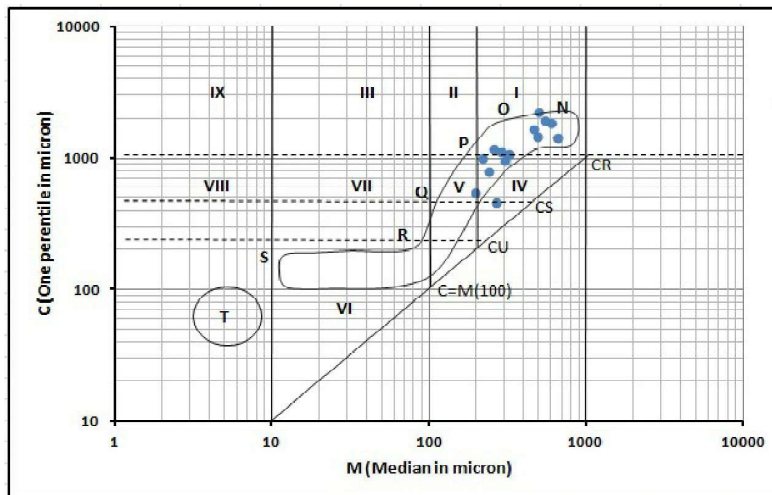


Fig. 9. C-M pattern (following Passega 1957 and 1964), note that most of the points fall in N-O and O-P segments and I, IV sectors indicating rolled and suspension modes of transport.

accordance with the other exposures of the Lameta Formation occurring at various places of central and western India e.g., Jabalpur (Tandon and Andrews, 2001), Nand-Dongargaon (Mohabey and Samant, 2005). Recently, Srivastava and Mankar (2012) studied the Lameta sediments of Bairam, Belkher and Salbardi area which are in a close vicinity of the studied locality and interpreted fluvial-lacustrine environments of deposition. The presently studied arenaceous unit of the succession is overlain and underlain by argillaceous and calcareous lithounits respectively which is broadly co-relatable with other Lameta sediments of central and western India, traditionally considered as the deposition of fluvial-lacustrine environments.

Energy Condition: Passega (1957) introduced C-M plot, in which, 'C' indicates coarsest one-percentile value in micron and 'M' denotes median value in micron,

plotted on log-probability scale. This plot establishes the relationship between texture of the sediments and the processes operated during the deposition therefore, significant to evaluate hydrodynamic forces working during the deposition of sediments (Passega, 1957, 1964; Passega and Byramjee, 1969). The plot shows different sectors and S-shaped plot which denotes different modes of transport and energy conditions of the depositing medium. In the present plot, most of the points are concentrated in N-O and O-P sectors indicating mostly rolling and suspension modes of sediments transport (Fig. 9). The restricted occurrence of points in sectors I and IV of the plot also support the same. This is also evident by the grain size values of the samples showing dominance of mean sand-size sediments followed by fine sand in the column. The very fine and coarse sand samples are represented by one each in total assemblage.

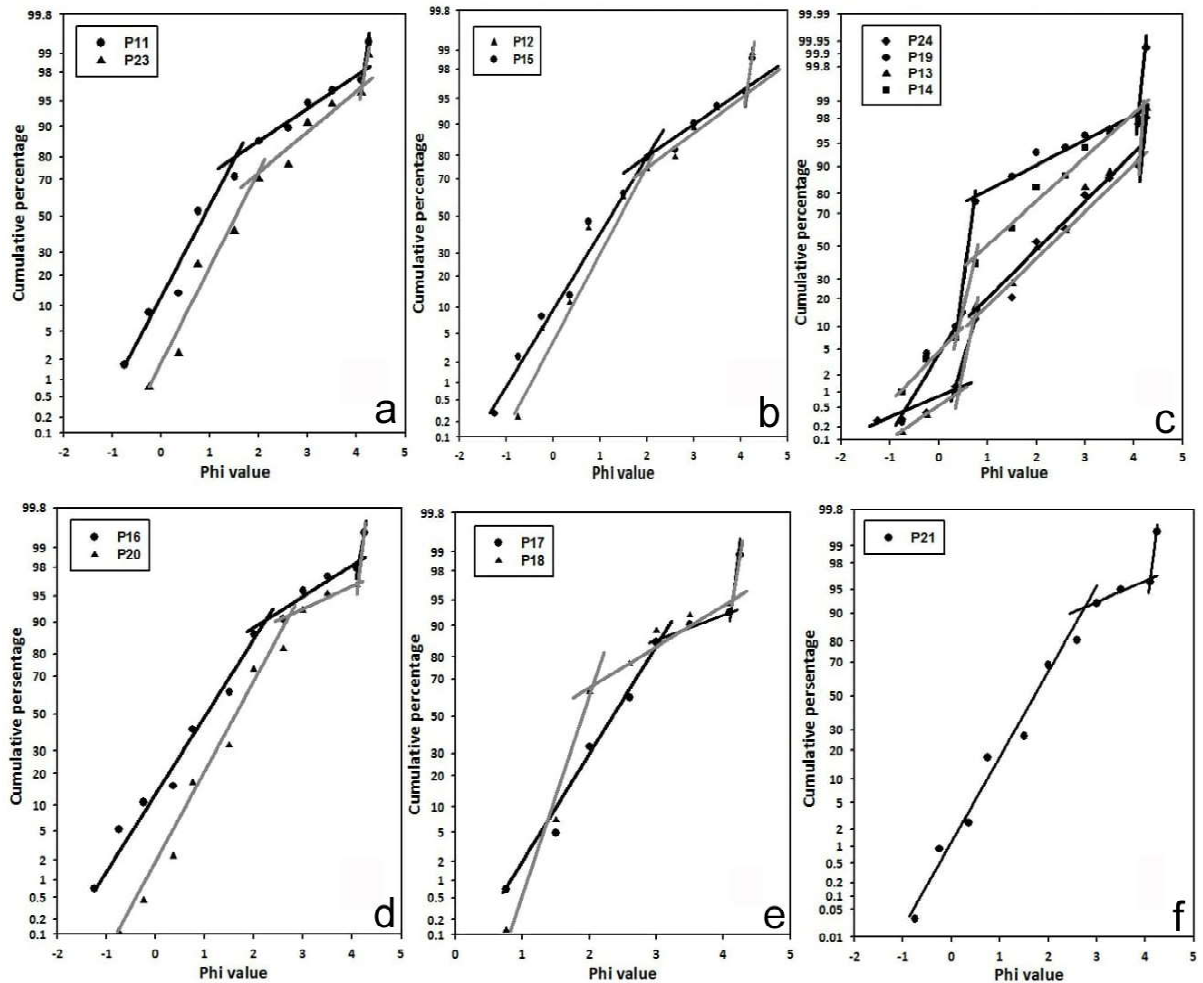


Fig. 10a-f. Log-probability curves of all the samples showing various populations. Note that most of the samples are dominated by traction and suspension populations.

The log-probability curve as proposed by Visher (1969) is an important tool to interpret the relationship of grain size distribution and sediment transport. Visher (1969) basically interpreted modes of sediment transport by this plot in the categories of traction, saltation and suspension. Plotting the cumulative grain size distribution on probability ordinate scale and phi values on horizontal axis provides a curve, on which, various straight line sectors can be identified joining maximum points. These straight lines are known as sub-populations and their length, slope and intersection points depend on mode of sediments transport i.e., traction, saltation and suspension. In the present study, these plots have been constructed for all the 14 samples and their trends have been compared which indicate that most of the samples are dominated by the sediments transported through traction mode (Fig. 10a-f). In general, the suspension mode is low and represented only in a few samples. In few samples, the traction population is further divisible into two showing local variation in the mode of transport possibly due to change in energy condition (Fig. 10c).

CONCLUSIONS

1. The Lameta succession of study area is about 37m thick column of argillaceous, arenaceous and calcareous sediments. The arenaceous sediments comparatively more constituting almost middle half of the column. The argillaceous sediments of the lower part are dominantly clayey with occasional presence of discontinued calcareous horizons. The upper calcareous unit is mostly represented by brecciated, nodular and chertified limestone as typical of the Lameta Formation.

2. Grain size analysis of 14 sandstone samples have been made to interpret the textural parameters of the sediments in order to interpret nature of the sediments, mode of their transport and environment of deposition. The significant conclusions drawn are as follows;

i. The histogram and cumulative frequency curve indicate medium to fine grained nature of the sediments.

ii. The textural parameter indicate that in general, the sediments are of mostly medium sand size, poorly to moderately sorted and leptokurtic in nature.

iii. Various inter-relationship plots indicate fluvial environment of deposition for the arenaceous unit of the succession.

iv. C-M pattern and log-probability curves indicate that the mode of sedimentation transport was both rolling and suspension.

Acknowledgement: Financial support for the work has been provided by UGC, New Delhi in the form of a major research project no. F.40/295/2011 (SR) awarded to one of authors (AKS) is thankfully acknowledged.

References

- Brookfield, H.E. and Sahni, A. (1987). Palaeoenvironments of Lameta Beds (Late Cretaceous) at Jabalpur, Madhya Pradesh, India: soil and biotas of a semi-arid alluvial plain. *Cret. Res.* 8, 1–14.
- Chanda, S.K. (1967). Petrogenesis of the calcareous constituents of the Lameta group around Jabalpur, M.P., India. *Jour. Sed. Petrol.* 37, 425–437.
- Dogra, N.N., Singh, R.Y. and Kulshreshta, S.K. (1994). Palynostratigraphy of infratrappean Jabalpur and Lameta Formations (Lower and Upper Cretaceous) in Madhya Pradesh, India. *Cret. Res.* 15, 205–215.
- Folk, R.L. (1980). *Petrology of Sedimentary Rocks*. Hemphill Austin, Texas, 159p.
- Folk, R.L. and Ward, W.C. (1957). Brazon river bar-A study in the significance of grain size parameters. *Jour. Sed. Petrol.* 27, 3-26.
- Friedman, G.M. (1961). Distinction between dune, beach and river sands from their textural characteristics. *Jour. Sed. Petrol.* 31, 514-529.
- Friedman, G.M. (1967). Dynamic process and statistical parameters compared for size frequency distribution of beach and river sands. *Jour. Sed. Petrol.* 37, 327-354.
- Hansen, H.J., Mohabey, D.M. and Sarkar, A. (1996). Lameta geomagnetic dating the main pulse of Deccan Trap volcanism. *Gond. Geol. Mag. Spec.* Vol. 4, 154-185.
- Ingram, R.L. (1971). Sieve analysis, In: Carver R. E. (ed.) *Procedures in Sedimentary Petrology*, Wilson Interscience. 49-68.
- Kumar, S. and Tandon, K.K. (1979). Trace fossils and environment of deposition of the sedimentary succession of Jabalpur, M.P. *Jour. Geol. Soc. India*, 20, 103-106.
- Mojala, R.J. and Weiser, D. (1968). Textural parameters and evolution. *Jour. Sed. Petrol.* 38, 45-53.
- Mohabey, D.M. (1996). Depositional environments of Lameta Formation (Late Cretaceous) of Nand-Dongargaon Inland Basin, Maharashtra: the fossil and lithological evidences. *Mem. Geol. Soc. India*, 37, 363–386.
- Mohabey, D. M. and Samant, B. (2005). Lacustrine facies association of a Maastrichtian lake (Lameta Formation) from Deccan volcanic terrain Central India: Implications to depositional history, sediment cyclicity and climates. *Gond. Geol. Magz.* 8, 37-52.
- Mohabey, D.M., Udhoji, S.G. and Verma, K.K. (1993). Palaeontological and sedimentological observations on non-marine Lameta formation, Upper Cretaceous. India: their palaeoecological and palaeoenvironmental significance. *Palaeogeog. Palaeoclimat. Palaeoeco.* 105, 83-94.
- Passega, R. (1957). Texture as a characteristic of clastic deposition. *Amer. Assoc. Petrol. Geol.* 41, 1952-1984.
- Passega, R. (1964). Grain size representation by C-M pattern as a geological tool. *Jour. Sed. Petrol.* 34, 830-847.
- Passega, R. and Byramjee, R. (1969). Grain size image of clastic deposits, *Sedimentology*, 13, 180-190.
- Saha, O., Shukla, U. K. and Rani, R. (2010). Trace fossils from the Late Cretaceous Lameta Formation, Jabalpur area, Madhya Pradesh: Palaeoenvironmental Implications. *Jour. Geol. Soc. India*, 76, 607-620.
- Sahni, A., Tandon, S.K., Jolly, A., Bajpai, S., Sood, A. and Srinivasan, S. (1994). Upper Cretaceous dinosaur eggs and nesting sites from the Deccan volcano-sedimentary province of peninsular India. In: *Dinosaur eggs and babies*. (Eds.) Carpenter K, Hirsch KF, Horner JR, Cambridge University Press, 204–226.
- Singh, I.B. (1981). Palaeoenvironment and palaeogeography of the Lameta group sediments, Late Cretaceous in Jabalpur area, India. *Jour. Paleontol. Soc. India*, 26, 38-53.
- Srivastava, A.K., Banubakode, P.D., Kale, V.M. and Patil, G.V. (1996). Record of trace fossils from Upper Gondwana succession of Bairam and adjoining area, district Amravati, Maharashtra. *Gond. Geol. Maz.* 11 (1), 33-44.
- Srivastava, A.K., Banubakode, P.D., Kale, V.M., Patil, G.V. and Manik, S.R. (1999). Lower Cretaceous plant fossil from Bairam-Belkher area, districts Amravati, Maharashtra and district Betul, Madhya Pradesh. *Curr. Sci.* 48, 39-48.
- Srivastava, A.K. and Mankar, R.S. (2012). Trace fossils from the Lameta successions of Salbardi and Belkher area, district Amravati, Maharashtra and their palaeoecological and palaeoenvironmental significance. *Arab. Jour. Geosci.* 5, 1003-1009.
- Srivastava, A.K. and Mankar, R.S. (2013). Revised palaeogeography of dinosaur bearing Lameta

- sediments, Central and Western India. National conference on 'Sedimentation and tectonics with special reference to energy resources of North-East India' & XXX convention of Indian Association of Sedimentologists, organized by Department of Earth Science, Manipur University, Manipur. 82 (Abstract).
- Tandon, S.K. and Andrews, J.E. (2001). Lithofacies associations and stable isotopes of palustrine and calcrete carbonates: examples from an Indian Maastrichtian regolith. *Sedimentology*, 48 (2), 339-355.
- Tandon, S.K., Sood, A., Andrews, J.E. and Dennis, P.F. (1995). Palaeoenvironment of the dinosaur bearing Lameta Beds (Maastrichtian), Narmada Valley, Central India. *Palaeogeogr. Palaeoclimatol. Palaeoecol.* 117, 153–184.
- Visher, G.S. (1969). Grain size distribution and depositional process. *Jour. Sed. Petrol.* 39, 1074-1106.

A Study on Reservoir Characteristics of the Tipam Sandstones of Miocene Age from Upper Assam Basin, India

ANANYA CHUTIA¹ AND JOGENDRA NATH SARMA²

¹Department of Geology, Cotton College, Guwhati- 781001, Assam

²Department of Applied Geology, Dibrugarh University, Dibrugarh- 786004, Assam

E-mail: ananyachutia@gmail.com

Abstract: The present study is on the reservoir characteristics of the Tipam sandstones from a few locations of Upper Assam Basin. Both exposed as well as subsurface sandstone samples have been studied and the methodologies used include petrography, clay mineralogy and well log analysis. The study has shown that after deposition, the sediments have undergone mechanical compaction due to which primary porosity has been reduced. On the other hand, secondary porosity has been developed by the diagenetic processes operative on the sediments after deposition. However, some of this secondary porosity has been lost latter due to precipitation of authigenic cement. Results of porosity determination have shown that the studied Tipam sandstones of NHK#332, NHK#322 and RGH#5 wells have average porosity percentages of 33.47, 31.11 and 31.41, respectively. The average permeability of the NHK#332, NHK#322 and RGH#5 wells are 454.79 md, 132.06 md and 279.99 md, respectively. Thus, the results indicate that most of the studied Tipam sandstones have very good to excellent porosity and good to very good permeability. The observed porosity and permeability values are good enough for the commercial accumulation of hydrocarbons.

Keywords: Tipam Sandstone Formation, Reservoir Characteristics, Petrography, Clay Mineralogy, Log Characteristics

INTRODUCTION

Oil and gas bearing rocks are generally referred to as reservoir rocks. The reservoir is an essential element of the petroleum system and it must be able to accommodate a significant volume of fluids to obtain its hydrocarbon charge and be produced (North, 1985). Successful exploration of oil and gas requires a thorough knowledge of the properties of reservoir rocks. Sandstones are very important as reservoirs for oil and gas; about 50% of the world's petroleum reserve is estimated to occur in sandstones (Berg, 1986). Depositional environment and diagenesis of sandstones determine their important reservoir characteristics which include properties such as porosity, permeability, etc. Reservoir characterization aims at better understanding of these properties to achieve the maximum efficiency in reservoir management for hydrocarbon production.

The pore spaces in clastic sediments may be altered by diagenetic processes such as compaction and secondary cementation following deposition (Beard and Weyl, 1973). Therefore, study on diagenesis is of very much importance in understanding the reservoir characteristics of particular sandstone. Local variations in reservoir properties depend on original depositional and diagenetic fabric of the reservoir, the relative timing of different mechanisms, lithologic and textural characteristics and structural and lithotectonic position (Mitra, 1988).

The Tipam Sandstone Formation of Miocene age is one of the most productive reservoirs of the Upper Assam Basin. The formation stratigraphically overlies undifferentiated grit beds of the Surma Group in the northeast and the Bokabil Formation in the southwest of Upper Assam Plains and underlies the Girujan Clay Formation of Tipam Group. The formation occurs in the subsurface of Upper Assam Plains and is exposed in the type area of Tipam Hills and different localities of the Naga Hill Ranges. In this study, an approach has been made to understand the reservoir characteristics of the sandstones from petrography, clay mineralogy and well log interpretation. The study deals with the Tipam Sandstone Formation exposed along three sections, namely Tipam Hills (Sita Kunda), Tipang Pani and Dilli Ghat (Fig. 1) as well as four OIL wells. The wells selected are from Nahorkatiya oil field (NHK#332, NHK#322), Jorajan oil field (JRN#2) and Rajgarh oil field (RGH#5) (Fig. 2).

PETROGRAPHIC APPROACH

For the study of reservoir characteristics, the nature of grain contacts between framework grains and their diagenetic alterations have been studied under petrological microscope. Diagenesis greatly influences reservoir characteristics and it may either enhance or reduce porosity. It has been observed that the Tipam sandstones have undergone mechanical compaction due

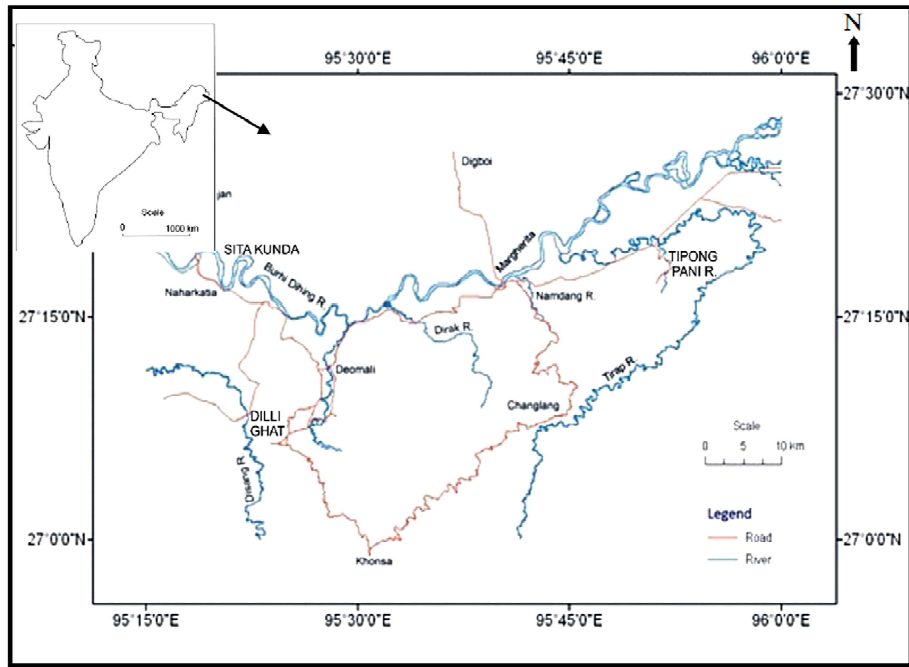


Fig. 1. Location map of the studied surface sections of the Tipam Sandstone Formation.

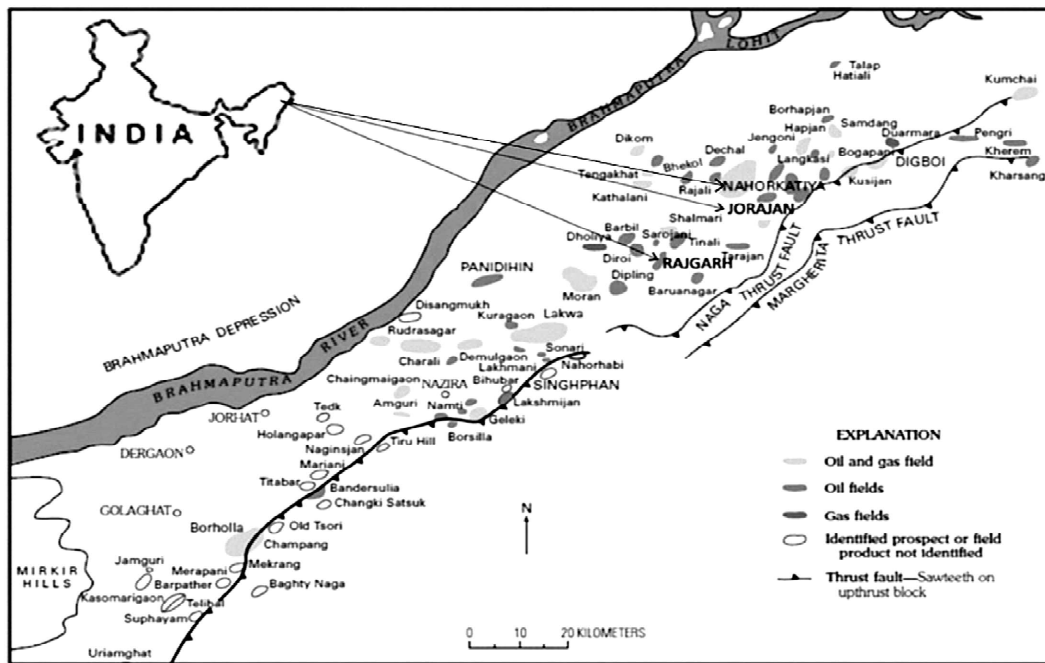


Fig. 2. Location map of the three oil fields from where the wells are selected for study (After OIL).

to the pressure of the overlying strata which have been evidenced by the presence of concavo-convex and sutured grain contacts, and bending of mica flakes and twin lamellae of plagioclase grains. Thus the primary porosity was reduced by the process of compaction. Porosity reduction was also influenced by the precipitation of different types of cements in the intergranular spaces. The types of cement present in the Tipam sandstones are argillaceous, siliceous, ferruginous and calcite cement. Argillaceous and ferruginous cement occur in the intergranular spaces as well as in the form of coating over the framework grains. Siliceous cement occurs in the form of quartz overgrowth. Calcite cement occurs in the intergranular spaces. Whereas development of secondary porosity has been evidenced by the presence of feldspar dissolution, corroded boundaries of quartz grains and fracturing of detrital grains. However, a significant amount of the produced secondary porosity has been lost by later cementation and authigenesis. Feldspar dissolution has seemed to contribute a significant part in the secondary porosity development. However, as the reprecipitation of clays generally occur near the dissolved feldspar and grain densities of both clays and feldspars are similar, the observed feldspar dissolution

has not resulted in a significant increase in total porosity. Thus, dissolution of feldspars in the studied Tipam sandstones has resulted in porosity redistribution. A number of representative photomicrographs showing the petrographic factors influencing reservoir characteristics of the studied Tipam sandstones have been presented in Plate 1. Figure- a and b show point and concavo-convex contacts and line contact between framework grains indicating compaction and porosity reduction of the Tipam sandstones after deposition. Figure- c shows floating framework grains which indicates that the porosity reduction due to compaction is insignificant in some places. Figure- d, e, f and g present different varieties of cement occurring in the intergranular spaces, which have contributed to the reduction of primary porosity. Figure- h presents dissolution of plagioclase grain indicating development of secondary porosity. Figure- i presents bending of a mica flake indicating compaction and porosity reduction of the studied Tipam sandstones.

CLAY MINERALOGICAL APPROACH

Clay minerals are considered as tools in the search for oil for a long time (Weaver, 1960; Burst, 1969). Many

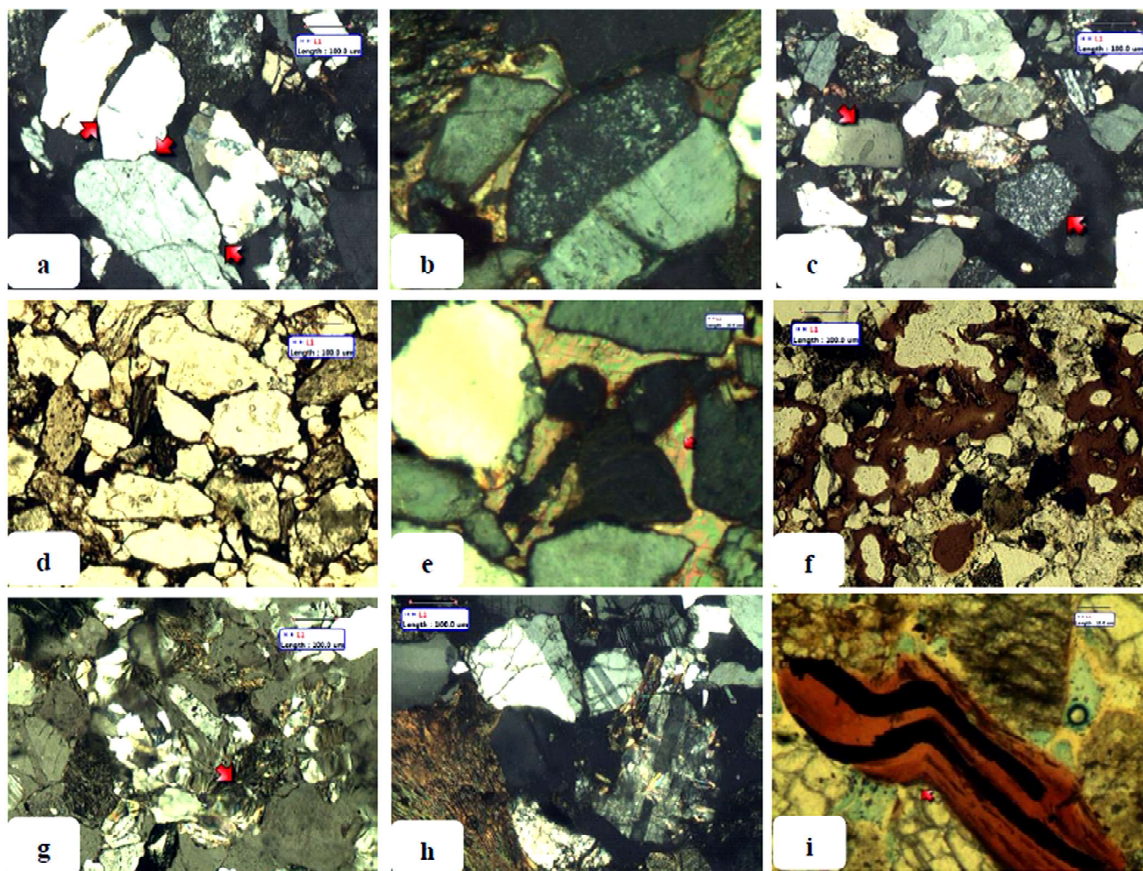


Plate 1. Petrographic factors influencing reservoir characteristics- Figure (a) Point and concavo-convex contact, (b) Line contact, (c) Floating grains, (d) Argillaceous cement, (e) Calcite cement, (f) Ferruginous cement, (g) Chalcedony, (h) Dissolution of plagioclase, and (i) Bending of a mica flake.

sandstones from productive oil wells contain diagenetic kaolinite only, while unproductive wells filled by saline water show the presence of both kaolinite and illite (Kulbicki and Millot, 1960; Chamley, 1989). The scanning electron microscope (SEM) study indicates that the Tipam sandstones contain kaolinite, montmorillonite and muscovite types of clay minerals. Neasham (1977) divided dispersed clay particles in sandstones into three general types: (i) discrete particles, (ii) pore-lining clays, and (iii) pore-bridging clays. In the studied sandstones, kaolinite occurs mainly as discrete particles and montmorillonite occurs as pore-lining particle. Development of book kaolinite, which reduces permeability in the sandstones, has been observed under the SEM in a number of cases. The water adsorption and expansion of smectite has been well-known for many years and has been accurately quantified in the laboratory (Mooney *et al.*, 1952). Even small expansions of this type may significantly affect reservoir property. Kaolinite crystals have the effect of reducing intergranular pore volume (Wilson and Pittman, 1977) but more importantly can act as migrating fines in the pore system (Neasham, 1977). SEM analysis of the Tipam sandstones suggests that kaolinite is mainly responsible for the observed permeability reduction, as the crystals are of relatively large size and also appear to be only loosely attached to the detrital grains. Presence of quartz overgrowth and framboidal pyrite has been observed under SEM in a number of cases, both of which contribute to the porosity reduction of the studied Tipam sandstones. Presence of fractures in the detrital grains contributes to the development of secondary porosity of the Tipam sandstones. A number of SEM photomicrographs of the studied sandstones have been presented in Plate 2. Figure- a presents kaolinite occupying intergranular spaces and Figure- b shows kaolinite books, both of which contributed to porosity reduction of the studied Tipam sandstones. Figure- c shows kaolinite loosely attached to detrital grains. There is an elongated pore in a quartz grain in this photograph indicating development of secondary porosity by detrital grain fracturing. Figure- d shows montmorillonite occurring as coating over grains and Figure- e shows pore-lining montmorillonite both of which reduces primary porosity. Figure- f shows framboidal pyrite which also contributes to the reduction of porosity.

WIRELINE LOG APPROACH

The reservoir characteristics of the Tipam sandstones have been studied from well logs. The wells selected are NHK#332, NHK#322 and RGH#5, which are under the operational areas of Oil India Limited, Duliajan. The types of logs used in this study are Spontaneous Potential (SP), Gamma Ray (GR), Resistivity, Caliper, Neutron and Density logs. The SP, GR, Resistivity and Caliper logs have been used for the

purpose of lithology identification and Neutron and Density logs have been used for the purpose of reservoir characterization. The subsurface study of the rocks based on well logs shows that the rocks of the Tipam Sandstone Formation consists of repetitive sequences of sandstone, shaley sandstone and shale facies (Fig.3). In the well NHK#332, the formation is penetrated at 2224.00 m and extends up to 2875.00 m. It extends from 1899.00 m to 2673.50 m and 2431.00 m to 3221.00 m in the NHK#322 and RGH#5 wells, respectively. The amount of sandy facies is considerably higher with thick sand bodies, which show dominance of channel facies as compared to overbank deposits of fluvial environments.

Fig. 4 represents porosity logs of the three wells under study, namely NHK#322, NHK#332 and RGH#5. The sandbodies show medium to high density indicating that the sandstones are compact. The density ranges from 2.09 to 2.40 gm/cc and from 2.19 to 2.45 gm/cc in the NHK#332 and NHK#322 wells, respectively. In the RGH#5 well, it ranges from 2.20 to 2.66 gm/cc. At some places low density values indicating high porosity and less compaction have also been observed. This is also evidenced by petrographic study by the presence of the floating framework grains. The less compact sandstones are appropriate reservoirs due to higher porosity.

All porosity logs deflect to the left for increasing porosity. Hydrocarbons increase resistivity compared to water zones, causing resistivity to deflect to the right. Thus, when porosity and resistivity logs deflect in opposite directions, the zone is identified to be hydrocarbon bearing. Most of the porous rocks of the studied Tipam sandstones show low resistivity indicating the presence of mainly water bearing zones. No marked increase in resistivity has been observed in all the three wells under study. However, at a few depths in these wells, increase in resistivity along with increase in porosity has been observed indicating probable occurrence of hydrocarbon. These depths include 2656 m, 2696 m and 2697 m in NHK#332 well; 2158 m and 2287 m in NHK#322 well; and 3131 m and 3209 m in RGH#5 well. Moreover, neutron density crossover has been observed in all the three wells under study, which infers the presence of gas. The maximum number of such crossovers has been observed in the NHK#332 well, followed successively by NHK#322 and RGH#5 wells.

CALCULATION OF PETROPHYSICAL PARAMETERS

Porosity is one of the key parameters evaluated during reservoir characterization studies. It is defined as the ratio of the volume of voids to the total volume of rock. Density, neutron and sonic logs have so far been used for porosity determination. Sonic log is less sensitive to borehole and mud cake variations than density and neutron logs. Thus the density, neutron or neutron – density combination has become the primary

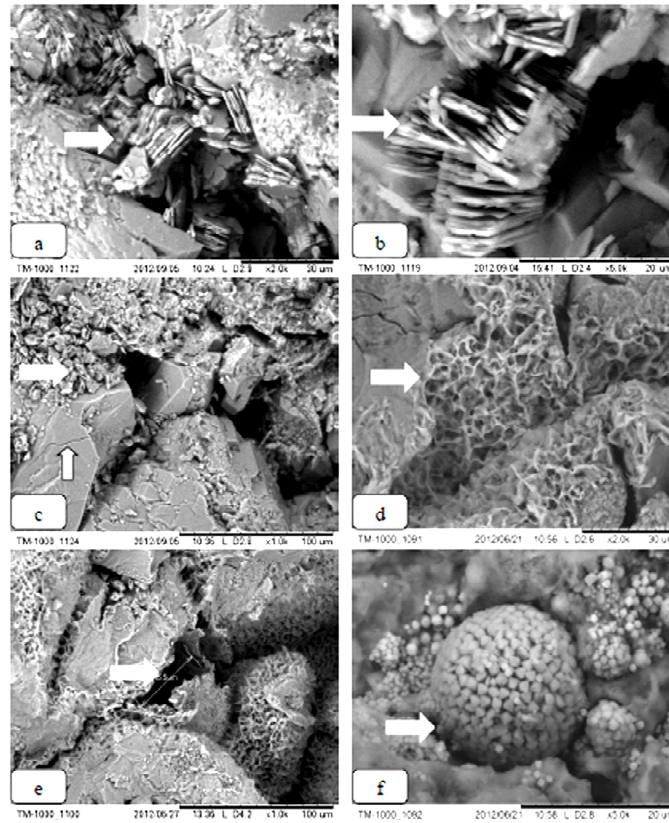


Plate 2. SEM photomicrographs of the studied sandstones- Figure (a) Kaolinite occupying intergranular spaces, (b) Kaolinite books, (c) Kaolinite loosely attached to detrital grains and elongate pore in quartz grain, (d) Montmorillonite occurring as coating over grains, (e) Pore-lining montmorillonite and (f) Framboidal pyrite.

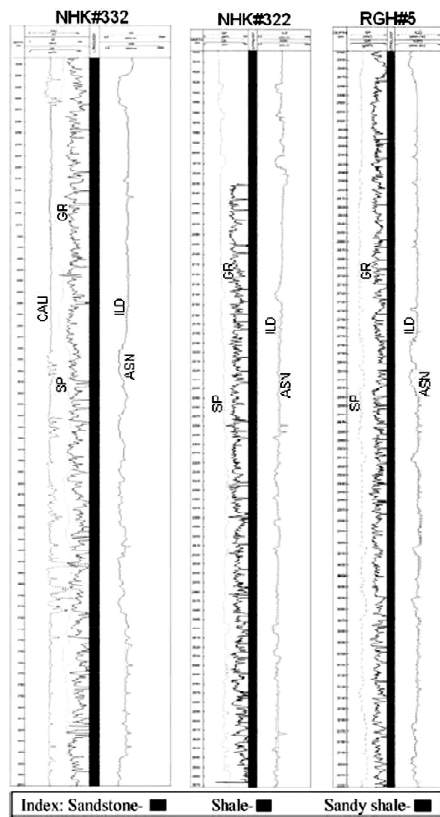


Fig. 3. Lithologs of the hydrocarbon wells under study.

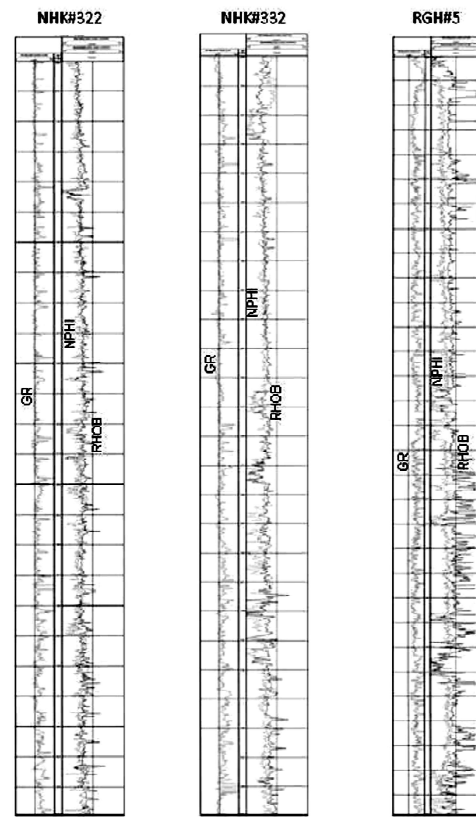


Fig. 4. Porosity logs of the wells NHK#322, NHK#332 and RGH#5.

source of porosity calculation, replacing the sonic (Dewan, 1983). In this study, porosity has been determined by using the combination of neutron and density logs. The values obtained from the neutron log have been corrected for sandstone by using standard correction chart. Then the values of neutron porosity and bulk density have been plotted in the Neutron – Density cross plot for the determination of porosity (Fig.5). The values of neutron porosity, corrected neutron porosity, density and the obtained porosity values from the cross plots for the three wells under study have been presented separately in Table 1, 2 and 3.

From the Tables 1, 2 and 3 it has been observed that the porosity values ranges from 25.20 to 45.50% (average 33.47%) for the NHK#332 well and from 18.50 to 38.50% (average 31.11%) for the NHK#322 well. The same values for the RGH#5 well ranges from 21.00 to 41.00% (average 31.41%). Table 4 after Rider (1991) gives a better explanation of calculated porosity values of the present study.

It is apparent from this table that in most of the calculated depths, the Tipam sandstones under study have very good to excellent porosity values.

Another petrophysical property commonly evaluated during reservoir characterization is permeability. Permeability is a measure of the ease with which fluids can flow through a formation. It is commonly determined from cores or a combination of cores and logs. However, in the absence of cores, it is evaluated from logs by using indirect methods. In the present study, an attempt has been made to evaluate permeability of the studied Tipam sandstones by studying logs due to the unavailability of cores.

Before starting calculations for the determination of permeability, water saturation (S_w) of the formation under study at different depths has been calculated by using Schlumberger approach. Water saturation of a

formation is defined as the fraction or percentage of the pore volume that contains formation water. S_w has been calculated by using the formula given by:

$$S_w = \sqrt{(F \cdot R_w / R_t)}$$

Here, 'F' stands for formation resistivity factor. It has been established experimentally that the resistivity of a clean, water-bearing formation is proportional to the resistivity of the brine with which it is fully saturated. The constant of proportionality is called the formation resistivity factor. 'R_w' and 'R_t' are formation water resistivity and true resistivity, respectively.

'F' is related to porosity (Φ) by:

$$F = 1 / \Phi^2$$

Thus, the values of 'F' are calculated from the already determined ' Φ_{N-D} ' values. The values of 'R_t' have been taken from the deep induction resistivity (ILD) logs. The values of 'R_w' for the NHK#332 and NHK#322 wells are 6.50 ohm-m. The same for the RGH#5 well is 6.00 ohm-m.

The values of 'R_t' at different depths of the three wells under study and the calculated values of 'F' and ' S_w ' are presented in Table 5. A zone or sand level where the water saturation is higher than 0.50 means that the zone is water-bearing, whereas if it is less than 0.50, then it is hydrocarbon-bearing. Water saturation at 0.50 implies that the zone has equal amount of water and hydrocarbons (Schlumberger, 1989).

It has been observed from Table 5 that the values of S_w indicate both water-bearing and hydrocarbon-bearing character of the studied Tipam sandstones. Moreover, at a depth of 2575 m of NHK#322 well, the value of S_w is 0.50 indicating a zone with equal amounts of water and hydrocarbon.

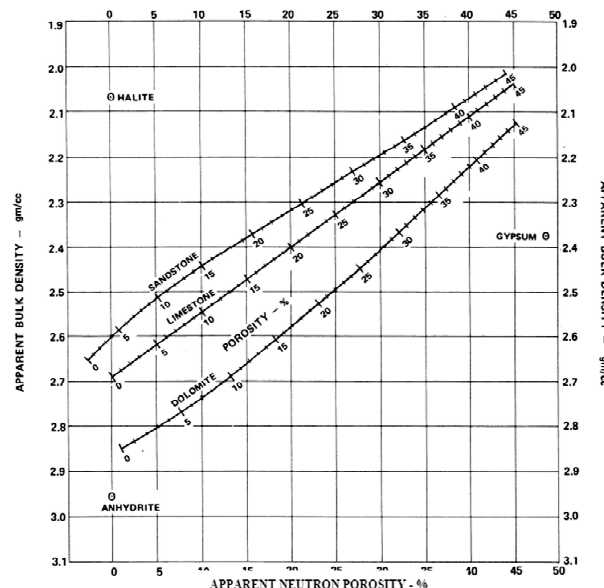


Fig. 5. Neutron – Density cross plot.

Table 1. Neutron porosity (Φ_N), Φ_N corrected, density (ρ) and cross plot derived porosity (Φ_{N-D}) for the NHK#332 well.

Depth (m)	Φ_N (PU)	Φ_N Corrected (PU)	P (gm/cc)	Φ_{N-D} (%)
2225	20	25.50	2.25	28.50
2250	17	22.50	2.19	28.00
2275	38	42.00	2.19	41.00
2300	30	35.00	2.27	34.50
2325	29	34.00	2.29	33.50
2350	29	34.00	2.26	34.50
2375	23	28.20	2.34	28.50
2400	30	35.00	2.26	34.80
2425	28	33.00	2.30	33.00
2450	27	32.00	2.27	32.80
2475	26	31.00	2.34	30.20
2500	27	32.00	2.34	30.50
2525	41	44.00	2.09	45.50
2550	31	36.00	2.31	33.80
2575	39	42.50	2.14	43.00
2600	31	36.00	2.27	35.00
2625	34	38.50	2.27	36.50
2650	41	44.00	2.26	40.50
2675	22	27.50	2.30	28.00
2700	32	37.00	2.26	36.00
2725	30	35.00	2.40	31.00
2750	28	33.00	2.30	32.80
2775	28	33.00	2.29	33.50
2800	25	30.40	2.30	30.50
2825	21	26.50	2.40	25.20
2850	27	32.00	2.31	31.00
2875	29	34.00	2.36	31.50

Table 2. Neutron porosity (Φ_N), Φ_N corrected, density (ρ) and cross plot derived porosity (Φ_{N-D}) for the NHK#322 well.

Depth (m)	Φ_N (PU)	Φ_N Corrected (PU)	ρ (gm/cc)	Φ_{N-D} (%)
2050	0.25	30.40	2.23	30.80
2075	0.29	34.00	2.19	34.60
2100	0.28	33.00	2.23	34.00
2125	0.37	41.00	2.25	38.50
2150	0.26	31.00	2.31	30.50
2175	0.23	28.40	2.25	29.00
2200	0.30	35.00	2.25	35.00
2225	0.28	33.00	2.35	31.50
2250	0.29	34.00	2.31	33.00
2275	0.27	32.00	2.29	30.50
2300	0.15	20.20	2.45	18.50
2325	0.22	27.50	2.30	28.00
2350	0.31	36.00	2.30	34.00
2375	0.28	33.00	2.30	32.00
2400	0.30	35.00	2.33	33.00
2425	0.27	32.00	2.28	30.50
2450	0.23	28.20	2.25	30.50
2475	0.23	28.20	2.23	30.80
2500	0.30	35.00	2.25	35.00
2525	0.25	30.40	2.32	30.50
2550	0.16	21.40	2.40	20.50
2575	0.37	41.00	2.33	36.50
2600	0.24	29.40	2.24	30.00
2625	0.21	26.50	2.29	28.50
2650	0.29	34.00	2.34	32.00

Table 3. Neutron porosity (Φ_N), Φ_N corrected, density (ρ) and cross plot derived porosity (Φ_{N-D}) for the RGH#5 well.

Depth (m)	Φ_N (PU)	Φ_N Corrected (PU)	ρ (gm/cc)	Φ_{N-D} (%)
2450	0.35	39.40	2.20	39.50
2475	0.37	41.00	2.40	34.00
2500	0.30	35.00	2.50	28.00
2525	0.31	36.00	2.29	34.20
2550	0.29	34.00	2.37	31.50
2575	0.29	34.00	2.52	37.50
2600	0.30	35.00	2.30	33.50
2625	0.26	31.00	2.31	31.00
2650	0.30	35.00	2.33	33.00
2675	0.25	30.40	2.35	29.50
2700	0.28	33.00	2.35	31.50
2725	0.26	31.00	2.37	29.00
2750	0.45	48.00	2.34	41.00
2775	0.24	29.40	2.40	27.50
2800	0.40	43.60	2.31	39.00
2825	0.42	45.00	2.27	41.00
2850	0.34	38.50	2.25	37.50
2875	0.23	28.40	2.50	24.00
2900	0.23	28.40	2.39	27.20
2925	0.35	39.40	2.24	38.50
2950	0.24	29.40	2.64	21.00
2975	0.30	35.00	2.45	29.50
3000	0.26	31.00	2.39	28.50
3025	0.22	27.50	2.39	26.80
3050	0.23	28.40	2.31	29.00
3075	0.16	21.40	2.25	26.00
3100	0.26	31.00	2.50	25.50
3125	0.17	22.50	2.35	22.80
3150	0.31	36.00	2.51	28.50
3175	0.44	47.30	2.47	37.50
3200	0.31	36.00	2.43	30.80

Table 4. Qualitative evaluation of porosity.

Porosity (%)	Qualitative Description
0 – 5	Negligible
5 – 10	Poor
15 – 20	Good
20 – 30	Very good
>30	Excellent

Table 5. Values of Rt, F and Sw at different depths in the studied wells.

Well No.	Depth (m)	Rt (ohm-m)	F	Sw (%)
NHK#332	2225	60.00	12.31	0.36
	2275	26.00	5.95	0.39
	2300	29.00	8.40	0.44
	2325	28.00	8.91	0.46
	2375	26.00	12.31	0.56
	2425	28.00	9.18	0.46
	2450	23.00	9.29	0.51
	2475	18.00	10.96	0.63
	2500	7.50	10.75	0.96
	2575	14.00	5.41	0.50
	2850	9.50	10.41	0.84
NHK#322	2100	26.00	8.65	0.47
	2250	16.00	9.18	0.61
	2350	15.00	8.65	0.61
	2475	14.00	10.54	0.70
RGH#5	2500	32.00	12.75	0.49
	2525	30.00	8.55	0.41
	2600	30.00	8.91	0.42
	2625	32.00	10.41	0.43
	2675	32.00	11.49	0.46
	2700	27.00	10.08	0.47
	2725	18.00	11.89	0.63
	2750	24.00	5.95	0.39
	2875	20.00	17.36	0.72
	3000	28.00	12.31	0.51
	3025	20.00	13.92	0.64

During the determination of permeability from logs, a very important point is that the log-derived permeability formulas are only valid for estimating permeability in formations at irreducible water saturation ($S_{w,irr}$; Schlumberger, 1977). Irreducible water saturation (sometimes called critical water saturation) defines the maximum water saturation that a formation with a given permeability and porosity can retain without producing water. This water, although present, is held in place by capillary forces and will not flow. Irreducible water saturation is the minimum water saturation obtainable in a rock. Water is usually the wetting fluid in oil or gas reservoirs, so a film of water covers each pore surface. The surface area thus defines the irreducible water saturation. Formations at irreducible water saturation cannot produce water until water encroaches into the reservoir after some oil or gas has been withdrawn. Small pores have larger surface area relative to their volume and thus, their irreducible water saturation is higher. If pores are small enough, the irreducible water saturation may be 1.0, leaving no room for oil or gas to accumulate (Crain, 2008).

To determine whether a formation is at irreducible water saturation or not, it is necessary to determine the bulk volume water (BVW) which is given by:

$$BVW = S_w \times \Phi$$

Where S_w = Water saturation (%)
 Φ = Porosity (%)

When the BVW values of a part of a formation are constant, the zone is at irreducible water saturation. The values of BVW at different depths in the studied wells have been determined and it has been observed that the values are equal or nearly equal in a number of depths in all the three wells under study. These depths and the respective BVW values have been presented in Table 6.

Equal values of BVW at different depths in a zone indicate that the zone is homogeneous and at irreducible water saturation. As permeability determination from logs is restricted to the zones with irreducible water saturation, it is now possible to attempt to determine permeability in the zones with equal BVW values. The formula which has been used in the present study for

Table 6. Calculation of bulk volume of water (BVW) and permeability (K) from Sw and Φ .

Well No.	Depth (m)	Sw (%)	Φ (PU)	BVW (%)	Sw (%)	Φ (%)	K (md)
NHK#332	2275	0.39	0.41	0.16	39	41.00	1115.99
	2300	0.44	0.34	0.15	44	34.50	410.24
	2325	0.46	0.33	0.15	46	33.50	329.78
	2375	0.56	0.28	0.16	56	28.50	109.26
	2425	0.46	0.33	0.15	46	33.00	308.66
NHK#322	2250	0.61	0.33	0.20	61	33.00	175.53
	2350	0.61	0.34	0.20	61	34.00	200.16
	2475	0.70	0.30	0.21	70	30.80	20.48
RGH#5	2500	0.49	0.28	0.14	49	28.00	132.02
	2525	0.41	0.34	0.14	41	34.20	454.66
	2600	0.42	0.33	0.14	42	33.50	395.58
	2625	0.43	0.31	0.13	43	31.00	268.28
	2675	0.46	0.29	0.13	46	29.50	188.47
	2700	0.47	0.31	0.14	47	31.5	240.94

Table 7. Qualitative evaluation of permeability.

Permeability (md)	Qualitative Description
<10.5	Poor to fair
15 – 50	Moderate
50 – 250	Good
250 – 1000	Very good
>1000	Excellent

permeability determination is after Timur (1968), which is given by:

$$K = (0.136 \Phi^{4.4}) / (Swirr)^2$$

The calculated values of permeability in these zones have been presented in Table 6. It has been observed that the average permeability values of the NHK#332, NHK#322 and RGH#5 wells are 454.79 md, 132.06 md and 279.99 md, respectively. Qualitative evaluation of permeability after Rider (1991) has been presented in Table 7. From the table it is apparent that most of the studied Tipam sandstones from the three wells have good to very good permeability. Exceptions are the sandstones from depths 2275 m in NHK#332 well and 2475 m in NHK#322 well where the permeability values are in the excellent and moderate ranges, respectively.

Since the determination of permeability in the present study is based only on log data, further study including both core and log data is needed for the determination of more accurate permeability values.

DISCUSSION AND INTERPRETATION

Petrographic study of the Tipam sandstones infers that the process of compaction has a significant effect in the primary porosity reduction. Presence of different

types of cements in the intergranular spaces as well as in the form of coating over framework grains also indicates primary porosity reduction by their precipitation. On the other hand, presence of features such as dissolution of feldspar grains, corrosion of quartz grains by cement and fracturing of detrital grains are indicative of development of secondary porosity in the Tipam sandstones. However, as indicated by the presence of cement in the intergranular spaces as well as in the form of coating over the detrital grains, most of the produced secondary porosity has been lost by later cementation and authigenesis. Although feldspar dissolution seemed to have contributed significantly to the development of secondary porosity, reprecipitation of clays near the dissolved feldspar has resulted in porosity redistribution instead of a considerable secondary porosity development.

From the SEM study, it has been observed that kaolinite occurs in the form of discrete particles as well as in book-like form. Development of kaolinite books has contributed to permeability reduction in the studied Tipam sandstones. Montmorillonite has a considerable effect on the reservoir characteristics of the studied Tipam sandstones as it is a type of expanding clay. According to Selley (1998), montmorillonite does not have significant effect on permeability in the presence

of hydrocarbons but has the ability to swell and greatly reduce permeability when saturated with water. According to Okiator *et al.* (2011), if this is the case in a reservoir, then the montmorillonite clay could pose a problem during production, in that, during production, high recovery rate may be experienced initially and after a while, productivity will decline due to formation damage. The principle is that when production begins, water displaces the crude hydrocarbons, causing the montmorillonite clay to expand and destroy the permeability of the lower part of the reservoir (Selley, 1998). Hence, if this is the case in the studied wells, during drilling of other wells in the same fields, use of oil-based mud would be more preferable than the conventional water-based mud.

It has been observed that presence of quartz overgrowths and framboidal pyrite has contributed to the porosity reduction. On the other hand, presence of fractures in the detrital grains contributes to the development of secondary porosity of the Tipam sandstones.

Interpretation of wireline logs of the three studied wells has shown that the sandbodies are of medium to high density indicating that they are compact in nature. At some places, the density values are low inferring high porosity and less compaction of the Tipam sandstones, which is also supported by petrographic study. Most of the porous rocks of the studied Tipam sandstones show low resistivity indicating that they are water-bearing. No marked increase in resistivity has been observed in all the three wells under study. Increase in resistivity along with increase in porosity has been observed at depth of 2656 m, 2696 m and 2697 m in NHK#332 well; 2158 m and 2287 m in NHK#322 well and 3131 m and 3209 m in RGH#5 well, indicating probable occurrence of hydrocarbons. Moreover, neutron density crossover has been observed in all the studied wells inferring the presence of gas. The maximum number of such crossovers has been observed in the NHK#332

well. Porosity determination from neutron density cross plot has shown that the studied Tipam sandstones of NHK#332, NHK#322 and RGH#5 wells have average porosity percentages of 33.47, 31.11 and 31.41%, respectively. Most of these values fall in the very good to excellent porosity ranges of Rider (1991). Gocon (1988) suggested that the minimum porosity for a hydrocarbon-bearing rock to be of economic importance is 10% - 20%. From the calculated values of porosity of all the three wells under study, it has been observed that all the porosity percentages are above this range. It infers that the Tipam sandstones of the wells under study have very significant reservoir characteristics with high porosity values.

The values of water saturation (S_w) of the studied Tipam sandstones indicate both water-bearing and hydrocarbon-bearing characters of the sandstones. Calculation of permeability of the studied Tipam sandstones have shown that the average permeability of the NHK#332, NHK#322 and RGH#5 wells are 454.79 md, 132.06 md and 279.99 md, respectively. Most of the permeability values fall in the good to very good ranges of Rider (1991). According to Okiator *et al.* (2011), for a rock to be considered as an exploitable hydrocarbon reservoir without stimulation, its permeability must be greater than approximately 100 md (however, depending on the nature of the hydrocarbons, gas reservoirs with lower permeabilities are still exploitable because of the lower viscosity of gas with respect to oil). In the present study, most of the calculated values of permeability are greater than 100 md, indicating good exploitable characteristics of the Tipam sandstones under study.

Acknowledgements: The authors are grateful to Oil India Limited, Duliajan, for extending financial assistance to carry out the study under the K. D. Malaviya Chair, Department of Applied Geology, Dibrugarh University, Assam.

References

- Berg, R.R. (1986). Reservoir Sandstones, Prentice-Hall, Inc, Englewood Cliffs, New Jersey, 481.
- Bread, D.C. and Weyl, P.K. (1973). Influence of texture on porosity and permeability of unconsolidated sand, American Association of Petroleum Geologists Bulletin, 57(2), 349-369.
- Burst, J. F. (1969). Diagenesis of Gulf Coast Clayey sediment sand, its possible relationship to petroleum migration, Bull. Am. Assoc. Petrol. Geologist, 53, 73-93.
- Chamley, H. (1989). Clay Sedimentology, Springer-Verlag, Berlin Heidelberg, 623.
- Crain, E. R. (2008). Hand book of Petrophysics, Internet book.
- Dewan, J. T. (1983). Essentials of modern open-hole log interpretation: Tulsa, PennWell Books, 361.
- Gocon (1988). Porosity Gradient Studies in Niger delta, Internet, 1-7.
- Kulbicki, G. and Millot, G. (1960). L'évolution de la fraction argilense gre's petrotiers Cambro-Ordovician du Sahara Central, Bull. Serv. Carta-Geol. AL-sace Lorraine, 13, 147-156.
- Mitra, S. (1988). Effects of Deformation Mechanisms on Reservoir Potential in central Appalachian Overthrust Belt, The American Association of Petroleum Geologists Bulletin, 72(5), 536-554.
- Mooney, R.W., Keenan, A.G., and Wood, L.A. (1952). Adsorption of water vapour by montmorillonite. II. Effect of exchangeable ions and lattice swelling as measured by X-ray diffraction, Journal of the American Chemical Society, 74, 1371-1374.

- Neasham, J.W. (1977). The morphology of dispersed clay in sandstone reservoirs and its effect on sandstone shaliness, pore space, and fluid flow properties, SPE paper 6858.
- North, F.K. (1985). Petroleum Geology, Boston Unwin Hyman Publishers, 631.
- Okiotor, M.E, Imasuen, I.O. and Etobro, A.A.I. (2011). Reservoir Evaluation of Well A, Field Y, North-Eastern Niger Delta: A Case of a Problematic Sandstone, *Advances in Applied Science Research*, 2(3), 114-126.
- Rider M. (1991). The Geological Interpretation of Well Logs, 3rd Ed., Whittles publishing, Caithness, 175.
- Sarma, J.N., Chutia, A. and Sarmah, P. (2011). Compositional study of subsurface Tipam Sandstone Formation from an oil field of Upper Assam, *Journal of the Indian association of Sedimentologist*, 30(1), 11-22.
- Schlumberger (1977). Log Interpretation Principle/ Application, Schlumberger Educational Services, Houston, Texas, U.S.A.
- Schlumberger (1989). Log Interpretation Charts, Schlumberger Well Serv. Inc., Houston, Texas, U.S.A.
- Selley R.C. (1998) Elements of Petroleum Geology, Academic Press Limited, London.
- Timur, A. (1968). An Investigation of Permeability, Porosity, and Residual Water Saturation Relationship for Sandstone Reservoirs, *The Log Analyst*, 9(4), 8.
- Weaver, C.E. (1960). Possible uses of clay minerals in search for oil: *Bull. Am. Assoc. Petrol. Geologists.*, 44, 1505-1518.
- Wilson, M.D. and Pittman, E. D. (1977). Authigenic clays in sandstones: Recognition and influence on reservoir properties and paleoenvironmental analysis, *J. Sediment. Petrology*, 47, 3-31.

Half-Graben Basin Filling Model and *New Constraints* on Continental Extensional Basin Development – A Case Study from the Kolhan Basin, Eastern India

SUBHASISH DAS, ROHINI DAS* AND SMRUTI REKHA SAHOO

Department of Geology and Geophysics, IIT Kharagpur, PIN:-721302, India

Email: romiyadas@gmail.com*

Abstract: The half-graben development and fault growth evolve differently through time and produce different basin-filling patterns. In the initial stage the fault model incorporates a basin-bounding fault that soles into a sub-horizontal detachment fault; the change in the rate of increase in the volume of the basin during uniform fault displacement is zero. Younger strata consistently pinch out against older syn-rift strata rather than pre-rift rocks. Both basin-bounding faults and the intervening fault blocks rotate during extension and as a consequence, there is a change in the rate of increase of the volume of the basin. The basin fill commonly forms a fanning wedge during fluvial sedimentation, whereas lacustrine strata tend to pinch out against older syn-rift strata. During the fault growth models, the Kolhan basin grew both wider and longer through time as the basin-bounding faults lengthen and displacement accumulates; the change in the rate of increase in basin volume is positive. The fluvial strata progressively onlap the hanging wall block, whereas the lacustrine strata pinch out against older fluvial strata at the centre of the basin but onlap along the lateral edges. The transition from fluvial to lacustrine deposition and hanging wall onlap relationships observed in numerous continental extensional basins are best explained by the fault growth models. The Kolhan Group in the studied basins of Chaibasa – Noamundi and Chamakpur-Keonjhar is usually marked by a sequence of clastic (+carbonate) association. This fining upward sequence, the vertical and lateral facies variation in the Kolhan implies superimposition of retrograding shorelines on an earlier prograding alluvial fan sand complex. The pronounced variations in thickness of the fan delta succession and the stacking pattern in different measured profiles reflect the overriding tectonic controls on fan-delta evolution. A strong asymmetry in vertical basin architecture and the linearity in the outcrop pattern of the preserved sedimentary sequence are presumed to have developed in an elongated trough during the initial basinal rifting stage, while the later stage is marked by the progressive overlaps and coalesce of the facies built-up.

The assumption of a tectonic setting for the NE-SW trending Kolhan basin possibly relate to the basin opening to the E-W extensional stress system that prevailed during the development of the Newer Dolerite dyke. The N-S oriented syn-Kolhan extensional regime may reflect orogenic collapse after the cessation of N-S orientated compression by collision or reactivation tectonics in the Singhbhum orogeny. The controlling factor for the location of half-graben development during a syn-Kolhan extensional regime is likely to have been reactivation along the Singhbhum shear zone (SSZ). Cratonic sutures such as the SSZ are likely to be prone to reactivation during any subsequent tectonic episodes, leading to complex structural and sedimentological relationships as basins are created, inverted and superimposed along a long-lived shear zone throughout successive tectonic regimes. The Kolhan serve as an example of sedimentary response to changing tectonic regimes associated with the SSZ.

Keywords: Half-Graben, Faults, Sedimentation.

INTRODUCTION

The Singhbhum Craton in eastern India is mainly composed of Archaean granitoids forming the nucleus rimmed by a Proterozoic mobile belt to the north and east (Saha, 1994). The oldest granitoid is referred to as Older Metamorphic Tonalite Gneiss (OMTG- 3.4 Ga) that includes enclaves of Older Metamorphic Group. The OMTG is intruded by several granitic plutons collectively referred to as Singhbhum Granite with three phases of emplacement between 3.4 and 3.1 Ga. In the western part of the Singhbhum granite Kolhan Group,

which represent youngest and the least studied Precambrian stratigraphic unit in Singhbhum geology. The 2.2-2.1 Ga pear shaped Kolhan basin in the Singhbhum craton is an enigma and significant in many respect. It occurs as a narrow strip-like outcrop pattern extending for 80-100 km in length with an average width of 10-12 km, controlled by the NE-SW trend. It occurs as isolated outliers present in four detached basins such as 1. Chaibasa - Noamundi basin, 2. Chamakpur - Keonjhar basin, 3. Mankarchua basin, and 4. Sarapalli - Kamakhyanager basin. It covers an area around 800sq km along the western margin of Singhbhum Granite. It

intervenes the Singhbhum granite to the east and the Iron Ore Supergroup to the west (Saha and. Sarkar, 1988).

No direct evidence of its age has been found, but inferences have resulted from its structural relationship with adjacent deformed and metamorphosed tectonosomes; that it ranges from Neo-archean (Roy.et.al.,2012) to Paleo-proterozoic (Saha,1994; Bandhopadhaya and Sengupta,2004) to Meso to Neo-proterozoic (Mukhopadhyay et.al.,2001). The undeformed and unmetamorphosed lithologic character of the Kolhans may be more compatible with deposition in the Meso- to Neo-Proterozoic time. (Bandhopadhaya and Sengupta, 2004).

The depositional environment of the Kolhans varied from braided fluvial-ephemeral pattern to a fan-delta-lacustrine type. The channel geometries and the climate exerted a major control on the processes of sediment transfer. Repeated upliftment of the source due to fault-controlled activity followed by subsidence and forced regression generated multiple sediment cyclicity that led to the fluvial-fan delta sedimentation pattern (Dalabhera, 2009). The lithofacies variation along with geophysical cross-sections generate predicted models for the basin filling pattern. The aim of this paper was to emphasise on the models probable to support the sedimentation and tectonics in Kolhans.

GEOLOGICAL SET-UP OF THE KOLHANS

The geological map of the Kolhan basin (Fig.1) shows various lithologic units. The various stratigraphic

units according to Saha (1994) are (a) Older Metamorphic Group (OMG) (b) Older Metamorphic Tonalite-gneiss (OMTG) (c) Singhbhum granite Phase II and Phase III (d) Iron Ore Supergroup {shales, tuffs, phyllites, banded iron formation (BIF), banded hematite jasper (BHJ), banded hematite quartzite (BHQ), sandstone, and conglomerate} (e) Jagannathpur and Malangtoli lavas, and (f) Kolhan basin.

The Kolhan basin consists of a low (2Ú - 10Ú) westerly dipping sequence of basal, purple conglomerate, pebbly sandstone, gray quartz arenite (locally arkosic), with several thin bands of purple to dusky red siltstone and shales. The Kolhans show a faulted contact with the Jagannathpur lavas and the Iron Ore Supergroup to the west and unconformably overlie the Singhbhum granite to the east (Saha,1994).

LITHOLOGY AND FACIES VARIATIONS IN KOLHANS

The lithofacies analysis based on the field descriptions, the detailed examination of outcrop patterns along with the variations in the sedimentary structures appears to be the most effective means for analyzing and interpreting the stratal geometries and the depositional and tectonic history. The architectural elements used in the present study are the field stratal characteristics, primary sedimentary structures, textures, fabrics of the lithofacies and their geometrical relationships.

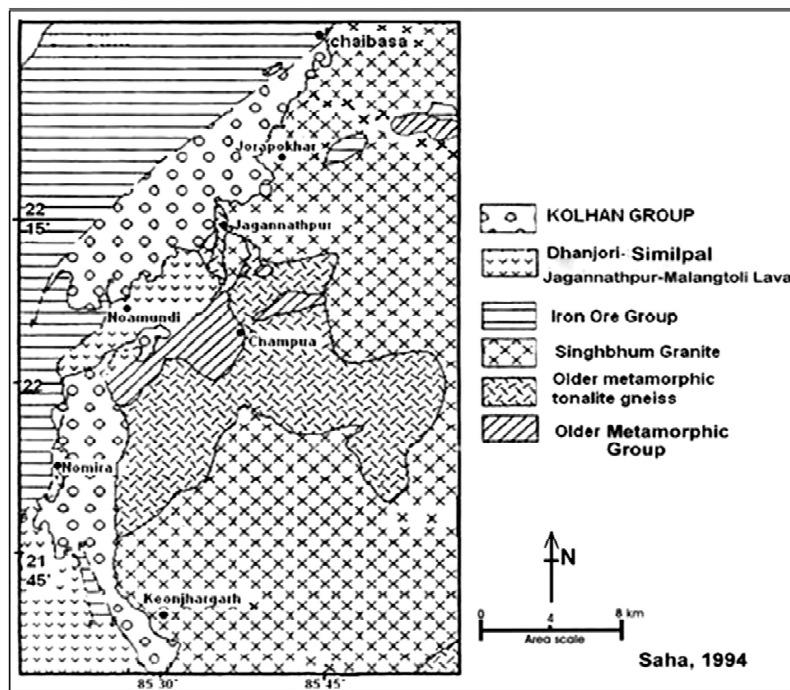


Fig.1. Geological map of West Singhbhum showing Chaibasa-Noamundi basin and North Orissa showing Chamakpur-Keonjhar basin (Saha, 1994) with the faulted contact against Iron Ore Group on the western side and angular unconformity with Singhbhum Granite on the eastern side of Chaibasa-Noamundi basin.

A. Lithology

The major lithounits have been described below.

- a. Kolhan shale
- b. Kolhan calcareous shale / limestone
- c. Kolhan sandstone
- e. Kolhan conglomerate

The Kolhan conglomerate rests unconformably on the Singhbhum Granite (Fig. 2a). A significant feature is that the pebbles of banded hematite jasper, jasper and iron ore which are commonly found in the conglomerate towards south progressively decrease in proportion northwards and their place is taken mainly by pebbles of quartz, quartzite and granite. The contact with the overlying sandstone is often transitional. The conglomerate grades upward to medium-fine grained plane bedded Kolhan sandstone.

The Kolhan sandstone is best developed at railway cutting near Chaibasa railway station, near Matgamburu, Bistampur, Rajanbasa, along Gumma Gara river, Nurda and Jagannathpur. In all these exposures the minimum thickness attained is 15ft while maximum goes up to 25 to 30ft. In other places the average thickness of the sandstone is nearly 5ft. The NE-SW trending outcrops of the sandstone are frequently interrupted, so that the maximum continuous exposure is never more than a mile and a half. The plane bedded sandstones are interbedded with minor thin beds and lenses of conglomerates, pebbly sandstones with thin

and impersistent layers of shale. The sandstone shows development of antidune /wavy lamination and planar cross stratification.

The Kolhan Limestone is an impersistent horizon. It is best developed towards SW of Chaibasa, near village Rajanka and Kondoia and N and NW of Jagannathpur. In all these places the minimum thickness attained is nearly 20 ft and the maximum ca. 65 ft. (Rajanka). The limestone can be divided (Fig. 2b) in the field into a white to pale grey, pink and pale green lower horizon consisting of thick bedded rock traversed by calcite quartz veins (Fig. 2c) in which rhombohedral calcite and partly euhedral transparent quartz crystals are developed. The darker upper horizon is very different in appearance with a foliated structure caused by parallel chloritic laminae. The contact between these two horizons is slightly transitional. This relationship is best seen in the A.C.C. Limestone quarry.

The Kolhan Phyllitic Shale (Fig2d) is the most dominant rock type of the Kolhan Formation, having the maximum areal extent within the area mapped. The maximum thickness is nearly 25 ft. The shales are traversed by innumerable massive quartz veins throughout the area, particularly towards the western extremity.

B. Tectonic Relation

Tectonically the Kolhan basin represents an epicontinental type with a NNE-SSW

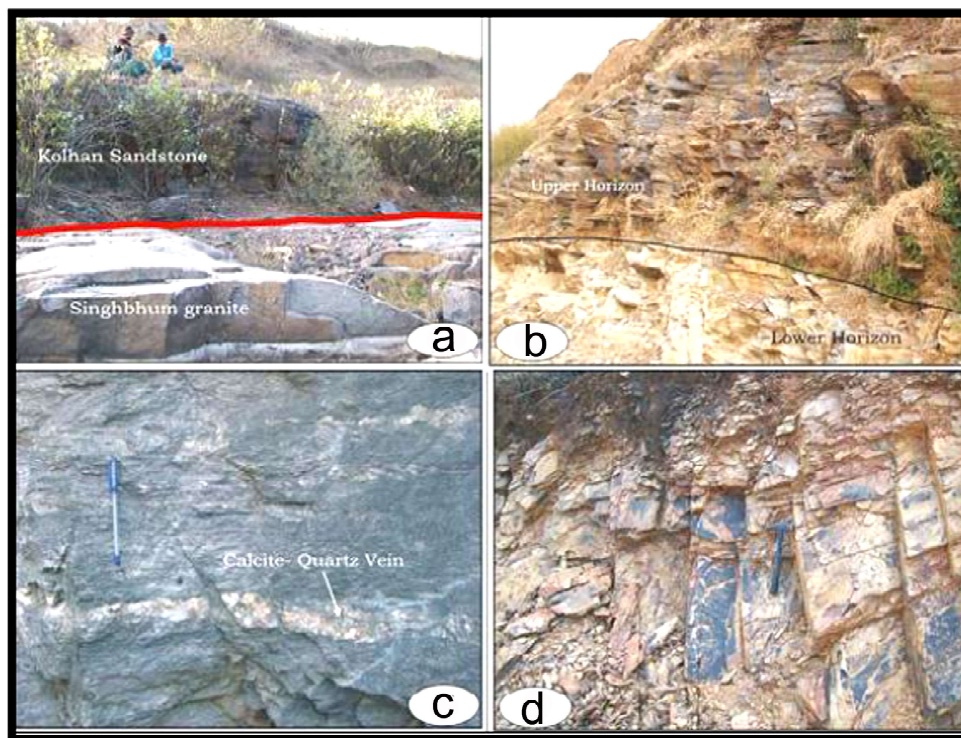


Fig.2a. Contact of Singhbhum granite with Kolhan sandstone at Gumua Gara river section; **b.** Upper and lower limestone horizons at Guira limestone mine (section height: 30m); **c.** Calcite-Quartz vein in limestone (scale: Pen, 15cm); **d.** Kolhan Shale formation at Harira (scale: Hammer, 27cm).

alignment, controlled by the similar trend of the Iron Ore Formation synclinorium (Eastern Ghat strike). Further west near the contact of the Iron Ore Formation, the Kolhan Shales show evidence of tectonic disturbance in the form of minor overturned isoclinal folds, numerous quartz veins (some of which are folded) and in the development of cleavage. It is remarkable however that major part of this Formation does not show any appreciable effect of the younger Singhbhum Orogeny (905-934 Ma, Sarakar & Saha, 1964). This is probably partly due to the distance of these rocks from the Copper-belt thrust zone and partly due to the blanketing effect of the basement Granite which acted as a shield to absorb the southwards directed thrust movements. In contrast where the basement consists of the incompetent Iron Ore phyllitic Shales, the Kolhan are highly disturbed with the development of minor folds, cleavage folds and minor faults (Fig.3).

C. Lithofacies

Six lithofacies have been recorded and are described individually as, 1. Granular lag facies (GLA) 2. Granular sandstone facies (GSD) 3. Sheet sandstone facies (SSD) 4. Plane laminated sandstone facies (PLSD) 5. Rippled sandstone facies (RSD) 6. Thin laminated sandstone facies (TLSD).

Granular lag facies (GLA): Granular lag facies, which directly overlies Singhbhum granite, is reddish brown in color and consists of moderately to poorly sorted, sub rounded to rounded pebbles of chert, vien quartz, phyllite, jasper and granite. It is characterized by the occurrence of laterally impersistent, massive, ungraded and fine matrix supported conglomerate which

is oligomict in character towards south and polymictic towards north. These conglomerates are mostly immature to sub-mature, and quite similar to the overlying sandstone (Fig. 4a-b). This fine matrix-supported GLA facies can be characterized as a more or less laminar, cohesive flow of relatively dense, sediment-fluid mixture of plastic behavior. Clasts float on the debris as a result of small density variation between the clasts and the debris, plus the cohesive strength of the clay-water slurry.

Granular sandstone facies (GSD): The GLA facies is overlain by reddish brown to brown color granular sandstone (GSD) facies. This facies is characterized by moderately to well sorted, moderate clast:matrix ratio, textural bimodality and development of normal grading with fining upward sequence. Planar cross-stratification is more commonly found in compare to trough cross-stratification (Fig. 4c-d).

Sheet sandstone facies (SSD): The SSD facies is defined by sheets of sub arkose and quartz arenite, sometimes intercalated with thin laminated siltstone. The facies shows profuse development of planar cross bedding (Fig. 4e) and locally developed herringbone cross-bedding (Fig. 4f).

Plane laminated sandstone facies (PLSD): The PLSD facies (Fig 5a) is defined by thick amalgamated well sorted sub arkose and quartz arenite, with a moderate - high grain: matrix ratio. The sandstone is medium to fine grained. The prominent structures are planar cross bedding (Fig. 5f), wavy lamination (Fig.5b), washed out/flat top ripples (Fig. 5e), herringbone cross-bedding (Fig. 5c) and antidunes (Fig. 5d). The wavy

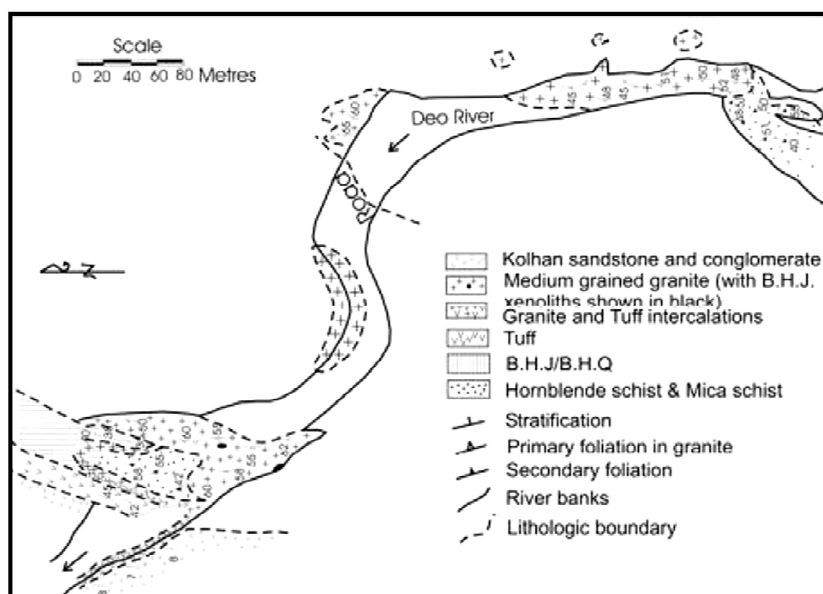


Fig. 3. Field relationship between Kolhans, Singhbhum granite, IOG and OMG rocks as seen in the Deo river section near Jagannathpur (Sarkar and Saha, 1977).

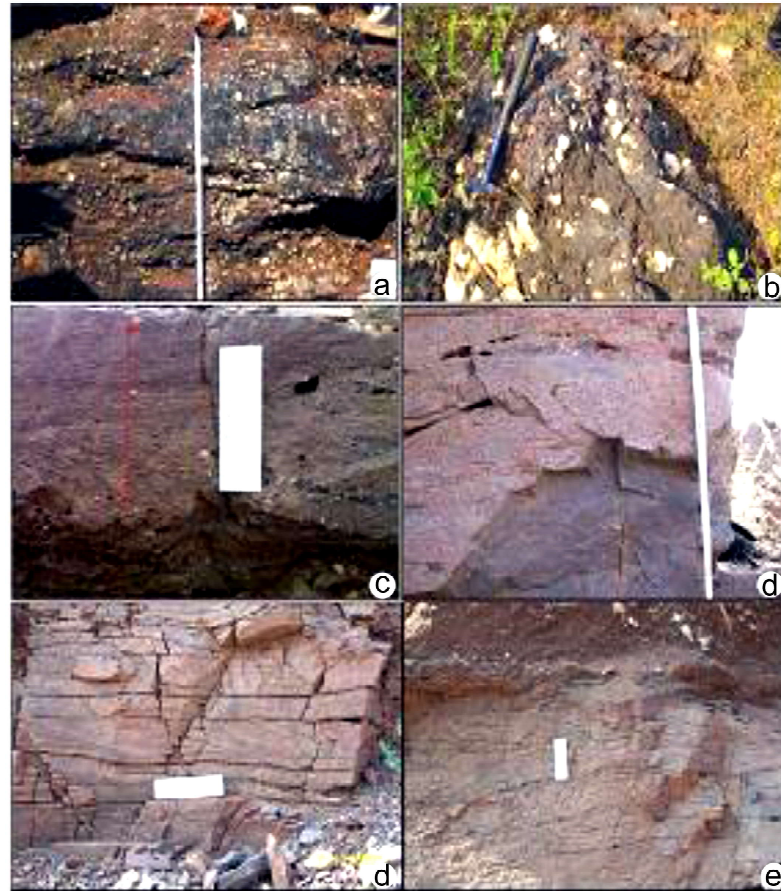


Fig.4a-b. Polymictic conglomerate with pebbles and granules of jasper, white chert, sandstone, banded hematite jasper (BHJ), quartzite fragments, volcanic and granitic rock fragments embedded in sandy-silty matrix (GLA facies). Scale: 45 cm. Location: Deo river section, Jagannathpur (a), Scale: Hammer. Location: Matgamburu (b). **c.** Pebbly sandstone at Rajanbasa showing upward fining sequence (GSD facies), 15 cm scale, **d.** Pebbly sandstone at Matgamburu (GSD facies) Note: outcrop thickness- 50 cm. **e.** Sandstone with sheet like morphology showing occurrence of planar cross stratification (SSD facies). Location: Matgamburu, Scale-15 cm. **f.** Herringbone cross bedding in sheet sandstone. Location: Rajanbasa, Scale- 15 cm.

lamination beds occur with thin ripple laminated shale parting between two successive beds. Sandstone beds in this facies tend to be sheet like with almost constant bed thickness.

Rippled sandstone facies (RSD): This facies is defined by predominance of packages of rippled sandstone with prolific development of both symmetrical and asymmetrical ripples (Fig. 6a), herringbone cross-bedding, hummocky cross-stratification and multiple toe scour like structures (Fig. 6b). It is very commonly associated with thinly laminated sandstone facies and plane laminated sandstone facies.

Thin laminated sandstone facies (TLSD): This facies is defined by the rhythmic alternation of sandstone and shale units (fig. 6c), in which sandy layers are thicker than shale layers. Prominent structures are convolute lamination (Fig. 6e), planar cross bedding (Fig. 6f) and asymmetrical ripples.

D. Lithologs and Fence Diagram

Chamakpur-Keonjharh Sub-Basin

Refer to Fig. 7 and Fig. 8

Chaibasa-Noamundi Sub-Basin

Refer to Fig. 9 and Fig. 10.

All the six lithofacies observed shows variation in the two sub-basins which are mapped (Fig.11 and Fig.12).

IMPLICATIONS FOR BASIN TECTONICS VIS-À-VIS HALF GRABEN TECTONICS

Active extension or stretching of continental lithosphere and high heat flow due to the effects of normal faulting and the resultant changes in crustal and mantle thickness, structure and state. The tectonic

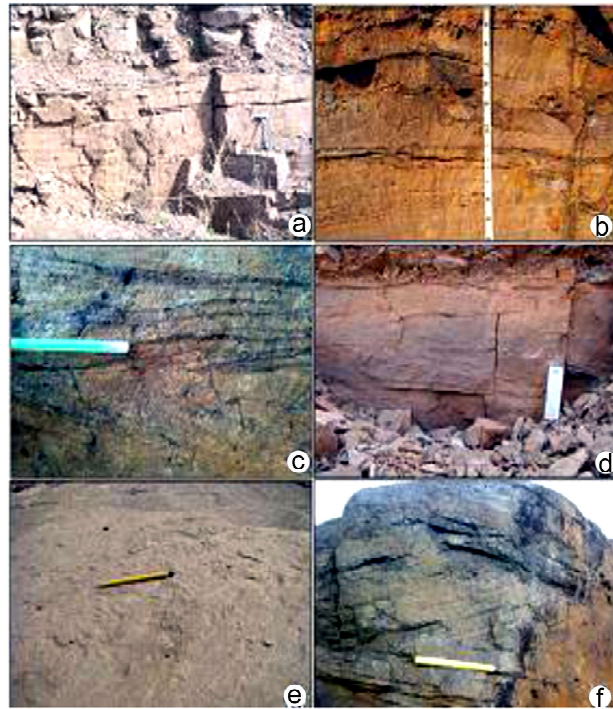


Fig. 5a-b. Wavy lamination/antidune in PLSD facies at Matgamburu, **c.** Herringbone cross bedding at Deo river section, Scale; Pen, 12cm. **d.** Antidune and low angle bar cross stratification at Gumua Gara river section, Scale:12cm. **e.** Washed out ripples/ flat top ripples with some current ripples, Scale: Pencil, 10cm, **f.** Planar cross bedding at Deo river section, Scale: Pen, 12cm.

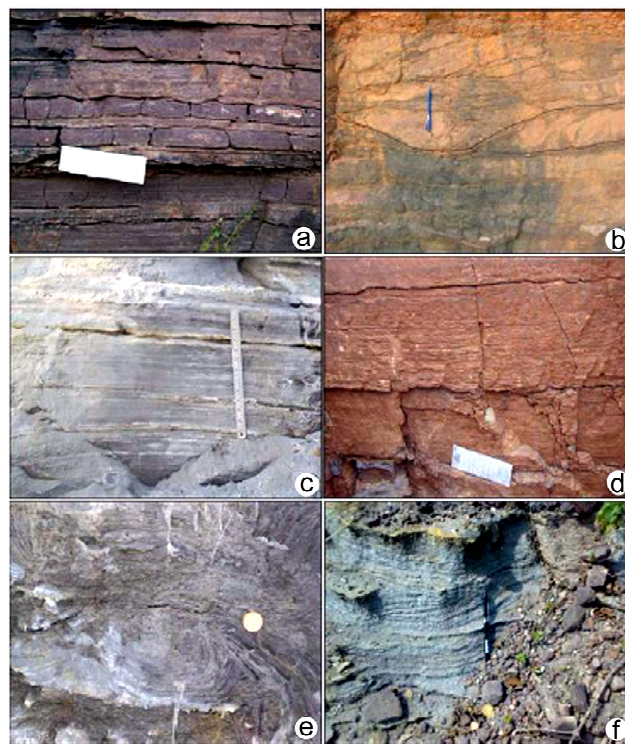


Fig. 6a. Rippled sandstone (RSD facies) with asymmetrical ripple marks location Bistampur, Scale: 12cm. **b.** Cross bedded unit with multiple toe scour like structure location Gumua Gara river section, Scale: Pen, 12cm. **c.** Rhythmic sandstone with alternate layers of sand and mud with thicker sand layer, location Bistampur, Scale: 30cm. **d.** Thinly laminated sandstone at Matgamburu, Scale: 12cm. **e.** Convolute lamination in rhythmic sandstone, 2.5cm diameter coin for scale, **f.** planar cross bedding in rhythmic sandstone, location Bistampur, Scale: Pen, 12cm.

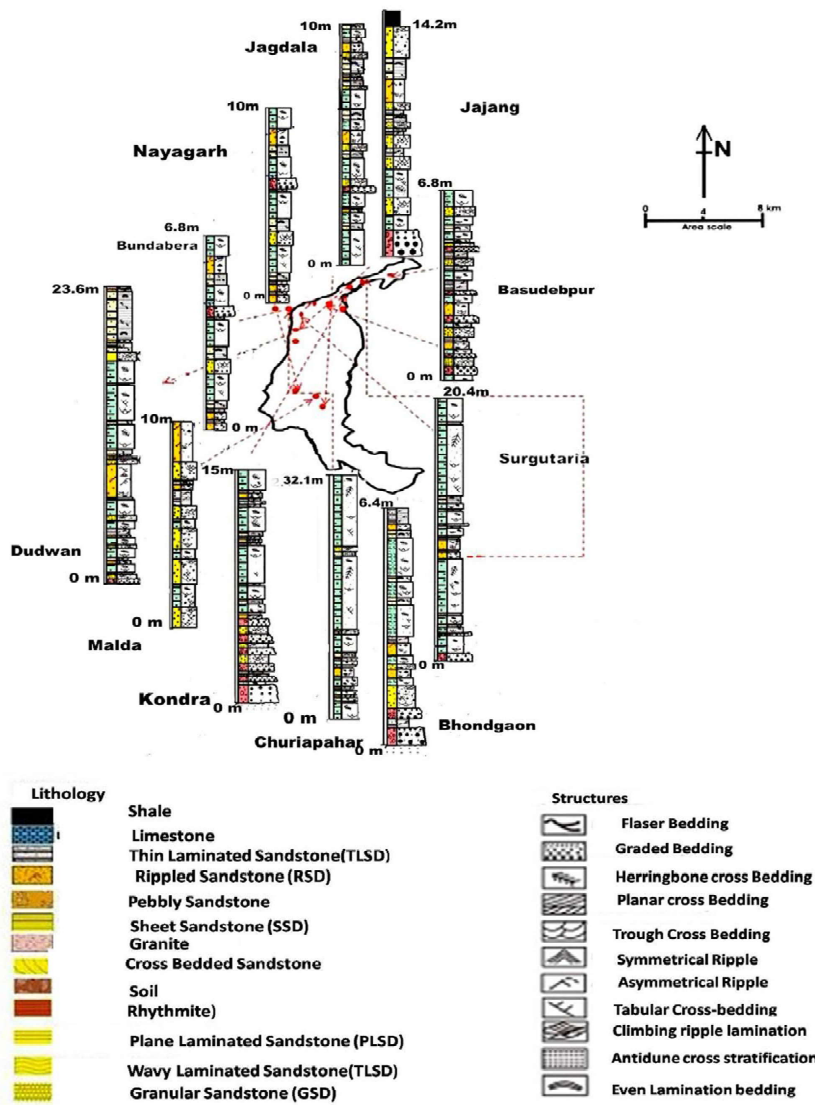


Fig. 7. Lithologs from different sections of the Sub-basin(0 m indicates Mean Sea Level).

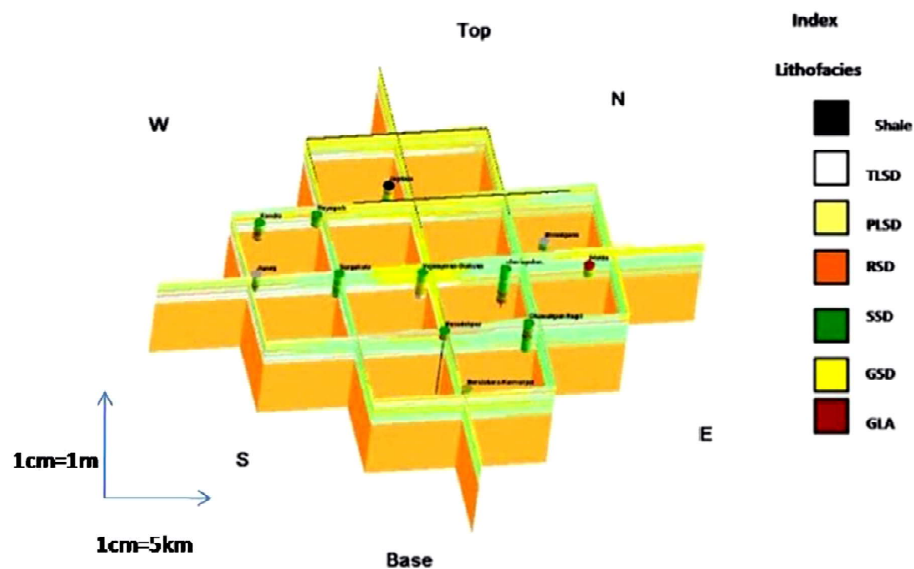


Fig. 8. Fence diagram showing facies variation across the sub-basin.

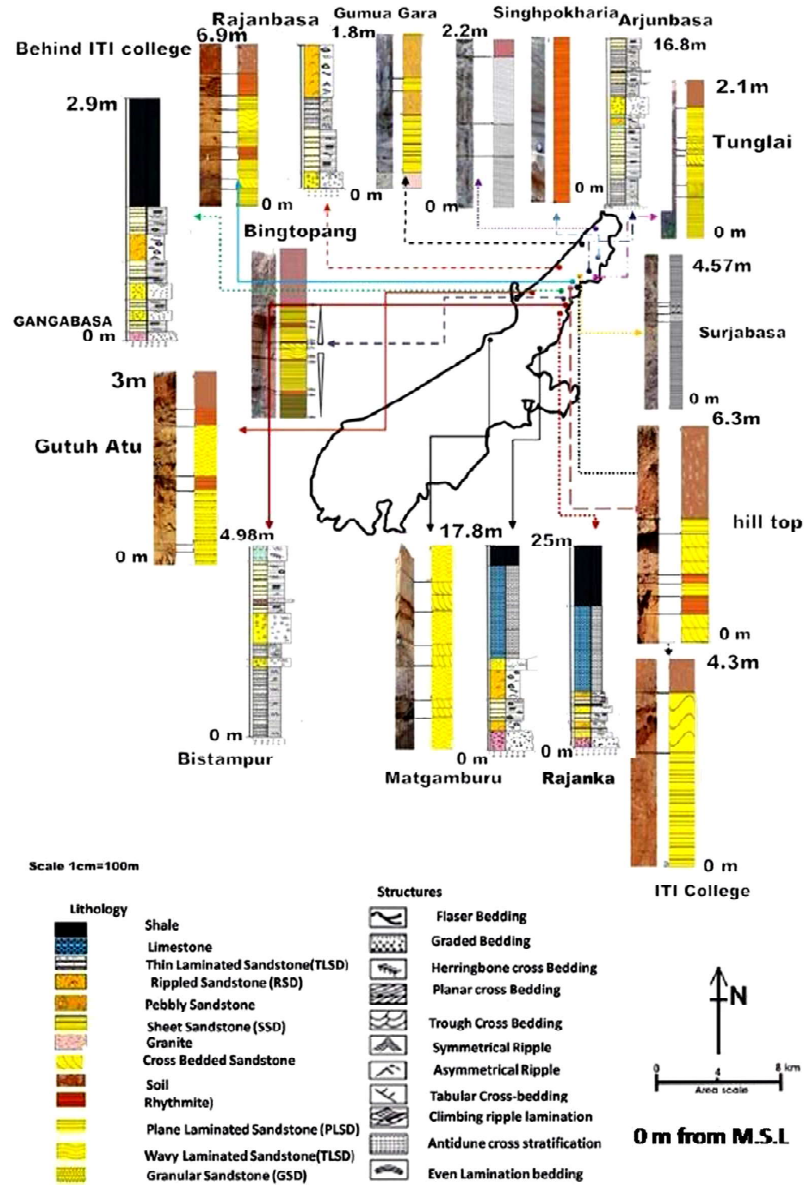


Fig. 9. Lithologs from different sections of the Sub-basin.

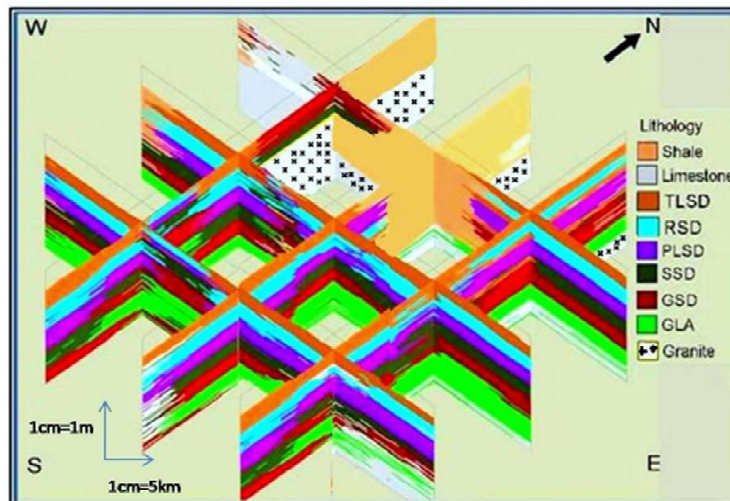


Fig. 10. Fence diagram showing facies variation across the sub-basin.

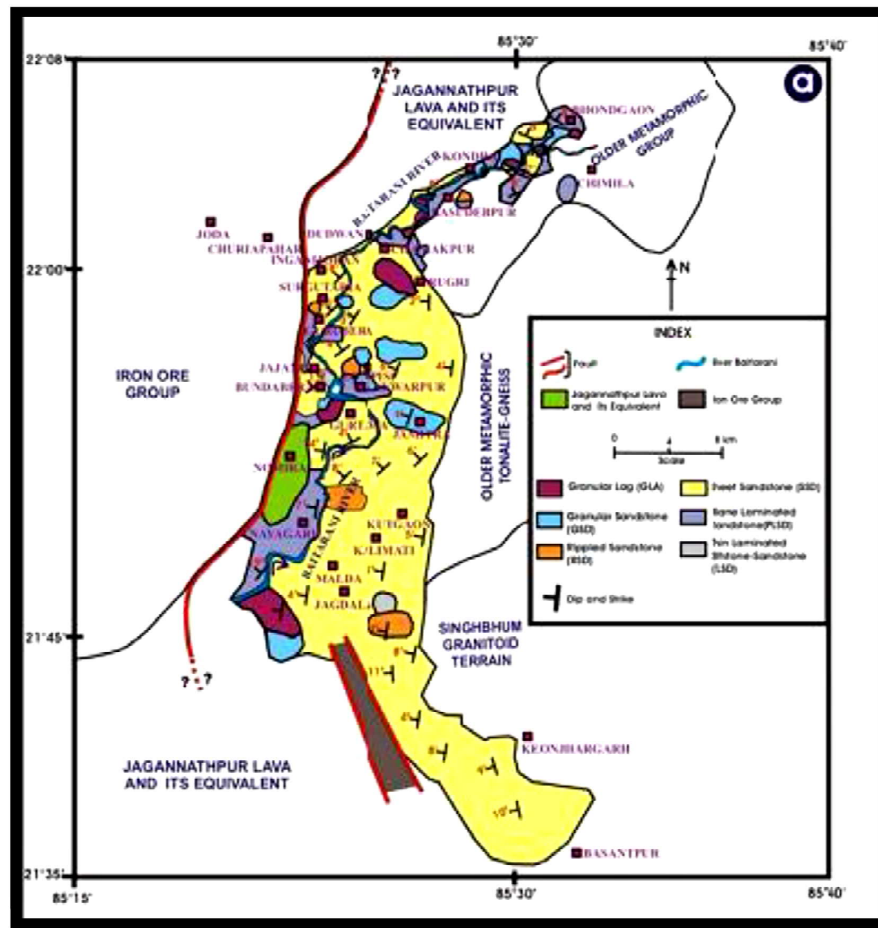


Fig.11. Geological map of the Kolhan basin around Chamakpur-Keonjhar showing the spatial distribution of the six lithofacies(Modified after Saha,1994).

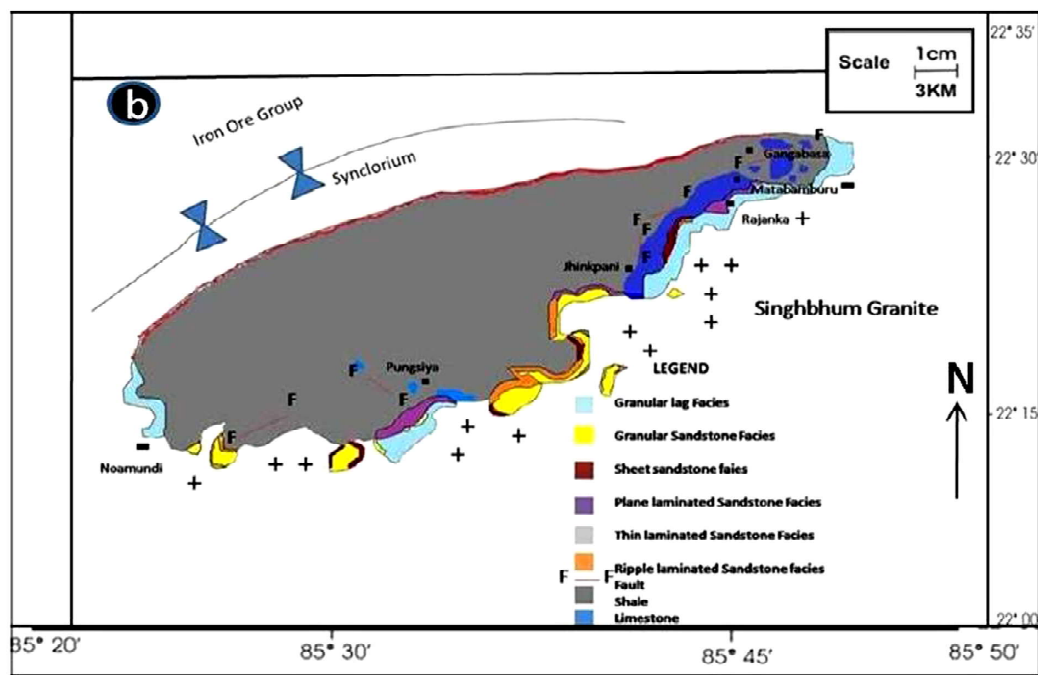


Fig.12. Geological map of the Kolhan basin around Chamakpur-Keonjhar showing the spatial distribution of the six lithofacies (Modified after Chatterjee and Bhattacharya, 1969).

environment of stretching is controlled by regional plate motions. Extension may occur in a variety of geodynamic settings, including continental crust adjacent to back-arc basins, continental interiors and thickened crustal orogens. Rifting may be passive (i.e. closed system, where the input of asthenospheric mass from outside the stretched lithosphere occurs passively as a response to lithospheric thinning) or active (i.e. open system, where rifting is accompanied by the eruption of voluminous volcanics, and the initial rising of the asthenosphere is independent of the magnitude of lithospheric extension.

A. Map and Sections

Change in dip and strike orientation of the fault evident from mapping of the structural data. Given are the map (Fig.13 and 15) showing structural data of two sub-basins. The strike of the boundary fault with IOG changes from NE to SW along with the dip which is steeper in the Chaibasa-Noamundi Basin and becoming progressively shallower toward the Chamakpur-Keonjhar Basin. The geophysical cross-sections

(Verma et al., 1984) shows the asymmetric half-graben nature of the basin (Fig.14 and Fig.16).

B. Field Evidences of Fault

Moreover field evidences of fault scarp, gouge (Fig.17 and Fig. 18) are potential supporter of the fact that there was a dominant fault activity within both the sub-basins.

C. Predicted Basin Filling Models In Kolhans

As revealed from field photographs, geological maps and geophysical sections alongwith variations of lithofacies in the two sub-basins with change in nature of dip and strike of the fault, it can be assumed that the basic structural element of a continental rift is now thought to be a half graben comprising a single basin-bounding fault with several intrabasinal faults.

Half-Graben Basin Filling Model:

Several structural models have been proposed for half graben development of which one appears more

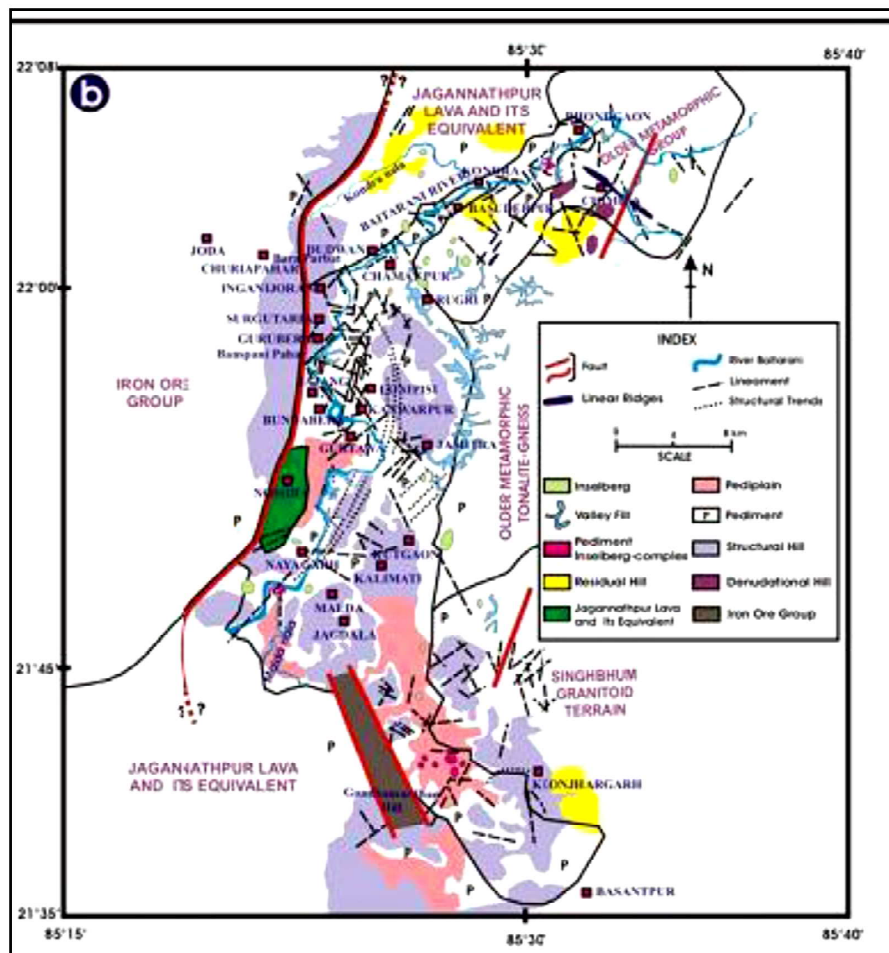


Fig. 13. Map of the Kolhan basin showing the structural control over the morphometric developments. (Modified after Saha, 1994).

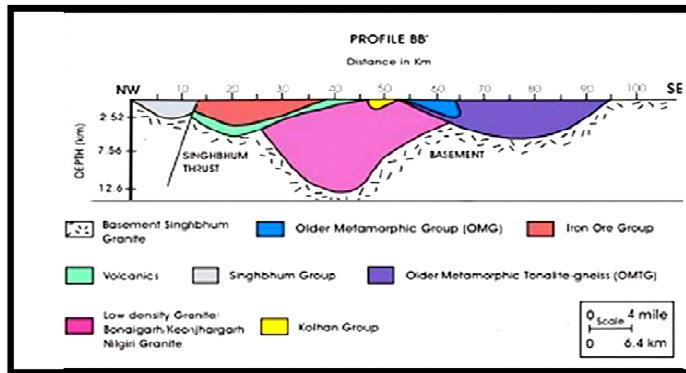


Fig.14. Geophysical Cross Section. Profile BB' across Singhbhum Group, IOG rocks, volcanics, Kolhan Group, and Older Metamorphics based on gravity data (Verma *et al.*, 1984 p.106). The thickness of the Kolhan basin is around 1.5 km. The Half-graben nature of the Kolhan basin shown in yellow is prominent.

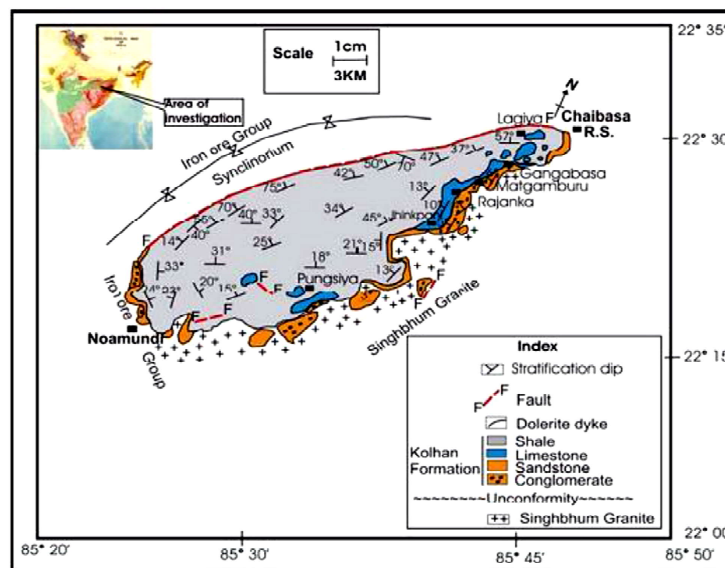


Fig.15. Geological map of the Chaibasa-Noamundi basin (Chatterjee and Bhattacharya, 1969) showing the structural control over the morphometric developments.

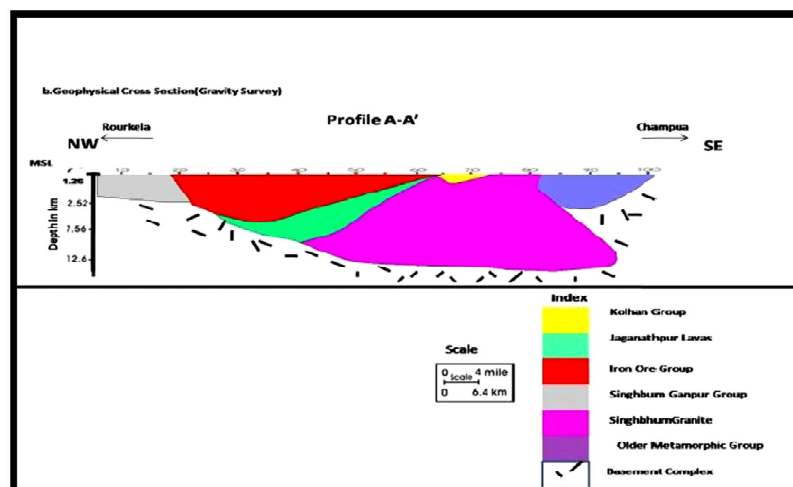


Fig.16. Geophysical Cross Section. Profile A-A' across the IOG rocks, volcanics, and Kolhan Group based on gravity data. (Verma *et al.*, 1984 p.106). The thickness of the Kolhan basin is around 1.5 km. The Half-graben nature of the basin can be seen marked in yellow.

probable in this context is that of listric normal faults, which terminate downwards into subhorizontal detachment faults of regional extent and fault blocks are highly rotated. It is presumed in this model that:

- In the initial stage the fault model incorporates an intrabasinal fault that soles into a sub-horizontal detachment fault; the change in the rate of increase in the volume of the basin during uniform fault displacement is zero (detachment type) (Groshong, 1989).

- Both basin-bounding faults, intrabasinal faults and the intervening fault blocks rotate during extension and as a consequence, there is a change in the rate of increase of the volume of the basin (domino type) (Wernicke & Burchfiel, 1982).

- During the fault growth models, the Kolhan basin grew both wider and longer through time as the faults lengthen and displacement accumulates; the change in the rate of increase in basin volume is positive (Gibson et al., 1989).

- Basin fill commonly forms a fanning wedge during fluvial sedimentation, whereas lacustrine strata tend to pinch out against older synrift strata.

The transition from fluvial to lacustrine deposition and hanging wall onlap relationships observed in the individual basins of Kolhans are best explained by these basin filling models (Fig. 19) (Schlische 1991).

Flexural-rotation (rolling hinge) model:

The second model that can be applied is that of a flexural-rotation (rolling hinge) model as proposed by (Seyitoglu, 2002), where an initially high-angle normal fault is progressively rotated to lower dips by isostatic uplifting resulting from tectonic denudation. Beneath these areas of extension, however, there is no upwarping of the Moho as would be anticipated if isostatic compensation of the extension occurred within the mantle. Thus, it is possible to find both heterogeneous upper crustal strain and uniform deep crustal structure across extensional domain boundaries resulting from the effects of intracrustal isostasy.

DISCUSSION

The tectonic set-up of the NE-SW trending Kolhan basin possibly relate to the basin opening to the E-W extensional stress system that prevailed during the development of the Newer Dolerite dyke system. The Paleoproterozoic age of the Kolhan basin is based on the consideration of the conformable stress pattern responsible both for the basin opening and the development of the conjugate fracture system veneered by the swarm of Newer Dolerite dykes.

The location of half-graben development during a syn-Kolhan extensional regime is likely to have been reactivation along the Singhbhum shear zone (SSZ). Cratonic sutures such as the SSZ may have been prone to reactivation during any subsequent tectonic episodes, leading to complex structural and sedimentological relationships as basins are created, inverted and superimposed along a long-lived shear zone throughout successive tectonic regimes.

The Kolhan is as an example of sedimentary response to changing tectonic regimes associated with the SSZ. The tectonism responsible for sedimentation and deformation of the Kolhans may be related to a ca. 2.0-2.2 Ga tectonic event or by intra-cratonic reactivation of structures within a previously assembled greenstone belt. The Kolhans, which may have been deposited in a half-graben set-up, unconformably overlie the Singhbhum granite. This establishes a sequence of tectonic regimes of north-south orientated compression, tectonic quiescence, denudation and north-south orientated extension, following the 2.0 Ga event in the Singhbhum region. The syn north-south orientated extension in the region may have been related to orogenic collapse of the Singhbhum shear zone.

The N-S oriented syn-Kolhan extensional regime may reflect basinal collapse after the cessation of N-S orientated compression by collision or reactivation tectonics in the Singhbhum orogeny.

The sedimentary rocks preserved in the trough-shaped Kolhan basin are older and thicker to the south,



Fig.17. Fault scarp present in Chaibasa Noamundi Sub-Basin.



Fig.18. Fault gouge present in Chaibasa Noamundi Sub-Basin. Scale Hammer-31cm.

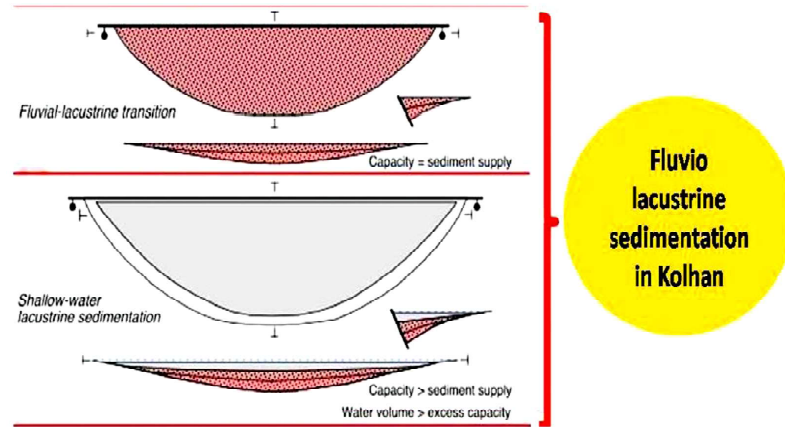


Fig. 19. Filling of an evolving half-graben basin shown in map view alongwith longitudinal cross section, and transverse cross section. Dashed line represents lake level. The relationship between capacity and sediment supply determines whether sedimentation is fluvial or lacustrine. For lacustrine sedimentation, the relationship between water volume and excess capacity determines the lake depth. Modified from Schlische and Anders (1996).

reflecting a single continuous period of sedimentation, with no evidence of stratal unconformities. As sedimentation appeared to have comprised predominantly of sandy bed load river systems with no evidence for rapid uplift of source areas, it is quite likely that the sedimentation occurred as a response to continuous downwarping and faulting. The Kolhan trough did develop almost perpendicular to the inferred edge of the craton, and that it has extended a considerable distance towards the craton interior (correlates of the Kolhan Group can be traced southwards and southwest wards for several kilometres).

General depositional models for sedimentation in half-graben set-up incorporate large-scale alluvial fans entering the half-graben from the low-gradient footwall. Significantly, the model predicts a contrasting facies change between the transverse alluvial fans and the major longitudinal trunk rivers flowing along the axis. The presence of lacustrine-related facies within the Kolhans proves significant development of lake sedimentation caused by interior drainage within the half-graben.

CONSTRAINTS

Sedimentation rates are generally difficult to determine in most continental strata (Schlische, 1991).

In a half-graben basin, the fluvial-lacustrine transition might occur as a consequence of decreasing the volume of sediment entering the basin per unit time or increasing the capacity of the basin, perhaps as a result of some tectonic event. However, it is noted that even if the volumetric sedimentation rate is constant, initial fluvial sedimentation will eventually give way to lacustrine sedimentation, reflecting the critical moment when the available supply of sediment no longer can completely fill the growing basin (Schlische, 1991).

The effects of erosion or sediment compaction are not considered. (Schlische, 1991).

Litho-facies variation is reverse in both the sub-basins and the boundary fault is opposite dipping. The intrabasinal faults play major role in sedimentation.

CONCLUSIONS

The fluvial environment of deposition recorded in the Paleoproterozoic Kolhan sediments of Chamakpur-Keonjhar basin, reflect variations in the rate of generated accommodation space. Six lithofacies recorded are arranged, in two genetic sequences, within the succession. The lower sequence records little available accommodation space with a high degree of reworking, which resulted in sheet-like, high-energy, bed load-dominated, braided fluvial deposits that lacked recurrent facies patterns. Channel deposits in the lower sequence reflect mixed-load, braided fluvial systems on stable channel banks with a low-moderate gradient. The channels retained an overall braided character with no evidence of meandering, despite indications that large fluctuations in discharge occurred within the mixed-load streams. As accommodation space increased upwards, the rate of reworking of the sediments was reduced, resulting in alternating fining and coarsening-upward sandstone-shale sequences. This led to the formation of alternation of sheet sandstones and sand-streaked siltstone-shale. The sheet sandstones record evidence of high-energy, unconfined ephemeral fluvial flash-flood deposition, internal erosion, and growth surfaces, while the shale-siltstone are interpreted to represent sand flat deposits. Variations in the style and order of the bedding contacts show that the deposits are products of subaqueous dune, bar, and channel migration. An expansion of braided channels may be present, which result in the formation of multilateral and multistoried sandstone bodies. The climatic change is the cause for the

reduced bed-load input seen in the overlying succession, which resulted in the ephemeral deposition style.

Repeated fault-controlled uplift of the source, followed by subsidence and basin margin progradation, generated multiple fining-upward cycles and a prograding fan-delta system in the Chaibasa-Noamundi Basin. The marked variations in thickness of the delta succession and the stacking pattern in different measured profiles reflect the overriding tectonic controls on delta evolution. The accumulated fault displacement in active sectors created higher accommodation and thicker delta sequences. Intermittent uplift of fault blocks exposed fresh bedrock to mechanical weathering, generated a large amount of detritus, and resulted in forced regressions, repeatedly disrupting the fining-upward pattern. The controls of source rock lithology or climate were of secondary importance to tectonic effects. Prograding fan deltas are rarely reported and may be a stratigraphic response of

connected rift basins at the early stage of extension. All the three end member half graben basin filling tectonic models are applicable in the Kolhans.

Fluvio-lacustrine sedimentation pattern that is taking place as we slowly move from one sub-basin to another and onlap of younger strata onto pre-rift rocks in the Kolhan is best explained by the half-graben basin filling tectonic models. Changing volumetric sedimentation rate along with the capacity of the basin is the controlling parameter for the development of fluvio-lacustrine facies in the Kolhans in spite of some constraints. The flexural-rolling hinge model unites two separate basins of Chamakpur-Keonjhar and Chaibasa-Noamundi with hinge point situated in between them as shown in map.

Acknowledgments: The author is grateful to the Head of Department of Geology and Geophysics, IIT Kharagpur for his constant support during the research work.

References

- Bandhopadhyaya, P.C. and Sengupta, S. (2004). Paleoproterozoic Supracrustal Kolhan Group in Singhbhum Craton, India and the Indo-African Supercontinent. *Gondwana Research*, 7 (4), 1228-1235.
- Chatterjee B.K and Bhattacharya, A.K. (1969). Tectonics and sedimentation in a Precambrian Shallow Epicontinental Basin, *Jour. Sedimentary Petrology*, 39 (4), 1566-1572.
- Dalabehera, L. (2009) Paleocurrents and paleohydraulics of Proterozoic Kolhan sediments in Chamakpur-Keonjhar basin, Orissa, India. *Int. Jour. Earth Sci. Engg.*, Vol: 2(1), 20-31.
- Gibson, J. R., Walsh, J. J., and Watterson, J. (1989). Modelling of bed contours and cross-sections adjacent to planar normal faults: *Journal of Structural Geology*, v. 11, p. 317-328
- Groshong, R. H. (1989) Half-graben structures: Balanced models of extensional fault-bend folds; *Geological Society of America Bulletin*, 101(1), 96-105.
- Gui, B., He, D., Chen, W., Zhang, W. (2014). Migration of growth axial surfaces and its implications for multiphase tectono-sedimentary evolution of the Zhangwu fault depression, southern Songliao Basin, NE China, *Jour. of Geodynamics*, 75, 53-63.
- Roy, A.K., Kroner, A., Rathore, S., Laul, V. and Purohit, R. (2012). Tectono-metamorphic and Geochronologic studies from Sandmata Complex, northeast Indian Shield: implications on exhumations of Late Palaeoproterozoic granites in and Archaean-early Palaeoproterozoic granite-gneiss terrane, *Journal of Geological Society of India*, 79, 323-324.
- Sarkar, S.N. and Saha, A.K. (1977). The present status of the Precambrian stratigraphy, tectonics and geochronology of Singhbhum-Keonjhar-Mayurbhanj region, Eastern India. *Ind. Jour. Earth Sci.*, Prof. S. Ray, 7-65.
- Saha, A.K and Sarkar, S.N. (1988). Early history of the earth. Evidence Eastern Indian Shield In: Mukhopadhyay, D. (Ed.), *Precambrian of the Eastern Indian Shield*. *Mem. Geol. Soc. Ind.*, 8, 13-37.
- Saha, A.K. (1994). Crustal Evolution of Singhbhum-North Orissa, Eastern India, *Memoir Geological Society of India*, 2, 341.
- Schlische, R. W., (1991). Half-graben filling models: New constraints on continental extensional basin development: *Basin Research*, 3, 123-141.
- Schlische, R.W., and Anders, M.H. (1996), Stratigraphic effects and tectonic implications of the growth of normal faults and extensional basins, in Beratan, K.K., ed., *Reconstructing the History of Basin and Range Extension Using Sedimentology and Stratigraphy*: Boulder, Colorado, Geological Society of America Special Publication, 303, 183-203.
- Seyitoglu, G., Tekeli, O., Cemen I., Sen S. and Isik, V. (2002). The role of the flexural rotation/rolling hinge model in the tectonic evolution of the Alaşehir graben, western Turkey, *Geological Magazine*, 139, 15-26.
- Schlische, R.W., and Anders, M.H. (1996). Stratigraphic effects and tectonic implications of the growth of normal faults and extensional basins, in Beratan, K.K., ed., *Reconstructing the History of Basin and Range Extension Using Sedimentology and Stratigraphy*: Boulder, Colorado, Geological Society of America Special Publication, 303, 183-203.
- Verma, R.K., Sarma, A.U.S. and Mukhopadhyay, M. (1984). Gravity field over Singhbhum, its relationship to geology and tectonic history. *Tectonophysics*, 106, 87-107.
- Wernicke, B., Burchfiel, B.C. (1982). Modes of extensional tectonics. *Journal of Structural Geology*, 4, 105-115.

Stratigraphic Implications of Seismites on Carbonaceous Shales within Siliciclastic Jhuran Formation in Western India

ASHWIN ARORA

Department of Earth Sciences, Indian Institute of Technology Bombay, Powai, Mumbai-400076
Email: ashwinarora.iitb@gmail.com

Abstract: This study presents occurrence of seismically-originated, basin-wide soft-sediment deformation structures within the predominantly siliciclastic Kimmeridgian-Tithonian Jhuran Formation of Kutch basin in western India and discusses its implications. Resting unconformably on the Dhosa Oolite, the Jhuran Formation exhibits overall shallowing upward trend and is unconformably overlain by the Cretaceous Bhuj Formation. The overall coarsening upward, three-tiered Jhuran Formation, deposited during the active rifting phase of the Kutch basin, exhibits thick organic-rich shale in the lower and middle segments, which are intervened by siltstone and sandstone interbeds of storm origin with variable thicknesses. Each of the lower two segments of the Jhuran Formation is marked by shallowing upward cycles, beginning with black shale of middle shelf to prodeltaic origin and terminating with deltaic sands. The black shale exhibits organic matter-rich shale laminae, with subordinate siltstone beds, attaining a maximum thickness of ~28 m in the middle segment of the Jhuran Formation. Total organic carbon (TOC) content of black shale ranges from 1.1% to 4.8%, indicating existence of suboxic to anoxic conditions in the depositional setting. Three distinctly disturbed layers, exhibiting wide range of syn-depositional deformation structures, occur within a 17 m thick interval near the top level of Middle Member. Beds occurring above and below the disturbed interval, as well as those intervening the disturbed layers are completely unaffected by deformation. Decimeter to meter scale features, including ball and pillows, pseudo-nodules, ptigmatic folds, shear folds, detached and isolated lobes and growth faults, traceable for more than 165 km, are interpreted as seismic shock-induced structures. Small-scale loading, growth faults, flame structures, dewatering structures are possibly of non-seismic origin, owing to their local or isolated occurrences. The evidence suggests seismologically active sedimentation and deposition during the Late Jurassic time, which is related to rift tectonics. The seismic shock must have induced a major change in the depositional settings as organic-rich shale deposition, overlying the deformed interval, is terminated in the shallower parts and is considerably insignificant in the deeper parts of the basin. The seismic shock possibly disrupted the restricted and stratified character of the basin, which was favoring deposition of black shale, to form a more open-marine depositional conditions.

Keywords: Syn-sedimentary deformation (SSD), Seismites, Jhuran Formation, Black Shale.

INTRODUCTION

The Jhuran Formation within Mesozoic of Kutch has been reported and observed to contain multiple soft-sediment deformation due to disruption of strata prior to the lithification (Seth et al., 1990). These contortions and transformations within an isolated bed contained in regionally undeformed sedimentary record is essentially a result of shock experienced by the sediments, prior to compaction and consolidation. A local or small scale event maybe a result of in-situ soft sediment deformation, however when single or multiple, large scale layer confined event(s) is correlatable on a basin-wide extent, then its genesis on account of seismic triggers can be assumed with robustness (Seilacher, 1969; Allen, 1975; Mills, 1983; Moretti and Van Loon, 2014; Van Loon, 2014, Sarkar et al., 2014). Although multiple mechanisms such as unstable density gradients, wave loading, sediment overloading, undercutting, basinal over-steepening and/or seismicity may be

responsible for clastic soft-sediment deformation structures (SSDS) (Seth et al., 1990) but, the structures produced may not be diagnostic of an individual process (Van Loon, 2009; Van Loon et al., 2014). This makes the search for an unambiguous rock record of seismicity difficult, even though seismicity related SSDS are commonly bounded to specific laterally extensive stratigraphical intervals (Seth et al., 1990). The SSDS in seismites may differ in form, size and intensity, because different types of unconsolidated sediment react in different ways to the earthquake-induced shock waves (see Bizhu and Xiufu, 2015) as the proximity to the epicenter, differential loading, the thickness of the deformed layers and several other factors have varied responses. Detection of unmistakable fingerprints of seismic events in ancient sequences remains to be of paramount importance as it may provide a valuable insight into basin dynamics (see Seilacher, 1984).

The present work reports and signifies numerous types of basin-wide Syn-Sedimentary Deposits (SSDS)

present in siliciclastic Kimmeridgian-Tithonian Jhuran Formation of the Mesozoic Kutch mainland basin (Fig. 1) in Western India. The seismically induced SSDS, seismites (Seilacher, 1984; Van Loon, 2014) such as syn-depositional faults, preferential basal brecciation of shale, frequent local intra-formational unconformities, mechanically sieved reverse graded beds, and sand volcanoes have been earlier reported by Seth et al. (1990). However, its sub categories, newer SSDS, their stratigraphic and geographic extents, along with implications on sedimentation patterns were little discussed. This study attempts recognize newly observed SSDS and integrate it with basinal repercussions in a litho-facies backdrop.

GEOLOGICAL BACKGROUND AND REGIONAL FACIES

The Formation under study, Jhuran Formation also referred to as Katrol Formation (Rajnath, 1932; Waagen, 1975; Krishna et al., 1998) was deposited in a pericratonic rift basin (Biswas, 1981) (Fig. 1). The generalized Mesozoic lithostratigraphy of Kutch and detailed subdivisions of the Jhuran Formation and its comparison with stratigraphic classification proposed by Rajnath (1932), Krishnan (1956), is provided in Table 1. The palaeontological boundaries (Rajnath, 1932; Waagen, 1975; Krishna et al., 1998) and lithostratigraphic boundaries (Biswas, 1977) are devoid of field correlatability hence the lithostratigraphic column has been shifted in Table 1. The formation unconformably

overlies the Dhosa Oolite of the Jhumara Formation and is overlain unconformably by the Bhuj Formation (Biswas, 1978). The transition from a predominantly carbonate rich environment in Oxfordian-Callovian to Kimmeridgian siliciclastic environment was marked by siliciclastic Jhuran Formation. A major transgressive phase resulted in basin-wide deposition of carbonaceous shales at the base of the Formation. An overall coarsening-up prograding sequence is also observed during field studies of Jhuran Formation. The overlying fluvial Bhuj Formation resulted from major basin-wide regression (Bardhan et al., 1989; Vail et al., 1977 and 1991; Krishna et al., 2000).

The Jhuran Formation is divided into Lower, Middle, Upper and Katesar Members (Biswas, 1977). Out of these four members, the Middle Member black shales has been deposited basin wide (Biswas, 1993) and is exposed throughout the mainland Kutch. Both the Lower and Middle Member of the Jhuran Formation are composed mainly of finer, well sorted clastics, Upper Member is dominated by thick sandstone bodies with subordinate shales and siltstones. The Katesar Member is exclusive to the western fringe of the basin. The Jhuran Formation has been reported (Seth et al., 1990; Arora et al., 2015) to contain numerous bi-directional prod marks, wave ripples, hummocky and swaley cross stratifications (Table 2), which are exclusive to deposition within storm wave base. Along with ample siliciclastic terrestrial influx, remnants of plant fragments within black shale laminae indicate unambiguous continental provenance. The Jhuran Formation represents a facies succession similar

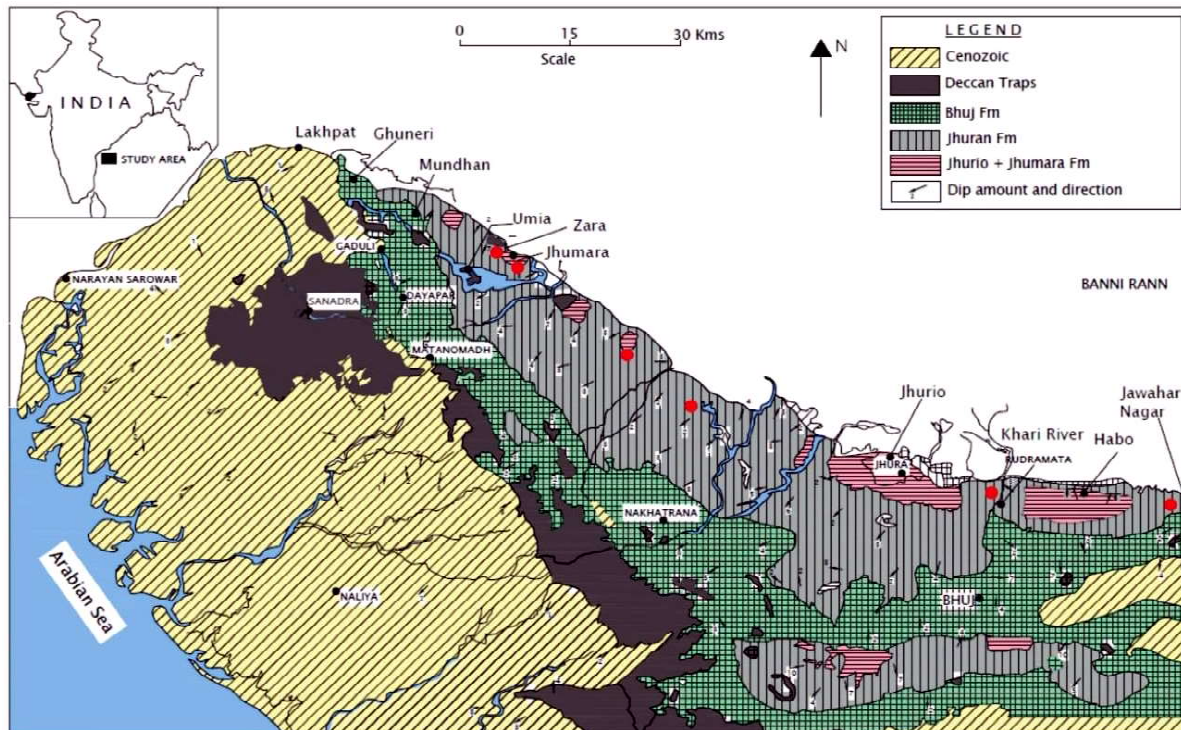


Fig. 1. A geological map (modified after Biswas, 1987), indicating extents the Jhuran Formation and solid red circles mark the observed localities.

Table.1. Stratigraphy of the Mesozoic succession of Kutch and detailed stratigraphy of the Jhuran Formation (Biswas, 1977) showing its relationship with Katrol Series (after Rajnath, 1932).

Age	Rajnath (1932)	Biswas (1977)	Members (Jhuran Fm)	Description	
Albian to ? Santonian	Umia Series	Bhuj Formation	Katesar (Tithonian to Valanginian)	Greenish grey to yellow, massive cross bedded sandstone with minor intercalations of shales, exposed only near Western margin near Katesar Temple.	
Aptian				Upper (Tithonian)	Predominantly arenaceous rocks. Red and yellow, massive cross bedded sandstone with intercalations of shales, siltstones.
Beriasian to Barremian					
Tithonian to Kimmeridgian	Katrol Series	Jhuran Formation	Middle (M. Kimmeridgian to Tithonian)	Predominantly shaley, dark grey to black shales, interbedded with ferruginous sandstones and laminated micaceous siltstone..	
Oxfordian to Callovian	Chari Series	Jhumara Formation	Lower (L. Kimmeridgian and older)	Alternating yellow and red sandstones and shale beds in almost equal proportion with some yellow fossiliferous, calcareous sandstones.	
Bathonian	Patcham	Jhurio Formation			

to those reported from ancient shallow shelves (Leithold and Bourgeois, 1984; Johnson and Baldwin, 1986; Bose and Das, 1986; Leckie, 1986; Reinson, 1992; Leckie and Reinson, 1993; Schieber, 1995; Aurther and Sageman, 2005; Suter, 2006).

Types of SSDS

The SSD structures that are observed are of multiple types and scales, and are listed as follows:

a. Sand Dyke

In the proximal part of the basin a near vertical, cylindrical, bifurcating, interconnected 8-12cm thick clastic dyke is present within the black shale facies (Fig.2d). There appears to be slight traces of crude lamination within the uniform grain sized dyke itself. The contacts of the dyke are sharp, straight or slightly sinuous with the adjacent, undeformed host shale beds. The base of the dyke is not observed in the outcrop.

Liquefaction along with fluidization processes may lead to the formation of fluid-escape structures. (Lowe, 1975 and references therein). Due to the presence of low permeability carbonaceous muds and their rapid burial, sand dykes may have been injected in the fissures/ fractures formed by pressure release from the underlying liquefied sand bodies (Potter and Pettijohn, 1977). There have been reports (Takashimizu and Masuda, 2000) of such dyke's formation due to a seismic

trigger, causing fluidization and escape of underlying unlithified sandy units. Dzulynski and Radomski (1956) had reported them also as a product of submarine slumping, but the absence of any such slump beds within proximity of these outcrops suits the former explanation. The wavy/sinuuous nature possibly indicates post burial lithification effects on both the injected dyke and the host medium.

b. Syn-sedimentary faults

Multiple occurrences of Syn-sedimentary faults are observed (Fig. 2b, 2c and 5c). This structural sequence is not more than 78cm thick and has a displacement of the order of few cm (av. 2cm). The top enveloping surface is sharp and abuts against undeformed lamination on top and the bottom enveloping surface gradually transitions to undeformed laminations. Seilacher(1969) identified these zones as liquefied zone, rubble zone, step-faulted zone and undisturbed sediment which were attributed to a seismic shock on unlithified fine grained sediments in quiet water basins. Furthermore, sudden shock stunned the development of deformational structures and made them static during early development thus devoiding them of major lateral transport. Prominently observed at multiple localities within the same horizon, this soft-sediment deformation may be interpreted as "seismites," and linked with growth faults being triggered by plasticization at the base while fluidization at top (Seilacher 1969, 1984).

Table 2. Summary table of facies assemblage observed within the coarsening upward Middle Member of the Jhuran Formation (adapted from Arora et al., 2015).

Facies	Detailed Description	Interpretation	Photograph
<p>A – Black shale</p>	<p>Thick beds of black shale with rare fine silt laminae ranging from a few mm to 2cm. Facies thickness ~ 6.8m, TOC – av. 3.4%. Shale beds are planar, massive or wavy laminated and have presence of few horizontal burrows and specs of plant fragments on bedding surfaces. Siltstone beds (fine-medium silt grain size) are hard, compact, with ferruginous cement and sharp lower contacts. Secondary sulfidic stains are present in a few horizons.</p>	<p>Deposition took place in deep sea conditions with minor silt input during episodic strong currents. Lack of circulation in the deep water column helped preserve organic matter. Absence of storm siltstone and sandstone beds is suggestive of deposition below the Storm Weather Wave Base (SWWB).</p>	
<p>B – Black shale with siltstone inter-bedding</p>	<p>Regular alternations between siltstone (av. 2cm) and black shale (av. 35cm). Facies thickness - 4.6m, TOC – av. 1.75%. Greater thickness and frequency of siltstone beds compared to facies A. Burrows are horizontal and vertical in nature. Siltstone beds are planar or ripple laminated, have sharp lower contacts and gradational top. Ripples are straight-crested with tuning fork bifurcations.</p>	<p>Increased frequency and thickness of siltstone beds indicate shallowing of depositional conditions as compared to Facies A. Sharp lower contacts of siltstones indicate storm action.</p>	
<p>C – Shale and siltstone alternations with minor sandstones</p>	<p>Black shale and siltstone (av. 4cm) alternations occasionally interrupted by thin sandstone beds (av. 6cm). Facies thickness - ?, TOC – av. 1.34%. Siltstone beds have planar or wavy laminated with NE-SW wave ripples and leaf impressions. Base of sandstone beds show NW-SE gutter casts.</p>	<p>Thin sandstones with gutter casts suggest storm action and deposition near Storm Weather Wave Base (SWWB).</p>	
<p>D – Siltstone-sandstone alternations</p>	<p>Siltstones (av. 8cm) and sandstone (av. 17cm) alternations with subordinate grey shale. Facies thickness - 7.4m. Black shales are absent. Sandstone beds have wavy and planar laminations along with crude normal grading. NE-SW straight-crested symmetrical wave ripples are present with tuning-fork bifurcation of crests. Bed base shows NW-SE gutter casts and bed undersurfaces show prod marks, groove casts and some flute casts.</p>	<p>Thick sandstone beds alternates with minor rippled siltstone indicates a proximal depositional condition.</p>	
<p>E – Plane laminated and hummock-swale cross-stratified sandstone</p>	<p>Hummock and swale cross-stratified, moderately well sorted sandstone alternating with planar laminated sandstone and minor siltstones. Facies thickness 47cm. Straight-crested ripples are present with tuning-fork bifurcation of crests. Mud clasts were observed at bed base along with NW-SE tool marks.</p>	<p>Presence of mud-clasts suggest high intensity storms causing erosion of underlying mud. Presence of erosional features like tool marks and absence of load casts suggest cohesive underlying mud.</p>	

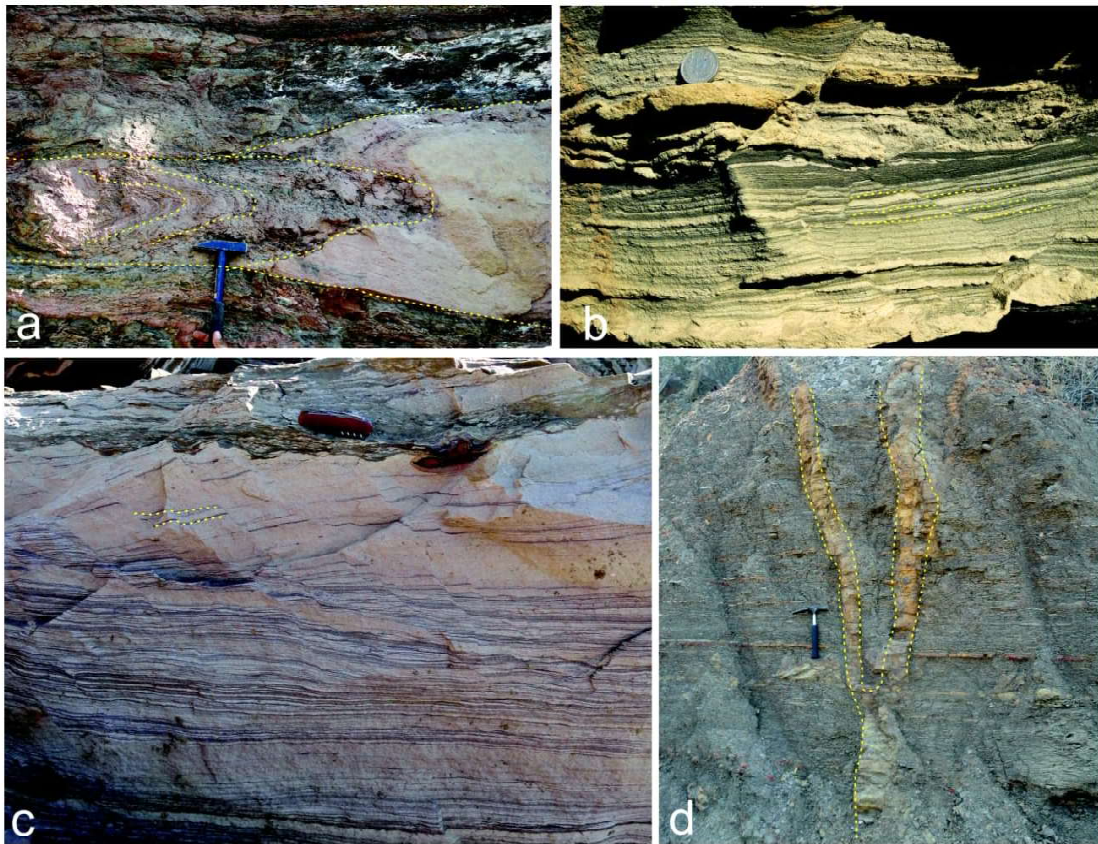


Fig.2a. An example of shock related folding and subsequent erosion of semi consolidated sandy units; **b & c.** Typical examples of graded faults resulting from seismic disturbances. Note the homogenized top of the faults while bearing segmented nature in the central portion, ultimately having undisturbed laminae at the base (see Seilacher, 1964); **d.** an example of classical sand injection dyke within a carbonaceous shale rich lithology.

c. Ball and Pillows

Throughout the study area, multiple ball and pillow structures of varying scales (0.08m to 1.2m) are observed (Fig. 3d, 3e). These structures are observed within lithologies of comparable grain sizes which range from fine-medium sand to coarse silt ranges. The features are layer confined and sandwiched between two totally undeformed sandstone layers. Along with balls and pillows, sand injections, small scale faults (Fig. 5c), multi lobate pillows and ptygmatic folds (Fig. 5b, 5d) are also observed. The descended lobes show a preferred direction possible indicative of palaeo- slope during the shock event. A combined effect of plasticization, liquefaction, fluidization and gravitational pull may be triggered by a seismic shock and may have yielded these large scaled structures in the present scenario (He et al., 2014).

d. Convolute beds:

Convolute beds occur at numerous levels within facies association C, D and E. Convolutions with a

height of meter scale are common and traceable (Fig. 3). Occasionally they are present in packages, with younger convolute structures truncating older ones (Fig. 3b, 3c). Affected individual layers may be as thick as 2.2m, and have no geometrical similarities of internal bedding structures with both underlying and overlying strata. Less commonly, these layers contain smaller centimeter scaled lobes with thoroughly deformed internal structures. In the basal part of some beds more complex and intense small-scale folding is also observed. The surfaces between the less and the more deformed parts within a layer or a set of layers are observed to be planar or slightly curved.

The isolated and unattached folds (Fig. 3b & 3d), present here in dominantly siltstones and sandstones, may have been a result of shock, which affected layers of contrasting density and rheology. The shearing in the host units creates plastic compressive deformation, necessary for ptygmatic folds to form. The absence of vertical loads at the time of the seismic shocks (in contrast with slumping) causes more “flattening” of the pillows and possible creation of the pseudonodules (Fig. 4e, 4f) (Mills, 1983).

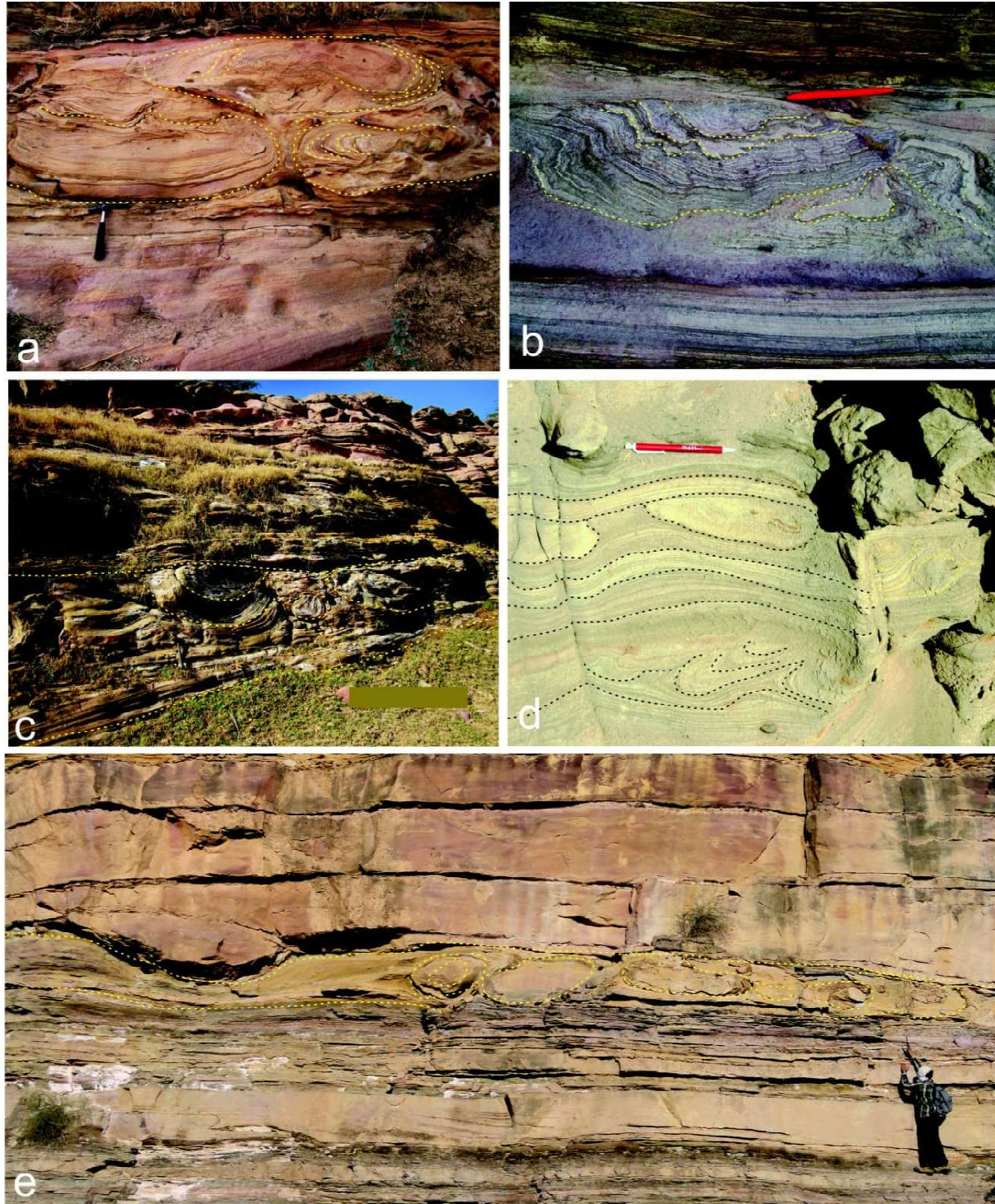


Fig. 3. (a-c) Examples of large scaled convoluted beds sandwiched in-between an otherwise undeformed lithology; (d, e) Small scale and large scale loading leads to formation of distinct load structures.

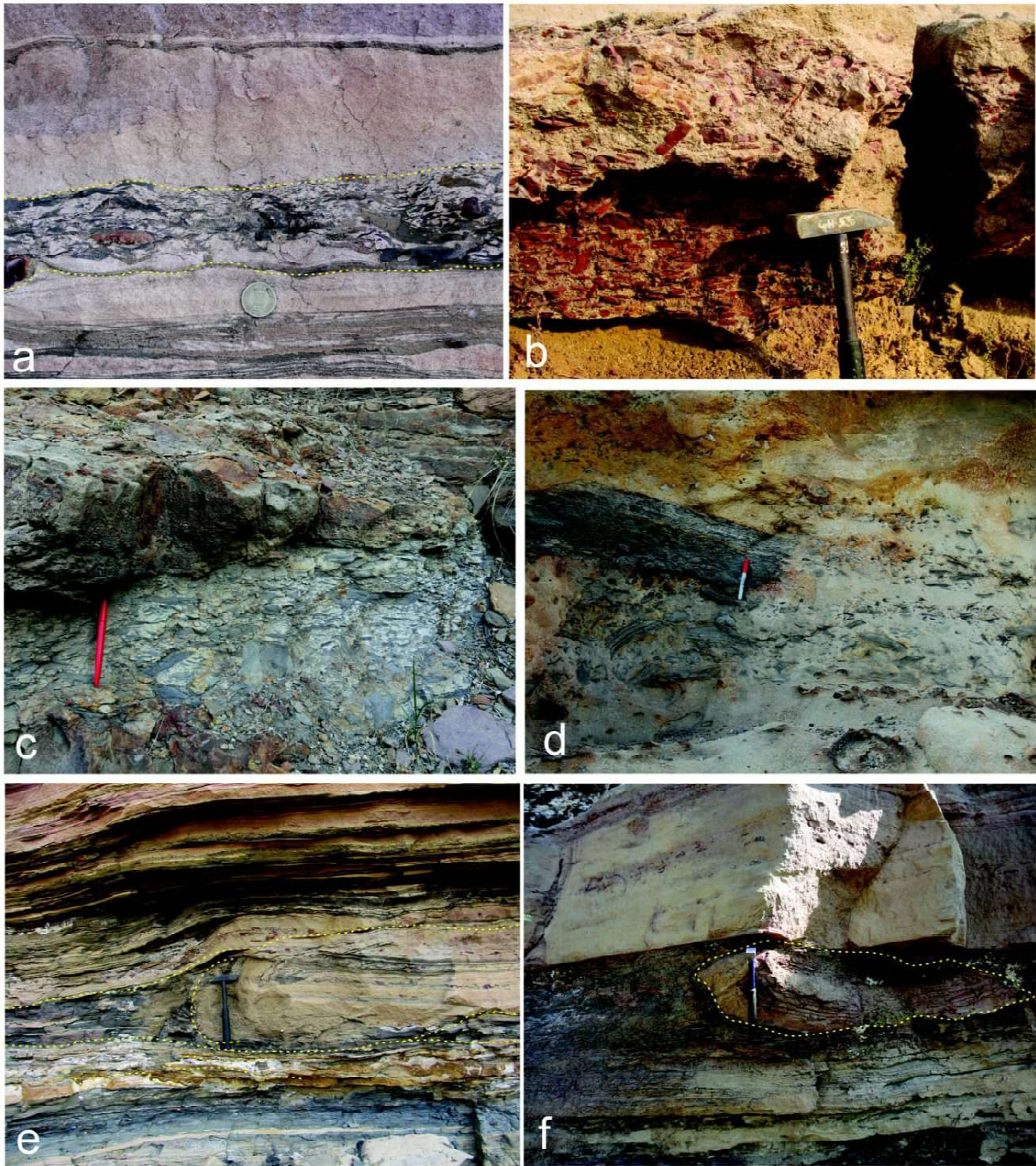


Fig. 4. (a-d) Multiple stages and degree of brecciation commonly observed. The clast sizes ranges from a few cm. (a) to more than half meter, (d) usually derived from underlying cohesive and plastically behaving shale lithologies. Note the consistent orientation of the clasts, (e, f) Advance stages of pillowing caused by sand loading in muddy substrate. sand locally thickened and overlying unconsolidated clay, leading to the pseudonodules generation enclosed in clay (see Blatt et al., 1980).

The overlapping of the convolutions is also observed, with younger ones affecting the older ones in the seismite level. The deformation and sedimentation of successive lobes must have taken place almost simultaneously with successive episodes of deformation bringing pulses of pore water necessary to recharge the pressure in the formation. Ghosh & Lahiri (1990) experimentally generated similar structures from a density-stratified mass by repeated shocks. Apart from the vertical motion some limited lateral sliding also took place, as indicated by the asymmetric convolutions and the minor shear folds at the base of each of the three seismites.

e. Brecciation

Multiple records have been observed (Fig. 4 a-d) of high density flow material to be 'frozen' in rock record. The clasts appear to be embedded in a fine grained matrix (usually fine-medium sand) and are often internally laminated, with bed parallel laminations which in some cases are of underlying facies A (Fig. 4d). The clasts range from pebble (few mm) to cobble (~70cm) size and are usually from underlying black shale facies of angular to sub-angular nature. The clasts are generally tabular in shape, elongated, internally laminated and positioned bed-parallel but vertically stacked clasts were also observed. The degree of brecciation is variable, ranging from highly transported (Fig. 4d), slightly transported (Fig 4c) to in situ brecciation (Fig 4a, 4b). In-situ brecciation locally characterizes the lower parts of some other beds. The boundaries between the brecciated and non-brecciated parts are highly irregular (Fig. 4c, 4d). Within a well-laminated layer, the clast presence creates bending or truncation of internal fabric of the beds, often with deformation at its brecciated base (Fig. 4a).

Breccia and clastic beds are usually associated with an erosional unconformity when marked by a sharp base. In present case the breccia observed is "frozen" within a particular horizon but bearing regular bed boundaries at both bed base and top. No evidences of deformation within immediately underlying or overlying beds suggests its confinement and development through a seismic disturbance, acting when the lithology was more or less unconsolidated (Sarkar et al., 2014).

f. Flame structures and load casts

The Jhuran formation is dominantly siliciclastic and has presence of cohesive mud, underlying the sand beds, which at certain traceable interval between Facies C and D form small scale (4-7cm) clay diapirs which may be referred to as flame structures (Fig 5a, 5b, 5c). Complementary to them are load casts (*c.* 5cm) of the overlying coarser and less cohesive sand bed. In a few occurrences pseudonodules were also observed, which are extremely amplified forms of flame structure and load cast (Fig. 4e, 4f) (Mills, 1983). The pseudonodules (Fig.

5e, 5f) are elongated (*c.* 28cm), bean-shaped sand nodules present in between shale beds and separated from the overlying sands (Kuenen, 1958). These structures seem to be formed by hydroplasticization and fluidization induced by seismic shock, in contrast to local slumping, as they are correlatable for hundreds of kilometers (Du et al., 2007).

g. Chaotic laminae

Combination of liquefaction, plasticization and fluidization produces chaotic laminae (Fig. 5e, 5f) (Duranti et al., 2002). The flowage of the matrix material (coarse-silt) within differential lithology (medium-sand) results in chaotic internal structures. This may be a result of rapid fluidization as a result of seismic shock and dewatering (Bizhu and Xiufu, 2015). Thixotropic liquidization and injection of clayey sediment, possibly caused further convolutions within an otherwise laminated beddings.

DISCUSSION AND CONCLUSIONS

The Jhuran Formation has been established to be deposited in shallow-marine to deltaic regime. Syn-sedimentary disturbances in the marine fan complex of Lower Member have been firstly reported by Seth et al., (1990) but the present work also suggests basin-wide development of soft sediment deformation at the top of the middle member (Fig. 6). The shallowing upward trends (Fig. 6) observed throughout most part of the basin, proximal to distal, initiates from organic-rich shales (Facies-A) and progrades to coarse sands (Facies-E). However, the litho-column above the syn-depositional deformation time plane possibly marks the initiation of Upper Member of the Jhuran Formation. This member's initiation is marked by organic matter poor silty shale units and eventually truncates unconformably with fluvial Bhuj Formation (Biswas, 1983). The pericratonic rift basin was undergoing active clastic sedimentation but was intermittently affected by seismicity of both low and high magnitudes, as suggested by the variability within scales of the soft-sedimentary deformation structures. It is evident that Late Jurassic Kutch rift basin was affected by palaeo-seismicity. Furthermore, the restricted depositional environment that was prevailing during the Lower and Middle Member which may have allowed preservation of high degree (~5% by wt.) (Arora et al., 2015) of carbonaceous matter was possibly perturbed and evolved into a more "open" marine regime (Arthur and Sageman, 1994 and references therein). The minor black shales (Fig. 6), overlying the syn-depositional deformation interval, at distal end of the basin, could be a product of sedimentological and basinal readjustment to the shock, which could not materialize in the shallower end of the basin. The seismic shocks possibly disrupted the restricted and stratified nature of the basin by both

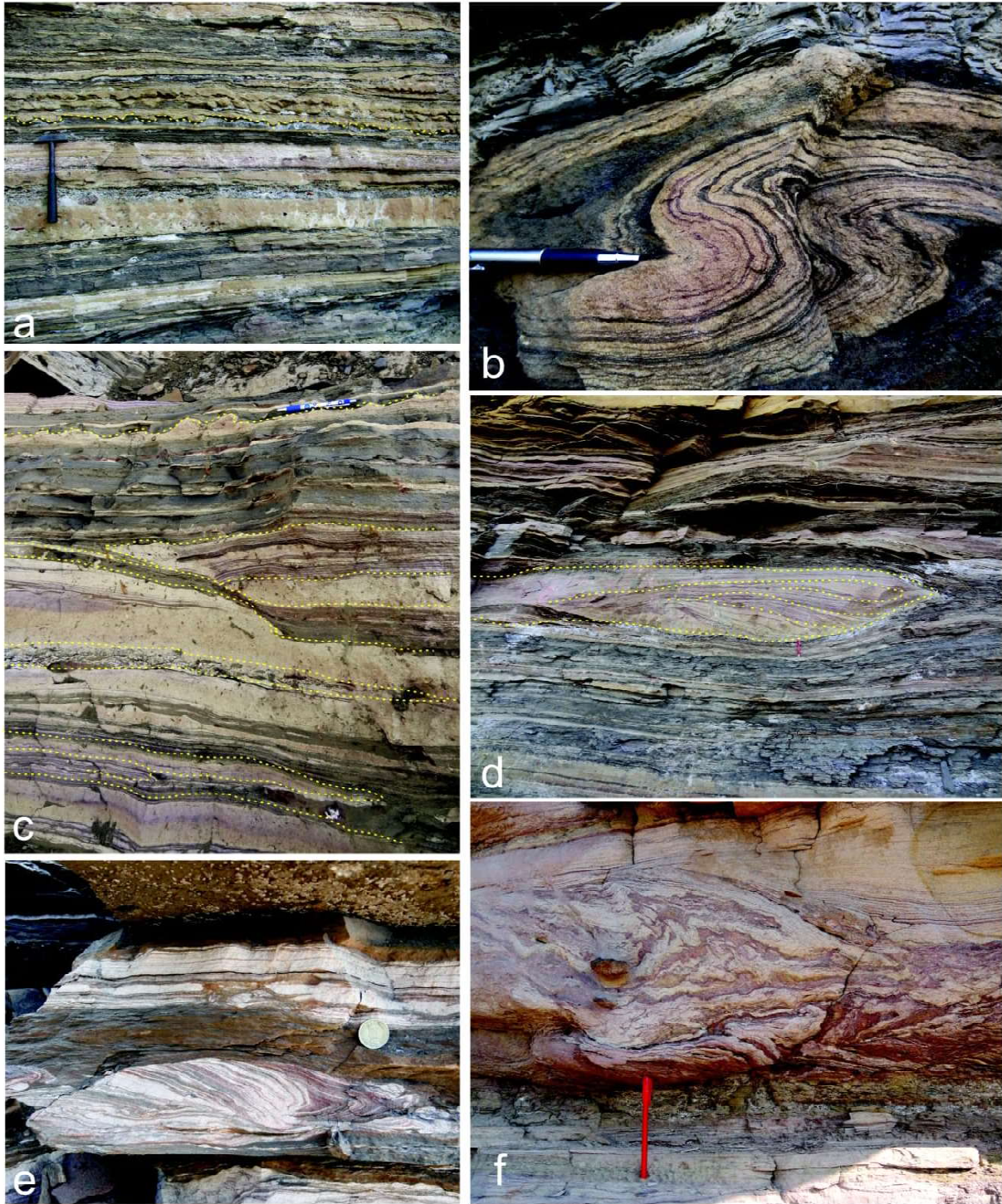


Fig. 5. (a, c) Small scale load casts and their complimentary flame structures observed within alternating lithologies. Note the presence of major syn-depositional ptygmatic, overturned fold (b, d) and faulting (c) in semi-plastic state but terminating in cohesive yet ductile mud layer; (e, f), a few examples of chaotic laminae creation by hydroplastication and subsequent drag.

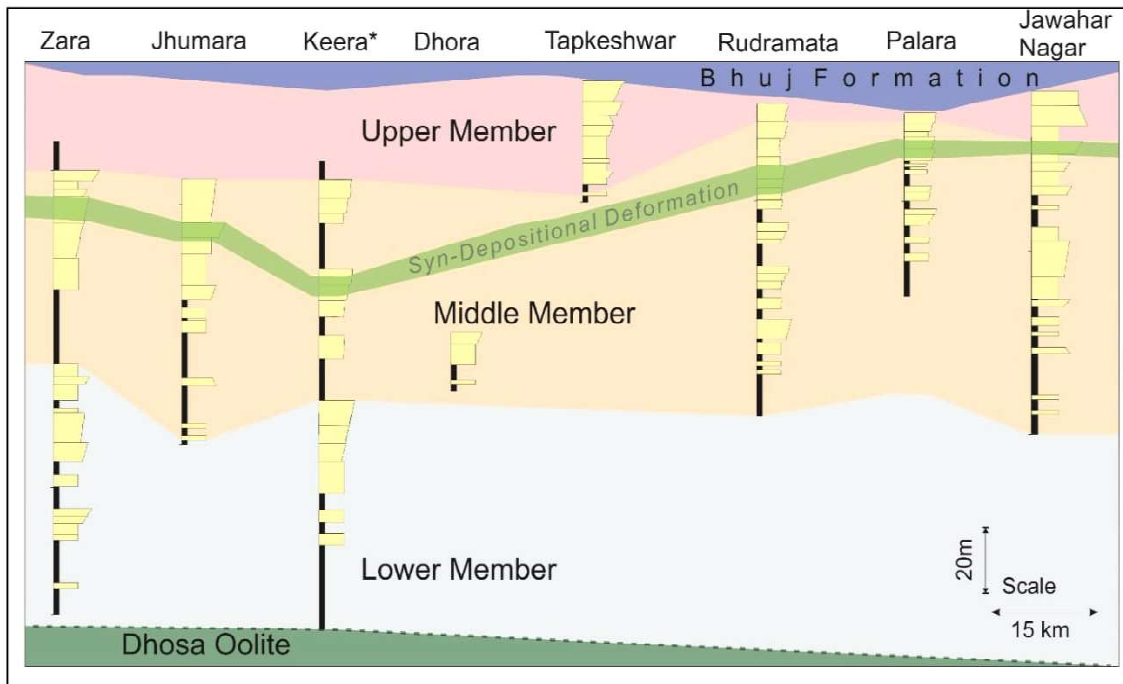


Fig. 6. Basin-wide lithological trends from multiple exposure showing a broad shallowing uptrend (see Biswas, 1987; *Seth et al., 1990; Arora et al., 2015). The lateral correlation (green band) marks the event of syn-depositional deformation throughout the mainland Kutch basin. Above this layer, the marked reduction in the organic content within shales suggests basinal opening and further deposition of shallowest Upper Member of the Jhuran Formation.

changing the tectonic settings or barrier breaching, (Arthur and Sageman, 1994) and affecting sedimentation patterns (Moretti and Sabato, 2007). This created a disturbance in the stratification which was favoring deposition of black shale, creating an openness to the basin and allowing favourable preservation of Type-III rich organic shales (Arora et al., 2015). It remains uncertain whether the coarsening upward trend was purely due to normal regression and subsequent reduction in accommodation space, or caused by uplift of basal surface of the basin by these seismic shocks. Nonetheless, combination of multiple factors for alteration in sedimentation trends, cannot be ruled out. The major conclusions of the study are as follows:

1. Abundant syn-depositional features within the Jhuran Formation suggest that deposition took place in

a seismically active setting, which played a significant role of perturbing an otherwise calm deposition environment.

2. The seismic event marks a correlatable time plane for basin wide reference at the top of the Middle Member of the Jhuran Formation.

3. The seismic events had a major role in disruption or readjustment within the oceanic water column stratification which was critical for organic rich shale preservation.

Acknowledgements: Author acknowledges Indian Institute of Technology Bombay for the infrastructural support and CSIR for financial support. Author is also thankful to Prof. Santanu Banerjee for constant guidance and ICGEN-IAS 2015 for providing a platform to this study.

References

- Allen, C. R. (1975). Geological Criteria for Evaluating Seismicity Address as Retiring President of The Geological Society of America, Miami Beach, Florida, November 1974. Geological Society of America Bulletin, 86(8), 1041-1057.
- Lowe, D.R., (1975). Water escape structures in coarse-grained sediments. *Sedimentology*, 22, 157-204.
- Arora, A., Banerjee, S., & Dutta, S. (2015). Black Shale in Late Jurassic Jhuran Formation of Kutch: Possible Indicator of Oceanic Anoxic Event? *Geological Society of India*, 85(3), 265-278.
- Arthur, M.A. and Sageman, B.B. (2005). Sea Level Control on Source Rock Development: Perspectives from the Holocene Black Sea, the mid-Cretaceous Western Interior Basin of North America, and the Late Devonian Appalachian Basin. In: N.B. Harris and B. Pradier, (Eds.), *The Deposition of Organic Carbon-rich Sediments: Models, Mechanisms and*

- Consequences, *SEPM Special Publication*, 82, 35-59.
- Bardhan, S., Shome, S., Bose, P.K. and Ghose, G. (1989). Faunal crisis and marine regression across the Jurassic-Cretaceous boundary in Kutch, India. *Mesozoic Research*, 2, 1-10.
- Bhattacharya, J. P., & Davies, R. K. (2004). Sedimentology and structure of growth faults at the base of the Ferron Member along Muddy Creek, Utah. The Fluvial-Deltaic Ferron Sandstone: Regional-to-Wellbore-Scale Outcrop Analog Studies and Applications to Reservoir Modeling, *American Association of Petroleum Geologists, Studies in Geology*, 50, 279-304.
- Biswas, S. K. (1977). Mesozoic rock stratigraphy of Kutch. *Quaternary Journal of Geological Mineralogical Metallurgical Society of India*, 49, 1-52.
- Biswas, S. K. (1987). Regional tectonic framework, structure and evolution of the western marginal basins of India. *Tectonophysics*, 135(4), 307-327.
- Biswas, S.K. (1993). Geology of Kutch v. 1, *Dehradun, KDM Institute of Petroleum Exploration*.
- Bizhu, H. E., & Xiufu, Q. I. A. O. (2015). Advances and Overview of the Study on Paleo earthquake Events: A Review of Seismites. *Acta Geologica Sinica (English Edition)*, 89(5), 1702-1746.
- Blatt, H., Murray, G. and Middleton, R., (1980). Origin of Sedimentary Rocks. *Prentice-Hall, Englewood Cliffs, N.J.*, 782.
- Bose, P.K. and Das, N.G. (1986). A transgressive storm- and fairweather wave dominated shelf sequence Cretaceous-Nimar formation, Chakrud, M.P, India. *Sedimentary Geology*. 46,147-167.
- Bowman, D., Bruins, H. J., & Van der Plicht, J. (2001). Load Structure Seismites in the Dead Sea Area, Israel: Chronological Benchmarking with ¹⁴C Dating. *Radiocarbon*, 43(3), 1383-1390.
- Chen, J., & Lee, H. S. (2013). Soft-sediment deformation structures in Cambrian siliciclastic and carbonate storm deposits (Shandong Province, China): Differential liquefaction and fluidization triggered by storm-wave loading. *Sedimentary Geology*, 288, 81-94.
- Du, Y., Shi, G. R., Gong, Y., & Xu, Y. J. (2007). Permian soft-sediment deformation structures related to earthquake in the Southern Sydney basin, Eastern Australia. *Acta Geologica Sinica-Chinese Edition*, 81(4), 511-518.
- Duranti, D., Hurst, A., Bell, C., Groves, S., & Hanson, R. (2002). Injected and remobilized Eocene sandstones from the Alba Field, UKCS: core and wireline log characteristics. *Petroleum Geoscience*, 8(2), 99-107.
- Dzulynski, S., & Radomski, A. (1956). Clastic dikes in the Carpathian Flysch. *Annual. Society Geologist Pologne*, 26(3), 225-264.
- Ghosh, S.K. & Lahiri, S., (1990). Soft sediment deformation by vertical movement. *Indian Journal of Earth Science* 17, 23-43.
- He, B., Qiao, X., Jiao, C., Xu, Z., Cai, Z., Guo, X., & Zhang, Y. (2014). Palaeo-earthquake events during the late Early Palaeozoic in the central Tarim Basin (NW China): evidence from deep drilling cores. *Geologos*, 20(2), 105-123.
- Johnson, H.D. and Baldwin, C.T. (1986). Shallow siliciclastic seas. In: H.G. Reading (Ed.), *Sedimentary Environments and Facies*. *Blackwell Oxford*, 229-282.
- Krishna, J., Pathak, D.B. and Pandey, B. (1998). Development of Oxfordian (Early Upper Jurassic) in the most proximal exposed part of Kachchh basin at Wagad outside the Mainland Kachchh. *Journal of Geological Society of India*, 52, 513-522.
- Krishna, J., Pathak, D.B., Pandey, B. and Ojha J. R. (2000). Transgressive sediment intervals in the Late Jurassic of Kachchh, India. *Geophysical Research*. 6, 331-332.
- Krishnan, M.S. (1956) Geology of India and Burma. *Higginbothams (pvt.) ltd., Madras, India*, 555.
- Knaust, D. (2002). Pinch-and-swell structures at the Middle/Upper Muschelkalk boundary (Triassic): evidence of earthquake effects (seismites) in the Germanic Basin. *International Journal of Earth Sciences*, 91(2), 291-303.
- Kuenen, P. H. (1958). I.—Experiments in Geology. *Transactions of the Geological Society of Glasgow*, 23(*centenary*), 1-28.
- Leckie, D.A. (1986). Rates, controls and sand-body geometries of transgressive-regressive cycles: Cretaceous Moosebar and Gates formations, British Columbia: *American Association of Petroleum Geologists*, 70, 516-535.
- Leckie, D.A. and Reinson, G.E. (1993). Effects of Middle to Late Albian sea-level fluctuations in the Cretaceous Interior Seaway, western Canada. In: W.G.E. Caldwell and E.G. Kauffman, (Eds.), *Evolution of the Western Interior Basin*. *Geological Association of Canada*, 39, 151-176.
- Leithold, E.L. and Bourgeois, J. (1984). Characteristics of coarse grained sequences deposited in nearshore, wave-dominated environments: examples from the Miocene of southwest Oregon. *Sedimentology*, 31, 749-775.
- Lowe, D. R. (1975). Water escape structures in coarse grained sediments. *Sedimentology*, 22(2), 157-204.
- Mazumder, R., van Loon, A. T., & Arima, M. (2006). Soft-sediment deformation structures in the Earth's oldest seismites. *Sedimentary Geology*, 186(1), 19-26.
- Mills, P. C. (1983). Genesis and diagnostic value of soft-sediment deformation structures—a review. *Sedimentary Geology*, 35(2), 83-104.
- Montenat, C., Barrier, P., & Hibsich, C. (2007). Seismites: An attempt at critical analysis and

- classification. *Sedimentary Geology*, 196(1), 5-30.
- Moretti, M., & Sabato, L. (2007). Recognition of trigger mechanisms for soft-sediment deformation in the Pleistocene lacustrine deposits of the Sant'Arcangelo Basin (Southern Italy): Seismic shock vs. overloading. *Sedimentary Geology*, 196(1), 31-45.
- Moretti, M.; Van Loon, A.J., (2014). Restrictions to application of 'diagnostic' criteria for recognizing ancient seismites. *Journal of Palaeogeography*, v. 3, 162-173.
- Myrow, P. M., & Chen, J. (2015). Estimates of large magnitude Late Cambrian earthquakes from seismogenic soft sediment deformation structures: Central Rocky Mountains. *Sedimentology*, 62(3), 621-644.
- Potter, P.E. and Pettijohn, F.J., (1977). Paleocurrents and Basin Analysis. *Springer, New York, N.Y.*, 425.
- Rajnath (1932). A contribution to the stratigraphy of Cutch. *Quaternary Journal of Geological Mineralogical Metallurgical Society of India*, 4 (4), 161-174.
- Ramberg, H. (1959). Evolution of pygmatic folding. *Nor. Geol. Tidsskr.*, 39(9).
- Rana, N., Bhattacharya, F., Basavaiah, N., Pant, R. K., & Juyal, N. (2013). Soft sediment deformation structures and their implications for Late Quaternary seismicity on the South Tibetan Detachment System, Central Himalaya (Uttarakhand), India. *Tectonophysics*, 592, 165-174.
- Reinson, G.E. (1992). Transgressive barrier island and estuarine systems. In: R.G. Walker and N.P. James (Eds.), *Facies Models, Response to Sea Level Change*. *Geol. Assoc. Canada, Toronto, ON*, 179-194.
- Rodríguez-Pascua, M. A., Calvo, J. P., De Vicente, G., & Gómez-Gras, D. (2000). Soft-sediment deformation structures interpreted as seismites in lacustrine sediments of the Prebetic Zone, SE Spain, and their potential use as indicators of earthquake magnitudes during the Late Miocene. *Sedimentary Geology*, 135(1), 117-135.
- Sarkar, S., Choudhuri, A., Banerjee, S., Van Loon, A. J., & Bose, P. K. (2014). Seismic and non-seismic soft-sediment deformation structures in the Proterozoic Bhandar Limestone, central India. *Geologos*, 20(2), 89-103.
- Seilacher, A. (1969). Fault graded beds interpreted as seismites. *Sedimentology*, 13(1 2), 155-159.
- Seilacher, A. (1984). Sedimentary structures tentatively attributed to seismic events. *Marine Geology*, 55(1), 1-12.
- Seth, A., Sarkar, S., & Bose, P. K. (1990). Synsedimentary seismic activity in an immature passive margin basin (Lower Member of the Katrol Formation, Upper Jurassic, Kutch, India). *Sedimentary Geology*, 68(4), 279-291.
- Schieber, J. (1995). Sedimentary expression and stratigraphic significance of erosion surfaces, condensation horizons, and hiatuses in the Chattanooga Shale of central Tennessee. *GSA Abstract volume*, v.27/6, 400.
- Shiki, T., Cita, M. B., & Gorsline, D. S. (2000). Sedimentary features of seismites, seismo-turbidites and tsunamiites—an introduction. *Sedimentary Geology*, 135(1), vii-ix.
- Soares, J. L., Nogueira, A. C. R., Domingos, F., & Riccomini, C. (2013). Synsedimentary deformation and the paleoseismic record in Marinoan cap carbonate of the southern Amazon Craton, Brazil. *Journal of South American Earth Sciences*, 48, 58-72.
- Suter, J.R. (2006). Facies models revisited: clastic shelves, In: H.W. Posamentier and R.G. Walker (Eds.), *Facies models revisited: SEPM Special Publication*, v. 84, 339-397.
- Takashimizu, Y., & Masuda, F. (2000). Depositional facies and sedimentary successions of earthquake-induced tsunami deposits in Upper Pleistocene incised valley fills, central Japan. *Sedimentary Geology*, 135(1), 231-239.
- Vail, P.R., Mitchum JR., R.M. and Thompson, S. (1977). Seismic Stratigraphy and global changes of sea level. Part 3: relative changes of sea level from Coastal onlap. In: C.E. Payton (Eds.), *Seismic Stratigraphy – Applications to Hydrocarbon Exploration*, *American Association of Petroleum Geologists. Memoir*, 26, 63-81.
- Vail, P.R., Audemard, F., Bowman, S.A., Eisner, P.N. and Percruz, C. (1991). The stratigraphic signatures of tectonics, eustasy and sedimentology—an overview. In: G. Einsele, A. Ricken and W. Seilacher (Eds.), *Cycles and Events in Stratigraphy*. *Springer-Verlag*, 617-659.
- Van Loon, A. J., & Brodzikowski, K. (1987). Problems and progress in the research on soft-sediment deformations. *Sedimentary Geology*, 50(1), 167-193.
- Van Loon, A. J. (2009). Soft-sediment deformation structures in siliciclastic sediments: an overview. *Geologos* 15, 3-55
- Van Loon, A. J. (2014). The life cycle of seismite research. *Geologos*, 20(2), 61-66.
- Waagen, W. (1875). Jurassic Fauna of Cutch. *Palaeontological Indica, Geological Survey of India, Memoir*, 9, 247.

Shale Gas Potential of North Cambay Basin, Gujarat, India

VAISHALI SHARMA AND ANIRBID SIRCAR

School of Petroleum Technology, Pandit Deendayal Petroleum University, Gandhinagar, India

Email: vaishali.sharma@spt.pdpu.ac.in, anirbid.sircar@spt.pdpu.ac.in

Abstract: Shale gas exploration and exploitation in India is in nascent stage, basic shale gas specific data requires to be generated. The prognosticated resource potential of Indian Shale gas basins is around 2000 TCF. The Cambay Basin is an intracratonic basin located along the western continental passive margin of Indian platform in the Western Indian state of Gujarat. The formation of this basin occurs due to the break-up of Gondwana super continent which makes it an intracratonic rift graben basin. The petroliferous Cambay basin in western India with interbedded carbonaceous in its thick Tertiary sequence forms a potential shale gas prospect. Cambay shale has been the main hydrocarbon source rock in the Cambay basin because of the high total organic carbon content and thermal maturity. Due to the favorable lithological change with structural support and short distance migration, Cambay formation has good generation, expulsion and accumulation of hydrocarbons. Fine grained, clastic and organic rich Cambay, Tarapur and other Tertiary shales have sources of oil and gas for the basin. The quantity, quality and type of organic matter play an important role in the generation of gas. In this study, around 10 sedimentary rock samples from the North Cambay Basin, Sanchor-Patan Tectonic Block were analyzed by Rock –Eval Pyrolysis - 6 to predict the generation and accumulation of gas in this basin. This technique was adopted to obtain the independent parameters on organic matter composition, its thermal maturity, and kerogen typing. Also, a mathematical expression of Hydrogen Index (HI) vs. Rock Eval maximum temperature (T_{max}) pathline for a particular kerogen is generated to understand the characterization of the kerogen with respect to its original generation potential. These results show that the sections are not mature at this moment but on complete thermal maturity they can act as a good source rock. The present study is suitable for good assessment of the petroleum potential of source rocks and rapid geochemical characterization of sedimentary organic matter.

Keywords: Shale, Thermal maturity, Kerogen Typing, Rock-Eval Pyrolysis

INTRODUCTION

The Cambay Basin, a rift sag Tertiary basin, in the western onshore part of India includes five tectonic blocks (i.e. Sanchor-Patan, Ahmedabad-Mehsana, Tarapur-Cambay, Broach-Jambusar and Narmada-Tapti), separated by faults aligned transverse to the general north-south axis of the rift (Fig. 1). It covers an aerial coverage of 53,000 sq. m trending NNW-SSE with a shale gas resource potential of 20 TCF (USGS, 2012). The dominant shale units are: Olpad formation of Paleocene age, Older Cambay Shale unit of Paleocene-Lower Eocene age, Younger Cambay Shale of Lower Eocene age followed by Kalol formation of Mid-Eocene-Oligocene age (Fig. 2). The Cambay Shale has been identified as the main hydrocarbon source rock in the Cambay Basin due to its high thermal maturity and richness in organic matter content. The quality, quantity and type of organic matter play an important in the generation and occurrence of hydrocarbons. However, it is difficult to generate the gas/oil – source genetic relationship due to complicated geology involving multiplicity of depressions, source rocks and reservoir (Banerjee *et al.*; 2000). The study area of this work is North Cambay Basin, Sanchor-Patan Tectonic Block (Fig. 3). Nearly 10

sedimentary samples have been collected to identify the best source rock for the generation and accumulation of gas in this basin. To generate the gas-source genetic relationship, geochemical characterization of these sedimentary samples is done. Geochemical parameters such as organic richness and kerogen typing are the prime requisite in shale gas exploration as these attributes control gas generation in shales. Rock Eval Pyrolysis is one of the most basic methods to study the thermal maturity of organic matter shales (Dayal *et al.*, 2013). The principal objective of this study is to predict the amount of hydrocarbons generated and organic matter type by analyzing the various parameters generated by Rock Eval Pyrolysis technique.

STRATIGRAPHY OF NORTH CAMBAY BASIN

Stratigraphy, tectonics and sedimentation of Cambay Basin have been worked out by various authors, the more significant contributions have been made by Sudhakar and Roy (1959), Zubov *et al.* (1996), Mathur *et al.* (1968), Chandra and Chaudhary (1969), Rao (1969), Sudhakar and Basu (1973), Bhandari and Choudhary (1975), and Raju *et al.* (1982). Stratigraphically, the basin has been divided

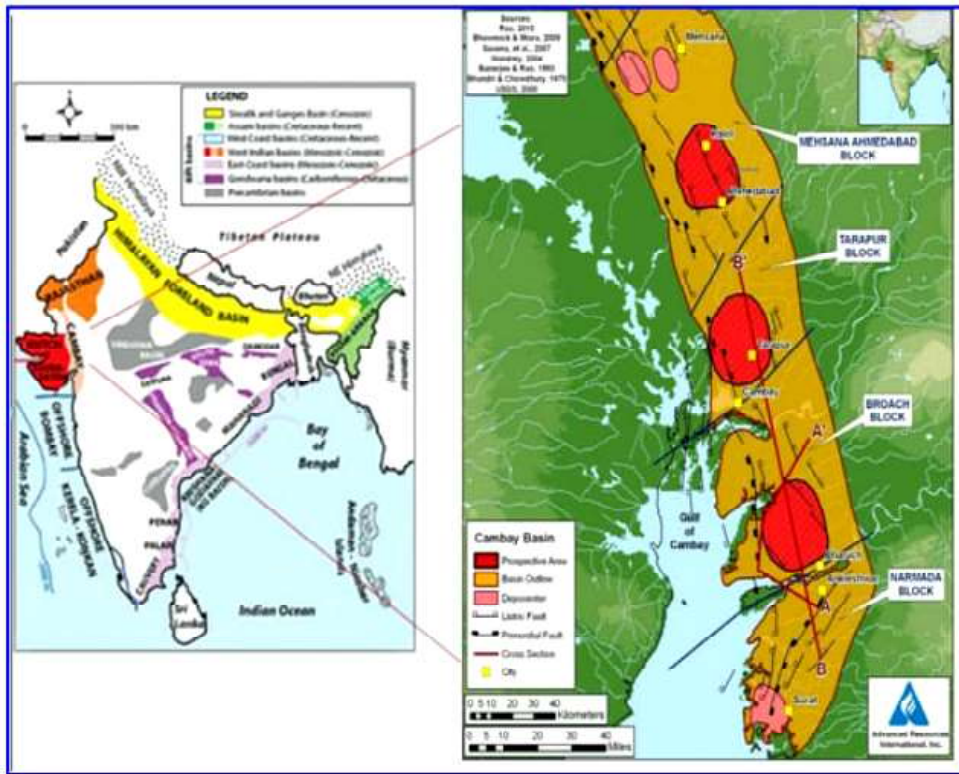


Fig. 1. Location Map of Study Area. Source: DGH.

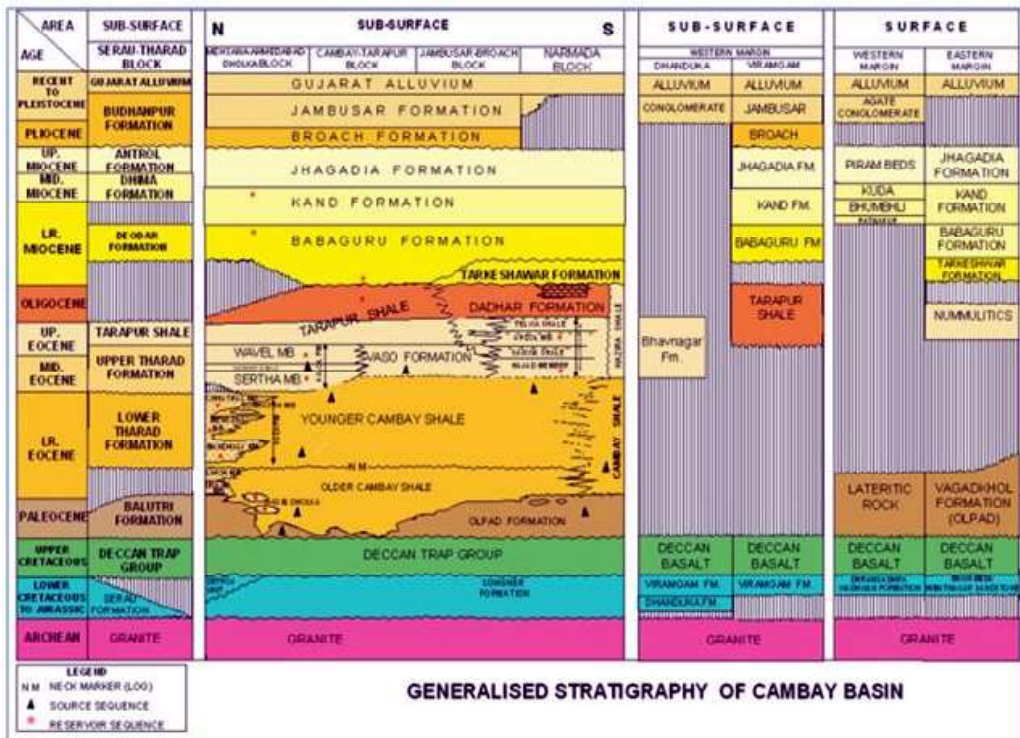


Fig. 2. Generalized Stratigraphy of Cambay Basin, Source: DGH.

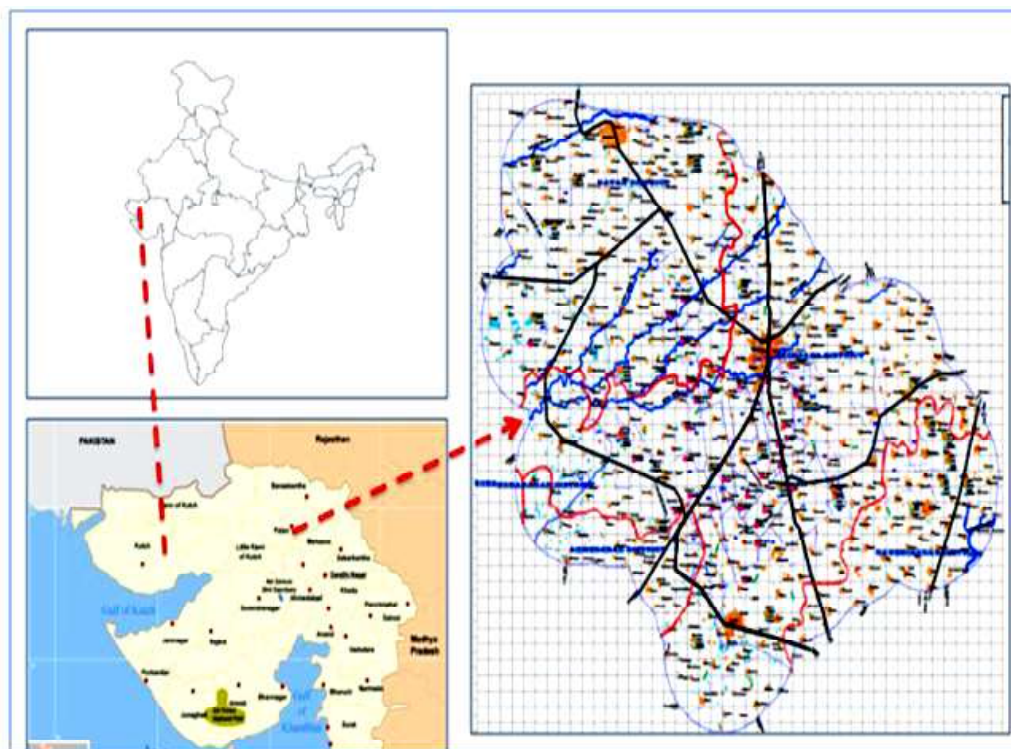


Fig. 3. Location Map of Patan, Source: DGH.

in to eleven formations with Deccan Trap as the basement (Fig. 2).

The dominant shale units of this basin are - *Olpad Formation (Paleocene)*, *Older Cambay Shale Formation (Paleocene-early part of Lower Eocene)*, *Younger Cambay Shale Formation (Lower Eocene)*, *Kalol/Ankleshwar Formation (Mid Eocene – Upper Eocene)* and *Tarapur Formation (Upper Eocene-Oligocene)*. The *Olpad Formation* unconformably overlies Deccan Traps which consists of volcanic conglomerates and trap wash sediments at the base followed by silts, claystones and shales. The thickness varies between 340 m to 2700 m (Dayal et al., 2013).

The *Older Cambay Shale Formation* has conformable to gradational relationship with underlying *Olpad formation*. It consists of grey to dark grey thin bedded shales, occasionally calcareous and carbonaceous. The thickness varies between 500-1900 m. These shales could form potential shale gas areas as they are thick, rich in organic content and placed at deeper levels.

Younger Cambay Shale Formation overlies unconformably the older Cambay shale unit and underlies the Kalol formation. It consists of grey to black massive siderites and pyritic shales along with occasional thin coal bands. Thickness varies between

520 m and 1500 m in Ahmedabad-Mehsana Tectonic block.

The *Kalol formation* is well developed in north Cambay basin while Ankleshwar Formation is in southern Cambay basin. They have conformable relation with overlying Tarapur shales. The thickness varies between 200 m and 300 m.

The *Tarapur Shale Formation* has conformable relationship with underlying Kalol formation and is unconformably overlain by Tarkeshwar Formation of lower Miocene age. It consists of greenish grey to dark grey shales and some argillaceous sandstones and thickness varies between 60 m and 400 m.

SAMPLES AND METHODS

The potential source rock samples from the field (10 samples) have been collected (Fig. 4 and Fig. 5) and significant amount of data is generated by using Rock-Eval Pyrolysis-6. Rock-Eval Pyrolysis is an appropriate method for a good assessment of petroleum potential of source rock and rapid characterization of sedimentary organic matter (Adel et al., 2007).

Rock Eval Pyrolysis allows us to identify the possible source rock sections and assess their quality and maturity (Banerjee et al., 1998). It involves



Fig. 4. Sample at different depth intervals.



Fig. 5. Samples in Powdered Form.

Table 1. Rock Eval Pyrolysis Data for rock samples.

Sample	Depth (m)	S1 (mg of HC/g of Rock)	S2 (mg of HC/g of rock)	Tmax (°C)	TOC%	HI	OI	TR	HCG	HCE
1	1230-35	0.09	1.13	431	1.67	61	140	-139	0.074	0.623
2	1235-40	0.04	0.35	429	1.12	42	131	-130	0.33	0.281
3	1240-45	0.21	0.42	433	1.14	56	120	-119	0.3	0.027
4	1245-50	0.14	0.61	437	1.13	57	119	-118	0.42	0.246
5	1250-55	0.3	0.34	432	1.12	106	261	-260	0.12	-0.261
6	1255-60	0.29	0.66	438	1.14	105	66	-65	0.25	-0.125
7	1260-65	0.17	0.29	435	1.13	107	6	-66	0.108	-0.112
8	1265-70	0.08	0.17	429	1.12	41	110	-109	0.165	0.061
9	1270-75	0.08	0.05	440	1.1	40	109	-108	0.05	-0.054
10	1275-80	0.17	0.12	438	1.1	39	71	-70	0.12	-0.097

TOC: Total Organic Content

OI: Oxygen Index

TR: Transformation Ratio

HCE: Hydrocarbon Expelled

S2: hydrocarbons from cracking of organic matter

HI: Hydrogen Index

T_{max}: Maximum Temperature

HCG: Hydrocarbon Generation

S1: thermo-vaporized free hydrocarbons

estimating the petroleum potential of rocks samples by pyrolysis according to a programmed temperature pattern (Dayal *et al.*, 2013). Released hydrocarbons are monitored by Flame Ionization Detector, forming the S1 (thermo-vaporized free hydrocarbons), S2 (hydrocarbons from cracking of organic matter) and S3 (milligrams of trapped carbon dioxide generated per gm of rock) peaks. The derived and direct parameters viz. Hydrogen Index (HI), maximum Temperature (T_{max}), Oxygen Index (OI) etc. generated from pyrolysis technique has been tabulated in Table 1. To identify the sections that most likely expelled the generated hydrocarbons, cross plots in between HI vs T_{max} has been plotted and a trendline equation (Banerjee *et al.*, 1998) has been used to determine the transformation ratio (TR), hydrocarbon generated (HCG) and hydrocarbons expelled (HCE).

SOURCE ROCK EVALUATION

Rock-Eval direct and derived parameters have been obtained from pyrolysis technique. A trendline equation (Banerjee *et al.*, 1998):

$$HI = \frac{1}{[a \exp b(T_{max} - 435) + c]}$$

where a, b and c are constants and c is equal to inverse of original hydrocarbon generation potential. HI_0 has been used to potentially evaluate the generation of hydrocarbons. The amount of hydrocarbons converted per gram of rock i.e. transformation ratio (TR) can be calculated as- $TR = 1 - (HI / HI_0)$

And the amount of hydrocarbons generated (HCG) and expelled (HCE) can be given as –

$$\begin{aligned} HCG &= S2 / (1-TR) \\ HCE &= HCG - S1 * 1.3 \end{aligned}$$

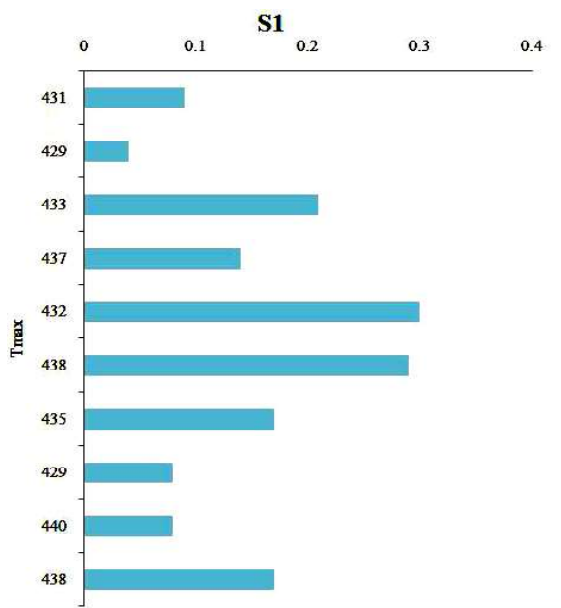


Fig. 6. Variation in S1 values with respect to Tmax.

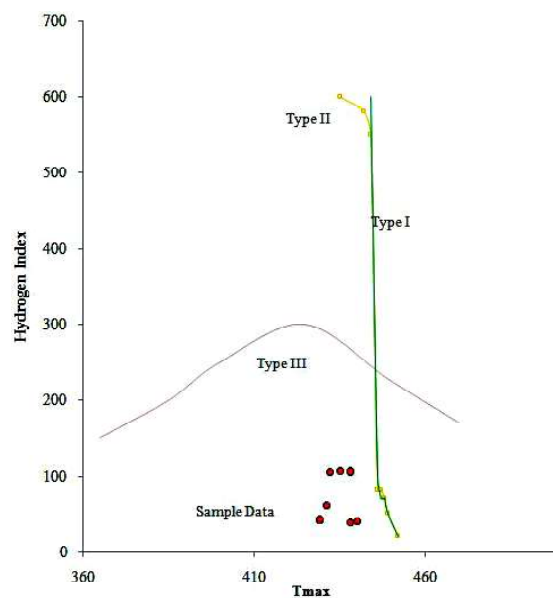


Fig. 7. Hydrogen Index vs Tmax Plot.

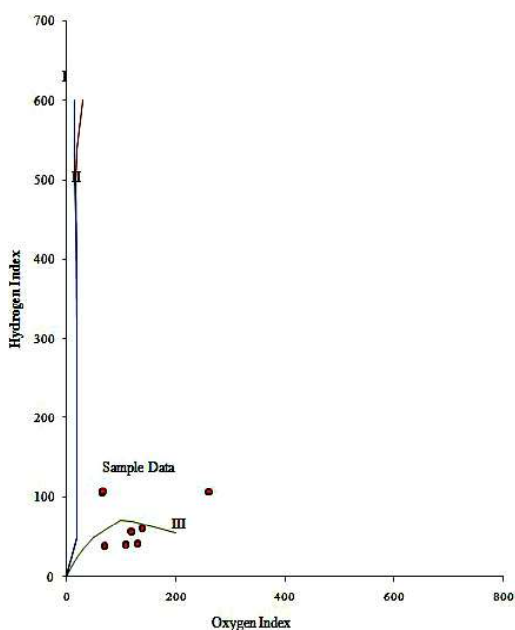


Fig. 8. Hydrogen Index vs Oxygen Index Cross Plot.

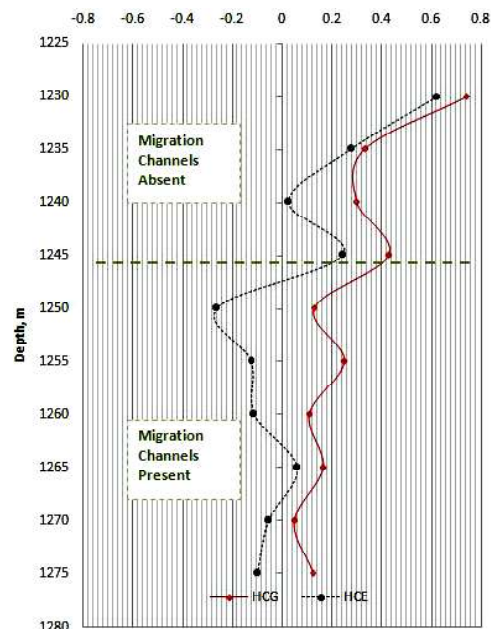


Fig. 9. HCG and HCE vs. Depth Plot.

where, the factor 1.3 has been used to account the loss of free volatile hydrocarbons that might have occurred before laboratory determination of S1 (Banerjee et al., 1998).

RESULTS AND DISCUSSIONS

The S1 value (thermally liberated free hydrocarbons) of the given samples ranges from 0.08 to 0.29 mg HC/g rock sample (Fig. 6). The S1 value equal to

1.0 mg HC/g dry rock indicates that the rock is a good source rock. The given samples show very low S1 values, which indicates that: i) it may not be a good source rock, or ii) significant amount of hydrocarbons are not yet produced from source rock due to low thermal maturity of organic matter or the produced hydrocarbons had migrated away from source rocks.

S2 values represent the hydrocarbon compounds originating from kerogen cracking up to 530°C. This value gives the residual petroleum potential of the rock,

expressed in mg HC/g of rock. The S2 value greater than or equal to 5.0 mg HC/g of rock is the minimum value for good source rock. The given samples show very low values of S2, which indicates that the rock may be immature at this particular depth of interval.

TOC content >2%, indicates that it is excellent source rock. The given samples have low abundance of TOC (in the range of 1.1 to 1.6%), which proves that with proper depositional environment and complete thermal maturity, it can lead to an excellent source rock. Low abundance of TOC suggests that a relative oxicity of the depositional environment affects the amount and elemental composition of the stored organic matter. (Tissot and Welte, 1984).

Cross plots, HI vs Tmax (Fig. 7) indicates Type-III Kerogen, which is suitable for the generation of gas. And the HI vs OI plot (Fig. 8) also shows that the organic matter is characterized by Type-III kerogen. This indicates that it is a woody i.e. gas prone humic zone.

The Hydrocarbon generation and expulsion can be calculated by the expressions suggested by Banerjee *et al.* (1998), and has been tabulated in the Table 1.

The stratigraphic log of HCG and HCE has been represented in Fig. 9. The plot suggests directly and indirectly the migration history, generation and expulsion of hydrocarbon. Although, nothing can be talked about this moment, about the tortuous path of hydrocarbon movement from source to reservoir but it can be concluded that the source and the reservoir coexists with each other in a cannibalistic manner.

Both the curves (HCG and HCE) have been studied in conjunction, which gives an idea about the movement of hydrocarbon when expelled.

The qualitative expulsion is demonstrated on the x-axis of the plot which is depiction of HC vs. depth. The positive correlation suggests that hydrocarbons have been most likely generated and expelled whereas, the negative HCE values suggests that the sections has migration channels/pathways or host accumulated hydrocarbons. Hence, it gives an indication that the generation has happened.

CONCLUSIONS

The pyrolysis results suggest that due to low abundance of S1, S2 and TOC values, the rock may not be mature at this moment, but it can be a good source rock with proper depositional environment and complete thermal maturity. And, the cross plots indicates that the sections are gas prone regions due to kerogen typing III. The plots of HCE and HCG indicates that the hydrocarbons have been significantly generated and expelled in the upper part (i.e. at shallow depth, 1225-1247.5 m) of the younger Cambay shale due to positive HCE and HCG correlation. However, in the lower part (i.e. at deeper depths, 1247.5-1280m) the hydrocarbons might have been migrated due to the presence of migration pathways or channels. The tortuous path of movement cannot be predicted at this moment.

Acknowledgements: The authors are grateful to School of Petroleum Technology, PDPU for granting the permission to publish this paper at Journal of the Indian Association of Sedimentologists. The authors are also thankful to the colleagues for their help and support rendered during this work.

References

- Arfaoui Adel, Montacer Mabrouk, Kamoun Fekri, Rigane Adel (2007). Comparative study between Rock Eval Pyrolysis and biomarkers parameters: A case study of Ypresian source rocks in central – northern Tunisia. *Marine and Petroleum Geology*, 24, 566-578.
- Banerjee, A., Jha, M., Mittal A.K., Thomas N.J. and Misra K.N. (2000). The effective source rocks in the north Cambay Basin, India. *Marine and Petroleum Geology*, 17, 1111-1129.
- Banerjee, A., Sinha, A. K., Jain, A. K., Thomas, N. J., Misra, K. N., & Chandra, K. (1998). A mathematical representation of Rock-Eval hydrogen index vs Tmax profiles. *Organic Geochemistry*, 28, 43–55.
- Bhandari, L.L., and Chowdhary, L.R. (1975). Stratigraphic analysis of Kadi and Kalol Formations, Cambay Basin, India. *AAPG Bulletin*. 59. 856-871.
- Chandra, P.K., and Chowdhary, L.R. (1969). Stratigraphy of the Cambay Basin. *Bulletin Oil and Natural Gas Commission (ONGC)*, Dehradun, India, 6, 37-50.
- Dayal A.M., Mani Devleena, Mishra Snigdharani, Patil D.J. (2013). Shale gas prospects of Cambay Basin, Western India. *Geohorizons*, 26.
- Mathur, L.P., Rao K.L.N., and Chaube, A.N. (1968). Tectonic framework of Cambay Basin, India. *Bulletin: Oil and Natural gas Commission (ONGC)*, Dehradun, India, 5, 29-40.
- Raju, A.T.R., Hardas, M.G., Srivastava, D.C., and Maindarkar, M.M. (1982). Depositional environment of oil bearing Lower and Middle Eocene sands of North Cambay Basin. *Bulletin, Oil and Natural Gas Commission (ONGC)*, Dehradun, India, 19, 55-72.
- Rao K.L.N. (1969). Lithostratigraphy of the Paleogene succession of Southern Cambay Basin. *Bulletin, Oil and Natural gas Commission (ONGC)*, Dehradun, India, 6, 24-37.
- Sudhakar, R., and Basu, D.N. (1973). A reappraisal of the Paleogene Stratigraphy of Southern Cambay Basin. *Bulletin, Oil and Natural gas Commission (ONGC)*, Dehradun, India, 10, 55-76.

- Sudhakar, R., and Roy, T.K. (1959). Progress report on the geology of Tertiary Formations of Broach and Surat District. unpublished report, Oil and Natural gas Commission (ONGC, Dehradun, India).
- Tissot, B.P. and Welte, D.H. (1984). Petroleum Formation and Occurrence. Springer, 699.
- USGS, 2012. United States Geological Survey. Retrieved from- <http://pubs.usgs.gov/fs/2011/3131/pdf/fs2011-3131.pdf>.
- Zubov, I.P, Naugolny I.K., Zapivalov N.P., and Chandra P.K. (1966). Problem of correlation and distribution of hydrocarbon bearing horizons in the Eocene of Cambay Basin: Bulletin, Oil and Natural gas Commission (ONGC, Dehradun, India, 3, 9-15.

Integrating Field Observations with Sub-Surface Geological Data for better understanding of Depositional Environment

SANKHADIP BHATTACHARYA, RUPA DAS AND W.W MOMIN
Forward Base Agartala, A&AA Basin, ONGC Ltd, Tripura, India
E-mail: bhattacharya_sankhadip@ongc.co.in

Abstract: Tripura Fold Belt constitutes the southern part of frontal fold belt of Assam-Arakan Basin. Tectonically, the area is characterised by a set of narrow, elongated, asymmetrical, doubly plunging, en-echelon anticlines, trending almost N-S to NNE-SSW with a slight convexity towards west. Anticlines are separated by broad synclines in between and became more tight eastward, exposing older rocks at culmination. The present study is restricted within eastern Tripura where ONGC Ltd has been awarded a NELP Block, which proved to be a significant gas reserve in Early to Middle Miocene formations. Conformable succession of thick Late Miocene Surma Group of clastic rocks is well exposed along road cuts near Jampai anticline, exhibiting plenty of primary sedimentary features of different scales. In this paper an attempt has been made to integrate sub surface geological data derived from cores, electro-log suites and 3-D seismic data available in the study area with the observed primary sedimentary structures to have a better understanding of the then depositional environment. This study utilizes the advantage of high resolution small scale primary sedimentary structures over seismic and electro-log data in identifying depositional environments. Our findings point towards a tidally influenced prograding deltaic system with migrating inter tidal bed forms which led to the deposition of Late Miocene upper part of Surma Group of rocks in the study area. This approach is to stimulate future lines of research for a better understanding of the sedimentological and structural evolution of the tertiary succession of the Tripura Fold Belt area.

Keywords: Fold belt, Surma Group, Depositional environment, Prograding deltaic system.

INTRODUCTION

Tripura Fold Belt (henceforth called TFB) constitutes the southern part of the Assam-Arakan fold belt. The state shares its international boundaries in all the three sides with Bangladesh and the remaining part with Assam and Mizoram. Systematic exploration activities began in early 1960s in this tough, logistically difficult terrain. However, recent gas discoveries in Early to Middle Miocene formations of the eastern part of TFB, where ONGC Ltd has been awarded a NELP Block, warrants an improved understanding of the depositional environment to know the stratigraphic as well as spatial distributions and architecture of reservoir-quality sandstones in order to optimise exploration and exploitation strategies.

The present study is restricted within eastern part of TFB (Fig. 1&2), where conformable succession of thick Late Miocene Surma Group of clastic rock is well exposed along Panisagar to Jampai road via Damcheera, showing plenty of primary sedimentary structures of different scales. The aim of the present study is to characterize the evolution

of the depositional environment during the Late Miocene time in the study area, which is achieved through: **i.** Detailed macroscopic field observation, **ii.** Integrating field data with available subsurface geological data with probable palaeo-environmental analysis and **iii.** Proposing a plausible depositional model for the Late Miocene upper part of Surma Group of rocks.

REGIONAL GEOLOGICAL SETTING

The initiation of the Bengal basin occurred during Late Mesozoic (ca. 125 Ma) with the break-up of Gondwanaland (Lindsay et al., 1991). Continued drifting and subsequent collision of the Indian and Eurasian plates resulted in formation of the Himalayan ranges. Thereafter, oblique collision of the Indian and Burmese plates during the Eocene–Oligocene (Curry et al., 1982) resulted in obduction of the accretionary prism, forming the Indo-Burma ranges (IBR). With continued subduction of the Indian plate, sediments within the Bengal basin have been compressed and uplifted to form the TFB (Anjelier, J., and Baruah, S., 2009).

Tectonically, the area is characterised by a set of narrow, elongated, asymmetrical, doubly plunging, en-echelon anticlines showing first order topography, trending almost N-S to NNE-SSW with a slight convexity towards west. Anticlines are separated by broad synclines in between and became more tight eastward, thus exposing much older rocks at culminations. Each anticline is bounded by longitudinal structure bounding reverse faults on one or either limb, which later got affected by the younger cross faults with dominantly strike slip components, accounting for the westward convexity of anticlines (Hiller and Elahi, 1988; Khar and Ganju, 1984; Ghosh, S. K., 1993).

Mio-Pliocene succession of clastic sediments comprising an intricate association of arenaceous and argillaceous sediments in varying proportions is well exposed all along the road cuts. Sediments in general are poorly fossiliferous, giving less chronostratigraphic control. The generalised litho-stratigraphic succession of exposed sedimentary rocks is given below in Table 1 (Baruah et. al, 1992).

DETAILED OBSERVATION IN FIELD

Middle to Late Miocene Surma Group of rocks are well exposed along Panisagar to Jampai road section via Damcheera, thus allowing us insight into part of the Middle to Late Miocene depositional environment. The exposed clastic succession has been broadly subdivided into two major litho units, namely *Unit-A* and *Unit-B*, based on grain size, degree of sorting, scale and type of sedimentary structures. The younger *Unit-A* being more

argillaceous, seems to be equivalent to the Late Miocene argillaceous Bokabil Formation. This unit is in turn sub divided into two subunits- A1 and A2 based on type of primary sedimentary structures and sand-mud ratio. *Unit-B* is comparatively more arenaceous and believed to be equivalent to the upper part of arenaceous Upper Bhuban Formation of Middle Miocene. Due to frequent lateral change of facies accompanied with absence of macro as well as trace fossil assemblages, detailed chronostratigraphic correlation could not be carried out, but the overall characters of the upper part of Surma Group of rocks as described by Ganguly, S., (1983 a, b), Srivastava, J. P., (1975), Baruah et. al, 1992, Evans, P., 1932, matches broadly with our present observations. We have documented all our field observations in detail in the following section with outcrop pictures, wherever possible.

Litho Units

Unit A: This litho unit, exposed near the Southern plunge of Langai anticline and laterally traceable up to western flank of Jampai anticline (location A' in Fig. 1, Table-1), is characterised as a heterolithic unit comprised of alternate clay and siltstone laminae with occasional intercalation of ripple cross laminated fine grained sandstone units. For the sake of simplicity, this unit is in turn subdivided into two subunits, namely- A1 and A2, based on type of primary sedimentary structures and sand-mud ratio. Though direct contact between the two subunits A1 and A2 could not be established in field, but based on the stratigraphic position of other

Table 1. Generalized litho-stratigraphic succession (Baruah et. al, 1992) of the exposed clastic rocks in the eastern part of TFB. *Stratigraphic position of both the *Litho Units- A* and *B* are shown here.

AGE	GROUP	SUB GROUP	FORMATION	LITHOLOGY	THICKNESS (m)	
Recent	-	-	Alluvium	Mainly arenaceous, loose, immature sediments turned into soil	100-300	
Plio-Pleistocene	Dupitila	-	Agartala		600-1000	
Early Pliocene	Tipam	-	Tipam Sandstone	Mainly arenaceous with claystone and siltstone interlamination	100-400	
Miocene	Late	Surma	Bokabil	Mainly argillaceous with thin interbedded siltstone and sandstone	400-1100	
			Bhuban	Upper Bhuban (<i>Unit-B*</i>)	Mainly arenaceous with alteration of thick shale and siltstone	500-1000
			↓	Middle Bhuban	Mainly argillaceous with siltstone and sandstone intercalations	500-1100
			(not exposed in our study area)	Lower Bhuban	Mainly arenaceous with shale and siltstone intercalations	500-1000?

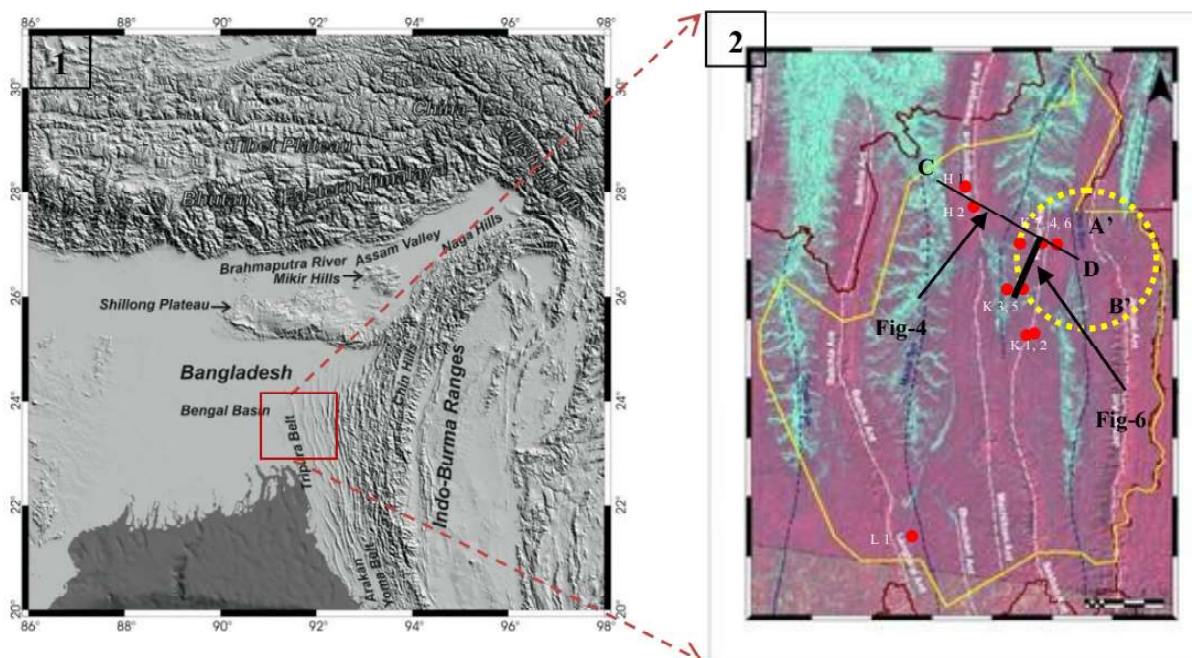


Fig. 1 & 2. Generalized relief map showing the tectonic elements of the Bengal Basin and surrounding areas (after Anjelier, J., and Baruah, S., 2009). Tripura Fold Belt (TFB) region is marked and eastern part of TFB is zoomed in (ONGC internal reports), showing study area (circled), locations of exposures (A', B'), location of the exploratory wells (K 1-7, H1, H2, L1) in the eastern part of TFB, line of electro-log correlation (C-D) shown in Figs. 4 and location of Seismic line (between wells K3-K4) shown in Figs. 6 (see text for explanation).

associated litho units, it is believed that subunit A2 is stratigraphically older than subunit A1. Unit-A is found to be unconformably overlain by a massive, medium to coarse grained sandstone unit with sharp erosional base, which seems to be equivalent to Tipam Formation (Fig.3A) and contains numerous 15-20cm long, brown coloured, very hard oval shaped clasts of very fine grained ferruginous materials, aligned almost sub parallel to erosional plane.

Subunit A1: This is the top most subunit of *Unit-A*, characterised by 8-10m thick, laterally traceable monotonous heterolithic unit. Thin, light brownish to light grey coloured, moderately sorted very fine sand to silty units with 1.5-2cm high ripple cross laminated beds and occasional bi-directional current features found to be interlaminated with grey coloured, massive, discontinuous, 0.50-0.75cm thick mud drapes in the trough of ripples, giving rise to the characteristic "Wavy bedding" (Fig. 3B). Mud couplets are often seen. Ripple cross laminations often incorporates small mud clasts in the trough. At places complete ripple form is preserved with thin mud draped foresets. Finer observation reveals small scale loading, water escape features in the grey coloured, soft, mud layer, lying beneath the sandy unit (Fig. 3C). Both sand and mud are present in equal proportion in this subunit, which is unconformably overlain by the massive sandstone unit. Noteworthy, steep structural dip (i.e. $\sim 65-70^\circ$ towards west) invariably indicates vicinity of a structure bounding

longitudinal fault on the western flank of Langai anticline (Fig. 3D).

Subunit A2: This 2-2.5m thick, laterally traceable, heterolithic subunit lies conformably over an interlaminated silt-mud rich unit and characterised by light yellowish, medium grained, moderate to well sorted, dominantly uni-directional, ripple cross laminated sandstones, with thin isolated mud drape on each foresets as well as on ripple troughs, forming Flaser bedding at lower part of the subunit. Towards top, it grades to purely isolated, light yellow coloured, medium to fine grained 0.50cm high and 1.5-2cm long, isolated sand lenticles encased well within laminated, dark grey coloured mud, forming Lenticular bedding (Fig- 3E, 3F). Lower part of subunit A2 is relatively sand dominated, whereas mud predominates over sand in the upper part of the subunit.

Unit B: Jampai anticline is situated in the easternmost part of TFB (Fig. 1). This 8 - 10m thick sub-horizontal litho unit is exposed near the crestal part of Jampai anticline on Damcheera to Phuldungsei road section (location B' in Fig. 1, Table-1), characterised by yellowish to light brownish coloured, medium grained, moderately sorted, hard, compact, dominantly sandstone unit with occasional thin intercalation of fissile Shale. Comparatively cleaner and better sorted lower portion of the exposed section contains a few 0.50 - 0.60m wide and 0.30-0.35m thick, isolated sandstone units with characteristic wavy lamination and low angle of

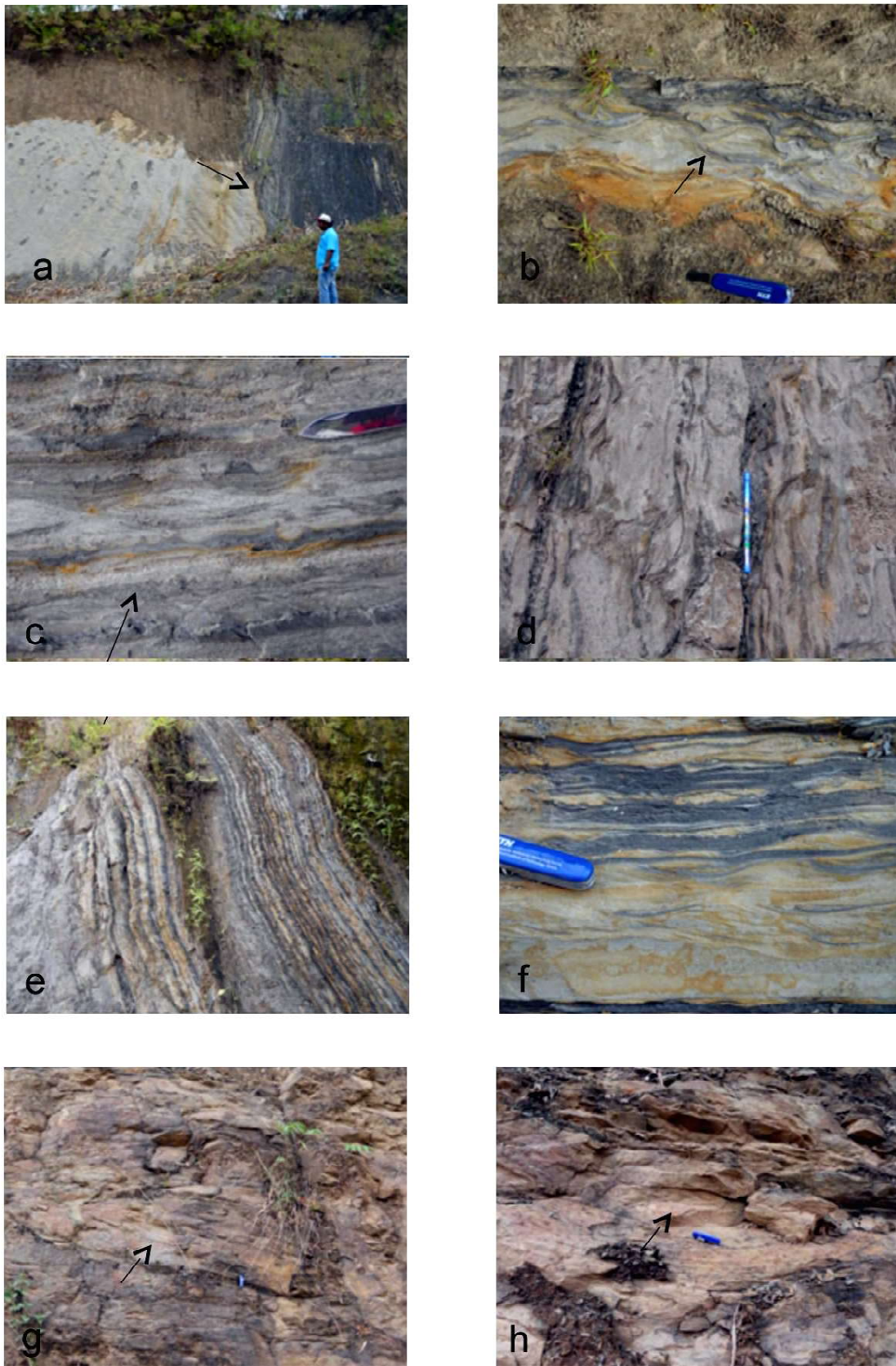


Fig. 3: (a-h) Selected outcrop photographs of *Litho Units A and B* from the clastic succession of Bokabil and upper part of Upper Bhuban formations, exposed along Panisagar to Jampai road section via Damcheera. (A) Erosional unconformity between Bokabil and Tipam formations (see arrow). (B-D) Subunit A1 of *Litho Unit-A*. (E-F) Subunit A2 of *Litho Unit-A*. (G-H) *Litho Unit-B*, Note the hummock is at the centre of G-H. Swiss Knife for scale (See text for explanation).

truncation, found interstratified with parallel bedded medium grained sandstone (Fig- 3G). These are believed to represent medium sized Hummocks. Fig- 3H depicts the geometry of both concave up swales at base & convex up hummocks at top, respectively.

INTEGRATING FIELD OBSERVATIONS WITH SUBSURFACE GEOLOGICAL DATA

In the eastern part of TFB, 10 exploratory wells (Fig.1) have been drilled by ONGC Ltd. In this section, an attempt has been made to analyse some available subsurface geological data which is being integrated with the palaeo-environmental inferences, drawn from the Middle to Late Miocene exposures. Based on the integrated result, a depositional model for the studied section will be proposed in the next section. Both surface and subsurface data were used to validate the depositional model.

Subsurface Data Available

The following data have been used in our study:

Electro-log Correlation,
Core-Log Integration,
3-D Seismic Data, and
Other Supporting Data

A brief account of each of the data type is given below:

Electro-log Correlation: Electro-log characters for Upper Bhuban and Bokabil formations along the line C-D (see Fig-1) have been studied through well correlation, depicting dominantly arenaceous nature of Upper Bhuban and argillaceous nature of Bokabil formations,

respectively. The Late Miocene sediments record an overall coarsening upward, progradational trend, as seen very clearly from the conventional electro-log correlation of the wells from our study area (Fig. 4).

Core-Log Integration: Because of non-availability of core data from Bokabil Formation in the study area, a core of the Bokabil Formation, cut in a field westward of the study area is integrated with a generalized log motif of Bokabil Formation. The salient features are mentioned in Fig. 5.

Log motif of Bokabil and upper part of Upper Bhuban formations show alternation of argillaceous and arenaceous litho units. Upper part of Upper Bhuban Formation seems to be dominantly arenaceous, while Bokabil Formation seems to be dominantly argillaceous in nature. Log characters show one distinct fining up sand in the upper part of Upper Bhuban Formation and blocky sands to an overall coarsening up trend in Bokabil Formation. The core, cut in the Bokabil Formation also shows fine alternation of mud and very fine grained sandstone, ripple cross lamination, Flaser bedding and occasional bi-directional current features, in the lower portion mainly.

Thin alternation of sand and mud along with profuse presence of Flaser bedding, occasional bi-directional current features in core, probably suggesting that the deposition took place in a tide dominated area with alternation of tidal currents and slack water phases (Reineck and Singh, 1973). Periods of current activity resulted in the deposition of sandy layers while the slack water periods gives rise to the deposition of muds from suspension. In the mud flat region (Fig- 8B), a vertical succession of thick shale with thin sand intercalations are expected and similar pattern is observed in Bokabil

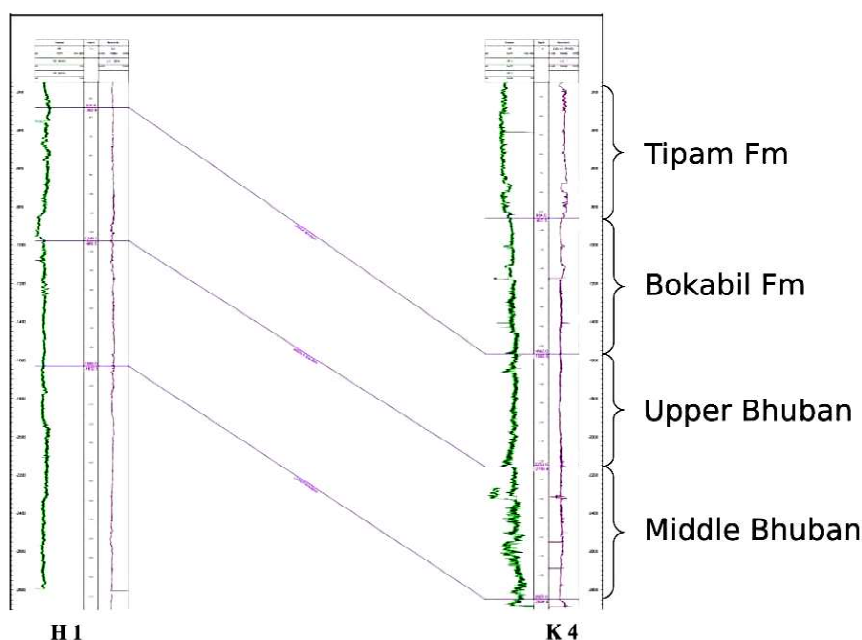


Fig. 4. Electro-log correlation along C-D line between wells H 1 and K 4 (see Fig- 1 for location of C-D line).

formation with dominantly coarsening up trend (**Fig. 5**), characteristic of a rapidly prograding tide dominated deltaic system. The well log signatures of Upper Bhuban Formation in general show dominantly arenaceous facies with one typical finning up sand unit with sharp base at the upper portion. Not much can be inferred from this about the Upper Bhuban Formation, because of paucity of data.

3-D Seismic Data: A 3-D seismic section (see location in Fig-1) is given in **Fig. 6** in order to provide a glance of subsurface stratigraphy of the region.

Other Supporting Data: Granulometric studies carried out in western part of TFB in both Upper Bhuban and Bokabil formations, clearly show classic grain size distribution as moderately well to well sorted sands with complete absence to minor presence of traction load which is expected in tidal flat setting (Chakrabarti, M. K. et. al., 1995; ONGC Internal Reports).

Integrating Surface and Subsurface Data:

In this section, an attempt has been made to integrate all the available data, ranging from outcrops to subsurface geological data. Based on the integrated result, a Late Miocene depositional model will be proposed in the next section.

Litho Unit A is an overall argillaceous facies and believed to be equivalent to the Late Miocene Bokabil Formation, with abundant Lenticular, Flaser and Wavy beddings. Lenticular bedding (Fig. 3F) records sediment starved current ripples deposited in a suspension load dominated mud rich environment. These may result from low sediment supply or from a current with insufficient velocity to transport sand (Reineck and Singh, 1973)

and usually found in mud flat region of an intertidal setting (Fig. 8B). Flaser bedding (Fig. 3F) occurs at an increased current velocity compared to the formation of Lenticular bedding, thus eroding the ripple crests and preserving muds within the troughs (Reineck and Wunderlich, 1968; Reineck and Singh, 1973). Flaser bedding is more common in the sand flat region of an intertidal setting (Fig. 8B), where bed load deposit predominate. Wavy bedding may be ascribed to an environment where current velocities and sediment supply are greater than during the formation of Lenticular bedding but lower than during the formation of Flaser bedding. Wavy bedding occurs usually in mixed flat region of an intertidal setting (Fig. 8B), where mud is deposited as suspension load during intermittent slack water periods over small scale rippled sands formed under tidal currents. Fine mud usually follows the alternating concave-convex nature of the ripples, creating a wavy appearance. Profuse occurrence of Flaser bedding, Lenticular bedding, characteristic 'Wavy or tidal-bedding' of Reineck and Wunderlich (1968), subordinate ripple cross-lamination with occasional bi-directional current features, mud couplets and thin mud drapes along the foresets (Fig- 3 B-F), all pointing towards the dominance of tidal influence during Late Miocene. The sedimentary structures in outcrops and core sample along with overall coarsening upward trend as depicted in electro-log signature in the upper part of Bokabil Formation substantiate our finding and suggesting that Bokabil Formation may have been deposited in an overall prograding intertidal depositional setting with migrating bed forms and unconformably overlain by Tipam Formation of continental fluvial origin. The nature of Tipam - Bokabil contact points to a sub-aerial

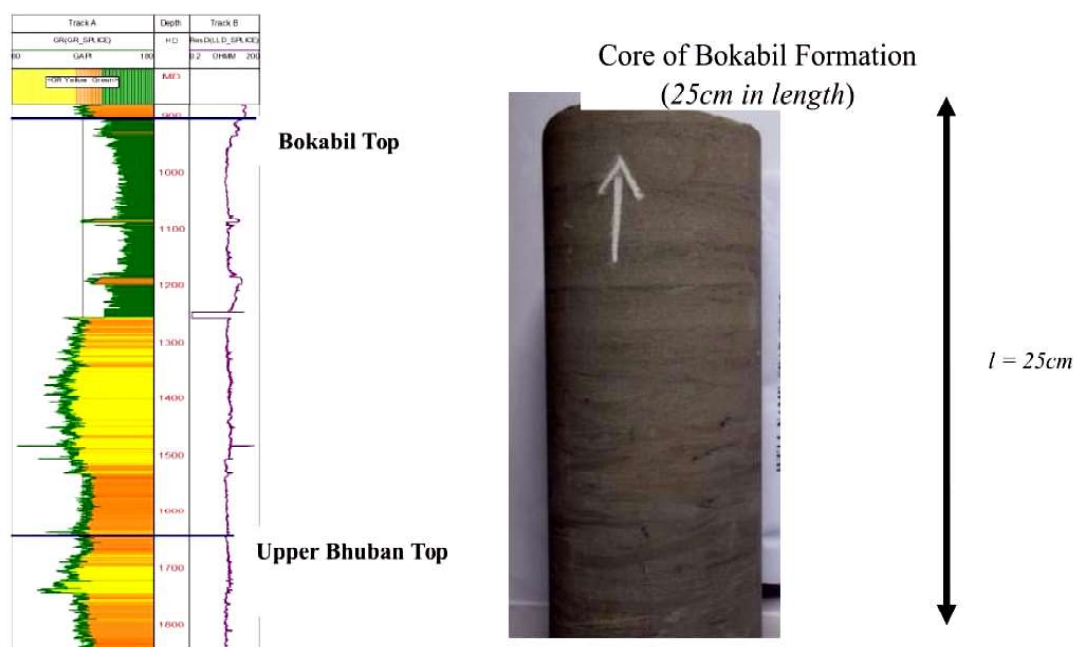


Fig. 5. Integration of Core and Electro-log data (see text for explanation).

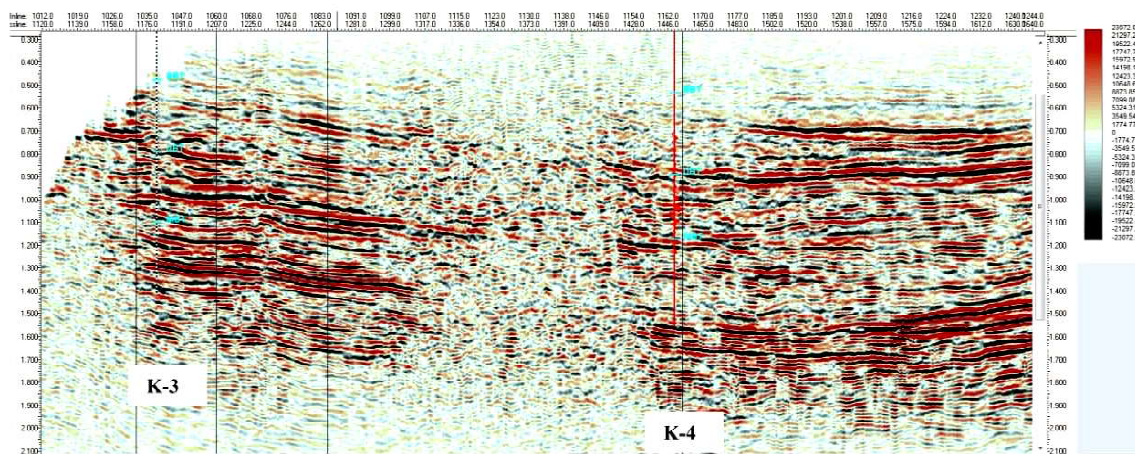


Fig. 6. 3-D Seismic section between wells K 3 and K 4 (see Fig- 1 or location of the line).

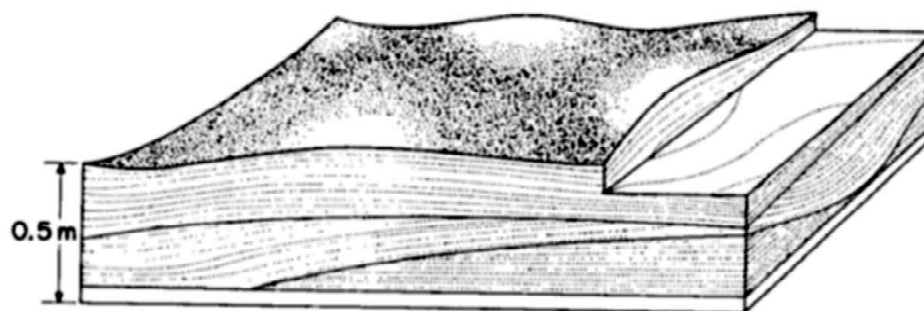


Fig. 7. Origin of Hummocky Cross-Stratification (after Harms et. al. 1975)

unconformity, likely to be due to sharp fall of relative sea level (Table 1).

Based on the observations, we may infer that *Litho Unit-B* is having close similarity with the upper part of arenaceous Upper Bhuban Formation of Middle Miocene, as described by earlier workers (Ganguly, S., 1983 a, b; Srivastava J. P., 1975). The unit is characterised by a few medium sized hummocks. Hummocky cross-stratification (HCS) optimally forms above or near storm wave base where aggradation rates during storms are high enough to preserve hummocks but unidirectional current speeds are sufficiently low to generate low-angle, isotropic cross-stratification. Swaley cross-stratification is also hypothesized to be deposited by an aggrading hummocky bed between fair weather and storm wave base, (Harms et. al. 1975) but in shallower water where aggradation rates are low enough to cause preferential preservation of swales (Fig. 7). Presence of HCS and dominantly fining up trend in electro-log signatures of upper part of Upper Bhuban Formation (Fig- 3 G-H; Fig- 5), strengthen our view that at least upper part of Upper Bhuban Formation had been deposited in a storm influenced shallow marine inner shelf condition between fair weather and storm wave base during Middle to Late Miocene.

DEPOSITIONAL MODEL

Understanding the tectonic setting of a region is a necessary pre-requisite to understand the paleogeography and sedimentation patterns of that region (Miall, A. D., 1997). Therefore, prior to propose a depositional model for the upper part of Surma Group of rocks of Late Miocene time, exposed in the study area based on integrating both surface and subsurface geological data, we will give a brief account of Late Miocene tectonic setting of the fold belt area.

During Eocene-Oligocene, oblique collision of the Indian and Burmese plates (Curry et al., 1982) resulted in obduction of the accretionary prism (Pivnik et. al. 1998), forming the Indo-Burma Ranges (IBR). Thereafter, the paleogeographic setting of the TFB included the westward migrating accretionary prism complex (Fig. 8A) in an arc-trench setting (Gani and Alam, 1999). The remnant ocean basin had been closing from northeast to southwest because of this oblique subduction (Gani and Alam, 2003; Alam et. al., 2003). Sediment source was believed to be largely from the newly uplifted Indo-Burman subduction complex to the east and north-east and carried most likely by Palaeo-Brahmaputra River (Uddin and Lundberg, 1999) to the closing Bengal Basin.

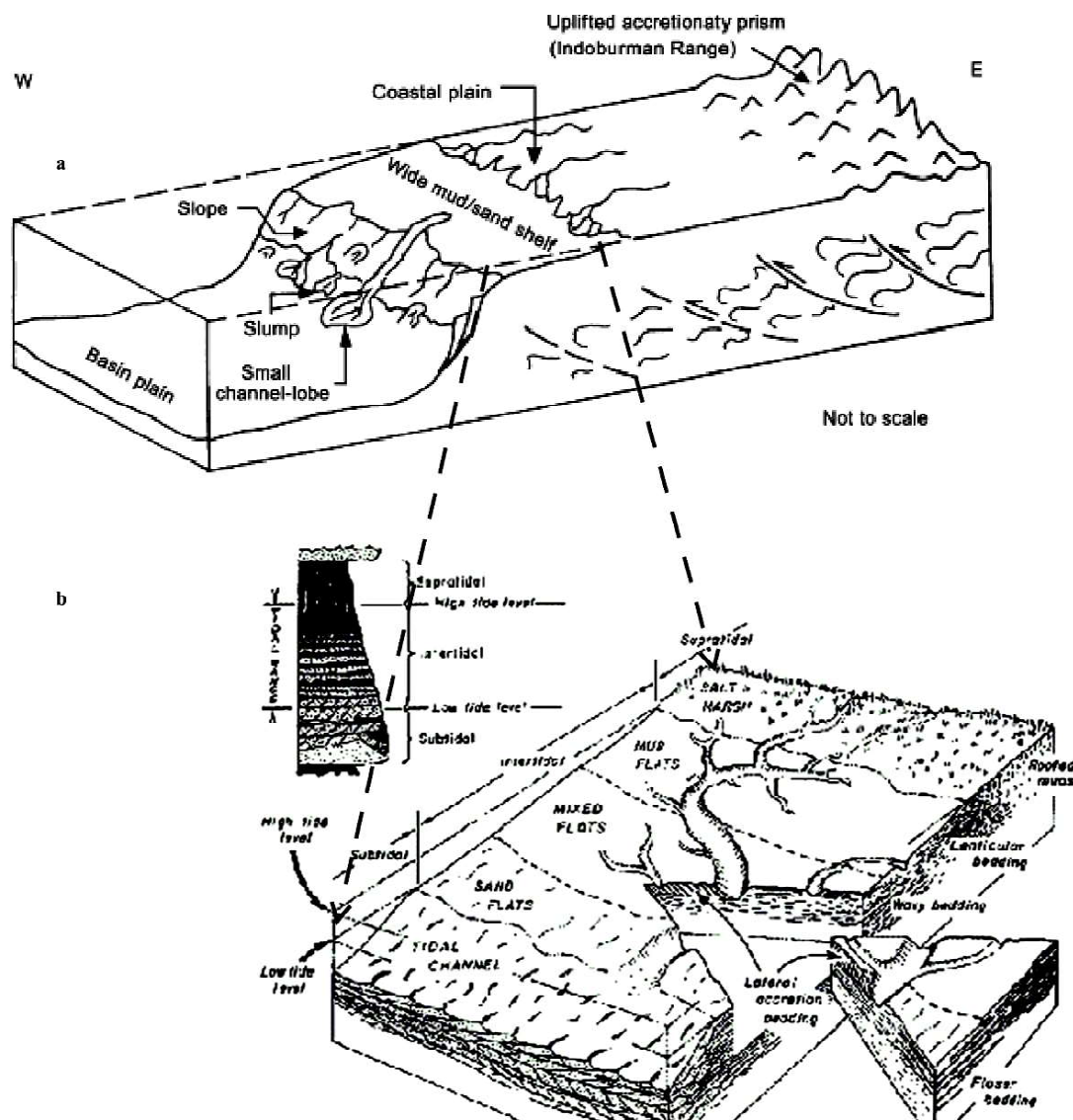


Fig. 8 (a-b). Depositional model during Late Miocene time (see text for explanation). Courtesy-8A-Gani and Alam, 2003; 8B-<http://www4.uwm.edu>.

Because of rapid sedimentation, the deep-water embayment had been smoothed to shallow water conditions with dominantly tidal influence, probably sometime in the Late Miocene (Curiale et. al. 2002). Alam (1995) has documented almost north-south palaeo-coastline trend from the paleocurrent analysis of the Upper Tertiary Baraichari Shale Formation, exposed in Sitapahar anticline of Bangladesh, southward of our study area.

Based on all the available data, ranging from Middle to Late Miocene clastic succession as exposed in the study area, integrated with available subsurface geological data, a conceptual palaeo- environmental model has been given (See the block diagram in Fig. 8A and B), where an overall basinward prograding sequence of Middle Miocene arenaceous Upper Bhuban Formation had been deposited under storm dominated

shallow inner shelf depositional setting between fair weather and storm wave base and grades conformably up the sequence to Late Miocene argillaceous Bokabil Formation, deposited dominantly under shallow intertidal mixed flat to mud flat depositional setting, with migrating bed forms due to sea level fluctuations (Fig-8B). Miocene Surma Group of rocks is unconformably overlain by Early Pliocene Tipam Group of rocks, most likely to be deposited in a continental-fluvial environment.

The significance of tidal influence in the shallow marine Miocene Surma Group was first discussed by Alam (1995). On the basis of detailed facies analysis of core samples and wire-line log interpretation, Alam (1995) envisaged a micro-tidal coastal setting with extensive development of intertidal and subtidal environments in the proto-Surma delta embayment, for the Surma Group

sediments in the Sylhet Trough. The modern, tidally influenced Bengal shelf is likely to provide an excellent analogue for the ancient tidal environment due to its similar basin physiography and high sediment and water discharge, thus validating the proposed depositional model (Davies et. al. 2003).

CONCLUSIONS

Exposed successions with a variety of primary sedimentary structures of different scales along with subsurface geological data permit a semi-detailed palaeo-environmental analysis of upper part of Surma Group of rocks. The Middle Miocene arenaceous Upper Bhuban Formation with a few isolated hummocks at the top part, probably suggesting a storm dominated shallow inner shelf depositional setting, grading conformably up to an argillaceous Late Miocene Bokabil Formation with profuse Flaser, Lenticular and Wavy bedding, which most likely point towards migrating intertidal mud flat to mixed flat environment of deposition in an overall prograding setup. Surma Group of rocks are unconformably overlain by arenaceous Tipam Group of rocks with a pronounced erosional unconformity, probably representing continental-fluvial depositional environment, which mark the final phase of regional fall of base level, aided by tectonic upheaval of the TFB.

This approach may be seen as an encouragement to stimulate further research work to study the lowermost part of the Surma Group to have a better understanding of the overall progradational nature of the basin fill history. A micro-paleontological, Ichnological, along with Palaeo-current analyses of the Surma Group of rocks in different areas of the TFB would be beneficial in this regard. This in turn will provide valuable insights into the exploration and exploitation strategies for hydrocarbons in terms of location and geometry of stratigraphic traps, outlining seal architecture and flow units.

Acknowledgements: The authors are extremely grateful to Shri N. K. Verma, Director (Exploration), ONGC Ltd for granting permission for oral presentation and publication of the work. They are highly indebted to Shri S. K. Jain, GGM- Basin Manager, A&AA Basin for his guidance and motivation throughout the study. The invaluable support of colleagues of Agartala Forward Base is thankfully acknowledged. Last but not the least, authors wish to thank Shri. A. K. Biswas, Shri. C. Chakrobarty, Dr. G. Bhattacharya, Shri. K. Kemas for critically reviewing the manuscript and providing invaluable comments. The views expressed here are solely of the authors and do not necessarily reflect the views of the organization, they belong to.

References

- Alam, M.M., (1995). Tide-dominated sedimentation in the Upper Tertiary succession of the Sitapahar anticline, Bangladesh. In: Flemming, B.W., Bortholoma, A. (Eds.), Tidal Signatures in Modern and Ancient Sediments. Int. Assoc. Sedimentol., Spec. Publ. 24, 329–341.
- Alam, M., Alam, M. M., Curray, Joseph R., Chowdhury, M. L. R., Gani, M. R., (2003). An overview of the sedimentary geology of the Bengal Basin in relation to the regional tectonic framework and basin-fill history. *Sedimentary Geology*, 155, 179–208.
- Anjelier, J., and Baruah, S. (2009). Seismotectonics in Northeast India: A stress analysis of focal mechanism solutions of earthquakes and its kinematic implications. *Geophys. Journal. Int.*, 178, 303–326
- Baruah, B., et. al. (1992). Geology of Jampai Anticline, Tripura State, Progress Report. IPE.
- Chakrabarti, M. K., et. al. (1995). Correlation of reservoir facies and sand geometry of western Tripura, ONGC Internal Reports.
- Curiale, J.A., Covington, G. H., Shamsuddin, A.H.M., Morelos, J.A. and Shamsuddin, A.K.M. (2002). Origin of petroleum in Bangladesh: AAPG Bulletin, 86 (4), 625-652.
- Curay, J.R., Emmel, F.J., Moore, D.G., Raitt, R.W. (1982). Structure, tectonics and geological history of the northeastern Indian Ocean. In: Nairn, A.E.M., Stehli, F.G. (Eds.), *The Ocean Basins and Margins*, Vol. 6. The Indian Ocean. Plenum Press, New York, 399–450.
- Davies, C., Best, J., Collier, R. (2003). Sedimentology of the Bengal shelf, Bangladesh: Comparison of late Miocene sediments, Sitakund anticline, with the modern, tidally dominated shelf, *Sedimentary Geology*, 155, 271–300.
- Evans, P. (1932). Tertiary succession in Assam. *Trans. Min. Geol. Inst. India* 27, 155–260.
- Ganguly, S. (1983a). Stratigraphy, Sedimentation and Hydrocarbon prospects of the Tertiary succession of Tripura & Cachar (Assam). *Indian Jour of Geol.* 145-180.
- Ganguly, S. (1983b). Geology and hydrocarbon prospects of Tripura–Cachar–Mizoram region. In: Bhandari, L.L. et al. (Eds.), *Petroliferous Basins of India*, Part 1. *Petrol. Asia J. Publ.*, Dehradun, 105–110.
- Gani, R. M., Alam, M.M. (1999). Trench-slope controlled deep-sea clastics in the exposed lower Surma Group in the south-eastern fold belt of the Bengal Basin, Bangladesh. *Sedimentary Geology*, 127, 221–236.
- Gani, M. R, Alam, M. M. (2003). Sedimentation and basin-fill history of the Neogene clastic succession exposed in the south eastern fold belt of the Bengal Basin, Bangladesh: a high-resolution sequence

- stratigraphic approach. *Sedimentary Geology*, 155, 227–270.
- Ghosh, S. K., *Structural Geology*. 1st Ed (1993).
- Harms, J. C., Southard, J. B., Spearing, D. R., and Walker, R. G. (1975). Depositional environments as interpreted from primary sedimentary structures and stratification sequences: SEPM Short Course Notes no. 2, 161.
- Hiller, K., Elahi, M. (1988). Structural growth and hydrocarbon entrapment in the Surma basin, Bangladesh. In: Wagner, H.C., Wagner, L.C., Wang, F.F.H., Wong, F.L. (Eds.), *Petroleum Resources of China and Related Subjects*, Houston, Texas. Circum-Pacific Council for Energy and Mineral Resources Earth Sci. Series, 10, 657–669.
- Khar, B. M., Ganju, J. L. (1984). Tectonics of Tripura folds- Probable mechanism of folding and faulting, *Petroleum Asia Journal*, 66-70.
- Lindsay, J.F., Holliday, D.W., Hulbert, A.G. (1991). Sequence stratigraphy and the evolution of the Ganges – Brahmaputra delta complex. *Am. Assoc. Pet. Geol. Bull.* 75, 1233–1254.
- Miall, A.D. (1997). *The Geology of Stratigraphic Sequences* Springer-Verlag, Berlin.
- Pivnik, D.A., Nahm, J., Tucker, R.S., Smith, G.O., Nyein, K., Nyunt, M., Maung, P.H. (1998). Polyphase deformation in a fore-arc/back-arc basin, Salin Sub basin, Myanmar (Burma). *Am. Assoc. Pet. Geol. Bull.* 82, 1837–1856.
- Reineck, H.E., Singh, I.B. (1973). *Depositional Sedimentary Environments*. Springer, Berlin.
- Reineck, H. E., Wunderlich, F. (1968). Classification and origin of flaser and lenticular bedding. *Sedimentology* 11, 99–104.
- Srivastava, J. P et. al. (1975). Photogeological Report of Jampai-Sakhan Anticline, Tripura State. ONGC Unpublished Reports.
- Uddin, A., Lundberg, N. (1999). A palaeo-Brahmaputra? Subsurface lithofacies analysis of Miocene deltaic sediments in the Himalayan– Bengal system, Bangladesh. *Sedimentary Geology*, 123, 239–254.

Sandstone Petrology of the Kolhan Basin, Eastern India: Implications for the Tectonic Evolution of a Half-Graben

ROHINI DAS

Department of Geology and Geophysics, IIT Kharagpur, PIN: 721302, India

Email: romiyadas@gmail.com

Abstract: The Palaeoproterozoic Kolhan Group (*Purana*) ensemble constitute the youngest lithostratigraphic basin in the Singhbhum Archaean craton. The Kolhan Group unconformably overlies both the Singhbhum granite and the Iron Ore Supergroup. Representing a typical sandstone-shale (\pm carbonates) sequence, the Kolhan Group is characterized by thin and discontinuous patches of basal conglomerates draped by sandstone beds. The faulted contact with the Iron Ore Supergroup limits the western 'distal' margin of the Kolhan basin showing evidence of passive subsidence subsequent to the initial rifting stage. The basin evolved as a half-graben under the influence of an extensional stress regime. The assumption of a tectonic setting for the NE-SW trending Kolhan basin possibly relate to the basin opening to the E-W extensional stress system that prevailed during the development of the Newer Dolerite dyke. The Paleoproterozoic age of the Kolhan basin is based on the consideration of the conformable stress pattern responsible both for the basin opening, and on the development of the conjugate fracture system along which the newer Dolerite dykes intruded the Singhbhum Archaean craton.

In general, the textural and mineralogical maturity of the Kolhan sandstone increases in vertical progression. The trend of variations in different mineralogical and textural attributes, however, exhibits inflections at different lithological levels. Petrological studies collectively indicate that the sandstones were dominantly derived from a weathered granitic crust under a humid climatic condition. Provenance-derived variations in sandstone compositions are therefore a key in unraveling regional tectonic histories. The basin axis controlled the progradation direction which was likely driven by climatically induced sediment influx, a eustatic fall, or both. In the case of the incongruent shift, increased sediment supply permitted the rivers to cross the basinal deep. Temporal association of the Kolhan sandstones with tectonic structures in the belt indicates that syn-tectonic thrust uplift, not isostatic uplift or climate, caused the influx of quartz.

The sedimentation pattern in the Kolhan basin reflects a change from braided fluvial-ephemeral pattern to a fan-delta-lacustrine type. The channel geometries and the climate exerted a major control on the processes of sediment transfer. Repeated fault controlled uplift of the source area followed by subsidence and forced regression, generated multiple sediment cyclicity that led to the fluvial-fan delta sedimentation pattern. Intermittent uplift of the faulted blocks exposed fresh bedrock to mechanical weathering that generated a large amount of detritus and resulted to forced regressions, repeatedly disrupting the cycles which may reflect a stratigraphic response of connected rift basins at the early stage of extension. The marked variations in thickness of the fan delta succession and the stacking pattern in different measured profiles reflect the overriding tectonic controls on fan delta evolution. The accumulated fault displacement created higher accommodation and thicker delta sequences. Intermittent uplift of fault blocks exposed fresh bedrock to mechanical weathering, generated a large amount of detritus, and resulted in forced closure of the land locked basin, repeatedly disrupting the fining upward pattern. The control of source rock lithology or climate was of secondary importance to tectonic effects. Such a retrograding fan delta could be a stratigraphic response of connected rift basins at the early stage of extension.

Keywords: Kolhan basin, petrology, sandstone, tectonics.

INTRODUCTION

The 2.2-2.1 Ga pear shaped Kolhan basin in the Singhbhum craton is an enigma and significant in many respect. It occurs as a narrow strip-like outcrop pattern extending for 80-100 km in length with an average width of 10-12 km, controlled by the NE-SW trend. It occurs

as isolated outliers present in four detached basins such as 1. Chaibasa - Noamundi basin, 2. Chamakpur-Keonjhar basin, 3. Mankarchua basin, and 4. Sarapalli - Kamakhyanager basin. It covers an area around 800sq km along the western margin of Singhbhum Granite. It intervenes the Singhbhum granite to the east and the Iron Ore Supergroup to the west (Saha and Sarkar, 1988).

It is one of the youngest and the least studied Precambrian stratigraphic unit in Singhbhum geology (Mukhopadhyay, 2001; Saha, 1994).

No direct evidence of its age has been made, but inferences have resulted from its structural relationship with adjacent deformed and metamorphosed tectonosomes; that it ranges from Neoproterozoic (Roy et al., 2012) to Paleo-proterozoic Saha, 1994; Bandhopadhyaya and Sengupta, 2004) to Meso-Neoproterozoic (Mukhopadhyay et al., 2006) The undeformed and unmetamorphosed lithologic character of the Kolhans may be more compatible with deposition in the Meso- to Neo-proterozoic time. The Kolhan basin is similar in many respects with Manganese-bearing Wyllies Port Formation of 1.8-1.96Ga of Soutpansberg Group, Northeast Kaapvaal Craton, South Africa suggesting a possible Indo-African connection during the Neo-Archean age (Bandhopadhyaya and Sengupta, 2004).

The depositional environment of the Kolhans varied from braided fluvial-ephemeral pattern to a fan-delta-lacustrine type. The channel geometries and the climate exerted a major control on the processes of sediment transfer. Repeated upliftment of the source due to fault-controlled activity followed by subsidence and forced regression generated multiple sediment cyclicity that led to the fluvial-fan delta sedimentation pattern (Dalabhera, 2009).

GEOLOGICAL SETTING OF THE KOLHANS

The geological map of the Kolhan basin (Fig.1) shows various lithologic units. The various stratigraphic units according to Saha(1994) are (a) Older Metamorphic Group (OMG) (b) Older Metamorphic Tonalite-gneiss (OMTG) (c) Singhbhum granite Phase II and Phase III (d) Iron Ore Supergroup {shales, tuffs, phyllites, banded iron formation (BIF), banded hematite jasper (BHJ), banded hematite quartzite (BHQ), sandstone, and conglomerate} (e) Jagannathpur and Malangtoli lavas, and (f) Kolhan basin .

The Kolhan basin consists of a low (2° - 10°) westerly dipping sequence of basal, purple conglomerate, pebbly sandstone, gray quartz arenite (locally arkosic), with several thin bands of purple to dusky red siltstone and shales. The Kolhans show a faulted contact with the Jagannathpur lavas and the Iron Ore Supergroup to the west and unconformably overlie the Singhbhum granite to the east (Saha,1994).

PETROLOGY AND GEOCHEMISTRY OF KOLHANS

A. Sandstone Petrology of the Kolhan

Petrographical investigation of the siliciclastic rocks of the Kolhan basin shows mainly sandstone,

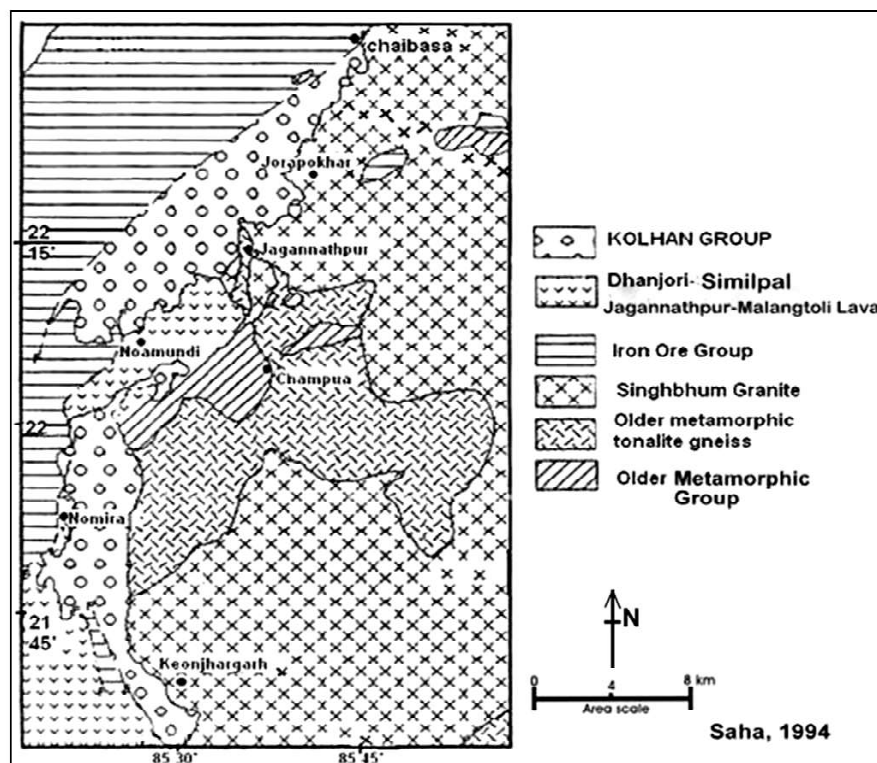


Fig. 1. Geological map of West Singhbhum showing Chaibasa-Noamundi basin and North Orissa showing Chamakpur-Keonjhar basin (Saha,1994)with the faulted contact against Iron Ore SuperGroup on the western side and angular unconformity with Singhbhum Granite on the eastern side of Chaibasa-Noamundi basin.

conglomerate, and shale. The minerals present are dominantly quartz, feldspar, (lithic fragments) rock fragments, and muscovite in minor amount, and heavy minerals like zircon, rutile, tourmaline, and opaques. The Kolhan sandstones display considerable compositional variety, ranging from subarkose to quartz arenite. They are composed mainly of an aggregate of sub-angular to sub-rounded quartz embedded in siliceous- ferruginous matrix, with subordinate amounts of feldspar, jasper, muscovite constitute about 1.5% or less. The grain size varies from 0.1 to 0.8 mm while the grains are subangular in shape coated with iron oxide. The matrix material consists of sericite or reconstituted complex aggregates of chert and sericite (Figs. 3a and 3 b). It usually occurs as fibrous or finer structured laths in the pore spaces, and constitutes about 3.21-6.96% of the bulk volume. The sandstones contain < 5% silt-size quartz grains and it is quite likely that the silica was precipitated over the detritals as secondary overgrowths (Goldstein,1948). The ferruginous cement may have been derived from the alteration of ferromagnesian minerals.

Quartz is dominant with slight undulose extinction and is usually monocrystalline. Polycrystalline, vein quartz and strongly undulose quartz are very subordinate in occurrence Polycrystalline quartz occurs in two varieties: (a) grains with a polygonal fabric of interlocking grains and (b) grains with elongate, lenticular, interlocking, sutured crystals (Fig. 2a). Quartz present in the matrix shows weak recrystallization and

presence of fused contacts with the framework grains (Fig. 2b). Quartz grains show bimodal distribution in quartz arenite (Fig. 2c). The grains are mostly coated with iron oxide and exhibit authigenic overgrowths which produce euhedral outline in a few cases. Such overgrowths are occasionally been replaced by the primary hematite coating living behind scattered relics of the latter. It is further observed that these overgrowths are rare on that side of the grain which is in contact with the “clay pellets”. Recycled quartz grains with abraded outgrowths are occasionally reported. The contacts between the grains are generally plane and rarely sutured and stylolitic. Inclusions of minute apatite, zircon and rutile are rare. They sometimes show gas vacuoles rarely arranged in trails. There is no preferred orientation of the grains, which are embedded in a clay matrix, replaced by hematite and rarely by calcite cement.

The detrital mineral grain in decreasing order of abundance is feldspar which varies in modal proportions from practically nil to about 3%. The feldspars are predominantly K-feldspars, microcline, and albite-rich plagioclase (in descending order of abundance). The grain size varies from 0.09 to 1 mm and the grains are mostly sub angular and coated with hematite. K-feldspars are highly altered and display microperthitic intergrowth with Na-plagioclase. The feldspar grains show rounded inclusions of quartz (Figs. 3(e)- (f)). Feldspar grains in arkosic arenite display lamellar and crosshatched twinning (cross nicols, 50x). The feldspars

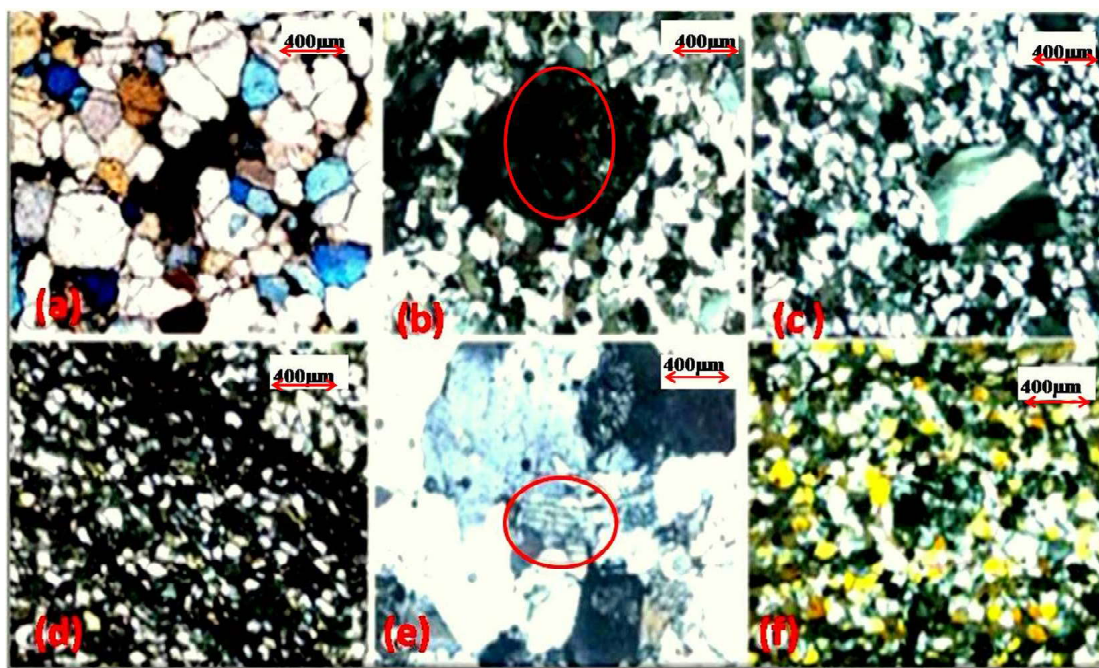


Fig. 2a. Moderately well sorted, medium-coarse grained sandstone, well rounded quartz grains with long and concavo-convex contact, **b.** Rounded to sub-rounded monocrystalline framework quartz grains in quartz arenite, matrix quartz shows feeble recrystallization and fused contacts with framework grains, **(c)** Quartz grains showing bimodal distribution in quartz arenite, **d.** sandstones, **e and f.** with rounded feldspar grains.

and microcline are sericitized in which few fresh relics are present. Micro faulting and bending of the twin lamellae are other features rarely observed in thin sections. Such detrital feldspars show evidence of having been replaced by the slightly recrystallized illite-clay matrix. In other cases, all stages of replacement by muscovite along cleavages are also observed. Authigenic overgrowths on detrital plagioclase are extremely rare. The low content of feldspar could be due to (a) the removal of feldspar during transport or (b) diagenetic removal of feldspars. Flakes of detrital muscovite measuring about 0.5 mm. are not commonly

seen in these sections. The flakes however show degradation to sericite mica and replacement of their detrital outline by hematite cement. The rock fragments are usually identified by compositional and textural criteria. Sedimentary rock fragments are intrabasinal, intraformational and extraformational.

The size of chert varies between 0.12 and 0.5 mm. The grains are mostly subrounded to round with haematite coating. They contain fine sericite flakes as inclusion and show occasional recrystallization. Other minor detrital components include biotite, chlorite, and kyanite. Biotite is mostly altered to colourless chlorite with

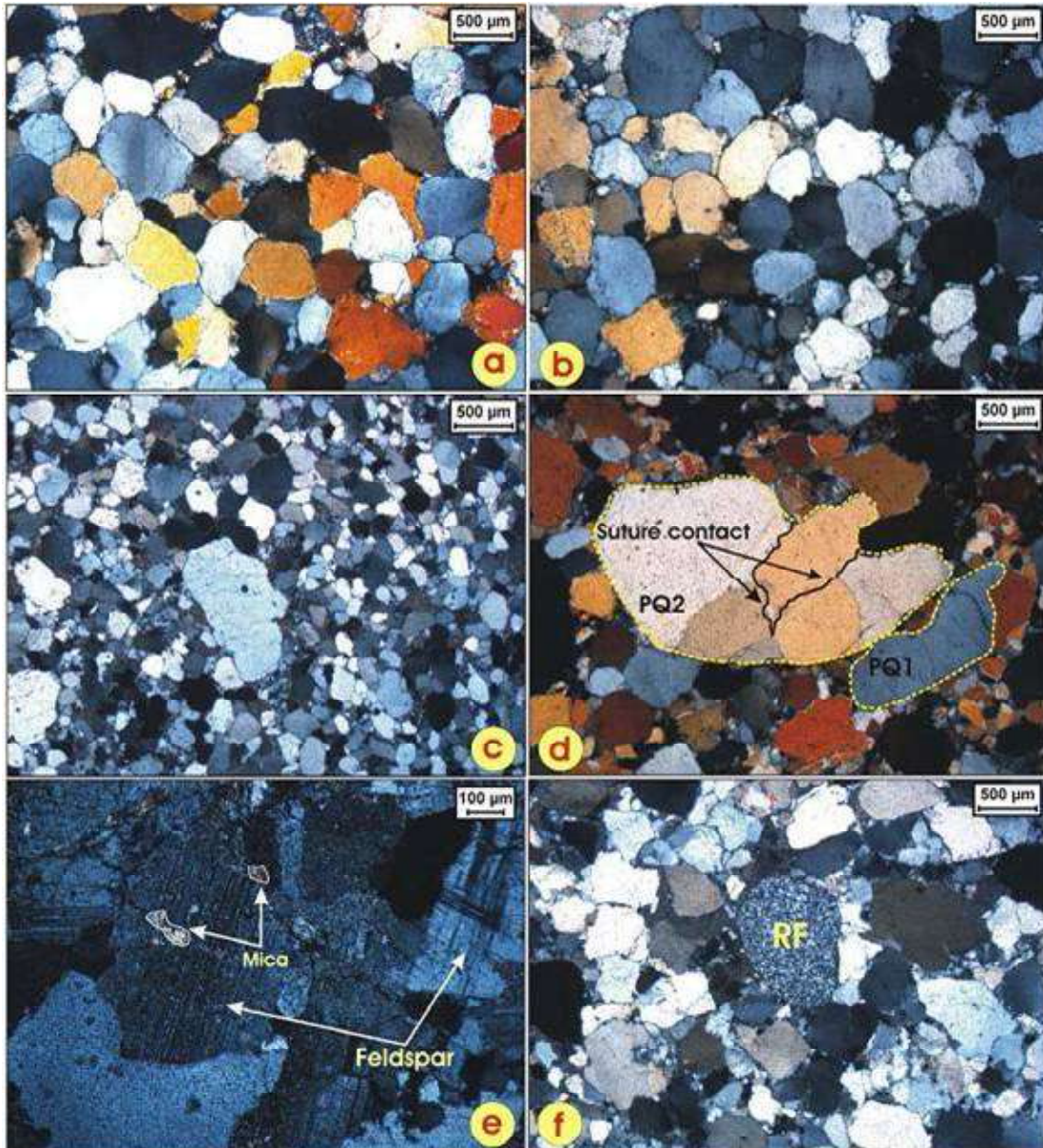


Fig. 3a and b. Moderately well sorted, medium-coarse grained sandstone (SSD facies) (Note: well-rounded recycled plutonic quartz with long and concavo-convex contact and volcanic quartz grains with cherty resorption structure are seen), **c.** Quartz grains showing bimodal distribution in quartz arenite, **d.** Elongate, oriented, and unoriented polycrystalline grains, commonly with strongly sutured contacts (Note: polycrystalline quartz with 2-3 grain (PQ1) and > 3 grain (PQ2) are present), **e.** Feldspar grains in sublitharenite (Note: mica inclusions are seen), **f.** Lithic fragment (RF) in recycled sandstone.

liberation of iron oxide and titanium oxide which form dusty hematite and minute rutile grains in the vicinity. Chlorite is greenish, feebly anisotropic to colourless and almost isotropic and is rarely found as pellets. It is mostly a prochlorite variety. Authigenic chlorite is also present. The kyanite is found as a single big crystal in only one thin section, with one set of prismatic cleavage and extinction angle of nearly 35° . It shows characters of replacement by muscovite flakes and by authigenic silica along the borders.

B. Geochemical Study of the Kolhans

Geochemical analysis of sandstones samples from the Kolhans show the following changes:

SiO_2 and Al_2O_3 vary in the range from 82.86 to 92.36% (average 86.66%) and 2.96 to 9.03% (average 6.20%) respectively.

K_2O , Na_2O , and CaO vary in the ranges from 0.60 to 3.65% (average 2.03%), 0.06-0.20% (average 0.10%), and 0.05 to 0.10% (average 0.08%) respectively (Fig. 4b).

The Kolhan shales are characterized by high values of SiO_2 , K_2O , Fe_2O_3 and low values of CaO , TiO_2 , Na_2O , Al_2O_3 , MgO as compared with the average Proterozoic shale (APS) (Figs. 5 and 6).

TERNARY PLOTS

Dickinson and Suzek (1979) and Dickinson et al. (1983) did not include the Precambrian suites in their provenance analysis because of uncertainty of plate tectonics in the Precambrian. However, an attempt has been made here to analyze the tectonic setting of the provenance in view of the fact that the Indian craton is

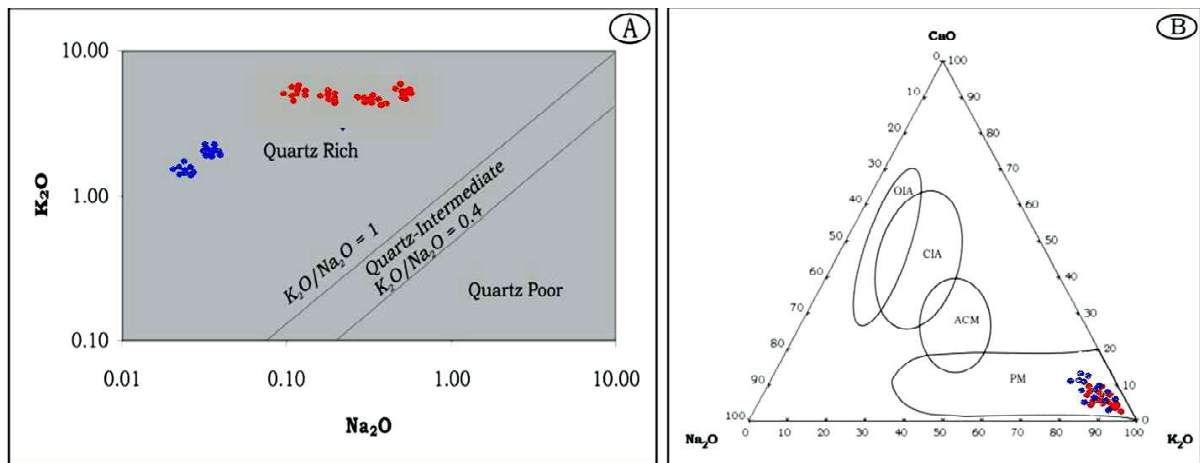


Fig. 4a. K_2O - Na_2O diagram classifying Kolhan siliciclastics as quartz rich type (Crook, 1974), **b.** CaO - Na_2O - K_2O triangular diagram showing Kolhan siliciclastics in the passive margin (PM) field; also shown are the fields of different tectonic settings, ACM-Active Continental Margin, OIA-Oceanic Island Arc, CIA - Continental Island Arc (Bhatia, 1983). The blue dots indicate the sandstone samples and the red dots indicate the shale samples. (Samples from Chamakpur-Keonjhar basin).

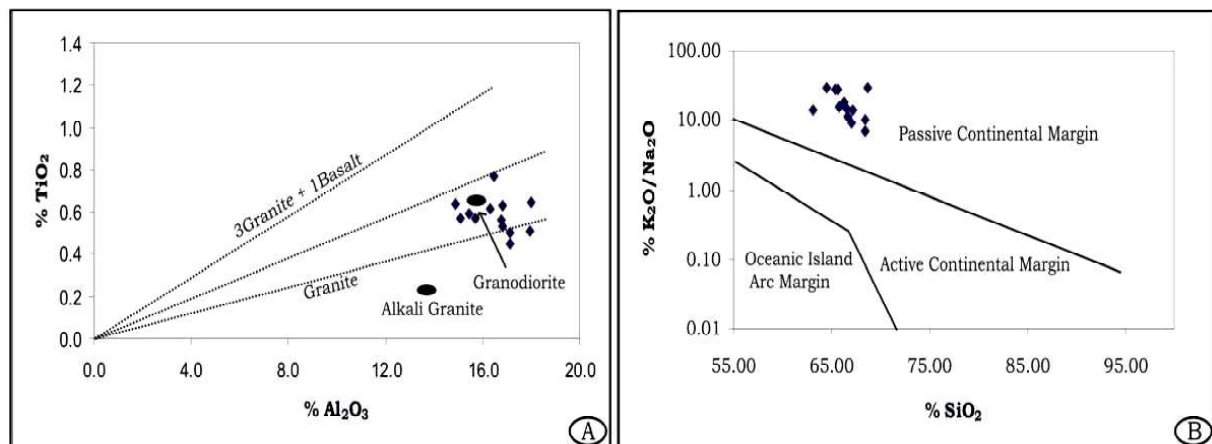


Fig. 5a. Bivariate plot between Al_2O_3 and TiO_2 , indicating source rock to be granitic (Schieber et al., 1992), **b.** Tectonic discrimination diagram for the Kolhan shale indicating the the passive margin setting, (Samples from Chaibasa-Noamundi basin).

a collage of several Archaean cratonic nuclei and mobile belts (Acharya,1984).The procedure suggested by Dickinson and Suzek (Dickinson and Suzek,1979) has been used though; a few departures had to be made for defining different elements for the modal analysis.The metasedimentary fragments such as argillite and phyllite showing definite signatures of metamorphism are of extrabasinal parentage and have been included within, Ls. Occurrence of few points in the transitional orogen provinces appears to have been caused by the modified classification of polycrystalline quartz (Qp) which has resulted in significant shift of the data points towards Lt pole. The recalculated modal components for Kolhans have been shown in Table 1, and the triangular plots have been shown in (Figs. 7 and 8). The observations from the triangular plots are:

1. QFL (quartz-feldspar-rock fragments) plots Folk (1980) shows that the clastics are quartz arenite-sublitharenite-subarkose-arkose (Fig. 7a).

2. QFL plots (Fig. 7b) (Dickinson et al.,1983) show that most of the samples fall in the zone of craton interior and some in transitional continental zone, nearly all the data points fall within the continental block tectonic field.

3. QpLyLs and QmPK. triangular plots show only partial grain populations, but reveal the character of polycrystalline and monocrystalline components respectively. Both of these plots serve to discriminate the increasing maturity or stability from continental block provenance (Fig. 8).

These plots indicate the possibility of a dual source for these sediments (both the Iron Ore basin of rocks

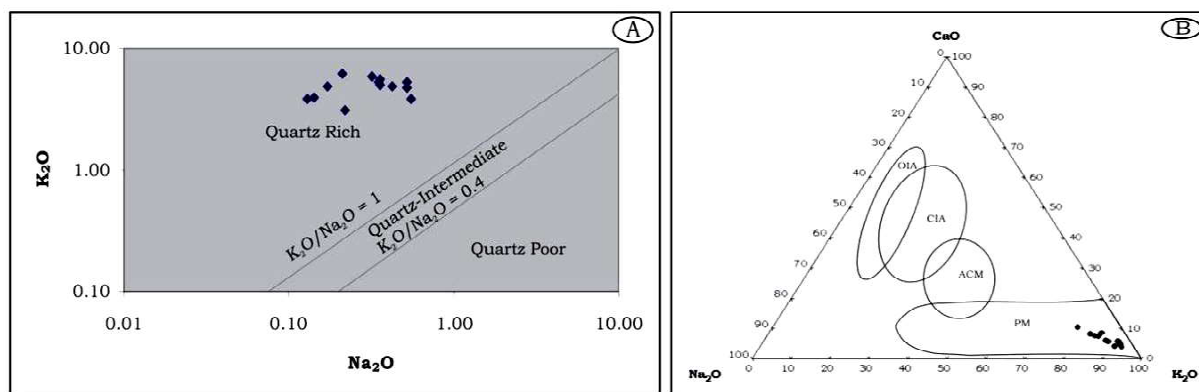


Fig. 6a. K₂O-Na₂O diagram (Crook,1974), b. CaO-K₂O-Na₂O triangular diagram (Bhatia,1983) showing Kolhan shale in the passive margin (PM) field; and also shown fields of different tectonic settings. CAN Active Continental Margin, OIA-Oceanic Island Arc, CIA-Continental Island Arc (Samples from Chaibasa-Noamundi basin).

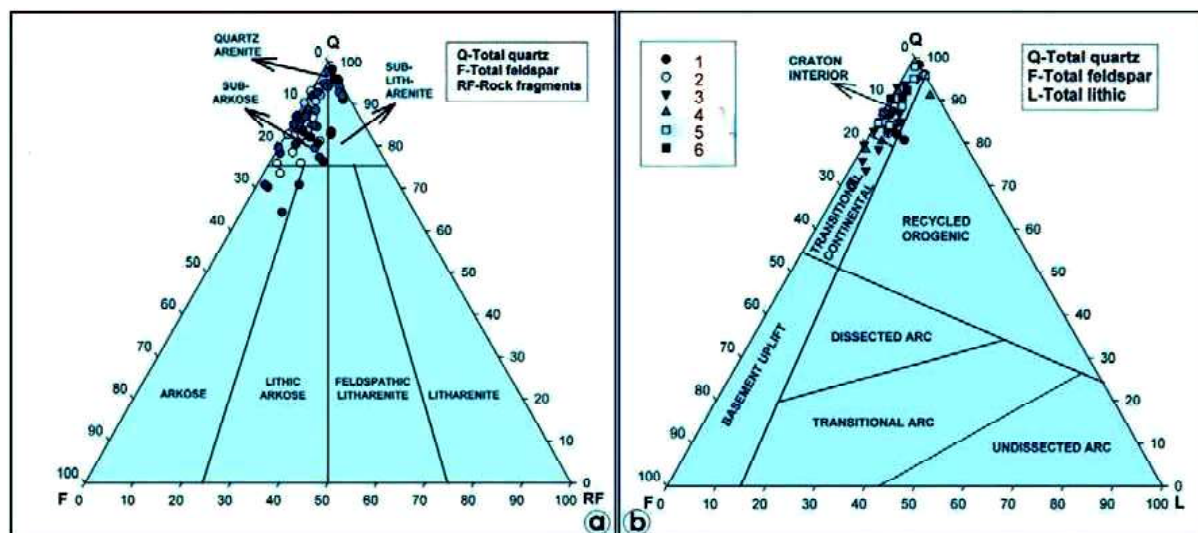


Fig. 7a. QFR plots: the clastics are mainly quartz arenite-subarkose, variety of sandstone (Folk, 1980), b. QFL plots: show that most of the samples fall in the zone of craton interior and few in the transitional continental zone (Dickinson et al., 1983). [Q:(Qm+Qp); F: Total Feldspar; RF: Rock Fragments; L: Total Lithics]. Plots are based on samples from Kolhan basin of Chamakpur-Keonjhar region.

Table 1. Recalculated parameters from modal analysis of thin sections.

Samples	1	2	3	4	5	6
Q	95.11	92.60	96.92	98.99	93.96	93.45
F	0.00	0.63	0.18	0.00	0.05	0.03
L	4.86	6.77	2.90	1.62	6.02	6.52
P/F	0.00	0.10	0.13	0.00	0.06	0.05
Qm	93.27	89.06	96.42	86.59	91.43	91.18
F	0.00	0.69	0.19	0.00	0.07	0.04
Lt	6.73	10.25	3.39	13.41	8.50	8.78
Qm/Qp	6.60	12.02	13.41	14.26	15.92	10.17
Qp	74.38	60.61	76.66	83.62	70.71	71.87
Lv	0.00	0.00	0.00	0.00	0.00	0.00
Ls	25.62	39.39	23.36	16.39	29.29	28.12
Qm/(Qm+F)	1.00	0.99	1.00	1.00	1.00	1.00
K/(K+P)	0.00	0.04	0.06	0.00	0.02	0.02
Lv/Ls	0.00	0.00	0.00	0.00	0.00	0.00
Chert/Q	0.02	0.01	0.01	0.00	0.02	0.01
Lv/Lt	0.00	0.00	0.00	0.00	0.00	0.00
Qm/Qm+Lt	0.78	0.81	0.86	0.92	0.79	0.76
Q	93.60	92.86	92.86	96.89	98.33	93.14
F	0.00	0.71	0.13	0.00	0.00	0.07
RF	6.40	6.43	2.98	1.67	7.00	6.93
Qm	100.00	99.20	99.79	100.00	99.93	99.96
P	0.00	0.57	0.13	0.00	0.05	0.03
K	0.00	0.23	0.07	0.00	0.02	0.01

(Using Gazzi-Dickinson Point Counting Method,). Parameters taken into Considerations: Qm: Monocrystalline Quartz; Qp: Polycrystalline Quartz, Q: (Qm+Qp); Kf: Potash Feldspar; Plag: Plagioclase Feldspar; F: Total Feldspar (Kf+Plag); Lv: Volcanic Lithics; Ls: Sedimentary Lithics; L: Total lithics (Lv+Ls); Lt: L+Qp; RF: Rock Fragments; L: (Lv+Ls+Chert);

1-6 are representative of several samples collected from the Kolhan basin of Jharkhand and Orissa.)

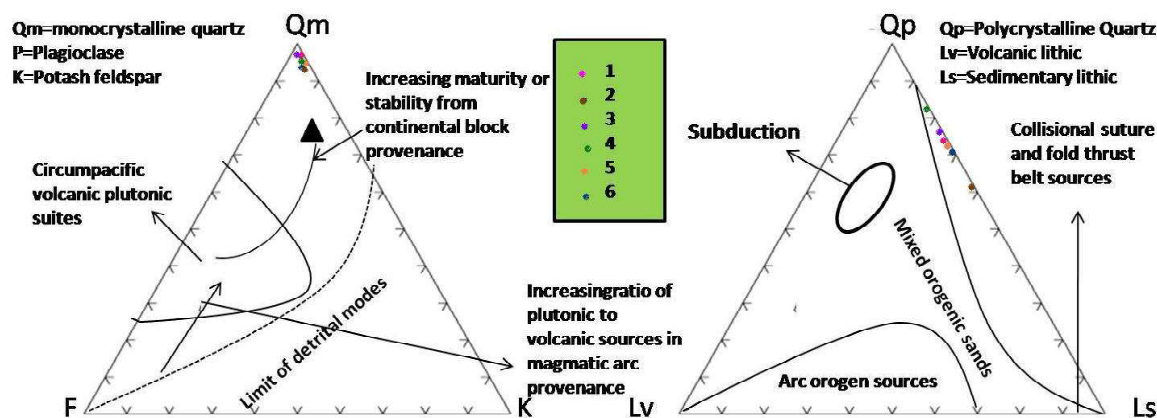


Fig. 8. The compositional fields in the triangular diagrams indicate the sandstone samples fall in the cratonic interior zone (Dickinson and Suczek, 1979). [Qm Monocrystalline F: Total Feldspar (Kf+Plag); Lv: Volcanic Lithics; Ls: Sedimentary Lithics; L: Total Lithics (Lv+Ls); Qp: Polycrystalline Quartz, Qt: (Qm+Qp); Kf: Potash Feldspar; Plag: Plagioclase Feldspar] Plots are based on samples from Kolhan basin of Chamakpur-Keonjhar region.

and the Singhbhum granite) and also focus on the grain stability including relief, weathering, maturity, and provenance.

CONCLUSIONS

Sandstone petrofacies are essential elements in paleotectonic reconstruction of the Kolhans. The association within a single half-graben of quartzose, arkosic and transitional subarkosic petrofacies of intermediate character, reflects the unusual geotectonic setting of the Kolhans as a segment of the Proterozoic basin. The close geographic and stratigraphic juxtaposition of petrofacies reflects derivation of detritus from the Iron Ore Supergroup and uplifted Singhbhum craton surface that are understandable in the paleogeographic context of the adjoining belt, but are otherwise puzzling. The geodynamic pattern that controlled Kolhan basin evolution and sediment provenance were apparently unique in the Proterozoic history of India, which led to the delivery into the same depocentre of multiple petrofacies and normally

indicative of disparate geotectonic settings. The Kolhans therefore records development of the half-graben and consists of fluvio-lacustrine deposits (Das and Sahoo, 2015).

The sandstone composition and regional relationship indicate that most of the western and central petrofacies are the distal equivalent of eastern margin proximal petrofacies of the basin. Equivalence of petrofacies in a basin supports a hypothesis for two-stage development of the half-graben. In the initial stage, an irregular east-tilted half graben was formed by high-angle faulting on cratonic basement reactivated structures. In the later stage, movement began on the fault system, and the Iron Ore Supergroup rose rapidly. In the process, the northern basin reversed its half-graben tilt to westward.

Acknowledgment: RD is grateful to her supervisor Prof. S.Das, and also to Prof.D.Sengupta, Ex Head of the Department of Geology and Geophysics, IIT Kharagpur for providing opportunity to carry out the research work.

References

- Acharya, S. (1984). Stratigraphic and Structural Evolution of the Rocks of Iron Ore Basins in Singhbhum-Orissa Iron Ore Province, India. *Special Issue, Indian Journal Of Earth Science, Seminar Volume, Crustal Evolution of the Indian Shield and its Bearing on Metallogeny*, 19-28.
- Bandhopadhyaya, P.C. and Sengupta, S. (2004). Paleoproterozoic Supracrustal Kolhan Group in Singhbhum Craton, India and the Indo-African Supercontinent. *Gondwana Research*, 7 (4), 1228-1235.
- Bhatia, M.R. (1983). Plate tectonics and geochemical composition of sandstones. *Journal of Geology*, 91, 611-627.
- Crook, A.W. (1974). Lithogenesis and geotectonics: the significance of compositional variations flysch arenites (greywakes). In: Dott, R.H. and Shaver, R.H. (Eds.), *Modern and Ancient Geosynclinal Sedimentation. Society of Economic Paleontologists and Mineralogists Special Publication*, 19, 304-310.
- Dalabehera, L. (2009). Paleocurrents and paleohydraulics of Proterozoic Kolhan sediments in Chamakpur-Keonjhar basin, Orissa, India. *International Journal of Earth Sciences and Engineering*, 2(1), 20-31.
- Das, S. and Sahoo, S. (2015). The Time Transgressive Kolhans in Fan Delta-Lacustrine Environment: Paleogeographic and Tectonic Implications. *International Journal of Earth Sciences and Engineering*, 8, 45-58.
- Dickinson, W.R. and Suczek, C.A. (1979). Plate tectonics and sandstone compositions. *American Association of Petroleum Geologists Bulletin*, 63, 2164-2182.
- Dickinson, W.R. (1983). Interpreting provenance relation from detrital modes of sandstones. In: G.G.Zuffa (eds.), *Provenance of Arenites* p.333-363. Dordrecht. Reidel Publication Company 1983.
- Folk (1980). *Petrology of Sedimentary Rocks*. Hemphill Publication Company, Austin, Texas, 182.
- Goldstein, A. (Jr.) (1948). Cementation of Dakota Sandstones of the Colorado Front Range. *Journal of Sedimentary Petrology*, 57, 405-416.
- Mukhopadhyay, D. (2001). The Archean nucleus of Singhbhum: the present state of knowledge. *Gondwana Research*, 4, 307-318.
- Mukhopadhyay, J., Ghosh, G., Nandi, A. K., Chaudhuri, A.K., Gutzmer, J. and Knock, M. D. (2006). Depositional setting of Kolhan group: Its implications for the development of a Meso to Neo Proterozoic deep water basin on South Indian Craton. *South African Journal of Geology*, 109, 183-192.
- Roy, A.K., Kroner, A., Rathore, S., Laul, V. and Purohit, R. (2012). Tectono-metamorphic and Geochronologic studies from Sandmata Complex, northeast Indian Shield: implications on exhumations of Late Palaeoproterozoic granites in and Archaean-early Palaeoproterozoic granite-gneiss terrane. *Journal of Geological Society of India*, 79, 323-324.

- Saha, A.K. and Sarkar, S.N. (1988). Early history of the earth. Evidence Eastern Indian Shield. In: Mukhopadhyay, D. (Ed.), Precambrian of the Eastern Indian Shield. *Memoir of. Geological Society of India*, 8, 13-37.
- Saha, A.K. (1994). Crustal Evolution of Singhbhum-North Orissa, Eastern India. *Memoir of. Geological Society of India*, 27, 341.
- Schieber, J. (1992). A combined petrographical-geochemical provenance study of the Newland formation, Mid-Proterozoic of Montana. *Geological Magazine*, 129, 223- 237.

Organic Petrology and Depositional Environments of Lignites of Nagaur, Rajasthan, India

ALOK K. SINGH AND ALOK KUMAR

Rajiv Gandhi Institute of Petroleum Technology, Rae Bareilly -229316, India

Email: asingh@rgipt.ac.in; drsinghalokk@gmail.com

Abstract: Investigation of lignites of Eocene age from the Nagaur Basin, Rajasthan was undertaken to characterize them petrographically and to discuss their evolution. These lignites are mostly dominated by the huminite group of macerals followed by liptinite and inertinite. According to microlithotype analysis, these lignites may be characterized as humite rich followed by clarite and huminertite. Mineral matters were mainly represented by argillaceous mineral followed by pyrite, siderite and marcasite. The petrographic composition reveals that these lignites have originated from bog forest under ombrotrophic to mesotrophic hydrological conditions. Gelification Index (GI) and the Tissue Preservation Index (TPI), suggests an accumulation of peat in marshy environment and wet forest swamp.

Keywords: Lignite, Nagaur Basin, Maceral, Microlithotype, Paleoenvironment.

INTRODUCTION

In the present global scenario, coal is an important source of energy, in which the lignite is one of the coal type having low calorific value as a fossil fuel. It is dark-brown to blackish-brown in colour, with moisture content ranges from 25% to 35 % and represents an intermediate stage in the alteration of wood into coal. Lignite deposits mostly occur in countries like Australia, China, Canada, Germany, U.S.A., Russia and India. The occurrence of lignite in India has been distinct according to their occurrence, age and depositional features with a strong paleogeographic control. In India lignite occurs in western, northwestern, and the southern part of the country (Singh et al., 2010). In the western part of Rajasthan, large deposits of lignite present in the Tertiary formations of Lower-Middle Eocene age (Sahni et al. 2006; Joshi, 2007) in the Barmer, Jaisalmer and Nagaur Basins of Barmer, Jaisalmer and Bikaner-Nagaur districts, respectively (GSI, 2011).

The area of western Rajasthan comprises one of the most important lignite bearing horizons of the country (Ex. Nagaur lignite is one amongst them). At present these lignites are mainly used for the power generation. The main objective of the study is to carry out the detail petrography and geochemistry of Nagaur lignites and to study the evolution of these lignites on the basis of petrography based depositional models (Teichmuller and Thomson, 1958; Hacquebard and Donaldson, 1969; Von der Brelie and Wolf, 1981; Diessel, 1986; Hagemann and wolf, 1987; Kalkreuth and Leckie, 1989).

GEOLOGY AND STRATIGRAPHY OF STUDY AREA

The Bikaner-Nagaur Basin is a shallow basin, which is established due to Malani magmatism giving rise to an intra-cratonic basin (Chauhan, 1999). It is structurally bordered by Delhi Sargodha Ridge in the north and northeast, Aravalli ranges in the east and southeast and in the south by Jodhpur-Chottan Malani Ridge. Nagaur district is occupied by the Delhi supergroup rocks (Lower to Middle Proterozoic), the Erinpura Granite, the Malani Igneous suite and the Marwar supergroup (Upper Proterozoic) and the Palana Formation of Paleocene age (Table 1; Fig. 1). In the northeast part of the Nawa Area in Nagaur district Mangalwar complex of the Bilwara Supergroup represented as few outcrops of gneisses. Lignite deposits of the study area occur in Bikaner-Nagaur Basin in Tertiary age of Palana Formation.

MATERIALS AND METHODS

Lignite samples (40) have been collected from the working faces of Matasukh mine (Seam No. I) in Nagaur following by the pillar sampling method. The megascopic study of lignite samples has been done following the ICCP (1993) classification scheme and macroscopic seam profile has been constructed. The lignite samples having the similar megascopic characteristics have been clubbed together as per the depth and form the composite band. The samples have been crushed and reduced in quantity with a quarter conning method to prepare composite particulate lignite pellets and then subjected to detailed petrographic analyses. The study was carried out on an advanced petrological microscope aided with MSP 200

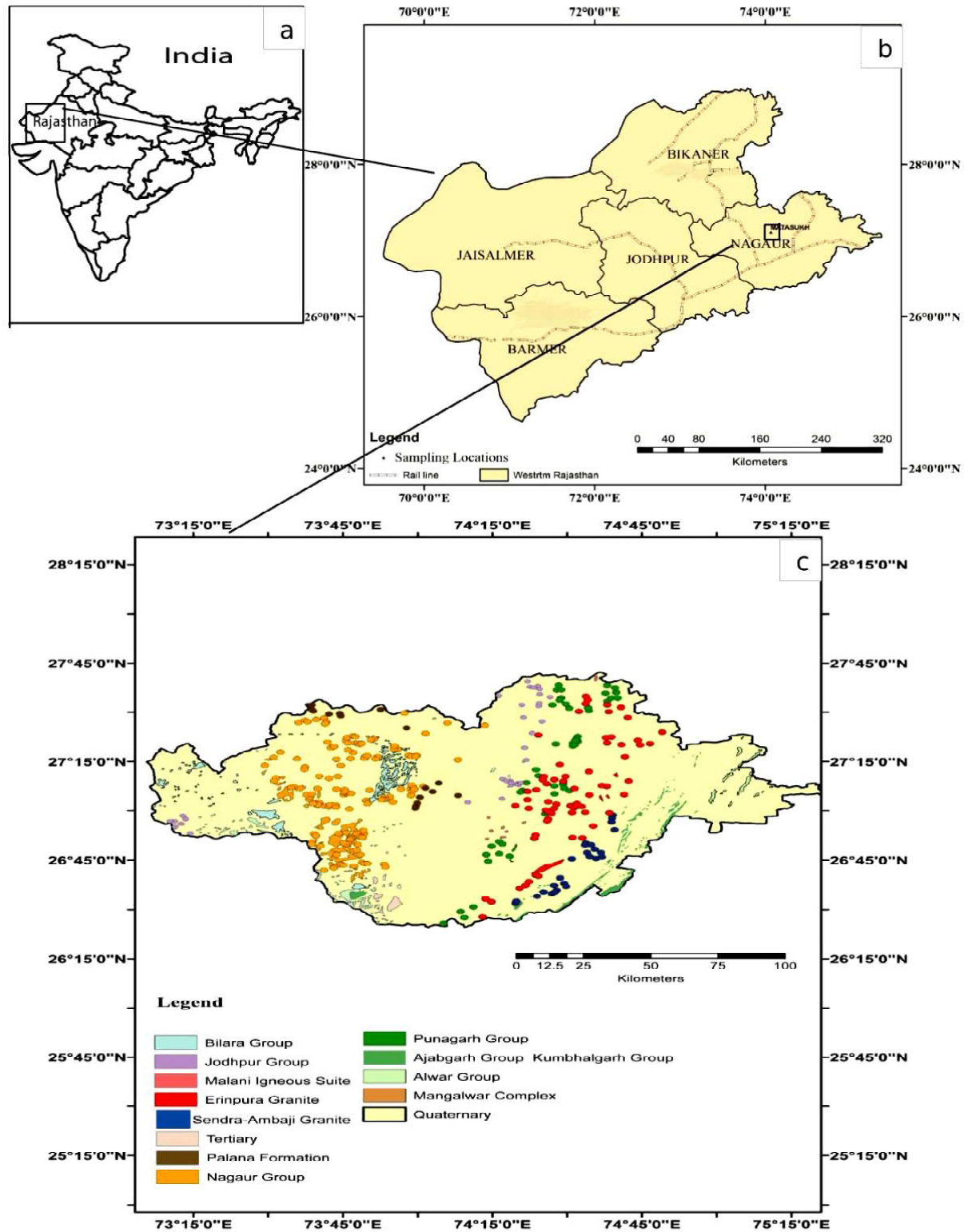


Fig. 1. Location and geological map of study area.

Table 1. The generalized stratigraphic succession of the rocks occurring in the Nagaur basin.

Age	Supergroup/Group	Formation	Rock Type
Quaternary			Aeolian mobile sand intermixed with clay, silt, polymictic conglomerate, calcrete and gypsite
Tertiary (Palaeocene)		Palana Formation	Sandstone, caly, grit, fuller's eath and shaly lignite seams
Marwar Supergroup (Upper Proterozoic)	{ Nagaur Group Bilara Group Jodhpur Group		Sandstone, grit, siltstone, with gypsum and clay clay pockets
			Limestone, dolomitic limestone, cherty limestone With calcareous clay, cherty dolomite, dolomite
			Gritty and pebbly sandstone with shale bands
Upper Proterozoic	{ Malani Igneous Suite Erinpura Granite		Rhyolite, trachyte, granophyres, granite
			Granite, granite gneiss, pegmatite and amphibolite
gnieiss Delhi Supergroup (Lower to Middle Proterozoic)	{ Punagarh Group Sendra-Ambaji Granite Ajabgarh Group/ Kumbhalgarh Group Alwar Group		Ferruginous quartzite, quartz mica schist, mica slate, phyllite, impure limestone, calc-silicate rock Granite, granite gneiss Quartzite with band of mica schist, calcitic marble
			Calc silicate rock
			Arkose, grit, conglomerate, schist
Archaean	Bhilwara Supergroup	Mangalwar complex	Gneiss

photometry system and fluorescence attachment. The identification of maceral was done as per the recommendation of I.C.C.P. (ICCP-94 system; 1998, 2001 & 2005). The maceral and microlithotype counting was done simultaneously. For microscopic study, a large number of composite samples were subjected for the detailed maceral and microlithotype analyses. The reflectance measurement was carried out as per the ISO standard (ISO, 7404-5). For the precise assessment of liptinite and dark huminite microscopic examination of macerals was carried out both under the white incident light as well as under blue irradiation.

RESULT AND DISCUSSION

Macroscopic characteristics

Macroscopically lithotypes of brown coal is categorized into four groups namely; matrix rich, xylite rich, charcoal rich and mineral rich (ICCP, 1993; Taylor et al., 1998). The lignites of Nagaur are mainly consisting of xylite rich coal followed by matrix rich coal while the charcoal rich coal is less in comparison to above mentioned lithotypes. Variations in lithotypes of Nagaur lignite are shown in Fig. 2.

Petrographic Composition

Maceral Composition

Nagaur lignites are dominated by a huminite group of macerals followed by liptinite and inertinite. Most of the huminite group of macerals are grey to dark grey in colour. Telohuminite characterized by variable degrees of retention of cell structures. In which textinite, has primary cell wall structure, showing grey to dark grey colour. Sometime it gives a brownish tint because of the presence of carbonate mineral matter (Fig. 3a). Another sub-group is ulminite, which shows cell walls more or less gelified with cracks and fractures often filled with clay and carbonate mineral matter (Fig. 3b). It is showing light to dark grey colour. Detrohuminite shows an intimate mixture of cell fragments and amorphous humic colloidal particles the major maceral sub-groups are attrinite and densinite. Attrinite consists of fine humic fragments, remains of cellulose and lignin. It looks like spongy, amorphous; porous substance which is often associated with carbonate and sulphate minerals (Fig. 3c). Therefore, they show dark grey colour with orange to brownish tint. Whereas densinite represented by cemented amorphous humic

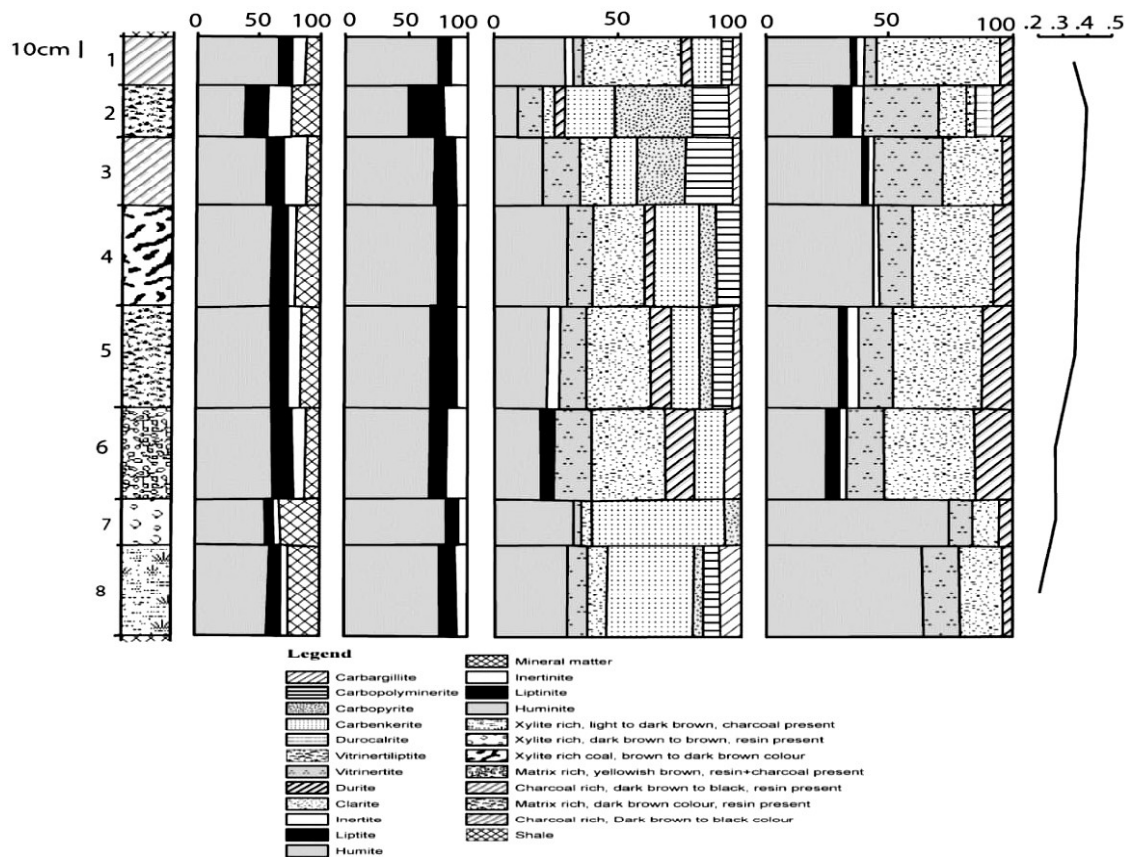


Fig. 2. Macropetrographic and microscopic section with range of mean vitrinite reflectance of lignite deposits of Nagaur.

gelified substance and grey in colour. In addition, gelohuminite which derived from gelified plant tissues, sub-group mainly represented by corpohuminite followed by gelinite and phlobaphinite. Corpohuminite occurs as discrete bodies of former cell filling, phlobaphinite occurs as the rounded bodies with reflectance are more than the other huminite group of macerals. While porigelinite/gelinite occurs as spongy, porous bodies, colour medium to light grey and has a discrete internal orange reflectance. The concentration of textinite ranges from 2.9-28.6% mean 13.9% (3.9-33.6%, mean 17.0% mmf basis), ulminite from 0.2-9.1% mean 3.1% (0.3-11.2%, mean 3.7% mmf basis), attrinite from 12.2-40.2% mean 29.4% (14.3-61.1%, mean 38.0% mmf basis), densinite from 0.2-5.4% mean 2.0% (0.2-8.2%, mean 2.7% mmf basis), corpohuminite from 2.8-16.1% mean 8.0% (4.3-18.8%, mean 9.9% mmf basis), gelinite from 0.4-1.4%, mean 0.7% (0.5-1.6%, mean 0.8% mmf basis) and phlobaphinite from 0.4-1.2% mean 0.7% (0.5-1.4%, mean 0.8% mmf basis).

Liptinite group of the study area are mainly represented primary liptinites (resinite, cutinite sporinite, liptodetrinite, suberinite and alginite) whereas secondary liptinites (exsudatinitite, bituminite and fluorinitite) are observed in minor concentration. Most of the samples having well rounded, oval shaped resinities. It is often found as the cavity filling, cell

lumens and fissures (Fig. 3d) of the ulminite. Resinite often shows light yellow to dark brown colour in white incident light and blue light excitation depending on maturity. But, in few samples resinite shows dark grey to black colour in the white light. Sporinite occurs as an individual, elongated thread like bodies. Megaspores are also recorded in these lignites. The colour of the spores varies from dark grey to black in white light while yellow to orange brown under blue irradiation. Cutinite is showing dark grey to black in white light and greenish yellow to orange in blue light. It occurs as elongated bodies in form of single or one-sided serrated margins (Fig. 3e). Suberinite often occurs with phlobaphinite and corpohuminite. It occurs as laminar mass and varies in size. Colour of suberinite is almost black to dark grey in white light while lemon-yellow to yellow orange and brown under blue light excitation (Fig. 3f). The maceral liptodetrinite occurs as small detrital lipid rich fragments which show black colour in white light and yellow-orange-brown colour under fluorescence mode. Exsudatinitite occurs as fissures, cracks and cavity. It is mainly originated from expelled hydrocarbon and showing orange to dark yellow colour under fluorescence light. In coals of Nagaur basin alginite occurs as fan or disc shape. Among liptinite group, concentration of resinite ranges from 3.0 to 9.0% mean 4.9% (0.4 to 10.0%, mean 5.7% mmf basis),



Fig. 3 a. Textinite, b. Ulminite, c. Funginite and carbonate mineral in attrinite, d. Resin and pyrite mineral, e. Cutinite, f. Suberinite, g. Semifusinite, h. Clusters of funginite.

sporinite from 0.4 to 8.2% mean 4.2% (0.6 to 11.4%, mean 5.4% mmf basis), cutinite from 0.6 to 4.3% mean 1.5% (0.7 to 5.3%, mean 2.0% mmf basis), liptodetrinite from 0.4 to 1.5% mean 0.8% (0.5 to 2.1%, mean 1.3% mmf basis), suberinite from 0.2 to 0.8% mean 0.5% (0.2 to 1.0%, mean 0.65% mmf basis) and alginite ranges from 0.2 to 0.6% mean 0.4% (0.2 to 0.8%, mean 0.5% mmf basis) respectively.

Inertinite group macerals mainly comprise of funginite, inertodetrinite and semifusinite in studied samples. However in few samples, fusinite, macrinite and micrinite are found but in minor concentration. The cell lumens of fusinite and semifusinite are often filled with argillaceous mineral matter, but sometimes it is also filled with huminite or other mineral matter. Semifusinite has intermediate reflectance between huminite and fusinite. It is showing preserved cell walls often filled with huminite or mineral matters (Fig. 3g). While, fusinite represented by well developed preserved cell wall structures and high reflectance as compared to semifusinite. The concentration of fusinite is very less. Well preserved funginites have been found to occur individually as well as in clusters. It represents ovoidal bodies of fungal remains, cell wall structure with high reflectance (Fig. 3h). Single, double, triples celled teleutospores occur in most of the samples of Nagaur lignites. Fine detrital masses of inert are scattered in huminite group macerals representing inertodetrinite. It has no structure and size is less than 10µm. Presence of macrinite and micrinite is also very less. Macrinite shows amorphous bodies of irregular shape and structure less (>10µm) with high reflectance, while micrinite having granular appearance with high reflectance. The concentration of main maceral sub-group of inertinite maceral is funginite 1.6-6.8% mean 4.2% (2.4-8.0%, mean 5.2% mmf basis), semifusinite 1.0-4.6% mean 2.6% (1.3-5.4%, mean 3.2% mmf basis) and inertodetrinite 0.4-10.4% mean 2.8% (0.5-13.8%, mean 3.5% mmf basis). The variations of three maceral groups in the Nagaur lignites have been shown in Fig. 2.

Mineral Matter

Mineral matter is regarded as highly indicative of depositional environment (Amijaya and Littke, 2005), therefore microscopic observation of mineral matter is also taking into account carefully. The determination of mineral matter is also very important for the utilisation point of view.

In the studied samples, mineral matter occurs in a variable concentration. The sulphides are represented by pyrites which occur as cavity filling, massive (Fig. 3c & d) and detrital grains (scattered tiny particles) associated with carbonate minerals. In addition, few samples also containing trambooidal pyrites occurs both as individual and clusters. This indicates the presence of marine influence. Siderites are the main component of carbonate mineral which occurs as

scattered on attrinite patches associated with pyrite, massive as well as fissure filling. Mineral matter is mainly dominated by carbonate 5.2-32.2% mean 12.3% followed by sulphides 1.8-14.8% mean 5.8% and argillaceous 2.2-4.8% mean 3.2%.

Microlithotype

Microlithotypes of brown coals are classified into monomaceral, bimaceral, trimaceral and carbominerite (Diessel 1992). Monomaceral microlithotype is represented by humite (24.5-74.5%, mean 42.8%; 9.4-32.5% mean 24.1% with carbominerite), liptite (0.5-6.8%, mean 2.9%; 0.2-5.1% mean 1.7% with carbominerite) and inertite (0.9-4.8%, mean 2.6%; 0.4-3.2% mean 1.6% with carbominerite) in which humite is dominating microlithotype. Clarite (10.9-49.9%, mean 26.8%; 3.9-40.4% mean 18.0% with carbominerite) and huminertite (3.9- 30.1%, mean 15.8%; 3.0-13.9% mean 8.7% with carbominerite) are dominating microlithotype in bimaceral group includes durite (0.4-1.4%, mean 0.8%; 0.2-0.5% mean 0.4% with carbominerite) which is less. In present study, the concentration of trimacerites is very less or absent and represented by huminertoliptite, clarodurite and duroclarite (2.8- 14.7%, mean 6.8%; 1.2-12.2% mean 4.4% with carbominerite). The carbominerite group are present in variable amount and represented by carbargilite (1.9-6.5% mean 3.5%), carbopyrite (1.4-29.2% mean 8.8%), carbenkerite (10.5-53.2% mean 21.4%) and carbopolyminerite (1.9-16.7% mean 8.4%).

RANK

To know the level of maturation/rank, samples were subjected to huminite reflectance measurement. The reflectance measurement has been done on ulminite submaceral, which were free from any contamination, inclusion and smooth surface. The random reflectance values of studied coal samples vary between 0.20% and 0.49%, with mean value 0.33 % Rom. The values of reflectance measurement entail coals are either transition phase to lignite or transitional phase between lignite to sub-bituminous (Fig. 4). Based on the reflectance value, Nagaur lignite may be classified as 'Low-rank B' (ISO-11760, 2005).

PALEOENVIRONMENT AND FACIES INTERPRETATIONS

The characteristics of coal depend on several factors such as peat-forming plant communities, types of deposition, nutrient supply, pH, bacterial activity, temperature, and redox potential (Sun et al., 2010; Lin and Tian, 2011). Variables of these conditions induce physical and chemical changes in the organic matter (Sun et al., 1998). Clastic input either by surface inundation or by the rise of water table may increase the

Rank		Rfl. Rm Oil	Vol. M. d.a.f. %	Carbon d.a.f. vitrinite	Bed Moisture	Cal. Value Btu/lb (Kcal/Kg)	Rank of Matasukh Lignite	Applicability of different rank parameters			
German	U.S.A						Vol.M. (d.a.f.)	Rfl. Rm oil			
Tort	Peat	0.2	68								
Welch-	Lignite	0.3	60	Ca. 60	Ca. 75						
Matt-		0.4	56		Ca. 35	7200 (4000)					
Glanz-	Sub-Bit. C	0.4	52								
Flamm-		0.5	48	Ca. 71	Ca. 25	9900 (5500)					
Gasflamm-	High Vol. Bituminous A	0.6	44								
Gas-		0.7	40	Ca. 77	Ca. 8-10	12600 (700)					
Fett-	Medium Volatile Bituminous	0.8	36								
Ess-		1.0	32								
Marger-	Low Volatile Bituminous	1.2	28	Ca. 87		15500 (8650)					
Anthrazit		1.4	24								
Meta-Anthr.	Semi-Anthracite	1.6	20								
		1.8	16								
	Anthracite	2.0	12								
		2.0	12								
	Anthracite	3.0	8	Ca. 91		15500 (8650)					
		4.0	4								
	Meta-A										

Fig. 4. Rank on the basis of Rm oil in the scheme representing different stages of colification according to German (DIN) and North American (ASTM) classification and their distinction on the basis of different physical and chemical parameters.

ash concentration of the coal and lignite. For the reconstruction of the paleomire of the Nagaur lignites, few models based on quantitative petrographic data have been applied.

The paleodepositional environment is reflected by the presence or absence of certain microscopic organic entities (Teichmüller, 1989). Two petrographic indices, the gelification index (GI) and tissue preservation index (TPI), were introduced by Diessel (1986) to characterize the paleodepositional environments of Permian coal deposits of Australia. Subsequently, a number of workers made serious efforts against their usage particularly for Tertiary coals and lignites (Lambersen et al., 1991; Crosdale, 1993; Dehmer, 1995; Scott,

2002; Moore and Shearer, 2003; Amijaya and Littke, 2005). However, the indices were further modified by Kalkreuth et al (1991), Petersen (1993), and Flores (2002) for low rank coals. In the present investigation, modified TPI and the GI have been calculated as suggested by Petersen (1993) to decipher the paleodepositional conditions. In the present study different depositional models based on the petrographic composition given by different workers

(Diessel, 1986; Mukhopadhyay, 1986; Calder et al., 1991) have been used. The GI and TPI indices are given below:

$$TPI = \frac{\text{Humotelinite} + \text{Carpohuminite} + \text{Semifusinite} + \text{Fusinite}}{\text{Gelinite} + \text{Macrinite} + \text{Humodetrinite} + \text{Inertodetrinite}}$$

$$GI = \frac{\text{All Huminite (except textoulminite \& detrohuminite)} + \text{Macrinite}}{\text{Semifusinite} + \text{Fusinite} + \text{Detrohuminite} + \text{Inertodetrinite}}$$

The gelification index (GI) indicates the relative water level during peat formation. The high values reflect the high water levels (Flores, 2002). GI also indicate the oxidation of tissue more accurately because it is ratio of huminite/vitrinite versus inertinite (Calder et al., 1991). In the present study, low tissue preservation index (TPI) indicates that kind of vegetation come from herbaceous plants, the source of detrohuminite (Teichmüller, 1989; Deissel, 1992). The lower value of TPI also suggests lignite contains an abundance of resinite and sporinite (Mavridou et al., 2003).

The few samples show the TPI value higher than 1 which suggests greater input of terrestrial plants than of microbial organic matter (Flores, 2002). In the present investigation, the values of gelification index higher than 2 and range from 2.98 -27.09. While the value of TPI varies between 0.26 - 3.11 and is higher in upper seam. Low values of TPI indicate the tree density decreases and high GI reveals for a transgressive setting. The moderate to high GI and low TPI values indicate that the accumulation of peat in marshy environment and few in wet forest mire (Fig. 5).

Another indices like groundwater influence index (GWI) and vegetation index (VI) proposed by Calder et al., (1991).

$$VI = \frac{\text{Textinite} + \text{Ulminite} + \text{Resinite} + \text{Suberinite} + \text{Semifusinite} + \text{Fusinite}}{\text{Attrinite} + \text{Densinite} + \text{Introdetrinite} + \text{Cutinite} + \text{Sporinite} + \text{Liptodetrinite} + \text{Alginite}}$$

$$GWI = \frac{\text{Gelinite} + \text{Carpohuminite} + \text{Densinite} + \text{Mineral matter}}{\text{Textinite} + \text{Textolulminite} + \text{Euulminite} + \text{Attrinite}}$$

It has been used to identify major mire paleoenvironmental and hydrological conditions. The value of GWI indicates the degree of gelification in the peat mire as well as the pH, whereas the VI related to the type of vegetation. GI ranges from 0.43 to 1.21, whereas the values of VI ranges from 0.26 to 1.91. As shown in GWI vs VI plot (Fig. 6), Nagaur lignite has been originated by bog forest under ombrotrophic to mesotrophic hydrological conditions. The contention is further supported by another facies critical maceral association model given by Mukhopadhyay, (1986) and

further modified by Kalkreuth et al. (1991), for low rank coals. The plot (Fig.7) shows that Nagaur lignites originated in mildly oxic to anoxic forest swamp with good tissue preservation and under reed marsh with increasing bacterial activity.

CONCLUSIONS

Lithotype association represents most of the lignites in the study area are matrix rich followed by xylite rich. Which entails coals consists of fine detrital humic groundmass and presence of xylite, well fossilized wood fragments such as stumps, trunks and branches must be present. Petrographic composition shows that main organic components are macerals of the huminite group in which detrohuminite and telohuminite occurs most frequently. In liptinite group predominant macerals are resinite, sporinite, cutinite and liptodetrinite. Whereas the inertinite group is mainly represented by inertodetrinite followed by funginite and semifusinite. In addition, mineral matter consisting of mainly carbonate and pyrite. Few coals represent framboidal pyrite which indicates the marine influence.

Huminite reflectance measurement on eu-ulminite B ranges from 0.20 to 0.49 entails rank of the seam in transition zone between lignite to sub-bituminous. The ratio of TPI vs GI indices suggests an accumulation of peat in marshy environment and few in wet forest swamp. GWI vs VI plot; coals were formed in bog forest under ombrotrophic to mesotrophic hydrological conditions. ABC ternary diagram represents coals of Nagaur Basin were formed in under oxic to anoxic

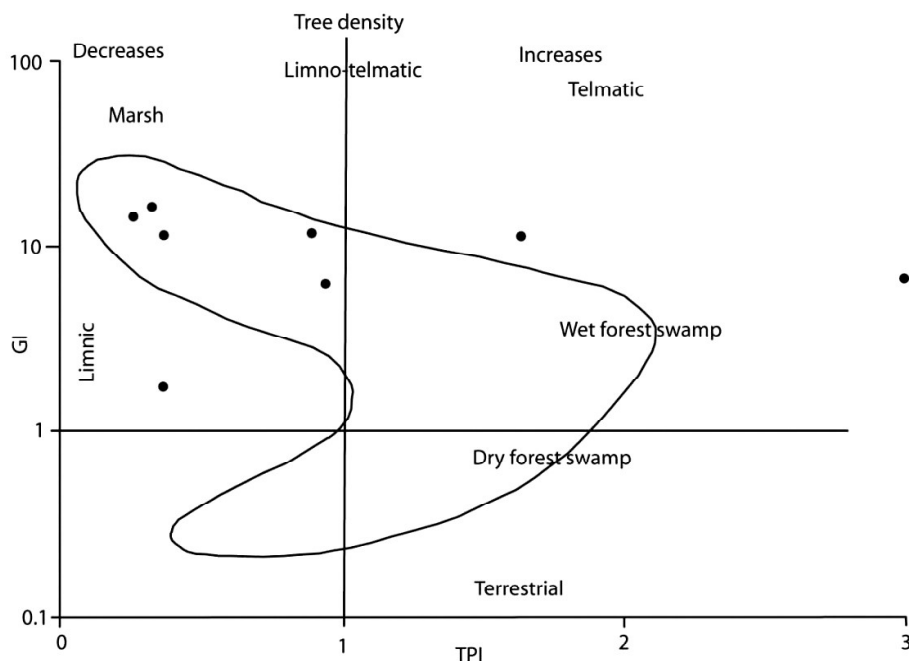


Fig. 5. Facies diagram, based on studied samples, illustrating facies – critical maceral association (after Diessel, 1986, modified by Kalkreuth et. al., 1991).

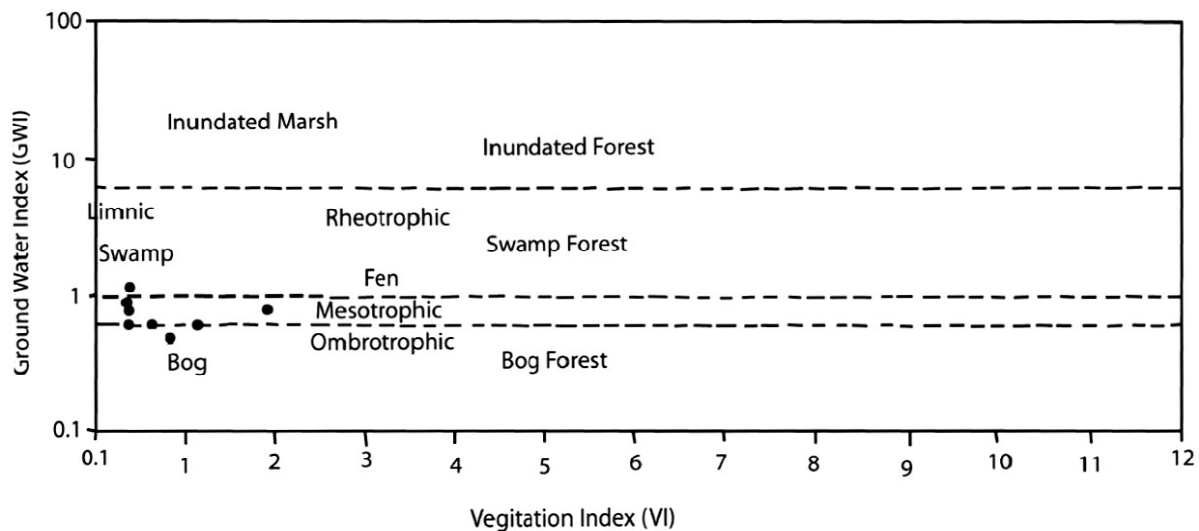


Fig. 6. GWI/VI mire palaeoenvironment diagram (modified after Calder et. al, 1991) for the lignite deposits of Nagaur basin.

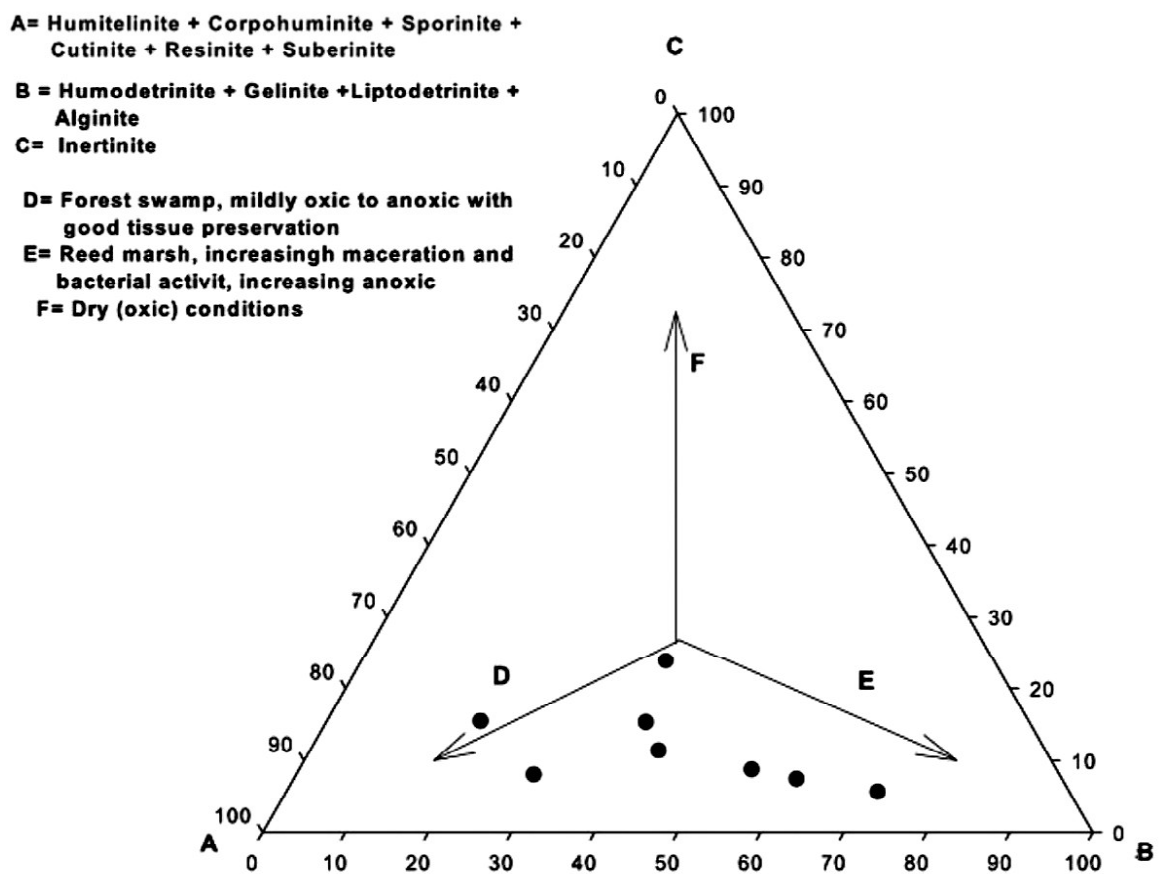


Fig. 7. Ternary diagram illustrating facies - critical maceral association based on the samples Matasukh lignite (Nagaur Basin) studied (after Mukhopadhyay, 1986 and modified by Kalkreuth et. al., 1991).

conditions. The facies model itself reveals, provide a complete and detailed description of coal evolution.

Acknowledgement: The authors are thankful to the Director, Rajiv Gandhi Institute of Petroleum Technology, Rae Bareilly, India, for extending all the necessary facilities. We sincerely thank the officials of Matasukh mine for extending their help during the

sample collection from lignite mines of Rajasthan State Mines and Minerals Limited, India. Authors are also thankful to Director, BSIP for granting the permission to utilize reflectance measurement facility. The financial support received from Department of Science & Technology (Project No. SB/S4/ES- 681/2013), Government of India is thankfully acknowledged.

References

- Amijaya, H., Littke, R. (2005). Microfacies and depositional environment of Tertiary Tanjung Enim low rank coal, South Sumatra Basin, Indonesia. *Int. J. Coal Geol.* 6, 197–221.
- Calder, J.H., Gibbing, M.R. and Mukhopadhyay, P.K. (1991). Peat formation in a Westphalian B piedmont setting, Cumberland Basin, Nova Scotia: Implication for the maceral-based interpretation of rheotrophic and raised paleomires. *Bulletin de la Societe Geologique de France* 162(2), 283–298.
- Chauhan, D.S. (1999). Tectonic and sedimentary evolution of the Marwar-basin: a Neoproterozoic–Early Cambrian sagbasin. In: Kataria, P. (Ed.), *Proceedings of Seminar on Geology of Rajasthan: Status and Perspective*. MLS University, Udaipur, 111–125.
- Crosdale, P.J. (1993). Coal maceral ratios as indicators of environment of deposition: do they work for ombrogenous mires? An example from the Miocene of New Zealand. *Org. Geochem.* 20(6), 797–809.
- Dehmer, J. (1995). Petrological and organic geochemical investigation of recent peats with known environments of deposition. *Int. J. Coal Geol.* 28(2–4), 111–138.
- Diesel, C.F.K. (1986). The correlation between coal facies and depositional environments. In: *Advances in the study of the Sydney Basin; Proceeding of 20th Symposium*, The University of Newcastle, 19–20.
- Diessel, C.F.K. (1986). On the correlation between coal facies and depositional environments. *Proceeding 20th Symposium of Department Geology, University of New Castle, New South Wales*, 19–22.
- Diessel, C.F.K. (1992). *Coal Bearing Depositional Systems*. Springer-Verlag, Berlin. 721p.
- Flores, D. (2002). Organic facies and depositional palaeoenvironment of lignites from Rio. Maior Basin (Portugal). *Int. J. Coal Geol.* 48, 181–195.
- GSI, MISC. PUB. No. 30. (2011). *Geology and mineral resources of Rajasthan; Geological Survey of India; Miscellaneous Publication No. 30 Part 12 3rd Revised Edition*.
- Hacquebard, P.A. and Donaldson, J.R. (1969). Carboniferous coal deposition associated with floodplain and limnic environments in Nova Scotia. In: E.C. Dapples and M.E. Hopkins (Editors), *Environments of Coal Deposition*. *Geol. Soc. Am. Spec. Pap.*, 114, 143–191.
- Hagemann, H. and Wolf, M. (1987). New interpretations of the facies of the Rhenish brown coal of West Germany. *Int. J. Coal Geol.* 7, 335–348.
- ICCP, (International Committee for Coal Petrology), (1993). *International handbook of coal petrography, 3rd Supplement to 2nd edition*. University of Newcastle upon Tyne, England.
- International Committee for Coal and Organic Petrology, (1998). *The new vitrinite classification (ICCP System 1994)*. *Fuel* 77, 349–358.
- International Committee for Coal and Organic Petrology, (2001). *The new inertinite classification (I.C.C.P. System 1994)*. *Fuel* 80, 459–471.
- International Committee for Coal and Organic Petrology, (2005). *Classification of huminite (ICCP System 1994)*. *Int. J. Coal Geol.* 62, 85–106.
- ISO, 11760, (2005). *Classification of coals*. International standard, pp 1–9.
- ISO, 7404-5, (2009). *Methods for the petrographic analysis of coals -Part 5: Method of determining microscopically the reflectance of vitrinite*
- Joshi, V.K. (2007). Pages of Past Environment entombed in a mine. www.boloji.com/environment/121.htm.
- Kalkreuth, W. and Leckie, D. (1989). Sedimentological and petrographical characteristics of Cretaceous strandplain coals; A model for coal accumulation from the North American western interior seaway. *Int. J. Coal Geol.* 12, 381–424.
- Kalkreuth, W.D., Marchioni, D.L., Calder, J.H., Lamberson, M.N., Naylor, R.D., Paul, J. (1991). The relationship between coal petrography and depositional environments from selected coal basins in Canada. In: Kalkreuth, W.D., Bustin, R.M., Cameron, A.R. (Eds.), *Recent Advances in Organic Petrology and Geochemistry. A Symposium honouring Dr. P. Hacquebard*: *Int. J. Coal Geol.* 19, 21–76.
- Lamberson, M.N., Bustin, R.M. and Kalkreuth, W. (1991). Lithotype (maceral) composition and variation as correlated with paleo-wetland environment, Gates Formation, Northeastern British Columbia, Canada. *Int. J. Coal Geol.* 18 (1–2), 87–124.

- Lin, M.Y. and Tian, L. (2011). Petrographic characteristics and depositional environment of the No. 9 Coal (Pennsylvanian) from the Anjialing Mine, Ningwu Coalfield, China. *Energy Exploration and Exploitation* 29(2), 197–204.
- Mavridou, E., Antoniadis, P., Khanaqa, P., Riegel, W., Gentzis, T. (2003). Paleoenvironmental interpretation of the Amynteon–Ptolemaia lignite deposit in northern Greece based on its petrographic composition. *Int. J. Coal Geol.* 56 (3–4), 253–268.
- Moore, T., Shearer, J. (2003). Peat/coal type and depositional environment - are they related? *Int. J. Coal Geol.* 56 (3–4), 233–252.
- Mukhopadhyay, P.K. (1986). Petrography of selected Wilcox and Jockson Group lignites from Tertiary of Texas. In: Finkelman, R.B., Casagrade, D.J. (Eds.), *Geology of Gulf Coast Lignites*. 1986, Annual Meet. Geological Society of America, Coal Geology Division, Field Trip, pp. 126–145.
- Petersen, H.I. (1993). Petrographic facies analysis of Lower and Middle Jurassic coal seams on the island of Bomholm, Denmark. *Int. J. Coal Geol.* 22(3–4), 189–216.
- Sahni, A., Saraswati, P.K., Rana, R.S., Kishor, K., Singh, H., Alimohammadian, H., Sahni, N., Rose, K.D., Singh, L., Smith, T. (2006). Temporal constraints and depositional paleoenvironments of the Vastan lignite sequences, Gujarat: analogy for Cambay shale hydrocarbon source rock. *Int. J. Petroleum Geol.* 15, 1–20.
- Scott, A.C. (2002). Coal petrology and the origin of coal macerals: a way ahead? *Int. J. Coal Geol.* 50 (1–4), 119–134.
- Shearer, J.C. and Clark, B.R. (1998). Whangamarino wetland: effects of lowered river levels on peat and vegetation. *Int. Peat J.* 8, 52–65.
- Singh, P.K., Singh, M.P. and Singh, A.K. (2010). Petrochemical characterization and evolution of Vastan Lignite, Gujarat, India. *Int. J. Coal Geol.* 82(1–2), 1–16.
- Sun, Y.Z., Wang, B.S. and Lin M.Y. (1998). Maceral and Geochemical Characteristics of Coal Seam 1 and Oil Shale 1 in Fault-controlled Huangxian Basin, China. *Org. Geochem.* 29(1–3), 583–591.
- Sun, Y.Z., Qin, S.J., Zhao, C.L. and Kalkreuth, W. (2010). Experimental study of early formation processes of macerals and sulfides. *Energy & Fuels* 24(2), 1124–1128.
- Taylor, G.H., Teichmüller, M., Davis, A., Diessel, C.F.K., Littke, R., Robert, P. (1998). *Organic Petrology*. Gebrüder Borntraeger, Berlin, Germany. 704p.
- Teichmüller, M. and Thomson, P. (1958). Vergleichende mikroskopische und chemische Untersuchung der wichtigsten Fazies-Typen im Hauptfloz der niederrheinischen Braunkohle. *Fortschr. Geol. Rheinl. Westfalen*, 2: 573–598.
- Teichmüller, M. (1989). The genesis of coal from the viewpoint of coal petrology. *Int. J. Coal Geol.* 12 (1–4), 1–87.
- Timell, T. (1967). Recent progress in the chemistry of wood hemicelluloses. *Wood Sci. Technol.*, 1, 45–70.
- Von der Brölie, G. and Wolf, M. (1981). Zur Petrographie und Palynologie heller und dunkler Schichten im Rheinischen Hauptbraunkohlenfloz. *Fortschr. Geol. Rheinl. Westfalen*, 29, 95–163.

Paleoclimatic Indicators in the Soil Blanket of Southern Western Ghats (Sahyadri), SW India

Divya V^{1*}, Padmalal D¹, Vimal K.C¹ and Mohanan C.N².

1. National Centre for Earth Science Studies, Thiruvananthapuram – 695011, Kerala, India

2. Institute for Climate Change Studies, Kottayam – 686004, Kerala, India

*Email: kukku.divyanair@gmail.com

Abstract: Although many attempts have been carried out to decode paleo-climate data from different onland and offshore sedimentary archives, soils are seldom being used as an archive for paleo-climate studies. But if used carefully, the top soils in the high altitude terrains of tropical regions can provide an excellent archive of climate records. The present study deals with climate records of Late Holocene age, which is preserved in the soil column of southern Western Ghats using multi-proxy studies. A total of 100 samples from ten trenches of 1m depth were examined for this study. The altitudinal heights of the sampling locations vary from 150 to 2000 m above mean sea level (msl). The soil types of the samples fall generally within clay, sandy clay and sandy clay loam categories with the colour index varying from dark brown to yellowish red. The average organic carbon and nitrogen contents in the samples are 1.81% and 0.09%, respectively. Among the various types of forests, the shola forests record high content of soil organic carbon. The soil organic carbon and nitrogen values show a strong positive correlation ($r = 0.89$; $n = 100$) indicating a common source for these elements. Carbon dating results of organic rich samples in soil profile of a shola forest trench indicate that, soil development in the studied section occurred in Late Holocene (3150 \pm 90 yrs BP). This study reveals the prevalence of high rainfall in Late Holocene with a marked interruption in the Mid-Late Holocene by a dry event.

Keywords: Late Holocene, Southern Western Ghats, Texture, Organic carbon

INTRODUCTION

Soil, the uppermost layer of variable thickness, consists of loose material, derived essentially from crustal weathering (Sannappa and Manjunath, 2013). The growth and productivity of forest vegetation cannot be interpreted without a better understanding of soil. A complex relationship exists between soil and vegetation, which influences the properties of soil to a great extent (Gairola et al., 2012). The physical and chemical attributes of soil regulates biological activity and interchanging ions between the solid, liquid and gaseous phases which influences nutrient cycling, plant growth and decomposition of organic materials. Soil properties mainly depend on climate, vegetation type, weathering, topography and soil derived age (Xiaoquan et al., 1998).

The Western Ghats (Sahyadri) comprises an area of 160,000 km² with an elevation ranging from 300-2700 m above mean sea level and the mountain ranges stretching between Tapti in the north and Kanyakumari in the south, along the western peninsular India. The Western Ghats (WG) form one of the four major watersheds of India, feeding the perennial rivers and moulding the rainfall regime of the Peninsula. The diverse topography, spectacular landscapes, high mountain forests of WG acts as 'water tower' for the region. The uniqueness of the overall zone is marked by the vertical

gradients in ecosystems and climate patterns. The region is also well-known for its capacity to support essential ecosystem goods and services, natural balance, forest based enterprises and livelihood opportunities to the society. Several major zones in WG appear to be highly vulnerable, particularly the southern Western Ghats due to the combination of global environmental changes and locally altered landuse changes. As a result of human interventions there has been progressive deterioration in the climate, elimination and destruction of habitats, impoverishment of biodiversity and regression of distributional ranges of RET (rare, endangered and threatened) species unique to the area (Brilliant et al., 2012). Recently WG has been considered under 'Natural Heritage Site' program of the UNESCO. Kerala part of Western Ghats is rich in biodiversity and vital for environmental protection and considered to be a repository of rare and endangered flora and fauna. The high floristic richness and restricted distribution of numerous endemics is due to geographical restrictiveness and other inherent factors like specialized altitude, vegetation type, habitat and microclimatic preferences of individual species. The mountain belt comprises of different forest types including tropical wet evergreen, moist deciduous, tropical dry deciduous, mountain subtropical and montane temperate forests (Rugmini and Balagopalan,

2006). The mountains and its forest cover play a pivotal role in regulating the climate system of the region. Among the various types of forests, tropical montane forest (shola forest) have high peat or organic matter rich layers, these samples are used for the investigation of paleo-climatic proxies (Sukumar et al., 1993). The montane forest in the southern Western Ghats is featured with stunted evergreen species interspersed with grasslands. These forests are largely confined to the sheltered folds of mountains and stream courses, whereas the grassland covers the hill slopes and the ecotone between forest and grassland is very sharp.

Study Area and its General Characters

The transect selected for the present study is aligned in the north eastern part of the Idukki district, Kerala, which is part of southern Western Ghats. The area is drained by the west flowing Periyar and east flowing Pambar Rivers of Kerala state and the altitude ranges from 150 to 2000 m above mean sea level (msl) (Fig. 1). The climate of the region is controlled by south-west and north-east monsoons. The south-west monsoon occurs in June to September and it contributes about 60% of annual rainfall and north-east monsoon contributes about 25% of annual rainfall and it starts in October; the remaining contributions are from summer showers. The mean annual rainfall in the windward side is 3200 mm and in the leeward side is 1800 mm. Geologically the study area forms part of the southern granulite belt of the Peninsular India. Major rock types

include hornblende-biotite-gneiss and granite gneiss with intrusions of pegmatite and dolerites at some places. The study area is considered as a potential site for megalithic cultures. Many dolmens (Portal grave) are seen on the hill tops of Marayoor, Kanthalloor and Chinnar regions (Nikhildas, 2014).

SAMPLING AND METHODOLOGY

A systematic field work was conducted for collecting primary and secondary data for the study. The location of the sampling points were fixed with a GPS (Trimble Juno SB) and 1 m deep trenches were made at 10 locations in the transect chosen from Neriamangalam in the west to Chinnar in the east. The vegetation pattern seen accordingly from Neriamangalam to Chinnar is a mosaic of wet evergreen, moist deciduous, sholas and grasslands (in the Eravikulam plateau) followed by hill top evergreen and dry deciduous forests in Chinnar. Table 1 shows the vegetational and altitudinal variation of the sampling sites. Each 1 m depth samples were sub-sampled at 10 cm intervals. Altogether there were about 100 samples analyzed for this study.

Colour was identified with the help of Munsell soil colour chart (1994), organic carbon by wet digestion method (Walkley and Black, 1934) and nitrogen by Kjeldahl digestion method (Maiti, 2003). Textural analysis was done by using pipette method (Lewis, 1984). The radiocarbon dating was carried out at Birbal Sahni Institute of Paleobotany, Lucknow using

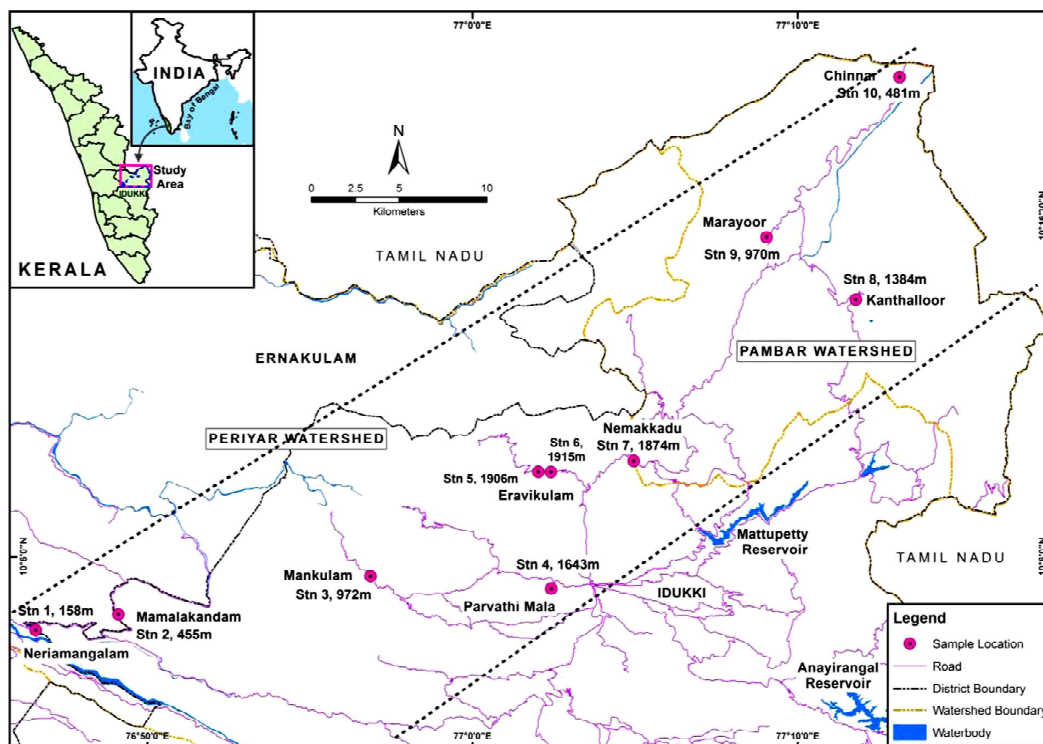


Fig. 1. Location map of the study area.

Table 1. Details of the sampling sites.

Stations	Location	Altitude (m)	Forest Type *
Stn 1	Neriamangalam	158	Evergreen
Stn 2	Mamalakandam	455	Moist deciduous
Stn 3	Mankulam	972	Evergreen
Stn 4	Parvathi mala	1643	Low elevation Shola
Stn 5	Eravikulam National Park	1906	Grassland
Stn 6	Eravikulam National Park	1915	Shola
Stn 7	Nemakkadu	1874	Hill top evergreen
Stn 8	Kanthalloor	1384	Dry deciduous
Stn 9	Marayoor	970	Sandal wood forest
Stn 10	Chinnar	481	Dry deciduous
*(Champion and Seth, 1968)			

conventional method (liquid scintillation counting of benzene), and calibration procedure was based on Stuiver et al. (1998). SPSS 16 software was used for statistical analysis.

General Features of the 1m Depth Trench Sample used for Climatic Study

Parvathi Mala (Station: 4)

The 1 m depth profile sample is collected from 10°5'0.62" N Latitude and 77°2'25.34" E Longitude at an altitude of 1643 m above mean sea level. The profile has been sub-sampled at every 10 cm intervals. The vegetation pattern seen in this area belongs to low elevation shola (Tropical montane forest). The colour of the samples in 1 m depth profile is dark yellowish brown. The soil profile is divided into two horizons, the top 60 cm gives the indication of A horizon and the rest is B horizon. Clay dominated soils are seen in the entire layers of the 1 m depth soil samples. Presence of organic matter content is very high in the upper layers. Broken roots, wood pieces, dead and decomposed leaflets are also present on the surface layers and these are the contributing factors to increases the organic matter content. Small and fibrous roots are present in the bottom layers.

Eravikulam National Park (Station: 6)

The 1 m length soil profile is collected from 10°8'37.68" N Latitude and 77°2'12.08" E Longitude at an altitude of 1915 m above mean sea level. The trench samples are sub-sampled at every 10 cm intervals. The vegetation pattern seen in this area is shola (Tropical montane forest). The colour of the samples ranges from very dark brown to black. The soil profile samples are distinctly divided into two horizons- A horizon extends upto 80 cm depth layer and the rest 20 cm bottom layer belongs to B horizon. The colour of A horizon is black and these layers are formed from dead and decayed

leaflets, wood pieces, broken roots and mineral matters. B horizon is of very dark brown colour and devoid of wood and root materials. Sand dominated soils are seen in the entire layers of 1 m depth trench sample and the soil type ranges from sandy loam to sandy clay loam.

RESULTS AND DISCUSSION

Textural Properties

Texture of the soil is important because it influences soil structure and aeration, water retention and drainage, ability of the soil to hold, exchange and fix the nutrients, root penetrability, and seedling emergence (Bockheim, 1982). The soil types identified in the area are clay, sandy loam and sandy clay loam categories. Out of the 100 samples 36% of the sample exhibits sandy clay loam type, 26% exhibits clay type and the remaining falls under sandy loam (17%), sandy clay (11%), clay loam (6%), loamy sand (2%), silty clay loam (2%) and sand (1%) categories (Fig. 2). The sand, silt and clay contents in the soil samples vary from 14.24 to 90.88%, 3.42 to 50.23% and 5.70 to 64.36%, respectively (Table 2). Out of the ten profiles studied, the Chinnar profile exhibits the highest sand content. At the same time, the silt and clay contents peak at station Parvathi mala. An overall evaluation of the textural characters reveals that silt and clay contents show a positive relationship with spot heights of the sampling locations, and sand particles shows a reverse trend. That is, the higher the elevation the lesser the content of sand in the soil cover. With increase in elevation and rainfall, the condition becomes favourable for higher rate of fragmentation / weathering of crustal rocks and formation of larger proportion of finer particles (Saeed et al., 2014). Moreover, the fraction of finer particles increases with a corresponding increase in organic matter and altitude. At higher altitudes, greater proportion of finer particles were firmly held, facilitated by the closer binding with higher proportion of organic matter (Balagopalan and Jose, 1995).

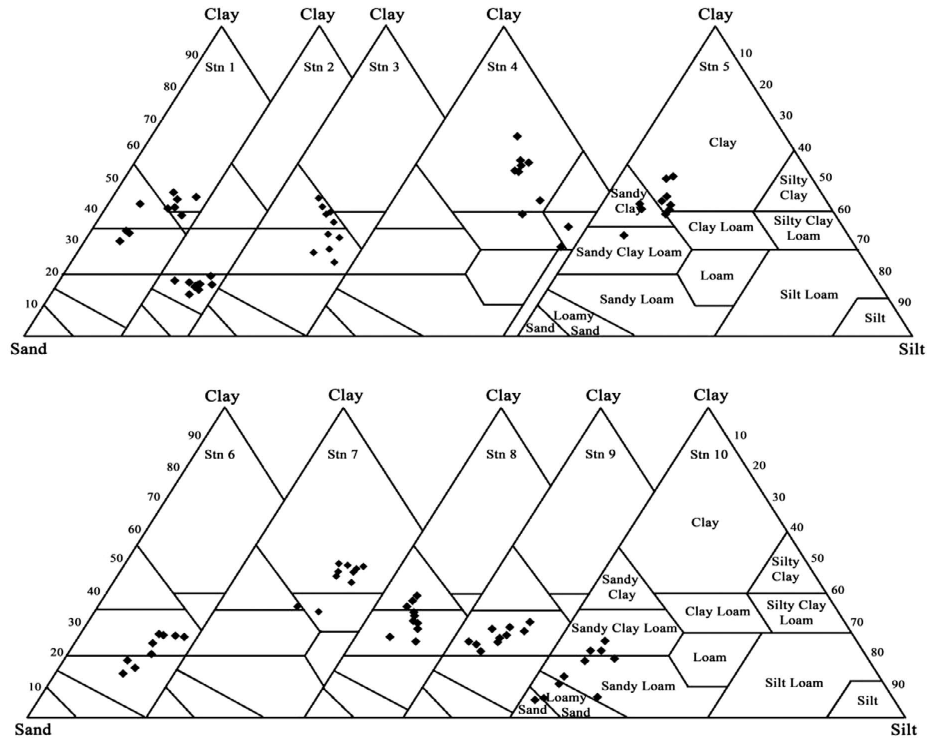


Fig. 2. Soil types of the different profiles examined for the present study.

Table 2. Depth-wise variation of textural properties and nutrient status in each samples.

Stations	Sample Depth (cm)	Sand (%)	Silt (%)	Clay (%)	C org (%)	Nitrogen (%)	Soil Type*
Stn 1 (Neriamangalam)	0-30	58.11	9.30	32.59	1.17	0.14	Sandy clay loam
	30-40	49.24	8.08	42.68	1.40	0.13	Sandy clay
	40-90	39.26	17.20	43.62	0.89	0.07	Clay
	90-100	40.65	20.42	38.94	1.19	0.003	Clay loam
Stn 2 (Mamalakandam)	0-100	72.89	10.60	16.51	1.29	0.07	Sandy loam
Stn 3 (Mankulam)	0-50	44.77	14.77	40.45	1.18	0.05	Sandy clay
	50-100	49.98	21.35	28.66	1.002	0.01	Sandy clay loam
Stn 4 (Parvathi mala)	0-10	21.07	50.23	28.70	3.91	0.27	Clay loam
	10-20	16.01	48.77	35.22	2.57	0.22	Silty clay loam
	20-30	18.89	37.36	43.74	2.13	0.14	Clay
	30-40	25.58	35.15	39.28	2.03	0.05	Clay loam
	40-100	17.57	26.08	56.35	1.08	0.02	Clay
Stn 5 (Eravikulam National Park)	0-10	56.6	10.57	32.83	1.03	0.08	Sandy clay loam
	10-20	47.93	11.02	41.05	0.87	0.04	Sandy clay
	20-80	39.01	15.36	45.63	0.51	0.03	Clay
	80-90	42.83	17.81	39.36	0.39	0.05	Clay loam
	90-100	47.60	9.72	42.68	0.41	0.05	Sandy clay
Stn 6 (Eravikulam National Park)	0-30	66.18	17.58	16.24	11.59	0.94	Sandy loam
	30-100	52.25	22.52	25.23	6.81	0.25	Sandy clay loam
Stn 7 (Nemakkadu)	0-20	41.48	23.60	34.93	2.50	0.18	Clay loam
	20-100	25.10	27.61	47.29	1.58	0.08	Clay
Stn 8 (Kanthloor)	0-70	57.74	12.62	29.64	0.78	0.02	Sandy clay loam
	70-100	53.72	8.73	37.55	0.62	0.003	Sandy clay
Stn 9 (Marayoor)	0-100	62.71	11.05	26.25	0.94	0.05	Sandy clay loam
Stn 10 (Chinnar)	0-20	69.31	17.80	12.90	0.77	0.09	Sandy loam
	20-50	66.24	11.1	22.66	0.83	0.08	Sandy clay loam
	50-70	75.91	8.33	15.76	0.65	0.04	Sandy loam
	70-90	85.41	6.04	8.56	0.40	0.05	Loamy sand
	90-100	90.88	3.42	5.70	0.22	0.03	Sand

* USDA, 1987

It is seen that, sand, silt and clay values are changing according to the sampling depth. Sand content exhibits decreasing trend in most of the samples except from stations 2, 3, 9 and 10 (Mamalaknadam, Mankulam, Marayoor and Chinnar), but in the case of clay values it shows increasing trend in most of the samples except in stations 3, 9 and 10 (Mankulam, Marayoor and Chinnar). Silt values increase according to its sampling depth in stations 1, 3, 6, 7 (Neriamangalam, Mankulam, Eravikulam, Nemakkadu) and in stations 2, 4, 8, 9 and 10 (Mamalakandam, Parvathi mala, Kanthalloor, Marayoor, Chinnar) shows a reverse trend.

Nutrient Status (Organic Carbon and Nitrogen)

Organic matter in the forest soil serves several important functions; it improves soil structure and increases soil porosity and aeration. Most organic matter is added to the forest soil in the form of litter, which includes freshly fallen leaves, twigs, stems, bark, cones and flowers. Soil organic carbon (SOC) values ranges from 0.13% to 13.89% with an average of 1.81% (Table 2). Higher organic carbon content is observed in the surface layers of the trench samples and this may be due to the rapid decomposition of forest litter in a favourable environment. The SOC content shows decreasing trend with increasing soil depth. The maximum carbon stock was present in the shola forest soils (Eravikulam National Park). The higher percent of soil organic carbon in shola forest may be due to dense canopy and higher inputs of litter which results in maximum storage of carbon. The low organic carbon content identified in Chinnar soil samples is due to the wider spacing trees, resulting in low litter inputs and less accumulation, in turn yielding less storage of carbon in these forest soils. This area experiences relatively hot climate and less seasonality compared to other areas. Climatic shifts in temperature and precipitation may have a major influence on the decomposition and amount of soil organic carbon stored within these forest soils.

Well decomposed organic matter will decide the status of nitrogen in the forest soils. Nitrogen values

vary from 0% to 1.09% with an average of 0.09% (Table 2). Shola forest in Eravikulam National Park and Parvathi mala invariably register higher values of nitrogen, because the vegetation pattern is very thick and organic matter and organic carbon content values are very high compared to other forest soils. The organic carbon shows a strong positive correlation with nitrogen ($r = 0.89$, $n = 100$), indicating that organic matter degradation is the major pathway of nitrogen to the soil substratum (Fig. 3). The SOC and nitrogen values show a positive relation with spot height also i.e., better nutrient status observed at higher altitudes and least values at lower altitudes.

Radiocarbon Dating

Radiocarbon dating of organic matter in the soil has been used to study the chronology of soil development. Samples from two locations namely Parvathi mala (Station 4) and Eravikulam National Park (Station 6) were subjected to radiocarbon dating in the present study, where the SOC content for radiocarbon dating was abundant. Once the living organisms die, the intake of carbon by these organisms stops, and the ^{14}C will continue its radioactive decay without replenishment, thereby, the time elapsed since death (radiocarbon age) can be determined (Suresh, 2014). The natural vegetation in the sampled site is tropical montane forest (Table 1), locally called shola forest. The diversity of the montane forest and grasslands have expanded and contracted, and thus in the process has undergone turnover in species composition, in response to the changing climate (Sukumar, 1995). The observed ^{14}C dates in station 6 are 790 ± 80 years BP at a depth of 45 cm below ground level (bgl) and 2060 ± 100 for the depth of 95 cm bgl (Fig. 4). This clearly indicates that the soil development in this area occurred in Late Holocene period. In station 4, ^{14}C data at 55 cm layer is 3150 ± 90 years BP and at the depth of 35 cm, reports modern age because the sample is young (Fig. 4). The modern age indicates these layers above 40 cm depth are formed recently by depositional activities. This station has

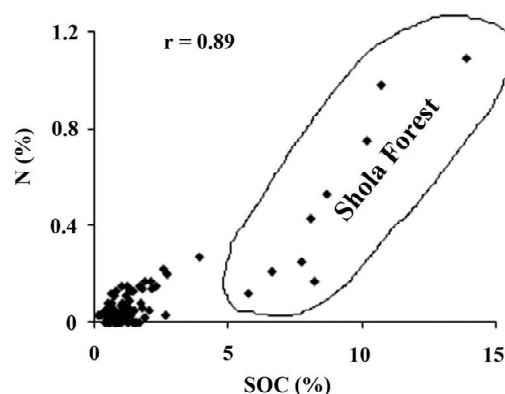


Fig. 3. Relationship of organic carbon with nitrogen.

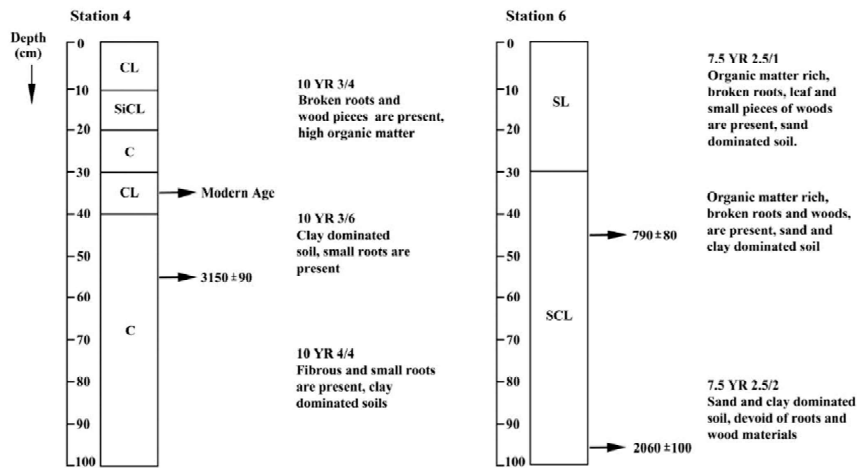


Fig. 4. Lithological and chronological bearings of trench sample in Eravikulam National Park (Station 6) and Parvathi mala (Station 4) (Soil type, colour, soil layer features and age are mentioned in this diagram) after Divya et al., 2016.

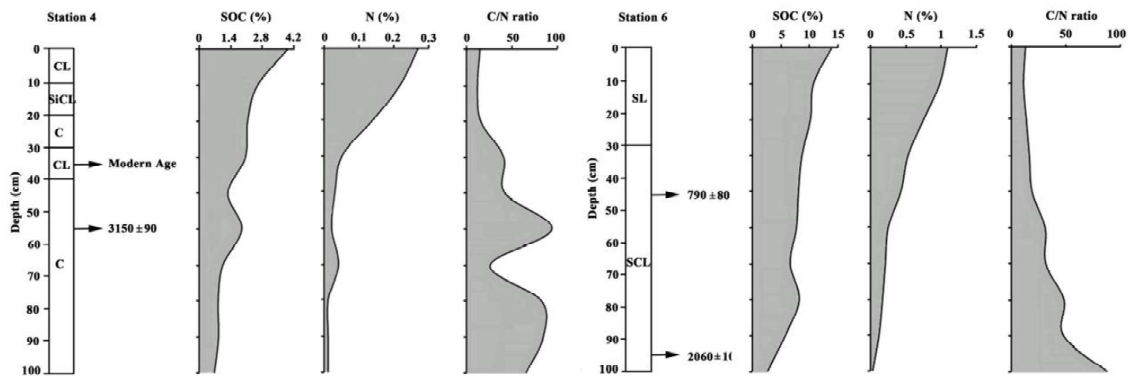


Fig. 5. Depth wise variation of SOC, nitrogen and C/N ratio in Parvathi mala (Station 4) and Eravikulam National Park (Station 6) after Divya et al., 2016.

steeply sloping terrain with maximum elevation of 2000 m above mean sea level.

The soil organic carbon and nitrogen content shows marked variation in the upper younger layers compared to the lower counter parts of both the profiles. But the C/N ratio exhibits reverse trend (Fig. 5). It indicates the stratified nature of soil profile with a period of break in the soil formation and it coincide with the age range of 1500-1000 yrs BP. Similar kind of break was observed by Veena et al. (2014) in lacustrine sediments of Pookot lake, which is located in the Wayanad district and in the coastal zones of southern Kerala (Rajimol et al., 2013; Vishnu Mohan et al., 2013). From these evidences and results of the study, it is revealed that the soil profile of the study area register records of three climate phases in the Late Holocene with the lower and upper strata evolved during two distinct events of high rainfalls, whereas the break in the profile is attributed to a dry phase.

SUMMARY AND CONCLUSION

Forest category has a significant influence on the soil carbon dynamics. From the study it can be seen that the SOC storage capacity or the sink capacity of various forest ecosystems- evergreen forest, moist and dry deciduous forest, shola forest, grassland and sandal wood forest in Idukki district vary and depend largely on the climatic condition, vegetation, soil texture, temperature and extent of human disturbances. The analytical results reveal that altitudinal changes have a significant bearing on the soil properties studied. The soil type ranges from sandy loam to clay. Nutrient status (Nitrogen content) of soil changes with the vegetation pattern. From the results it is clear that shola forest soils are very rich in organic matter and nutrients than other forest soil types. This forest also helps in moisture conservation which increases soil fertility. Carbon dating values in

montane forest ecosystems helps to determine the period of soil development. Geochronological examination reveals that the soil profile of the study area register records of three climate phases in the Late Holocene with the lower and upper strata evolved during two distinct events of high rainfalls, whereas the break in the profile is attributed to a dry phase.

Acknowledgements: We thank the Director, National Centre for Earth Science studies, Thiruvananthapuram for encouragement and support. The financial assistance from Kerala State Council for Science, Technology and Environment (KSCSTE) is gratefully acknowledged. We also thank C.M. Nautiyal (Birbal Sahni Institute of Palaeobotany) for providing the ^{14}C results.

References

- Balagopalan, M., Jose, A.I. (1995). Altitudinal effect on tropical and subtropical forest soils in Kerala, India. *Annals of Forestry* 3, 87-95.
- Bockheim, J.E. (1982). Forest Soils. In: Young, R.A. (Ed.), *Introduction to forest science*. University of Wisconsin, John Wiley & sons Publishing, Madison, Wisconsin, pp. 93-111.
- Brilliant, R., Varghese, V.M., Paul, J., Pradeepkumar, A.P. (2012). Vegetation analysis of montane forest of Western Ghats with special emphasis on RET species. *International Journal of Biodiversity and Conservation* 4, 652-664.
- Champion, H.G., Seth, S.K. (1968). *A revised survey of the forest types of India*. Govt. of India press, Nasik.
- Divya, V., Padmalal, D., Mohanan, C.N. (2016). Soils of southern Western Ghats (India) – a potential archive of late Holocene climate records. *International Journal of Scientific and Research Publications* 6, 302-306.
- Gairola, S., Sharma, C.M., Ghildiyal, S.K., Suyal, S. (2012). Chemical properties of soils in relation to forest composition in moist temperate valley slopes of Garhwal Himalaya, India. *Environmentalist* 32(4), 512-523.
- Lewis, D.W. (1984). *Practical Sedimentology*. Hutchinson Ross publishing company, Pennsylvania, 227p.
- Maiti, S.K. (2003). *Handbook of methods in Environmental studies- Air, Soil and Overburden Analysis*. ABC publishers, Jaipur 2, 171-175.
- Munsell soil colour chart (1994). Gretag Macbeth, New York, 10p.
- Nikhildas, N. (2014). *Archeology of the Anjunad valley, with special reference to the megaliths and rock art, Idukki district, Kerala*. (Ph.D. Thesis) Deccan College Post Graduate and Research Institute, Pune, 246p.
- Rajimol, T.R., Ramdev, P. R., Baburaj, B., Maya, K., Padmalal, D. (2013). Coastal plain rivers of Thiruvananthapuram District, Kerala – River characteristics, human interventions and management strategies. *Proceedings of the 23rd Swadeshi Science Congress, Mahatma Gandhi University, Kottayam*, pp. 336-340.
- Rugmini, P., Balagopalan, M. (2006). Evaluation of factor patterns of soils in different plantations and natural forests in the Western Ghats, Kerala. *Indian Journal of Forestry* 29(3), 271-275.
- Saeed, S., Barozai, M.Y.K., Ahamad, A., Shah, S.H. (2014). Impact of altitude on soil physical and chemical properties in Sra Ghurgai (Takatu mountain range) Quetta, Balochistan. *International Journal of Scientific & Engineering Research* 5(3), 730-735.
- Sannappa, B., Manjunath, K.G. (2013). Fertility status of soils in the selected regions of the Western Ghats of Karnataka, India. *Scholars Academic Journal of Biosciences* 1(5), 200-208.
- Stuiver, M., Reimer, P.J., Braziunas, T.F. (1998). High-precision radiocarbon age calibration for terrestrial and marine samples. *Radiocarbon* 40(3), 1127-1151.
- Sukumar, R., Suresh, H.S., Ramesh, R. (1995). Climate change and its impact on tropical montane ecosystems in southern India. *Journal of Biogeography* 22, 533-536.
- Sukumar, R., Ramesh, R., Pant, R.K., Rajagopalan, G. (1993). A $\delta^{13}\text{C}$ record of late quaternary climate change from tropical peat in Southern India. *Nature* 364, 703-706.
- Suresh, P.O. (2014). Organic carbon dynamics in a soil profile and an alluvial deposit from India. *International Journal of Earth and Atmospheric Science* 1(1), 54-57.
- USDA (1987). *United States Department of Agriculture, Textural classification study guide*.
- Veena, M.P., Achyuthan, H., Eastoe, C., Farooqui, A. (2014). A multi-proxy reconstruction of monsoon variability in the late Holocene, South India. *Quaternary International* 325, 63-73.
- Vishnu Mohan, S., Padmalal, D., Santhosh, V. (2013). Paleoclimatic records and organic carbon loading in the Holocene sediments of Polachira wetlands, southern Kerala, SW India. In: Sundaresan J., Sreekesh S., Ramanathan A. L., Sonnenschein L., Boojh R. (Eds.), *Climate change and environment*. Scientific Publishers, New Delhi, pp. 211-224.
- Walkley, A., Black, I.A. (1934). An examination of the Deglgareff method for determining soil organic matter and a proposed modification of the chromic acid titration method. *Soil Science* 37, 29-38.
- Xiaoquan, Z., Chaoshu, S., Qinghua, Z. (1998). Effect of vegetation and land use on soil fertility in Wutai Mountains of Shanxi province. *Journal of Forest Research* 9(4), 249-252.

Periphyton Diatom Assemblages and their relationship to Environmental Characteristics in Cauvery River of Tamil Nadu (Bhavani) by Canonical Correspondence Analysis

KARTHIKEYAN, P. AND VENKATACHALAPATHY, R.

Department of Geology, Periyar University, Salem 636 011, Tamil Nadu, India

Email: pkarthikeyangold@gmail.com

Abstract: The community structure of periphyton diatom was studied in relation to physico-chemical characteristics of the Cauvery river environmental condition by industrial effluents and domestic sewage from Bhavani. We revealed a diatom diversity consisting of 37 diatom species in the Cauvery River. The distributions of species over the 7 higher taxa were very similar for both rivers with diatom prevailing. As a result of Canonical correspondence analysis (CCA), we revealed components group sensitive to highly polluted due to industrial effluents and sewage evidenced. Thus species which develop well in polluted *Fragilaria intermedia*, *Gomphonema lanceolatum*, *Gomphonema parvulum*, *Nitzschia palea*, *Nitzschia thermalis*, *Pleurosigma salinarum* may also occur in fairly clean water. Their values indicate is their presence in polluted water.

Keywords: Diatom, Cauvery, Canonical correspondence analysis (CCA), Industrial effluents.

INTRODUCTION

Diatoms are a major group of algae and are one of the most common types of phytoplankton. According to our research, diatoms diversity is significantly influenced by changes in the environmental parameters. However, the major parameters used in bioindication are individual for each species, while the reaction of the entire community is left unseen. To change this situation, in this research we reveal the reaction of the entire diatom community present in Cauvery rivers in Bhavani, Tamil Nadu (Fig. 1) as a result of the changes in water parameters under industrial effluents, sewage and anthropogenic pollution. Therefore, we have assumed that water quality during the summer season can represent the sum of all climatic influences and sewage impacts in both regions.

The distribution in the number of species between the groups in the different indicator systems shows the total range of environmental conditions in the river, on one hand, and the prevailing conditions, on the other. The summit of the trend line corresponds to the optimal conditions in respect to the given variable. Out of the many possible ordination methods available we have chosen to use Canonical correspondence analysis (CCA). We were able to obtain quantitative information on the relationship between species and environmental variables using CCA with the STATISTICA for Windows 4.5 package. Estimation of the explanatory power for each environmental variable was performed using the variable as the sole constraining variable. Statistical significance for each variable was assessed using the

Monte Carlo unrestricted permutation test involving 100 permutations (Ter Braak 1990).

MATERIAL AND METHODS

Study Area

The study area lies at 77°40' E to 77°42' E longitude and 11°25'N to 11°27' N latitude with an area of 9.05 sq. km (Fig. 1). The Cauvery River is one of the major rivers of South India. The Cauvery rises at Talakaveri on the Brahmagiri Range of Hill in Western Ghats of India. The river has an approximate length of 760 km flows in the South and East through Karnataka and Tamil Nadu States. The expansion of the city at the moment does not meet the technical standards that should go with it in terms of streets, sewage treatment and collection of garbage, urban drainage, water supply, road system and recreational area. The council also does not have an adequate system of sorting and disposal of waste. River in the study area, therefore, receive untreated or semi-treated effluent from various domestic and industrial sources as well as other diffuse sources as they pass through the city of Bhavani. In 2011, the population of Bhavani was approximately 54,645.

Diatom Sampling and Analyses

Diatom and water quality sampling was done during pre-monsoon (May 2012). The samples were obtained by scooping up for phytoplankton and by scratching for periphyton and were fixed in 3% formaldehyde. In

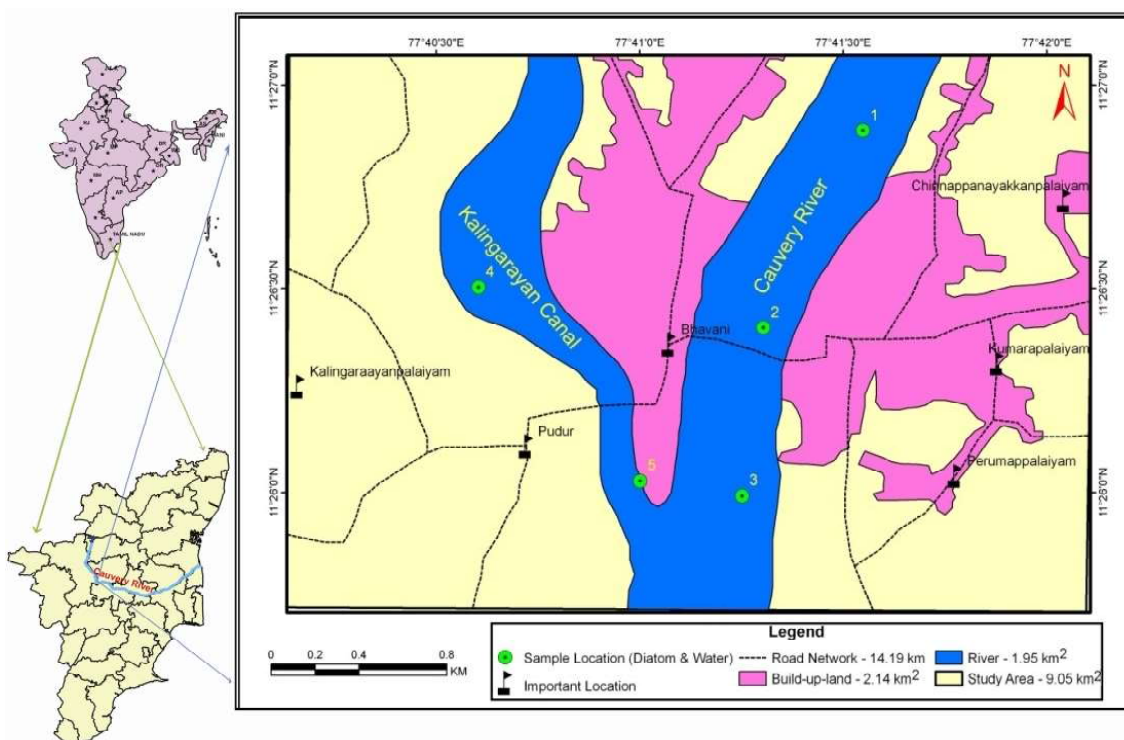


Fig. 1. Map of the Study area with sample locations.

laboratory, the diatom valves were cleaned using 40% H₂O₂ and HCl. Clean valves were mounted in a resin (Naphrax[®]). At least 40 valves from each sample were counted and identified using a light microscope (100 × magnifications). The abundances of all observed taxa were expressed as relative counts. Identifications were carried out using Krammer and Lange-Bertalot (1986–1991) to species and sub-species level.

Physical and Chemical Sample Analyses

Physical and chemical analyses were carried-out at the same sampling sites (Tab. 1). Dissolved oxygen and conductivity were measured in the field. For nitrogen (TKN), PO₄³⁻, Na⁺, Ca²⁺, Cl⁻, K⁺, Mg²⁺, Biological oxygen demand (BOD), Chemical oxygen demand (COD), water samples were collected and analysed in the laboratory according to standard procedures (APHA, 1995).

Species Relationships to Environmental Variables

The CCA biplot represents the ordination of species in relation to the combination of the different environmental variables (Fig. 2). We used canonical correspondence analysis (CCA) to determine the amount of diatom variation explained by water quality. Analyses were performed with the software package Statistics (STATISTICA). Separate CCAs were performed using taxa relative and absolute abundance data to determine which data type was best reflected by water quality. All water quality variables listed in Table 1 were

included in CCAs except for diatoms pH, Temperature, Electrical Conductivity, Total Dissolved Solid, Dissolved Oxygen, Biological oxygen demand (BOD) and Chemical oxygen demand (COD) which had variability at sampled sites. The proportion of variation in the assemblage data captured by the environmental variables was examined to explore the ability of measured water quality to explain the diatom species variation in absolute and relative abundance datasets. Similarly, CCAs were also performed for both data formats using the 5 location variables.

RESULTS

Species Distribution

The present study recorded a total of 37 diatoms belonging to 17 genera species *Achnanthes inflata*, *Achnanthes minutissima*, *Amphora ovalis*, *Caloneis pulchra*, *Cocconeis placentula*, *Caloneis silicula*, *Cyclotella catenata*, *Cyclotella meneghiniana*, *Cymbella aspera*, *Cymbella cymbiformis*, *Cymbella tumida*, *Cymbella tumidula*, *Cymbella turgida*, *Cymbella ventricosa*, *Eunotia fallax*, *Fragilaria intermedia*, *Gomphonema gracile*, *Gomphonema lanceolatum*, *Gomphonema olivaceum*, *Gomphonema undulatum*, *Navicula mutica*, *Nitzschia palea*, *Nitzschia pseudofonticola*, *Nitzschia recta*, *Nitzschia sigma*, *Nitzschia thermalis*, *Melosira granulata*, *Pinnularia acrosphaeria*, *Pleurosigma indica*, *Pleurosigma salinarum*, *Stauroneis anceps*, *Surirella*

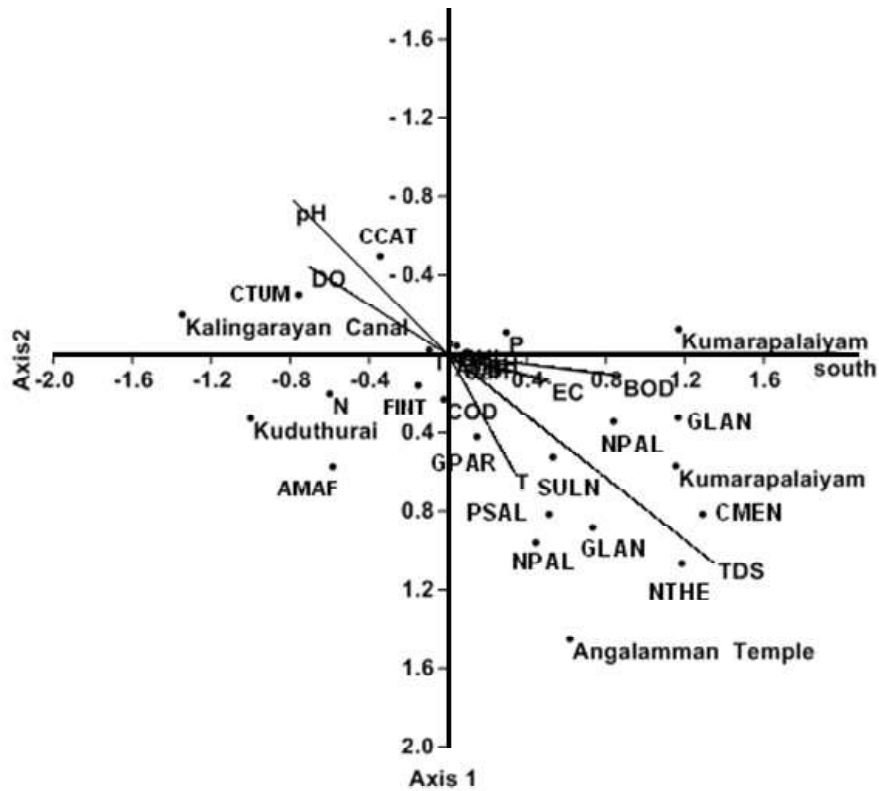


Fig. 2. Ordination diagram based on Canonical Correspondence Analysis (CCA) of most frequently occurring diatom species composition in 5 sampling sites with respect to five environmental variables (pH, T, EC, TDS, DO, BOD and COD). *Achnanthes minutissima* AMAF, *Fragilaria intermedia* Grun FINT, *Cymbella tumida* CTUM and *Cyclotella catenata* CCAT, *Synedra ulna* (Nitzsch) SULN, *Pleurosigma salinarum* Grun PSAL, *Nitzschia palea* (Kutzing) W. Smith NPAL, *Nitzschia thermalis* Kutz v minor Hilse NTHE, *Gomphonema parvulum* GPAR, *Gomphonema lanceolatum* Ehr GLAN, *Fragilaria intermedia* Grun FINT.

Table 1. Anions & Cations Concentration in river water Samples (All values in the table are expressed in ppm except EC in μScm^{-1} and pH / TDS in ppm).

Locations	Angalamman Temple	Kumarapalaiyam	Kumarapalaiyam South	Kalingarayan Canal	Kuduthurai
pH	7.52	7.67	7.81	7.12	7.15
T	27.8	26.57	26.6	24.33	24
EC	1203.23	1015.67	1223.33	843.33	404
TDS	560.67	937	769.33	535	270
DO	5.67	5.81	6.89	3.87	3.6
BOD	13.8	12.89	7.9	3.2	2.92
COD	80.01	42.32	65.08	10.91	10.65
N	0.013	0.014	0.012	0.014	0.123
P	0.024	0.03	0.014	0.005	0.002
TH	236.67	243.97	322.93	119.33	131
CaH	91.23	89	82.23	79.67	76.93
MgH	57.83	56.19	57.58	33.35	18.51
CHL	272.12	285.34	277.81	65.96	42.4
ALK	151	151.11	159.01	115.33	110

linearis, *Surirella robusta*, *Surirella splendida*, *Surirella tenera*, *Synedra rumpens*, *Synedra ulna* genera with wide range of community composition and species distribution across the river. Among all species (relative abundance >0.05% of all sites),

Water Quality Assessment

The Physicochemical analytical results of water sample are given in Table 1. The pH, EC, BOD, COD and alkalinity are the parameters showed marked difference among various samples. The pH is ranged from 7.12 to 7.81 highest being 7.81 at Kumarapalayam South. Water temperature had a wide range, 24.00 to 27.80 (mean 25.86, SD 1.62) which is mainly dependent on the time of sampling. The EC is varying much (mean 937.912, SD 336.1217) having low at Kuduthurai (404 ppm) and high value noticed at Kumarapalayam south (1223.33 ppm) which is beyond the permissible limits. High electric conductivity is mainly due to high ionic concentrations. Nutrients such as nitrates and phosphates varied from 0.01-0.12 ppm and 0.002-0.030ppm respectively within the permissible limits. The alkalinity ranged from 110mg/L at Kuduthurai and high to 159.01mg/L at Kumarapalayam south. Both COD and BOD values were high at Angalamman temple (80.01mg/L, 13.80 mg/L) and low at Kuduthurai (10.65 mg/L, 2.92mg/L) respectively. Among 5 sample locations, the Angalamman temple and Kumarapalayam south sites recorded with high ionic concentrations while low values within the permissible limit (WHO 1996) were recorded in Kalingarayan Canal and Kuduthurai.

Canonical Correspondence Analysis

The results of CCA are presented in Fig 2. The CCA explained a large proportion of the diatom species variance; CCA axis 1, eigenvalue = 0.04 and axis 2, eigenvalue = 0.4. Monte Carlo unrestricted permutation test indicated that axis 1 (100 permutations) and axis 2 (100 permutations of axis 2 with axis 1 as a covariable) were statistically significant ($p < 0.05$). The CCA axis 1 and 2 roughly separated relatively less polluted sites (Kalingarayan Canal and Kuduthurai) from highly polluted sites (Angalamman temple, Kumarapalayam and Kumarapalayam South). The former group of sites is associated with slightly pH and DO (which was highly positively correlated with T, EC, TDS and BOD). The parallel Canal, relatively less polluted sites (Kalingarayan Canal and Kuduthurai) were characterized by such species as *Achnanthes minutissima*, *Fragilaria intermedia* Grun, *Cymbella tumida* and *Cyclotella catenata*. These species were highly negatively associated with CCA axis 1. On the other hand, down river, highly polluted sites (Angalamman temple, Kumarapalayam and Kumarapalayam South) were characterized by *Gomphonema parvulum* (Kützing) Cleve and *Nitzschia palea* (Kützing) Smith which have

been reported to be highly pollution tolerant (Duong et al., 2006) and *Pleurosigma salinarum* Grun, *Nitzschia thermalis* Kutz v minor Hilse, *Gomphonema parvulum*, *Gomphonema lanceolatum* Ehr, *Fragilaria intermedia* Grun were positively associated with CCA axis 2.

DISCUSSIONS

Achnanthes minutissima Kutz, *Cyclotella meneghiniana* Kützing, *Cyclotella catenata* Brun, *Cymbella tumida* (Breb) Van Heurck, *Cymbella turgida* (Greg) Cleve, *Cymbella ventricosa* Kutz, *Fragilaria intermedia* Grun var. *robusta*, *Gomphonema lanceolatum* Ehr, *Gomphonema parvulum*, *Nitzschia sigma* (Kutz) W Smith, *Nitzschia thermalis* Kutz v minor Hilse, *Nitzschia palea* (Kützing) W. Smith, *Pleurosigma salinarum* Grun, *Synedra ulna* (Nitzsch) Ehr. *Cyclotella meneghiniana* Kützing, *Gomphonema parvulum* and *Nitzschia palea* (Kützing) W. Smith were the most abundant species. These species were cosmopolitan which are reported from North America (Stevenson and Pan, 1999) Europe (Bella et al., 2007) & Africa (Facca and Sfriso, 2007) and well recognized diagonally inhabiting sensible to extremely polluted in the river. *Cyclotella meneghiniana*, a pollution tolerant species was abundant at Kumarapalayam, representing water quality as rich with ionic concentration. *Gomphonema parvulum* and *Nitzschia palea* with environmental characteristics of highly tolerant to nutrients and ions is abundant at Kumarapalayam south, which is having the highest electrical conductivity and ionic concentrations. However Kalingarayan canal, unlike from rest of the river (low ionic level) is dominated by *Achnanthes minutissima* Kutz species which occurs in slightly too moderate waters. The equivalent as contamination greater than before, low pollution tolerant species such as *Achnanthes minutissima*, *Fragilaria intermedia* Grun, *Cymbella tumida* and *Cyclotella catenata* were replaced by high pollution tolerant species such as *Fragilaria intermedia*, *Gomphonema lanceolatum*, *Gomphonema parvulum*, *Nitzschia palea*, *Nitzschia thermalis* and *Pleurosigma salinarum*. The high pollution group of species has been reported to be associated with waters of comparatively high ionic strength and high conductivity (Potapova and Charles, 2003) that accompanied the downriver gradient in this study. Similarly, Angalamman Temple, Kumarapalayam and Kumarapalayam south sites are highly polluted due to anthropogenic activities and industrial effluents evidenced by CCA. *Nitzschia palea* to be tolerant of organic pollution due to sewage effluent in the river of Yamuna, Delhi, India (Dakshine and Soni, 1982). Similarly this species is most abundant at Kumarapalayam site due to highly sewage effluent in these sites. *Gomphonema parvulum* has also been shown to be tolerant of organic pollution (Lobo et al., 2004) which is also similar to Kumarapalayam South and Kumarapalayam are most abundances of the location

due to highly sewage effluent and dyeing factories. Thus species which develop well in polluted *Fragilaria intermedia*, *Gomphonema lanceolatum*, *Gomphonema parvulum*, *Nitzschia palea*, *Nitzschia thermalis*, *Pleurosigma salinarum* may also occur in fairly clean water. Their values indicate their presence in polluted water which was also characteristic of the Angalamman temple, Kumarapalayam and Kumarapalayam South.

In Cauvery river we revealed diatoms variety consisting of 37 species. Species variety in the rivers is significantly different but the distributions of species

over the higher taxa were very similar for river side. The CCA determines the most significant factors affecting the species variety in both river sides. As we know, the most effective application of this statistical approach is the comparison of community's preferences from different phytogeographical provinces. The environment distinguishing every diatom taxa in occurrence and distribution as community composition is significant at every sampling location. The significance of water quality difference among the sampling sites is expressed in CCA gradient.

References

- American Public Health Association (APHA) (1995). Standard Methods for Examination of Water and Wastewater, 19th edition.
- Bella V. D., Puccinelli C., Marcheggiani S. and Mancini L. (2007). Benthic diatom communities and their relationship to water chemistry in wetlands of central Italy. *Ann. Limnol. - Int. J. Lim.* 43(2), 89-99.
- Daskshine K. M. M. and Soni J. K. (1982). Diatom distribution and status of organic pollution in sewage drains. *Hydrobiologia*, 87(3), 205-209.
- Facca C. and Sfriso A. (2007). Epipelagic diatom spatial and temporal distribution and relationship with the main environmental parameters in coastal waters, *Estuarine, Coastal and Shelf Science*, 75, 35-49.
- Krammer, K., Lange-Bertalot, H. (1986-1991). *Bacillariophyceae* 1. Teil: Naviculaceae. 876 p.; 2. Teil: Bacillariaceae, Epithemiaceae, Surirellaceae, 596 p.; 3. Teil: Centrales, Fragilariaceae, Eunotiaceae, 576 p.; 4. Teil: Achnantheaceae. Kritische Ergänzungen zu Navicula (Lineolatae) und Gomphonema. 437 p. In: Ettl, H., Gerloff, J., Heynig, H., Mollenhauer, D. (Eds.), *Susswasserflora von Mitteleuropa*. Band 2/1-4. G. Fischer Verlag, Stuttgart.
- Lobo E. A., Callegaro V. L. M., Hermany G., Bes D., Wetzel C. A. and Oliveira M. A. (2004). Use of epilithic diatoms as bioindicators from lotic systems in southern Brazil, with special emphasis on eutrophication. *Acta Limnol. Bras.*, 16(1), 25-40.
- Potapova M. and Charles D. F., 2003. Distribution of benthic diatoms in US rivers in relation to conductivity and ionic composition. *Freshwater Biology*, vol. 48, no. 2, p. 1311-1328.
- Stevenson, R. and Pan Y. (1999). Assessing environmental conditions in rivers and streams with diatoms. In: *The Diatoms: Applications for the Environmental and Earth Sciences*. Cambridge University Press, Cambridge, (eds Stoermer, E. F. and Smol, J. P.). 11-40.
- Ter Braak, C.J.F. (1990). Interpreting canonical correlation analysis through biplots of structural correlations and weights. - *Psychometrika* 55, 519-531.

Uncertainty in Ecological Status Assessments of the Cauvery River, Tamil Nadu, India using of Biological Diatom Indices (IBD)

KARTHIKEYAN, P. AND VENKATACHALAPATHY, R.

Department of Geology, Periyar University, Salem 636 011, Tamil Nadu, India

Email: pkarthikeyangold@gmail.com

Abstract: This paper deals with biological diatom indices proved successful in indicating general ecological status and assessment of water quality, namely the Biological Diatom Index (BDI) and also successfully indicates levels of ecological status determined in the Cauvery River, Tamil Nadu, India. Diatom-based indices are more becoming significant tools for the assessment and ecological status in river waters. They are reactive to the scenery of the physical, chemical and biological characteristics in all aquatic systems. However, diatom-based indices developed for a specific geographic region may not be appropriate elsewhere. In this paper, diatom indices such as the Biological Diatom Index (BDI), Shannon Index, Berger-Parker Index, diatom assemblages and trophic condition were analyzed and discussed. Results of the present study cautions the indiscriminate dumping and release of pollutants into rivers which might lead to serious environmental deterioration which could be considered as a potential source of threat to the biotic life.

Keywords: Diatom, IBD, Ecology, Cauvery river

INTRODUCTION

Diatom-based indices might be particularly valuable in assessing rivers because a one-time assay of species composition of diatom assemblages within the system could provide better characterizations regarding physicochemical conditions than one time measurement of those conditions (Stevenson and Pan, 1999, Venkatachalapathy and Karthikeyan 2015 & 2014). This scrupulous guide gives a means with regard to identification of the entire diatom taxa utilized in the Biological Diatom Index (BDI) regarding Lenoir of Coste (1996) created for use within national river quality assessment networks in France. Kelly (2000) developed a comparable guide for that identification involving common benthic diatoms in Great Britain. Work on the usage of diatoms as bioindicators has in reality proceeded to such an extent that in some cases diatom indices replaced invertebrate indices because of the choice of biomonitoring methods (Prygiel and Coste, 1993). Diatom-based indices will be very useful for monitoring habitats in conditions where other sorts of monitoring tools are difficult or inappropriate to be utilized. Diatoms are utilized carefully for biomonitoring all aquatic ecosystems due to their common occurrence, simplicity of selection in addition to maintenance, and as well their particular speedy reaction to environment changes in addition to wear and tear involving water top quality, especially coming from has an effect on for instance nutrient enrichment, acidification and metal contamination (Descy 1979; Kelly and Whitton 1995;

Stoerme and Smol 1999; Hirst et al. 2002). Strong relationships in between diatom assemblage in addition to water chemistry are established and lots of diatom indices pertaining to water quality assessment of associated with rivers and lakes are developed (Kelly and Whitton 1995; Schonfelder et al. 2002; Kelly et al. 2008; Beltrami et al. 2012). However, some studies have established that diatom indices vary within their capacity to help predict trophic reputation, ionic composition and organic pollution in rivers (Gomez and Licursi 2001; Taylor et al. 2007). In this paper, an attempt has been made to assessment and ecological status of biological diatom indices in Cauvery River.

DESCRIPTION OF STUDY AREA

The Cauvery River is one of the major rivers of South India which originates in the Western Ghats and flows in eastward direction passing through the states of Karnataka, Tamil Nadu, Kerala and Pondicherry before it drains into Bay of Bengal. The total length of the river from its source to merger into Bay of Bengal is about 800 km². The Cauvery basin extends over an area of 81,155 km² lies in the states of Tamil Nadu, Karnataka, Kerala and Pondicherry. The shape of the basin is somewhat rectangular with a maximum length and breadth of 360 km² and 200 km², respectively. The study area lies at 77°40' E to 77°42' E longitude and 11°25' N to 11°27' N latitude with an area of 41.1 sq. km (Fig. 1.1).

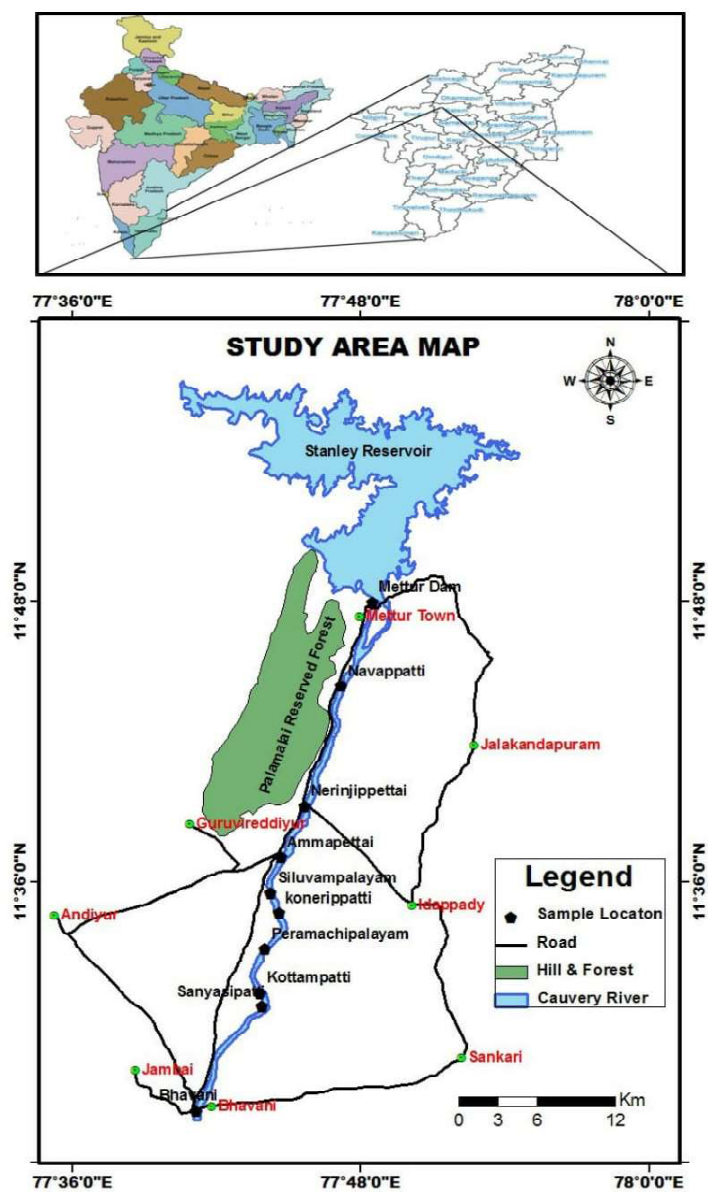


Fig. 1. Location of the Study area.

Table 1. Sample locations in Cauvery River, parts of Tamil Nadu.

S.No.	Location	Latitude and longitude		Altitude (Feet)
1	Mettur Dam	77°48'28.92"E	11°47'58.64"N	658
2	Navappatti	77°47'02.37"E	11°44'27.74"N	638
3	Neringipettai	77°45'38.46"E	11°39'17.18"N	611
4	Ammappettai	77°44'41.23"E	11°37'10.05"N	595
5	Siluvampalayam	77°47'58.86"E	11°35'28.07"N	590
6	Koneripatti	77°44'36.72"E	11°34'41.58"N	586
7	Peramachipalayam	77°47'58.86"E	11°33'14.07"N	567
8	Kottampatty	77°43'34.23"E	11°31'37.22"N	557
9	Sanyasipatti	77°43'14.22"E	11°30'14.03"N	548
10	Bhavani	77°40'59.96"E	11°25'59.87"N	524

METHODOLOGY

Macrophytes, epilithic and water samples were collected from the Cauvery river during 2011 to 2013. We usually started our sampling from Mettur Dam to Bhavani with the Global Position System (GPS) and location of all the sampling points were noted down. All the macrophytes and epilithic samples were packed for different laboratory analysis appropriately in well-insulated zip-lock polythene cover added with formaldehyde (4%) for preservation. Different methods mentioned in this study were used for sampling diatoms from different habitats for environmental studies in the Cauvery River. Epiphytic diatoms grow attached to macrophytes and large algae. Phytoplankton samples were collected ideally by manual collection. The attached microalgae, of which diatoms are a dominant component, were collected by scraping natural substrates in river, streams and lake. Floating filamentous algae and plant materials are often full of loosely attached diatoms.

Concentrated diatom samples were boiled in 50-60% nitric acid to oxidize the organic materials and then the acid was washed off with demineralised water by settling or centrifugation. The final ‘cleared’ diatom samples, an ash colored material was mounted in a mounting medium Naphrax with a refractive index close to 1.7 and placed on a hotplate until the solvent in the medium evaporates. The slide was cooled immediately, by removing from the hotplate. The diatom slide thus obtained is permanent. The diatoms cleaned cells in permanent slides were observed under X 40 and photographed using black and white for best results or by digital photography. In the present study, the systematic classification of Diatoms by Round et al. (1990) “The Diatoms, Biology & Morphology of the Genera” is followed. In addition, the work of John (2012) on “Diatoms in the Swan River Estuary, Western Australia: Taxonomy and Ecology” and Karthik et. al. 2013 “An Illustrated Guide to Common Diatom of Peninsular India” widely used along with the published literatures for comparison of taxa.

Biological Diatom Index (BDI) index (Prigiel & Coste, 2000) indicates general ecological status of rivers. This practical index is a good compromise between reliability and efficiency. It is based on some hundreds of most common diatom taxa. The scale runs from 1 to 20 (Table 2 and Table 3).

Table 2. Index score and Ecological status of BDI.

Index score	Ecological State
17.0 to 20.0	Very good
13.0 to 17.0	Good
09.0 to 13.0	Moderate
05.0 to 09.0	Low
01.0 to 05.0	Very low

Ecological diversity was calculated for each sample using diversity indices, Shannon Weiner’s (H’), Simpson’s D and Berger-Parker.

Shannon - Wiener Diversity index (Shannon and Weiner, 1949) was employed to determine species diversity (H’).

$$H2 = - \sum_{i=1}^S pi \ln pi \dots\dots\dots(2)$$

where
Pi: proportion of individuals of ith species

Remarks: The value ranges between 1.5 and 3.5 and rarely surpasses 4.5

Berger and Parker 1970;

$$d = \frac{Nmax}{N} \dots\dots\dots(3)$$

where Nmax is the number of individuals in the most abundant species and N is the total number of individuals in the sample. Remarks: The number of individuals in the dominant taxon relative to n, where n is the total number of species.

RESULTS AND DISCUSSION

In ten different stations in aquatic systems of Cauvery river showed rich and diverse diatom taxa population. 102 (One hundred and two) diatom taxa belong to 3 Classes, 5 Subclasses, 16 Orders, 24 Families and 35 genera recorded in the study area were as follows:

Cyclotella atomus, Cyclotella catenata, Cyclotella meneghiniana, Cyclotella stelligera, Cyclotella striata, Melosira granulata, Melosira moniliformis, Melosira varians, Aulacoseira distans, Aulacoseira granulata, Terpsinoe musica, Pleuosira indica, Pleuosira laevis, Ctenophora pulchella, Fragilaria intermedia, Fragilaria tenera, Fragilaria ulna, Fragilaria rumpens, Meridion circulare, Synedra rumpens, Synedra ulna, Tabellaria flocculosa, Tabellaria ventricosa, Eunotia bilunaris, Eunotia fallax, Eunotia pectinalis, Cymbella aspera, Cymbella cymbiformis, Cymbella ehrenbergii, Cymbella helvetica, Cymbella lanceolata, Cymbella microcephala, Cymbella tumida, Cymbella turgidula, Encyonema minutum, Achnanthes brevipes, Achnantheidium eutrophilum, Achnantheidium exiguum, Achnantheidium latecephalum, Achnantheidium minutissima, Cocconeis pediculus, Cocconeis placentula, Anomooneis sphaerophala,

Table 3. Class limit values for Diatom indices (Eloranta & Soininen, 2002).

Index score	Class	Trophy
>17	High quality	Oligotrophy
15 to 17	Good quality	Oligo-mesotrophy
12 to 15	Moderate quality	Mesotrophy
9 to 12	Poor quality	meso-eutrophy
<9	Bad quality	Eutrophy

Gomphonema affine, *Gomphonema clavatum*, *Gomphonema augur*, *Gomphonema gracile*, *Gomphonema lanceolatum*, *Gomphonema olivaceum*, *Gomphonema parvulum*, *Gomphonema truncatum*, *Neidium affine*, *Neidium productum*, *Diadesmic confervacea*, *Frustulia rhomboids*, *Gyrosigma acuminatum*, *Pinnularia acrosphaeria*, *Pinnularia maior*, *Pinnularia gibba*, *Sellaphora pulchra*, *Stauroneis phoenicenteron*, *Caloneis silicula*, *Navicula atomus*, *Navicula cryptocephala*, *Navicula elginensis*, *Navicula mutica*, *Navicula radiosa*, *Navicula subrhynchocephala*, *Navicula salinarum*, *Navicula symmetrica*, *Navicula tripunctata*, *Navicula viridula*, *Craticula cuspidata*, *Stauroneis anceps*, *Pleurosigma angulatum*, *Pleurosigma elongum*, *Pleurosigma angulatum*, *Pleurosigma salinarum*, *Mastogloia braunii*, *Amphora holsatica*, *Amphora veneta*, *Amphora ovalis*, *Tryblionella apiculata*, *Tryblionella debilis*, *Tryblionella levidensis*, *Bacillaria paxillifer*, *Nitzschia acicularis*, *Nitzschia angustata*, *Nitzschia dissipata*, *Nitzschia heufleriana*, *Nitzschia linearis*, *Nitzschia lorenziana*, *Nitzschia microcephala*, *Nitzschia palea*, *Nitzschia pseudofonticola*, *Nitzschia recta*, *Nitzschia sigma*, *Surirella angusta*, *Surirella linearis*, *Surirella ovalis*, *Surirella robusta*, *Surirella splendida* and *Surirella tenera* recorded from Cauvery River.

Biological Diatom Index

In most dominant species, taxa were recorded such as *Achnanthes brevipes* (5.1%), *Cymbella aspera* (5.4%), *Cocconeis placentula* (7.6%), *Craticula cuspidata* (5.8%) and *Navicula cryptocephala* (5.4%) in Mettur dam. The IBD values in Mettur dam (14.4) indicated good ecological status in 2011 due to the inflow of water to Mettur dam changing the water quality as oligo-mesotrophy i.e. good quality. The similar result was reported Hasan Kalyoncu and Burcu Serbetci (2013) in Dari Stream, Isparta Turkey with good water quality were associated with such species as *Cocconeis pediculus* and *C. placentula*. In most dominant species, taxa were recorded such as *Achnanthidium minutissima* (9.7%), *Amphora ovalis* (6.1%), *Cymbella microcephala* (6.7%), *Caloneis silicula* (6.1%), *Cymbella tumida* (9.7%), *Gomphonema olivaceum* (5.5%) and *Navicula viridula* (9.7%). The IBD values in Mettur dam (14.2) indicated good ecological status in 2012. In most dominant species taxa were recorded such as *Aulacoseira granulata* (11.7%), *Cymbella cymbiformis* (12.9%), *Navicula elginensis* (9%), *Nitzschia obtusa* (8.9%), *Navicula subrhynchocephala* (6.3%), and *Synedra rumpens* (7.4%). The IBD values in Mettur dam (16.5) indicated good ecological status in 2013. The similar result reported in with good water quality were associated with such species as *Achnanthidium minutissimum* Kalyoncu 2013 in Dari Stream, Isparta Turkey and Barlas (1988) say that *A. minutissimum* is an

organism of moderate quality. In present study Mettur Dam has water quality of oligo-mesotrophy condition and therefore it is of good quality in ecological status.

In most dominant species taxa were recorded such as *Amphora veneta* (5.4%), *Aulacoseira distans* (9.7%), *Cyclotella atomus* (8.6%), *Craticula cuspidata* (8.6%), *Diadesmic confervacea* (1.4%), *Fragilaria rumpens* (5.4%), *Gomphonema gracile* (8.6%) and *Synedra ulna* (6.5%). The IBD values in Navappatti (14.2) indicated good ecological status in 2011. In most dominant species taxa were recorded such as *Achnanthidium minutissima* (6.8%), *Amphora veneta* (8.4%), *Aulacoseira granulata* (9.1%), *Cymbella turgidula* (6.8%), *Cymbella tumida* (6.8%), *Melosira granulata* (9.8%), *Nitzschia lorenziana* (6.8%), *Navicula subrhynchocephala* (6.8%), *Nitzschia microcephala* (6.8%), *Surirella ovalis* (9.1%) and *Surirella robusta* (6.8%). The IBD values in Navappatti (13.3) indicated good ecological status in 2012. The most dominant species taxa were recorded such as *Achnanthidium eutrophilum* (6.8%), *Anomoeoneis sphaerophora* (6%), *Cymbella microcephala* (8.3%), *Ctenophora pulchella* (6.8%), *Fragilaria rumpens* (5.8%), *Neidium productum* (4.6%), *Nitzschia obtusa* (6.8%), *Surirella ovalis* (6.8%) and *Tryblionella victoriae* (6.8%). The IBD values in Navappatti (16.5) indicated good ecological status in 2013. In present study of Navappatti there is no change for ecological status and continues to be of good ecological status as during 2011-2013.

In present study of Nerinjipettai most dominant species taxa were recorded such as *Cymbella aspera* (4.9%), *Cocconeis placentula* (4.9%), *Neidium productum* (4.9%) and *Nitzschia palea* (8.9%). The IBD values in Nerinjipettai (11.29) indicated moderate ecological status in 2011. The similar result reported by Kalyoncu and Serbetci (2013) with moderate to bad water quality were associated with *Nitzschia palea* taxa determined to be tolerant of pollution in Dari Stream, Isparta Turkey. It was described that this species had high relative abundance in alfamesosaprobic critically polluted water quality, an indication that it is tolerant of high pollution. In this study IBD values in Nerinjipettai (11.29) indicated moderate ecological status due to sewage influences in this area. In present study most dominant species taxa were recorded such as *Amphora holsatica* (5.6%), *Amphora veneta* (9.5%), *Amphora ovalis* (4.8%), *Aulacoseira granulata* (9.3%), *Cymbella tumida* (4%), *Encyonema minutum* (5.6%), *Gomphonema lanceolatum* (5.6%), *Gyrosigma acuminatum* (5.6%) and *Surirella angusta* (5.6%). The IBD values in Nerinjipettai (13.6) indicated moderate ecological status in 2012. In present study most dominant species taxa were recorded such as *Cymbella tumida* (5.1%), *Frustulia rhomboids* (4.3%), *Nitzschia acicularis* (5.1%), *Navicula elginensis* (9%), *Nitzschia obtusa* (8.9%), *Navicula subrhynchocephala* (6.3%), *Synedra rumpens* (7.4%) and *Synedra ulna* (5.1%). The IBD values in Nerinjipettai (10.3) indicated poor

ecological status in 2013. Similarly, Hosmani (2012) reported that the diatoms indicating anthropogenic pollution were *Amphora ovalis*, *Synedra ulna*, *Cymbella tumida*, *Gomphonema olivaceum*, *Navicula subrhynchocephala* in Doddakere lake of Mysore city. In present study, Nerinjipettai was affected in anthropogenic pollution and sewages IBD values of (10.3) were indicating ecological states in poor quality.

In present study of Ammapettai most dominant species taxa were recorded such as *Cyclotella striata* (58%), *Diademsis confervacea* (5.8%), *Gomphonema gracile* (5.8%), *Neidium affine* (5.8%) and *Pinnularia gibba* (5.8%). The IBD values in Ammapettai (12.52) indicated moderate ecological status in 2011. In similar study, Hosmani S. P (2012) reported the diatoms indicating anthropogenic pollution were *Pinnularia gibba* in Dadadahally Lake, Doddakere lake of Mysore city. In present study, Ammapettai was slightly polluted due to sewage and anthropogenic activity. In present study most dominant species taxa were recorded such as *Achnantheidium minutissima* (5.2%), *Amphora veneta* (9.7%), *Amphora ovalis* (5.8%), *Cymbella microcephala* (5.2%), *Caloneis silicula* (5.2%), *Cymbella tumidula* (8.4%), *Gomphonema parvulum* (7.7%), *Navicula elginensis* (9.7%) and *Synedra ulna* (5.2%). The IBD values in Ammapettai (11.4) indicated moderate ecological status in 2012. Hosmani S. P (2012) reported that the most common indicators of organic pollution were *Nitzschia intermedia*, *Cyclotella meneghiniana*, *Navicula cryptocephala*, *Cyclotella atomus*, *Melosira varians* in Dadadahally Lake, Doddakere lake of Mysore city. In present study most dominant species taxa were recorded such as *Achnantheidium eutrophilum* (6.8%), *Anomooneis sphaerophora* (6%), *Cymbella microcephala* (8.3%), *Ctenophora pulchella* (6.8%), *Fragilaria rumpens* (5.8%), *Neidium productum* (4.6%), *Nitzschia obtusa* (6.8%), *Surirella ovalis* (6.8%) and *Tryblionella victoriae* (6.8%). The IBD values in Ammapettai (14.4) indicated good ecological status in 2013.

In present study of Siluvampalayam most dominant species taxa were recorded such as *Achnantheidium eutrophilum* (4%), *Amphora ovalis* (4%), *Anomooneis sphaerophora* (2.4%), *Cyclotella atomus* (4.8%), *Ctenophora pulchella* (4%), *Cymbella ventricosa* (6.4%), *Gomphonema gracile* (4.8%), *Gomphonema olivaceum* (4%), *Meridion circulare* (4%), *Navicula viridula* (6.4%), *Synedra rumpens* (6.4%) and *Surirella splendida* (4%). The IBD values in Siluvampalayam (13.5) indicated good ecological status in 2011. The similar result reported by Kalyoncu 2013 with mean moderate water quality were associated with such species as *Melosira circulare*, *Gomphonema olivaceum* represents excellent quality class, *Gomphonema olivaceum*, good quality class taxa determined in tolerant of pollution in Dari Stream, Isparta Turkey. In study of Siluvampalayam the IBD score (13.5) indicated in good ecological status. In present study most dominant

species taxa were recorded such as *Achnanthes brevipes* (53%), *Bacillaria paxillifer* (6.1%), *Cymbella turgidula* (3.0%), *Cymbella ventricosa* (6.1%), *Fragilaria ulna* (5.3%), *Gomphonema gracile* (9.1%), *Gomphonema parvulum* (8.6%), *Gomphonema lanceolatum* (7.6%) and *Nitzschia palea* (9.1%). The IBD values in Siluvampalayam (11.1) indicated moderate ecological status in 2012 Hosmani S. P (2012) was reported the most common indicators of organic pollution were diatoms indicating anthropogenic pollution were *Gomphonema parvulum* in Doddakere lake of Mysore city.

In present study of Siluvampalayam most dominant species taxa were recorded such as *Aulacoseira granulata* (4.9%), *Cymbella microcephala* (5.6%), *Frustulia rhomboids* (5.6%), *Gomphonema affine* (6.8%), *Meridion circulare* (7.2%), *Neidium affine* (8.5%), *Nitzschia recta* (6.2%), *Synedra ulna* (9.3%), *Tabellaria ventricosa* (1.2%), *Tryblionella victoriae* (4.9%), *Fragilaria intermedia* (1.6%), *Navicula festiva* (1.3%), *Pleurosigma angulatum* (1.4%) and *Pleurosira indica* (2.6%). The IBD values in Siluvampalayam (14.5) indicated good ecological status in 2013.

In present study of Koneripatti most dominant species taxa were recorded such as *Achnanthes brevipes* (5.1%), *Amphora veneta* (4.7%), *Amphora ovalis* (4.3%), *Cymbella aspera* (5.4%), *Cocconeis placentula* (7.6%), *Craticula cuspidata* (5.8%), *Navicula cryptocephala* (5.4%) and *Neidium affine* (4.3%) in Koneripatti. The IBD values in Koneripatti (10.4) indicated moderate ecological status in 2011. In present study of Koneripatti most dominant species taxa were recorded such as *Aulacoseira granulata* (4.1%), *Cymbella microcephala* (5.4%), *Cocconeis pediculus* (4.1%), *Diademsis confervacea* (9.4%), *Gomphonema lanceolatum* (8.8%), *Gomphonema olivaceum* (8.2%), *Navicula viridula* (9.4%) and *Surirella robusta* (5.4%). The IBD values in Koneripatti (10.4) indicated moderate ecological status in 2012. In present study of Koneripatti most dominant species taxa were recorded such as *Aulacoseira granulata* (7.3%), *Caloneis silicula* (6.1%), *Diademsis confervacea* (6.1%), *Navicula cryptocephala* (6.1%), *Nitzschia linearis* (6.1%), *Surirella robusta* (6.1%), *Synedra rumpens* (9.8%), *Synedra ulna* (7.8%) and *Tabellaria flocculosa* (7.9%). The IBD values in Koneripatti (10.4) indicated moderate ecological status in 2013.

In present study of Peramachipalayam most dominant species taxa were recorded such as *Achnantheidium eutrophilum* (9.4%), *Amphora veneta* (6.8%), *Cymbella cymbiformis* (7.9%), *Cocconeis placentula* (7.3%), *Cyclotella striata* (6.3%), *Cymbella ventricosa* (5.8%), *Fragilaria rumpens* (6.3%), *Navicula elginensis* (8.9%), *Navicula viridula* (7.9%) and *Pinnularia acrospheria* (8.4%). The IBD values in Peramachipalayam (13.5) indicated moderate ecological status in 2011. In present study of Peramachipalayam most dominant species taxa were recorded such as *Achnantheidium minutissima* (3.9%), *Amphora veneta*

(8.4%), *Cymbella tumida* (7.1%), *Gomphonema affine* (5.8%), *Navicula elginensis* (5.8%), *Navicula salinarum* (5.8%), *Surirella linearis* (4.5%) and *Synedra ulna* (5.2%). The IBD values in Peramachipalayam (10.1) indicated moderate ecological status in 2012. In present study of Peramachipalayam most dominant species taxa were recorded such as *Achnantheidium minutissima* (9.6%), *Anomoeoneis sphaerophora* (9.6%), *Eunotia fallax* (9.6%), *Nitzschia acicularis* (8.4%), *Nitzschia microcephala* (8.4%) and *Synedra ulna* (8.4%). The IBD values in Peramachipalayam (11.4) indicated moderate ecological status in 2013.

In present study of Kottampatty most dominant species taxa were recorded such as *Amphora veneta* (6.6%), *Cyclotella atomus* (6.6%), *Cymbella aspera* (5.7%), *Cymbella cymbiformis* (6.6%), *Craticula cuspidata* (6.6%), *Cyclotella striata* (9%), *Encyonema minutum* (1.6%), *Fragilaria rumpens* (9.8%), *Gomphonema gracile* (6.6%) and *Synedra ulna* (9.8%). The IBD values in Kottampatty (12.6) indicated moderate ecological status in 2011. In present study of Kottampatty most dominant species taxa were recorded such as *Amphora veneta* (9.3%), *Cocconeis pediculus* (5%), *Ctenophora pulchella* (8.7%), *Surirella linearis* (6.8%), *Surirella robusta* (6.8%), *Gomphonema affine* (6.8%) and *Synedra ulna* (9.8%). The IBD values in Kottampatty (13.2) indicated moderate ecological status in 2011. In present study of Kottampatty most dominant species taxa were recorded such as *Anomoeoneis sphaerophora* (9.2%), *Cyclotella atomus* (7.6%), *Cymbella cymbiformis* (8.6%), *Cocconeis pediculus* (9.8%), *Nitzschia microcephala* (9%), *Nitzschia recta* (8%) and *Synedra rumpens* (6.1%). The IBD values in Kottampatty (10.3) indicated moderate ecological status in 2013.

In present study of Sanyasipatti most dominant species taxa were recorded such as *Cyclotella atomus* (7.1%), *Ctenophora pulchella* (7.1%), *Gomphonema parvulum* (7.1%), *Gomphonema olivaceum* (1.8%), *Surirella tenera* (8.8%) and *Nitzschia palea* (8.8%). The IBD values in Sanyasipatti (11.9) indicated moderate ecological status in 2011. In present study of Sanyasipatti most dominant species taxa were recorded such as *Amphora veneta* (5%), *Encyonema minutum* (8.4%), *Fragilaria rumpens* (5.7%), *Gomphonema olivaceum* (6.5%), *Gomphonema parvulum* (9.2%), *Melosira granulata* (5.7%), *Nitzschia obtusa* (8.5%), *Navicula salinarum* (5.7%) and *Navicula viridula* (8.5%). The IBD values in Sanyasipatti (11.5) indicated moderate ecological status in 2011. In present study of Sanyasipatti most dominant species taxa were recorded such as *Cocconeis placentula* (9.6%), *Diadesmis confervacea* (3.9%), *Gomphonema parvulum* (6.1%), *Nitzschia dissipata* (3.9%), *Navicula mutica* (5%), *Surirella ovalis* (4%) and *Synedra ulna* (9.8%). The IBD values in Sanyasipatti (8.8) indicated moderate ecological status in 2013. In similar reported, Hosmani 2012 was reported the most common indicators of organic

pollution were *Gomphonema parvulum* (6.1%), *Synedra ulna* (9.8%) in Dadadahally Lake, Doddakere Lake of Mysore city. In present study, Sanyasipatti was affected in organic pollution due to dying factory effluent and sewages. So Sanyasipatti has IBD values of 8.8 indicating moderate ecological statuses.

In present study of Bhavani most dominant taxa were recorded such as *Achnantheidium eutrophilum* (3.8%), *Amphora ovalis* (4.8%), *Cymbella lanceolata* (4.8%), *Cymbella turgidula* (1.9%), *Ctenophora pulchella* (4.8%), *Fragilaria rumpens* (3.8%), *Gomphonema parvulum* (8.3%), *Gomphonema olivaceum* (3.8%), *Navicula viridula* (3.8%), *Pinnularia acrospheria* (3.8%), *Synedra rumpens* (3.8%), *Surirella splendida* (3.8%), *Nitzschia palea* (8.3%), *Tryblionella levidensis* (5.7%). The IBD values in Bhavani (10.22) indicated moderate ecological status in 2011. Similarly, Lobo et al. 2004 described *Nitzschia palea* as a medium pollution-tolerant species and *G. parvulum* as a relatively abundant species in downstream eutrophic sites with high organic pollution as alfamesosaprobic from lotic systems in southern Brazil. This taxon represented quality class from moderate to poor quality. Similarly, *Nitzschia palea* (8.3%) was most dominant taxa in this area. In present study most of Bhavani dominant species taxa were recorded such as *Amphora ovalis* (3%), *Gomphonema gracile* (9%), *Gomphonema lanceolatum* (9%), *Gomphonema olivaceum* (7.2%), *Gomphonema parvulum* (9.8%), *Navicula viridula* (7.8%) and *Nitzschia palea* (8.9%). The IBD values in Bhavani (11) indicated moderate ecological status in 2012. Similarly Lobo et al. 2004 described *Nitzschia palea* as a medium pollution-tolerant species and *Gomphonema parvulum* is a relatively abundant species at downstream eutrophic sites with high organic pollution as alfamesosaprobic from lotic systems in southern Brazil. This taxon represented quality class was moderate to poor quality. In present study, *Gomphonema parvulum* (9.8%) and *Synedra ulna* (8.9%) were most dominant in this area affected to sewages and dying factories. In present study most dominant species taxa were recorded such as *Amphora veneta* (4.4%), *Cymbella cymbiformis* (4.4%), *Cocconeis pediculus* (9.6%), *Cyclotella stelligera* (9.4%), *Ctenophora pulchella* (4.4%), *Eunotia bilunaris* (4.4%), *Frustulia rhomboids* (4.4%), *Gomphonema truncatum*, (8%), *Gomphonema parvulum* (9.8%), *Nitzschia acicularis* (7.9%), *Navicula subrhynchocephala* (4.4%), *Pinnularia acrospheria* (4.4%), *Surirella angusta* (7.9%), *Nitzschia palea* (9.6%) and *Synedra rumpens* (7.9%). The IBD values in Bhavani (7.7) indicated moderate ecological status in 2013. In similar result of Kalyoncu and Serbetci (2013) was studied both taxa richness and diversity declined due to a mixture of waste water to stream. All of the taxa determined in this site are tolerant of pollution. These taxa are *N. palea*, *G. parvulum* and *Navicula cryptocephala* in Dari Stream, Isparta Turkey and however, this species had high relative abundance at alfamesosaprobic with critically

polluted water quality, an indication that it is tolerant of high pollution. In present study during 2011-2013 was determined to moderate in ecology status due to In present study, Bhavani in receives untreated domestic and industrial wastewaters from Bhavani region, The pollution in the river is due to the merger of sewages and industrial pollution. The industry in this area seems to discharge effluents in the river without treating it posing danger to human health and animal habitat.

Shannon diversity index (H') computed as per equation 2 takes into account the number of individuals as well as number of taxa (Fig. 2). This varies from 0 for communities with only a single taxon to high values for communities with many taxa, each with few individuals. Low H' was recorded in Sanyasipatti (2.86), *Surirella tenera* and *Synedra ulna*, representing (8.8%) in 2011 (Table 4). Low H' was recorded in Navappatti (2.87), *Aulacoseira distans* representing (9.7%) in 2012 (Table 5). Low H' was recorded in Ammapettai (2.36), *Cymbella microcephala* representing (8.3%) in 2013 (Table 6).

Berger-Parker index was calculated (equation 3) from the number of individuals in the dominant taxon relative to the total number of species (Fig. 3). *Synedra ulna* and *Tryblionella levidensis* are the dominant species (with 8.3% abundance) showing a high index value in Bhavani during 2011 (Table 4). *Synedra ulna* and *Tryblionella levidensis* are the dominant species (with 8.3% abundance) showing a high index value in Bhavani

during 2012 (Table 5). In Bhavani *Navicula viridula* (9%), *Nitzschia palea* (8.9%) of the population from a macrophytes habitat. *Cyclotella atomus* (5.8%), *Cyclotella striata* (5.8%), *Diadlesmis confervacea* (5.8%), *Gomphonema gracile* (5.8%), *Neidium affine* (5.8%) in Ammapettai 2013 (Table 6).

Dominance is the total of a particular species with respect to different species in an ecological community predominate, ranging from 0 (all taxa are equally present) to 1 (a taxon dominates the community completely). The dominance analysis shows that the Bhavani locality in Cauvery river has species with *Synedra ulna* (8.3%) and *Tryblionella levidensis* (8.3%) as dominant species (dominance: 0.15), while *Surirella tenera* (8.8%) and *Synedra ulna* (8.8%) are dominated in Sanyasipatti, (dominance 0.08), and *Achnanthisidium eutrophilum* (9.4%), and *Cyclotella atomus* (6.2%) in Peramachipalayam (dominance 0.07), Navappatti (dominance 0.07). Remaining sites showed dominance index value between 0.1- 0.4 (Table 4) in 2011 (Table 4). The dominance analysis shows that the Bhavani locality in Cauvery river has species with *Navicula viridula* (9% as dominant species (dominance: 0.09), while *Melosira granulata* (9.8%) dominated Navappatti (dominance 0.08) and Kottampatti and Sanyasipatti (dominance 0.06) *Nitzschia palea* (9.8%), *Navicula viridula* (8.5%) dominance respectively. The dominance analysis shows that the Mettur dam, Siluvampalayam,

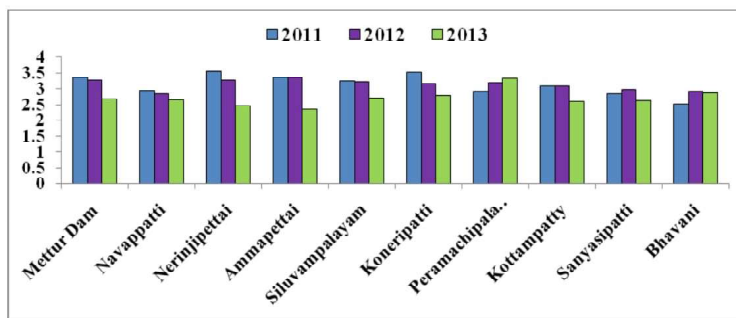


Fig. 2. Shannon diversity Index in different areas under study.

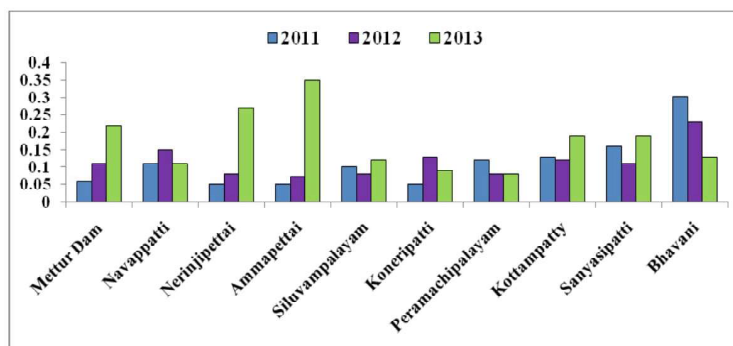


Fig. 3. Berger-Parker Index in different areas under study.

Table 4. Diversity of Diatom taxa in 2011.

Diversity Indices	Mettur Dam	Navappatti	Nerinjipettai	Ammappettai	Siluvampalayam	Koneripatti	Peramachipalayam	Kottampatty	Sanyasipatti	Bhavani
Dominance D	0.04	0.07	0.03	0.04	0.04	0.03	0.07	0.06	0.08	0.15
Shannon H	3.37	2.94	3.56	3.35	3.26	3.54	2.92	3.08	2.86	2.53
Berger Parker	0.06	0.11	0.05	0.05	0.10	0.05	0.12	0.13	0.16	0.30

Table 5. Diversity of Diatom taxa in 2012.

Diversity Indices	Mettur Dam	Navappatti	Nerinjipettai	Ammappettai	Siluvampalayam	Koneripatti	Peramachipalayam	Kottampatty	Sanyasipatti	Bhavani
Dominance D	0.05	0.08	0.04	0.04	0.05	0.05	0.05	0.06	0.06	0.09
Shannon H	3.27	2.87	3.29	3.35	3.23	3.18	3.19	3.07	2.97	2.93
Berger Parker	0.11	0.15	0.08	0.072	0.08	0.13	0.08	0.12	0.11	0.23

Table 6. Diversity of Diatom taxa in 2013.

Diversity Indices	Mettur Dam	Navappatti	Nerinjipettai	Ammappettai	Siluvampalayam	Koneripatti	Peramachipalayam	Kottampatty	Sanyasipatti	Bhavani
Dominance D	0.09	0.07	0.12	0.16	0.07	0.06	0.04	0.09	0.10	0.07
Shannon H	2.7	2.68	2.46	2.36	2.72	2.81	3.32	2.60	2.63	2.89
Berger Parker	0.22	0.11	0.27	0.35	0.12	0.09	0.08	0.19	0.19	0.13

Koneripatti, Peramachipalayam has the dominances of 0.05. Remaining Nerinjipettai and Ammapettai sites showed dominance index value 0.4 (Table 4) in 2012 (Table 5). The Dominance analysis shows that the Ammapettai locality in Cauvery river has species with *Cymbella microcephala* (8.3%), as dominant species (dominance: 0.16), while *Nitzschia palea* (9.8%), dominated Sanyasipatti (dominance 0.16) in 2013 (Table 6).

In present study, of Sanyasipatti most dominant species taxa were recorded such as *Cyclotella atomus* (7.1%), *Gomphonema gracile* (7.1%), *Surirella tenera* (8.8%) and *Synedra ulna* (8.8%), *Encyonema minutum* (8.4%), *Gomphonema parvulum* (9.2%), *Melosira granulata* (5.7%), *Nitzschia obtusa* (8.5%), *Cocconeis placentula* (9.6%), *Diademesmis confervacea* (3.9%), *Synedra ulna* (9.8%) which are more tolerant to high levels of pollutions in Sanyasipatti.

In Bhavani, cosmopolitan extreme pollution resistant species *Synedra ulna* (8.3%), *Tryblionella levidensis* (8.3%), *Gomphonema gracile* (9%), *Gomphonema lanceolatum* (9%), *Gomphonema olivaceum* (7.2%), *Gomphonema parvulum* (7.8%), *Cocconeis pediculus* (9.6%), *Cyclotella stelligera* (9.4%), *Surirella robusta* (9.6%) and *Synedra rumpens* (7.9%) were dominant species highlighting eutrophic status of water with higher electrolyte. Xiang Tan *et.al* (2013) reported to Biological Diatom Index (IBD) and diatom based eutrophication/pollution index (EPI-D) were strongly related to trophic status and ionic content were related to organic pollution and conductivity. Yet, the diatom indices showed weak relationships with physical and chemical variables during the wet season in Han River in the Yangtze River basin is the water source area of China. It is concluded that IBD have strong correlations with some water quality variables in subtropical rivers in China, especially in the dry season, despite differences in taxonomy, geographic setting (e.g., climate, geology) and the nature of the pollutant gradient.

Mettur dam has IBD (14.2), mesotrophic indicating moderate quality in 2011, IBD (14.2), mesotrophic indicating moderate quality in 2012 and IBD (16.5), oligo-mesotrophic indicating good quality in 2013 due to the inflow of water to Mettur dam changing the water quality as oligo-mesotrophy i.e. good quality. Finally, Mettur Dam has water quality of oligo-mesotrophic condition and therefore good quality in ecological status. Navappatti was IBD (14.2), mesotrophy- indicate to moderate quality in 2011, IBD (13.3), mesotrophy indicate to moderate quality in 2012 and IBD (16.5), oligo-mesotrophy indicates to good quality in 2013.

In Navappatti there is no change for ecological status this area had good ecological status during 2011-2013. Nerinjipettai has IBD (11.29), meso-eutrophic indicating poor quality in 2011, IBD (13.6), mesotrophic indicating moderate quality in 2012 and IBD (10.3), meso-eutrophic indicating poor quality in 2013. Nerinjipettai was affected in anthropogenic pollution and sewages IBD values of (10.3) were indicating ecological states in

poor quality. Ammapettai has IBD (12.52), mesotrophic indicating moderate quality in 2011, IBD (11.4), meso-eutrophic indicating poor quality in 2012 and IBD (14.4), Mesotrophic- Moderate quality in 2013. Ammapettai was slightly polluted due to sewage and anthropogenic activity. Siluvampalayam was IBD (13.5), mesotrophy indicated moderate quality in 2011, IBD (11.1) meso-eutrophy indicated poor quality in 2012 and IBD (14.5) Mesotrophy indicated moderate quality in 2013. Siluvampalayam was affected in organic pollution, anthropogenic pollution and sewages.

Koneripatti has IBD (12.1) mesotrophy indicated moderate quality in 2011, IBD (11.5) meso-eutrophy indicated poor quality in 2012 and IBD (13.7) mesotrophy indicated moderate quality in 2013. Koneripatti was affected in discharge by effluents and untreated sewage into the river by dying units from Koneripatti. Peramachipalayam has IBD (13.5) mesotrophy indicated moderate quality in 2011, IBD (10.1) meso-eutrophy indicated poor quality in 2012 and IBD (11.4) meso-eutrophy indicates to poor quality in 2013. In during 2011-2013, Peramachipalayam was affected in sewage, industrial effluent and dying factory. Kottampatti has IBD (12.6) mesotrophy indicated moderate quality in 2011, IBD (13.2) mesotrophy indicated moderate quality in 2012 and IBD (10.3) meso-eutrophy indicated poor quality in 2013. Kottampatti study area affected to sewages and dying factories. Sanyasipatti has IBD (11.9) meso-eutrophy indicated poor quality in 2011, IBD (11.5) meso-eutrophy indicated poor quality in 2012 and IBD (8.8) eutrophy indicated bad quality in 2013. Sanyasipatti was affected in organic pollution due to dying factory effluent and sewages. Bhavani has IBD (10.22), meso-eutrophy indicated poor quality in 2011, IBD (11) meso-eutrophy indicated poor quality in 2012 and IBD (7.7), eutrophy indicated bad quality in 2013.

CONCLUSIONS

The present study is an attempt, first of its kind, in this study area to use biological diatom indices for indicating general ecological status and assessment of river water quality determined at various sites in the Cauvery River. The studies on Diatoms indices reveal that water qualities of the Cauvery River are good quality (oligo-mesotrophy) at Mettur where as it is heavily polluted (eutrophic) at Bhavani sites.

Bhavani areas of Cauvery River are grossly polluted due to the discharge of untreated sewage disposal and industrial effluents directly into the river.

The pollution in the river is due to the merger of sewages and industrial pollution. The industry in this area seems to discharge effluents in the river without treating it posing danger to human health and animal habitat. The present study cautions the indiscriminate dumping and release of pollutants into rivers which might lead to serious environmental deterioration which could be considered as a potential source of threat to the biotic life.

References

- Barlas, M. (1988). Limnological investigations other Fulda with special emphasis on fish parasites, your Host specificity range and the water quality. Dissertation. PhD Thesis. Universitat Kassel.
- Beltrami, M. E. Ciutti, F. Cappelletti, C. Losch, B. Alber, R. and Ector, L. (2012). Diatoms from Alto Adige/ Südtirol (Northern Italy): characterization of assemblages and their application for biological quality assessment in the context of the Water Framework Directive. *Hydrobiologia*. DOI 10.1007/s10750-012-1194-x
- Berger, W.H. Parker, F.L. (1970). Diversity of planktonic Foraminifera in deep sea sediments. *Science* 168, 1345–1347.
- Descy, J.P. (1979). A new approach to water quality estimation using diatoms. *Nova Hedwigia* 64: 305-323.
- Eloranta, P. and Soininen, J. (2002). Ecological status of some Finnish rivers evaluated using benthic diatom communities. *J. Appl. Phycol.* 14, 1/7
- Gomez, N. and Licursi, M. (2001). The Pampean Diatom Index (IDP) for assessment of rivers and streams in Argentina. *Aquatic Ecology*, 35, 173-181.
- Hirst, H. Juttner, I., and Ormerod, S. (2002). Comparing the response of diatoms and macroinvertebrates to metals in upland streams of Wales and Cornwall. *Freshwater Biology* 47, 1652-1665.
- Hosamani, S. P. (2012). Freshwater Diatoms as Indicators of River Water Quality Paripex - Indian Journal of Research, Vol: 1, Issue: 1, 36-38.
- Jacob John (2012). Diatoms in the Swan River Estuary, Western Australia: Taxonomy and Ecology, Koeltz Scientific Books, Algae-456.
- John, J. (2012). A Diatom Prediction Model and Classification for Urban Streams from Perth, Western Australia. Germany: Koeltz Scientific Books.
- Kalyoncu and Burcu, S. (2013). Applicability of Diatom-Based Water Quality Assessment Indices in Dari Stream, Isparta Turkey Hasan. *World Academy of Science, Engineering and Technology International Journal of Environmental, Chemical, Ecological, Geological and Geophysical Engineering*, 7(6).
- Karthick, B. Hamilton, P. B. and Kocielek, J.P. (2013). Illustrated Guide on Common Freshwater Diatoms of Western Ghats. Gubbi Labs. ISBN: 978-81-924461-1-0
- Kelly, M. Juggins, S. Guthrie, R. (2008). Assessment of ecological status in U.K. rivers using diatoms. *Freshwater Biology*, 53, 403-22.
- Kelly, M.G. and Whitton, B.A. (1995). The Trophic Diatom Index: a new index for monitoring Eutrophication in rivers. *Jour. Applied Phycol.*, 7, 433-444
- Kelly, P. M. (2000). 'Towards a Sustainable Response to Climate Change', in Huxham, M. and Sumner, D. (eds.), *Science and Environmental Decision-Making*, Pearson Education, Harlow, 118–141.
- Lenoir, A. and M. Coste. (1996). Development of a practical diatom index of overall water quality applicable to the French National Water Board Network. In Whitton, B. A. and E. Rott (eds), *Institut für Botanik. Universität Innsbruck*, 29-43
- Lobo EA, D. Bes. L, Tudesque. and L. Ector. (2004). Water quality assessment of the Pardino river, RS, Brazil, using epilithic diatom assemblages and faecal coliforms as biological indicators. *Vie et Milieu – Life and Environment* 54, 115-125
- Prygiel, J. and M. Coste. (1993). The assessment of water quality in the Artois-Picardie water basin (France) by the use of diatom indices. *Hydrobiologia*. 269, 343–349.
- Round, F.E. Crawford, R.M. and Mann, D.G. (1990). *The diatoms. Biology and Morphology of the Genera*. Cambridge University Press, Cambridge, pp. 747.
- Schonfelder, I. Gelbrecht, J., Schonfelder, J. and Steinberg, C.E.W. (2002). Relationships between littoral diatoms and their chemical environment in northeastern German lakes and rivers. *Journal of Phycology*, 38, 66-82.
- Shannon, C.E. and Weaver, W. (1949). *The Mathematical Theory of Communication*. University of Illinois Press, Urbana.
- Stevenson, R.J. and Pan, Y. (1999). Assessing environmental conditions in rivers and streams with diatoms. In: Stoermer, E.F., Smol, J.P. (Eds.), *The Diatoms: Applications for the Environmental and Earth Sciences*. Cambridge University Press, Cambridge, UK, 11-40.
- Stoermer, E.F. and Smol, J. P. (1999). *The Diatoms: Applications for the Environmental and Earth Sciences*. Cambridge University Press, Cambridge, UK.
- Taylor, J.C. (2007). The application and testing of diatom-based indices in the Vaal and Wilge Rivers, South Africa, *Water SA*, 33 (1).
- Venkatachalapathy, R. and Karthikeyan, P. (2014). Diatom Indices for Water Quality Assessment in Cauvery River, Tamil Nadu, India. *Gondwana Geological Magazine*. Spl. Vol. No. 15, pp.109-116.
- Venkatachalapathy, R. and Karthikeyan, P. (2015). Diatom Indices and Water Quality Index of the Cauvery River, India: Implications on the Suitability of Bio-Indicators for Environmental Impact Assessment. Springer, Earth System Sciences, DOI 10.1007/978-3-319-13425-3-31.
- Xiang Tan, Fran Sheldon, Stuart E. Bunn, Quanfa Zhang (2013). Using diatom indices for water quality assessment in a subtropical river, China. *Environ Sci Pollut Res* 20(4), 164–4175 DOI 10.1007/s11356-012-1343-9.

INVITATION TO CONTRIBUTORS

Contributions on every aspect of sediments and sedimentary rocks in the form of articles, notes, reviews, etc. will be considered for publication in *Journal of the Indian Association of Sedimentologists*. An article accepted becomes the copy right of the Journal.

Manuscripts

The contributions should be sent to Prof. D. Rajasekhar Reddy, Chief Editor, *Journal of Indian Association of Sedimentologists*, 49-53-8/1, Sneha Apartments, Balaji Hills, Visakhapatnam - 530 013. A certificate should accompany that the contribution is the author's / author's own original work and has not been published or sent for publication elsewhere.

It is desirable that the size of the article is kept to about 3000 words and is submitted in duplicate to enable quick pre-publication processing. Each article should be accompanied by short informative abstract not exceeding 300 words, summarizing the main points and important conclusions arrived at in the article.

The manuscript should be typed on one side of the paper, double spaced, with a margin of at least 4 cm on each side. It should bear title of the contribution, name(s) and affiliations(s) and full postal address for communication. All pages should be numbered on top right hand corner. The relative importance of respective headings should be indicated by the author by use of ringed capital letters, i.e. (A) for the main heading, (B) for the second heading, etc.

Tables, Figures and Illustrations: Tables should be typed on separate sheets and numbered consecutively with Arabic numerals. All illustrations, including photographs and / or photomicrographs are to be classified as figures and should be numbered consecutively. Line drawings should be in Indian ink on glossy tracing paper. Figures and lettering should be suitable for 50% reduction and should be drawn or grouped so that on reduction they fit within the typed area of 200 X 130 mm and the minimum lettering size must not be less than 1 mm on reduction. Figures and illustrations should be drawn neatly and be lettered with proper stencils. Authors are asked to send to the Editor all the original illustrations along with the manuscript and one set of sharp copies of drawings, reduced to publication size, if possible. Good quality glossy prints should be sent un mounted and without lettering. Details of lettering (A, B, C, D etc.) to be used on photographs should be written properly with stencils on a separate sheet. Each table and figure including photograph should have the author's name and number as cited in the text, written on the back in pencil. Legends should be typed on a separate sheet, and the approximate position of tables and figures be indicated in the margin of the text.

References: References should be made by giving the author's name with the year of publication in parenthesis. References should be listed in alphabetical order at the end of the paper in the following standard form.

Article: Walker, R. C. (1969). Geometrical analysis of ripple-drift cross-lamination. *Can. Jour. Earth Sci.*, 6(3), 383-392.

Book: Fuchtbauer, H. (1974). *Sediments and Sedimentary Rocks I*. Stuttgart Schweizerbart'sche Verlagsbuchhsndlung.

Chapter in book: Fyfe, W. S. and Bischoff, J. C. (1965). Calcite aragonite problem. In: L. C. Pray and R. C. Murray (eds.), *Dolomitization and Limestone Diagenesis*, pp. 3-13. *Soc. Econ. Palaeontologists and Mineralogists, Spec. Pub.*, No. 13.

Reprints. The author/first author will receive 25 reprints at a cost @ Rs. 25/page for printed pages.

Published by

INDIAN ASSOCIATION OF SEDIMENTOLOGISTS